A FUNDAMENTAL STUDY OF ACTIVE NOISE CONTROL SYSTEM DESIGN

SCOTT D. SNYDER

Department of Mechanical Engineering

University of Adelaide

GPO Box 498

Adelaide, South Australia 5001

Thesis in fulfillment of the degree of Ph.D. in Mechanical Engineering,

submitted December 7, 1990, revised August 30, 1991.

A FUNDAMENTAL STUDY OF ACTIVE NOISE CONTROL SYSTEM DESIGN

CONTENTS

A FUNDAMENTAL STUDY OF ACTIVE NOISE CONTROL SYSTEM DESIGN

ABSTRACT

Active noise control has become the topic of a great deal of research in recent years. Despite this, it has remained largely a laboratory exercise rather than a practical noise control technique, with commercial systems being available only for the relatively simple case of controlling plane wave propagation in air handling ducts. One of the principal reasons for this is a lack of complete understanding of the physical mechanisms involved in the active control of noise. Another reason is a lack of information available to the potential user of active noise control on how to design an efficient system, and on the effect which structural / acoustic, geometric, and electronic variables have upon active noise control system performance.

The goal of this thesis is to help alleviate these two problems. It aims to examine physical control mechanisms, provide general analytical models, and quantify the effect of system variables, for some of the most commonly targeted active noise control problems.

This thesis is divided into two parts; examination of the physical system arrangement, and examination of the electronic control system. The physical arrangement section is concerned first with the study of the control of a simple, single mode system (plane wave sound propagation in an air handling duct). It then progresses on to more complex structural/ acoustic systems. The electronic control system section examines the least mean square (LMS)

algorithm as implemented in active noise control systems. In this way, the effects of system variables upon the stability and convergence characteristics of a class of transversal filter-based adaptive architectures can be qualitatively determined.

NEW WORK

New work presented in this thesis includes:

1. Development of an analytical model for the active control of plane wave sound propagation in air handling ducts. The model describes the acoustic control mechanisms involved in terms of acoustic power flows from both primary and control sources (Chapter 2).

2. Experimental verification of the analytical plane wave control model for duct noise using a novel means of directly measuring the acoustic power flow from all sources (Chapter 2).

3. Extension of the analytical model to examine the influence of several system parameters on the ability of the active system to control plane wave sound propagation in air handling ducts (Chapter 2).

4. Development of a generalized model to enable the assessment of the effect of applying active noise control to structural radiation problems where the fluid medium is air. This model accommodates the use of acoustic and/or vibration control sources, and is suitable for implementation as a design tool for this type of active noise control system (Chapter 3).

5. Experimental verification of this generalized structural radiation model for the control of both sound radiation from a planar surface into free space, and sound transmission into a weakly coupled enclosure (Chapters 4 and 5).

6. Use of the analytical model and experimental results to examine the physical mechanisms of active control using vibration control sources on a vibrating structure (Chapter 4).

7. Use of the analytical model to examine the effect which various structural / acoustic and geometric system parameters have upon the performance, and control mechanisms, for systems actively controlling sound radiation into free space from a planar surface (Chapter 4).

8. Development of a methodology for the design of systems to actively control sound radiation from planar vibrating structures into free space (Chapter 4).

9. Analytical development of the bounds of stability for the filtered-x LMS algorithm as applied to active noise control systems, and examination of the effects which system variables have upon these stability bounds (Chapter 7).

10. Analytical development of the bounds of stability for the multiple input, multiple output filtered-x LMS algorithm as applied to active noise control systems, and examination of the effects which system variables have upon these stability bounds (Chapter 8).

STATEMENT OF ORIGINALITY

To the best of my knowledge, except where otherwise referenced, all of the work presented in this thesis is my own original, and has not been presented previously for the award of any other degree or diploma in any University. If accepted for the award of the degree of Ph.D., I consent that this thesis be made available for loan and photocopying.

Scott D. Snyder

ACKNOWLEDGEMENTS

The work presented in this thesis would not exist without the encouragement and support of a large number of people. In particular, I would like to acknowledge the following.

Firstly, I would like to thank my parents, Ralph and Nancy Doss, and Daniel Snyder, for encouraging an interest in academic pursuits and engineering from an early age. I would like to thank Prof. R.E. (Sam) Luxton for allowing me the opportunity to conduct research in his department. Also, I am grateful to Dr. Pan Jie, for his many enlightening comments, and Prof. C.R. (Chris) Fuller, for giving me the opportunity to conduct research at both Virginia Tech and NASA Langely. I was also fortunate to have excellent technical support during my research, and would like to especially thank Matthew Woodland, for his electronics work, and George Osborne, for his craftsmanship in building experimental apparatus (and for keeping my stomach from growing too much).

Finally, I would like to thank the two people who had the greatest influence upon my research. Firstly, my supervisor, Dr. C.H. (Colin) Hansen, who provided me with all of the support and incentive I could ever want to make my research both fruitful and enjoyable. Secondly, to my wife, Gillian, who provided endless encouragement and kept my emotions on a somewhat even keel.

CHAPTER 1.

INTRODUCTION TO PHYSICAL SYSTEM ANALYSIS

1.1 OVERVIEW

The chief obstacle still standing in the way of active noise control being realized as a viable, practical technique is the complexity of most structural/acoustic systems for which active noise control is targeted. For global sound attenuation to be achieved, the dominant offending acoustic or coupled structural/acoustic modes present under primary excitation (without the addition of active control) must be observable to, and controllable by, the active noise control system. For the relatively simple single mode problem of controlling plane wave sound propagation in ducts, a single control source (actuator) and error sensor (providing a measure of the residual sound field) can achieve the desired result. For multi-modal problems, the required number of control sources and error sensors generally increases dramatically.

To design efficient active control systems for these complex noise problems, the design of both the "physical" control system, comprising the arrangement of the actuators and sensors, and the design of the electronic control system, must be optimized. The physical control system will set the bounds on the levels of noise control which are achieveable, while the design of the electronic control system will determine how close to these bounds the actual levels of attenuation will be. This thesis will consider only control systems which are feedforward in structure. In this type of control system the principle aim is to alter the impedance of the structural / acoustic system to the impending primary source disturbance. This is in contrast to

feedback control systems, whose principle aim is to alter the transient response characteristics of the structural / acoustic systems. It will be divided into two sections; chapters 1-5 will be devoted to the design of the physical control system, while chapters 6-8 will be devoted to the design of the electronic control system (note that chapter 6 is a separate introduction explicitly for the electronic control system, as opposed to this chapter which is concerned with the physical control system).

To optimize the design of the physical control system, a thorough understanding of the physical control mechanisms employed must be gained. As outlined in the next section, several mechanisms for the use of acoustic control sources have been suggested in the past. These include cancellation, absorption, reflection, and impedance changes. These suggested mechanisms remain largely unverified experimentally, owing to the difficulty of measuring the physical quantities which they address. Clearly more work is required here, which will be undertaken in Chapter 2.

Also, work is still required to clarify the physical control mechanisms employed when vibration sources are used to actively control sound radiation (Thomas et al, 1990). A reduction in the amplitude of the dominant radiating structural modes has been shown to be one control mechanism (Fuller and Jones, 1987), but experimental results would appear to indicate that this explanation may be incomplete in some instances (Thomas et al, 1990). This topic will be addressed in chapter 4.

Further, there is a need to appreciate that the performance of an active noise control system is not dependent only on the performance of the electronic controller; of equal importance is the

physical arrangement of the control sources and error sensors. It is this physical arrangement that will determine the maximum achievable level of sound attenuation. The design of the electronic control system will dictate how close to this maximum achievable level the actual sound attenuation will come. Each of these two sub-systems must be optimally designed if the overall active noise control system is to be maximally effective.

It has thus far proved, in general, impossible to directly analytically determine the optimal physical arrangement of the control sources and error sensors for a given single or multiple channel active noise control problem (Nelson et al, 1985). There are two reasons for this. First, the maximum level of achievable sound power and pressure attenuation is not a linear function of location. Secondly, the optimum error locations are dependent upon the control source locations. What is required, therefore, is a means of analytically predicting the effectiveness of a given active noise control system, as well as a means of analytically predicting the influence which various structural / acoustic and geometric parameters have upon this effectiveness, which can be implemented in a multi-dimensional optimization routine. In this way, a "trial and error" approach can be used to optimize the physical system arrangement.

As will be outlined in the next section, many analytical models have been put forward for use in a variety of active noise control problems. They are, however, specific to their single topic of interest; generalization would allow inference of control mechanisms and parameter influences. Many of these models are idealized to the point where they cannot assess the physical system limitations such as control source size and structural / acoustic damping. Many are unverified experimentally. Also, many of the previously developed analytical models are not suitable for practical implementation, owing to the degree of computational power required to solve them.

The aim of the physical control system arrangement section of this thesis is to shed light on some fundamental issues which must be taken into account in the design of the physical arrangement of the control sources and error sensors in active noise control systems. Central to this is a thorough examination of the physical mechanisms employed by active noise control systems. This examination leads to an understanding of how physical design variables, such as control source and error sensor arrangement, influence the performance of the active noise control system. Incorporated in this examination is the development of generalized analytical models suitable for use in the design of active systems to control plane wave sound propagation in air handling ducts (in Chapter 2), and for controlling structural sound radiation (in Chapter 3), where the fluid medium is air.

1.2 HISTORICAL BACKGROUND

It has been widely published that the origins of active noise control can be traced back to the German inventor, Paul Lueg, in the 1930's (Warnaka, 1982; Leitch and Tokhi, 1987; Guicking, 1990). His physical concepts, however, were far in advance of the technology required for practical implementation, and this coupled with the political climate in Germany at that time hindered any further development (Guicking, 1990).

Active noise control surfaced as a research topic again in the 1950's, from work conducted by two main researchers. Firstly, Olson (1953, 1956) began to experiment with an "electric sound absorber". This was basically a loudspeaker and cabinet arrangement, with a microphone located in close proximity to the face of the speaker cone. The loudspeaker was driven so as to

null the sound pressure at this microphone, effectively creating an area of quiet encompassing it. Olson proposed the use of his sound absorber for a number of applications, including headsets and air handling ducts. However, although his results showed promise, the electronics technology of that period was still not sufficiently advanced to enable practical (rather than laboratory) implementation.

The other researcher working on active noise control during this period was Conover (1956), who was interested in attenuating noise radiated from large transformer tanks. He placed loudspeakers near a 15 MVA transformer, and adjusted the phase and amplitude of these active sources to reduced the sound pressure at a point 100 ft. from the tank, normal to its surface. His results, however, would appear to indicate that local, rather than global, sound attenuation was achieved.

Following the work of Olson and Conover, interest in active noise control again waned for a period of time. It was not until the late 1960's that sustained research in the field began in earnest. This was spurred on by parallel advances in electronics technology which made the practical implementation of active noise control realizable. Early research of this period was directed mainly at attenuating plane wave sound propagation in air handling ducts, and sound radiation from transformer tanks. More recently, there has been a large body of research directed towards controlling sound transmission into weakly coupled enclosures, particularly into aircraft fuselages.

Possibly the most popular active noise control research topic is the attenuation of plane wave propagation in air handling ducts. This is partly because of potential widespread industrial

applications, and partly because working experimental systems can be readily built. Commercial systems for this active noise control application are currently available (Eriksson and Allie, 1988).

Practical active noise control systems require some means of sensing the unwanted primary noise disturbance so that the electronic control system has a reference signal to modify, producing the control disturbance. This can present a problem for duct active noise control systems using a single control source (Leventhall, H.G. and Eghtesadi, Kh., 1979), as the controlling disturbance propagates both upstream and downstream, "contaminating" the reference signal if a microphone is used. Much of the early work on duct active noise control systems was directed towards developing novel control source arrangements to help overcome this problem. Arrangements were developed in which the control source disturbance was constrained to propagation in one direction (Jessel and Mangiante, 1972; Swinbanks, 1973), and in which the control source disturbance was nulled in certain locations (Leventhall, 1976; Eghtesadi and Leventhall, 1981). In general, however, the bandwidth of these arrangements was limited (Poole and Leventhall, 1976; Canevet, 1978), although it was shown that with some modification to the basic ideas broadband noise control could be achieved (La Fontaine and Shepherd, 1983). Despite this, the majority of more recent research has considered the use of the relatively simple, single control source system.

Much of the early work (Burgess, 1981; Eghtesadi and Leventhall, 1982; Chaplin, 1983) and some recent work (Eghtesadi et al, 1985, 1986; Hong et al, 1987; Eriksson and Allie, 1988) on active noise control in ducts describes the acoustic mechanism as one of cancellation; that the attenuation of the sound from the primary source is due to the destructive interference caused by

an injection of an "antiphase" wave from a secondary source or sources. Other investigators have suggested that this apparent cancellation is actually a reflection of the primary source wave at the secondary source (Trinder and Nelson, 1983; Poole and Leventhall, 1976). This reflection is caused by the impedance change at the secondary source resulting from the source maintaining a sound pressure null in front of itself. Several researchers have also demonstrated analytically that it is possible to arrange two secondary sources so that they will completely absorb all incident energy from the primary source (Elliott and Nelson, 1984; Berengier and Roure, 1980a; Nelson and Elliott, 1987). However the analyses are incomplete as the effects on the primary source and the downstream power radiation when the secondary sources are misadjusted from their optimum are not considered.

Although much of the analytical work in the past has centered on idealized point sources (Burgess, 1981; Eghtesadi and Leventhall, 1982; Eghtesadi et al, 1985, 1986), some work has been directed at finite size rectangular sources mounted in the wall of the duct (Berengier and Roure, 1980, 1980a; Hong et al, 1987; Curtis et al, 1987; Sha and Tian, 1987; Tichy et al, 1984). Point source modelling is not sufficiently rigorous, and finite size source modelling is essential if theoretical analyses are to be useful in predicting the performance of practical active control systems.

Recently it has been suggested that the secondary source may have an effect on the primary source power output (Ffowcs-Williams, 1984; Ffowcs-Williams et al, 1985; Roebuck, 1990). Papers (Nelson and Elliott, 1987; Curtis et al, 1987) have appeared in which it is suggested that the secondary source(s) can unload the primary source by changing its radiation impedance, thus reducing its overall sound power output; and analytical models have begun to appear which

consider both primary and secondary sources and how each reacts in the presence of the other's sound field (Sha and Tian, 1987; Elliott and Nelson, 1986). These models, however, are developed for source configurations that are seldom found in practice, and the results can be misleading if attempts are made to extrapolate to more realistic configurations. The problem is that the primary source is modelled as radiating from the plane of the duct wall and having a finite length along the duct axis, whereas most practical primary noise sources are in the plane of the duct cross section. Modelling the primary source as extending in the plane of the duct wall results in waves incident from the secondary source(s) having a phase variation across the primary source face, leading to different results and conclusions from the configuration of the primary source in the plane of the duct cross section, in which case there is no phase variation across the primary source face. It should be noted that modelling the primary source in the plane of the duct cross section and analysing the interaction between primary and secondary source(s) is *not* equivalent to assuming a downstream propagating plane wave and analysing the interaction between this plane wave and the secondary source(s), as is done by many previous investigators.

A second major drawback of the existing models is that no one has been successful in quantitatively measuring simultaneously both primary and secondary source acoustic power flows or impedances, and thus the models remain unverified experimentally. Attempts have been made to measure changes in the electrical power flow to the sources but the results are inconclusive (Sha and Tian, 1987). The problem with measuring electrical power flow to determine changes in acoustic power flow is the low acoustical efficiency of speaker sound sources; thus extremely accurate electrical current and voltage to current phase measurements are needed to determine acoustic power flows with even just moderate accuracy.

Finally, if the physical mechanism of active noise control is related to sound source interaction, it can be surmised that the placement of the control source with respect to the primary source will have an influence upon the attenuation achieved. Although, as mentioned previously, a great deal of early research was directed towards examining the effect of geometric variations amongst multiple control sources, the effect of placement of a single control source with respect to the primary source has not been adequately investigated. This, and the preceding problems of adequate modelling and experimental verification for controlling plane wave sound propagation in ducts, will be the topic of chapter 2 in this thesis.

In parallel to the research directed towards controlling plane wave sound propagation in ducts, a body of research was being undertaken towards actively attenuating sound radiation from transformer tanks using acoustic control sources (Kido, 1975; Kempton, 1976; Hesselman, 1978; Angevine, 1978; Ross, 1982; Berge et al, 1987). As with the control of plane wave sound propagation in ducts, the popularity of this research topic was partially a result of the potential commercial applications of such a system. Also, as the noise originating from a transformer is deterministic, and very stable, the electronic control system design could be greatly simplified. Despite the considerable effort directed towards this problem, the majority of the results were not sufficiently satisfactory to warrant serious commercial consideration, and no such systems are currently available.

The problems arising in this free space radiation problem would appear to stem from an incomplete understanding of the physical control mechanisms at work, and the effect which structural / acoustic and geometric system parameters have upon them. Therefore, a greater

component of recent research has been directed towards idealized systems to enhance the knowledge in this area. Early work in this vane included an examination of the control of free field sound radiation from monopole acoustic sources (Nelson and Elliott, 1986; Nelson et al, 1987), followed by a progression to the control of sound radiation from a baffled, rectangular panel using acoustic control sources (Deffayet and Nelson, 1988). This latter work, however, was limited to cases where the wavelength of the sound was much larger than the size of the radiating structure. Further, there was no consideration of the implications of the fact that a practical active noise control system minimizes sound pressure at discrete locations, rather than the total radiated sound power (as would be ideal). These points will be discussed in chapter 4.

More recently, the possibility of using vibration control sources to minimize sound radiation from a vibrating structure has been investigated (Fuller and Jones, 1987; Fuller, 1988, 1990; Thomas et al, 1990, Meirovich and Thangjitham, 1990). This would appear to have advantages over the use of acoustic control sources in terms of system compactness, especially if low cost, lightweight piezoelectric ceramic actuators are used (Dimitriadis and Fuller, 1989). However, work in this field has thus far been restricted to the development of specific analytical models to predict the effect which applying vibration control has upon the structural / acoustic system under certain conditions. Some fundamental investigation of the physical mechanisms is still required (Thomas et al, 1990). Also, the effect which structural / acoustic and geometric system parameters, such as control source and error sensor number and location, damping, modal density, and structure size, have upon both the mechanisms of control and the levels of achievable sound attenuation in each case have not been investigated adequately. It is plausible that these effects will be different here, for sound radiation control, than for the related field of

active control of vibratory power flow (Meirovitch and Bennighof, 1986; Mace, 1987), but more investigation is required. This will be undertaken in chapter 4.

In the last decade, research into the use of active methods to control structural sound radiation has been extended from free space problems to the control of sound transmission into weakly coupled enclosures. This has been spurred on largely by the desire to use new, fuel efficient turboprop engines on aircraft (Magliozzi, 1984), which will require some form of lightweight, low frequency noise control. Also, there has been interest from the automotive manufacturers in developing a similar system to control interior noise levels in cars.

There was some early flight testing conducted to determine the feasibility of the application of active control to reduce aircraft interior noise (Zalas and Tichy, 1984); however, the general research path seems to have been a progression from the active control of sound transmission into enclosure models of simple geometry through to more realistic, complex systems. The initial work was directed at using acoustic sources to control deterministic sound fields in simple rectangular (Nelson et al, 1987a; Bullmore et al, 1987; Elliott et al, 1987; Tohyama and Suzuki, 1987; Doelman, 1989) and cylindrical (Bullmore et al, 1986; Lester and Fuller, 1986; Silcox et al, 1987; Abler and Silcox, 1987; Lester and Fuller, 1987; Silcox et al, 1987a; Silcox and Lester, 1988; Silcox et al, 1989; Bullmore et al, 1990) enclosures. In much of this work, quadratic optimization theory was used to determine the optimal control source volume velocities which would provide the maximum levels of acoustic potential energy attenuation possible for a given control source arrangement (Nelson et al, 1985). This has since been extended to incorporate the use of boundary element methods in more complex structural / acoustic systems (Mollo and Bernhard, 1987). Also, the deterministic sound field assumption

has been relaxed to examine the ability of active systems to control random incidence sound fields (Joseph et al, 1989; Nelson et al, 1990; Joplin and Nelson, 1990).

This line of research has lead to some recent flight tests (Elliott et al, 1989; Dorling et al, 1989; Elliott et al, 1990) and automobile trials (Berge, 1983; Nadim and Smith, 1983;). However, it is apparent that the control source and error sensor arrangement has a significant influence upon the overall levels of sound attenuation obtained (Fuller and Jones, 1987a; Silcox et al, 1987a; Pan and Hansen, 1990a; Elliott et al, 1990), and more work is required to develop a practical means of optimizing the locations of these physical control system components. An analytical approach is developed in chapter 3 directed towards helping to overcome this problem.

More recently, the use of vibration sources to control structural sound transmission has been investigated. These have been applied initially to the control of sound transmission into both rectangular (Pan et al, 1990) and circular (Fuller and Jones, 1987; Jones and Fuller, 1987; Mandic and Jones, 1989) enclosures, for which the modal coupling characteristics are very different. Whilst this technique shows great promise, especially when piezoelectric ceramic actuators are used, it is apparent that the ability of the system to achieve substantial levels of sound control is dependent upon the modal coupling characteristics of the structural / acoustic system, and the energy distribution in this system, and more work is required to quantify this. The analytical models developed in chapter 3, and verified in chapter 5, of this thesis are suitable as tools for such an examination; however, no such examination will be undertaken in this thesis work.

CHAPTER 2:

THE ACTIVE CONTROL OF PLANE WAVE SOUND PROPAGATION IN AIR HANDLING DUCTS

2.1 INTRODUCTION

As outlined in the introduction chapter 1, the active control of plane wave sound propagation in air handling ducts has been the subject of considerable research in recent years. Despite this, no analytical model has so far been developed which adequately describes the acoustic mechanisms involved, and which allows the power flows associated with both primary and control sources to be calculated for any control source arrangement, strength and phase difference. Also, as stated in the introduction, no one has yet been successful in quantitatively measuring simultaneously both primary and control source acoustic power flows or impedances, and thus the models previously developed remain largely unverified experimentally. Attempts have been made to measure changes in electrical power flow to the sources but the results are inconclusive (Sha and Tian, 1987). The problem with measuring electrical power flow to determine changes in acoustic power flow is the low acoustical efficiency of speaker sound sources; thus extremely accurate electrical current and voltage to current phase measurements are needed to determine acoustic power flows with even just moderate accuracy.

The purpose of the work presented in this chapter is two-fold; firstly, to analytically and experimentally demonstrate the physical mechanism of active noise control when using an acoustic control source, and secondly to analytically examine the effect which varying physical system parameters such as control source location have upon the performance of systems actively controlling plane wave sound propagation in air handling ducts. To do this, analytical models are first developed which describe the effect of applying this form of active noise control in terms of the acoustic power flows from both the primary and control sources. Following the development of these models, a novel means of measuring the acoustic power flow from all sources (primary and control) is used to provide experimental verification. The models are then utilized to examine the previously mentioned physical system variable effects.

2.2. MODEL OF SINGLE SOURCE ACTIVE NOISE CONTROL IN A DUCT: SINGLE CONTROL SOURCE

In the following analysis, it will be assumed that the frequency range of interest is below the duct cutoff frequency, so that only plane waves can propagate down the duct. Also, to develop the model based on source acoustic power flow changes, it will be assumed that both primary and control sources are constant volume velocity sources. This assumption will be relaxed later in this chapter to examine the control of a constant pressure acoustic source. For convenience, the time dependent term $e^{i\omega t}$ will be omitted from the analysis.

It is worthwhile noting that the assumption of constant volume velocity sources is equivalent to assuming infinite impedance sources, something that is not practically possible (Mungal and Eriksson, 1988). It was found that for the speaker source and frequency used in the experiments described later in this article the assumption of infinite impedance was sufficiently accurate. However, aerodynamic sources and low frequency speaker sources may be better modelled as constant pressure sources, and the theoretical model will be modified later in the chapter to consider the effect of constant pressure sources on the active control problem.

The acoustic power radiated (into the duct) by each source is determined by calculating the product of the volume velocity amplitude Q and complex conjugate of the acoustic pressure amplitude P^* at the surface of the source:

$$W = \frac{1}{2}QP^* \tag{2.1}$$

The real, or active, part of this product will determine the real, or active, acoustic power output of the source. This is the part of the acoustic power which propagates away from the source, and travels down the duct. (It should be noted that in an active control system the real acoustic power can be positive or negative, corresponding to power flow or absorption, respectively). The imaginary or reactive sound power associated with equation (2.1) is stored in the near field (in evanescent modes) and does not propagate down the duct.

The case of interest here, where there is only one control source (the monopole system), will be examined using the coordinate system shown in Figure 2.1. The primary source occupies the entire cross sectional area of the duct at one end (z=0), and the duct is assumed to be infinitely extending in the positive z-direction. This is achieved approximately in practice by using an anechoic termination wedge. (Note that the same result would be achieved if the primary source only occupied part of the cross-sectional area and the remainder was baffled).

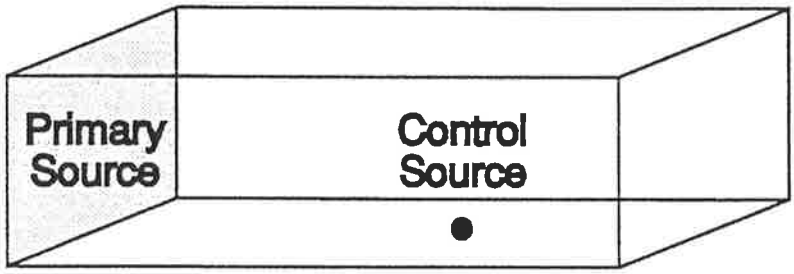

2.1 Standard monopole system arrangement.

In order to calculate the acoustic power output of the primary and control sources, both operating alone and together, it is necessary to first derive expressions for the acoustic pressure field generated by these two sources. Consider first the primary source sound pressure field. The sound pressure produced by the primary source operating alone (with no other sources active), at a frequency ω, can be calculated using the Green's function, G, for an infinite duct (Morse and Ingard, 1968):

$$G(\vec{x},\vec{x}_o,\omega) = \sum_n \frac{\Psi_n(\vec{x})\,\Psi_n(\vec{x}_o)}{\Lambda_n\sqrt{\kappa_n^2-k^2}}\, e^{-ik_n|z-z_o|} \tag{2.2}$$

Here, $\vec{x}$ is the location of some point in the duct whose coordinates are (x,y,z), $\vec{x}_0$ is the location of a point on the surface of the acoustic source whose coordinates are (x_o,y_o,z_o), S is the cross-sectional area of the duct, k is the acoustic wave number, κ_n is the eigenvalue of the n^{th} mode, Ψ_n is the n^{th} duct mode shape function, and Λ_n is the n^{th} mode normalization term, defined as twice the integral of Ψ_n^2 over the duct cross-section

$$\Lambda_n = \int_S \Psi_n^2(\vec{x})\, d\vec{x} \tag{2.3}$$

As only the plane wave mode will be considered here, this can be simplified to

$$G(z,z_o,\omega) = -\frac{i}{Sk_o} e^{-ik_o|z-z_o|} \tag{2.4}$$

where k_0 is the free space acoustic wave number, ω/c_0, and c_0 is the speed of sound in free space.

This simplified Green's function can be used to find the pressure, p(z), at the axial location z in the duct (Fahy, 1985):

$$p(z) = i\rho c_o k_o \int_S q_p(\vec{x}_o) G(\vec{x},\vec{x}_o,\omega)\, d\vec{x}_o \tag{2.5}$$

where q_p is the complex particle velocity amplitude at a position $(\vec{x}_o)=(x_0,y_0,z_0)$ on the face of the primary source.

Substituting equation (2.4) into equation (2.5), and writing the result in terms of primary source volume velocity amplitude, Q_p, produces the expression for the primary source generated sound field

$$p_p(z) = \frac{\rho c_o}{S} Q_p e^{-ik_o|z-z_0|} \tag{2.6}$$

Now consider the sound pressure field generated by the control source, in particular in the region between the control source and the primary source, located at the terminated end, distance d away. Referring to figure 2.2, the total sound pressure at some position z in this region is the sum of a positive (downstream) travelling wave of complex amplitude P_+, and a negative (upstream) travelling wave of complex amplitude P_-. With positive time dependence, this sum is

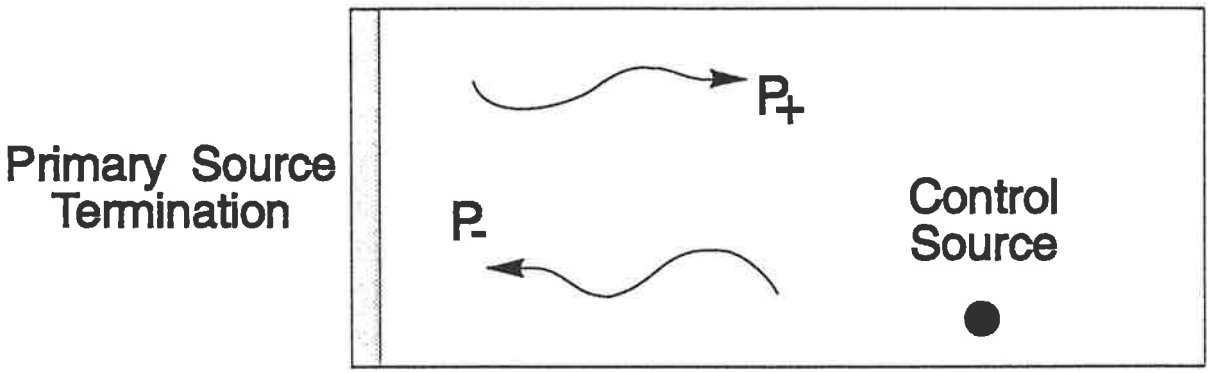

2.2 Control source sound pressure components.

$$p_c(z) = P_+ e^{-ik_o z} + P_- e^{ik_o(z-z_c)} \tag{2.7}$$

The ratio of the (complex) amplitudes of the reflected and incident waves at the origin of the duct system (the terminated primary source end) can be expressed in exponential form as (Morse and Ingard, 1968)

$$\frac{P_+}{P_- e^{-ik_0 z_c}} = e^{-2\psi} \tag{2.8}$$

where

$$\psi = \pi\alpha + i\pi\beta \tag{2.9}$$

Note that $2\pi\beta$ is the phase angle between the positive and negative travelling waves at the primary source termination, and $e^{-2\pi\alpha}$ is the scalar magnitude ratio of these waves.

Substituting equation (2.8) into equation (2.7) yields the expression for the acoustic pressure between the primary and control sources

$$\begin{aligned} p(z) &= P_{-}e^{-\psi}e^{-ik_0 z_c}(e^{-\psi}e^{-ik_o z} + e^{\psi}e^{ik_o z}) \\ &= 2P_{-}e^{-\psi}e^{-ik_0 z_c}\cosh(\psi - ik_o z) \end{aligned} \tag{2.10}$$

The variables α and β can be determined directly by measuring the standing wave in the section of the duct between the primary and control sources, in the same way that an impedance tube is used to measure the specific acoustic impedance of a sample placed at its end. The scalar magnitude of the sound pressure at any location in this region is

$$|p(z)| = \sqrt{p(z)p^{*}(z)} = 2P_{-}e^{-\pi\alpha}\sqrt{\cosh^2(\pi\alpha) - \cos^2(\pi\beta + k_0 z)} \tag{2.11}$$

This can be re-expressed as

$$|p(z)| = 2P_{-}e^{-\pi\alpha}\sqrt{\cosh^2(\pi\alpha) - \cos^2(\pi\beta')} \tag{2.12}$$

where

$$\beta' = \beta + \frac{z}{\lambda/2} \tag{2.13}$$

where λ is the wavelength of sound at the frequency of interest. From this, it can be seen that the pressure amplitude is a minimum where β' is an even multiple of ½, and is a maximum where β' is an odd multiple of ½. From equation (2.13) it is apparent that the distance between successive points of minimum or maximum sound pressure is ½ wavelength, and that the distance between the first acoustic pressure minimum and the terminated end, divided by ½ wavelength, is equal to 1-β. The ratio of the sound pressure amplitudes between the minimum and maximum pressure locations in the standing wave will be equal to

$$\frac{|p(z)|_{min}}{|p(z)|_{max}} = \frac{\sqrt{\cosh^2(\pi\alpha)-1}}{\sqrt{\cosh^2(\pi\alpha)}} = \tanh(\pi\alpha) \tag{2.14}$$

Equation (2.10) describes the sound field between the control source and the end termination for an idealized point source model of the control source; that is, one which has no physical size. However, as real acoustic sources are of finite size, some modification to equation (2.10) must be made to account for this. As shown in figure 2.3, the acoustic control source can be modelled roughly as a rectangular piston of width B and axial length L, whose centerline is located a distance ($z=z_c$) from the primary source terminated end. To find the total sound pressure generated by the

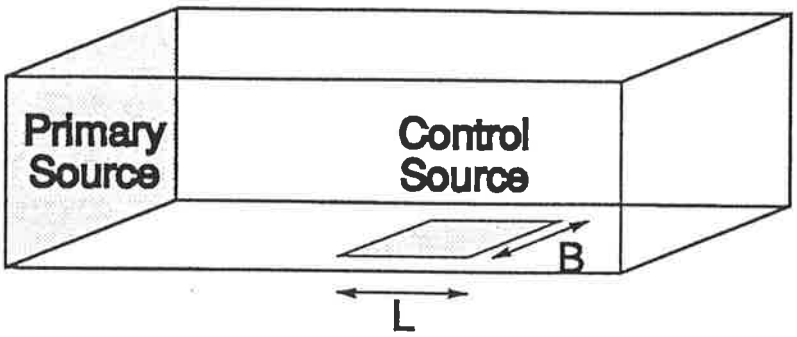

2.3 Finite size control source model.

motion of this source, it is necessary to integrate the contributions from all points on the source. To do this, equation (2.10) must first be written in terms of source volume velocity, rather than in terms of pressure. The amplitude of the acoustic pressure travelling away from the control source, P_-, will be equal to that produced by the source operating in a duct which is infinitely extending in both directions (which is equivalent to looking into an infinitely extending duct of twice the cross-sectional area). From equation (2.6),

$$P_- = Q_c \frac{\rho_o c_o}{2S} \tag{2.15}$$

Therefore, equation (2.10) can be written as

$$p(z) = Q_c \frac{\rho_o c_o}{S} e^{-\psi} e^{-ik_o z_c} \cosh(\psi + ik_o z) \tag{2.16}$$

The form of equation (2.16) is amenable to finding the pressure distribution produced by a finite size control source. Considering only the plane wave mode, and assuming that the velocity distribution across the face of the piston is uniform, the total acoustic pressure at some location z between the control source and the primary source terminated end is

$$p(z) = B \int_{z_c - L/2}^{z_c + L/2} u_c \frac{\rho_o c_o}{S} e^{-\psi} e^{-ik_o z_c} \cosh(\psi + ik_o z)\, dz \tag{2.17}$$

where u_c is the particle velocity at any point on the source, taken to be uniform.

Evaluating this integral produces the expression for the pressure distribution produced by the control source operating alone between the control source and the terminated end

$$p(z) = Q_c \frac{\rho_o c_o}{S} \gamma e^{-\psi} e^{-ik_o z_c} \cosh(\psi + ik_o z) \tag{2.18}$$

where the variable γ is defined as a control source size factor

$$\gamma = sinc\left(\frac{k_o L}{2}\right) \tag{2.19}$$

Equations (2.6) and (2.18) can be used to determine the total acoustic pressure at the surface of both the primary and control sources, thereby enabling the calculation of the (real) acoustic power output of these sources, which is to be minimized by the active noise control system. Consider first the primary source, located at a position (z=0). Evaluating equations (2.6) and (2.18) at this location shows the total acoustic pressure at the primary source to be

$$p(z=0) = Q_p \frac{\rho_o c_o}{S} + Q_c \frac{\rho_o c_o}{S} \gamma e^{-\psi} e^{-ik_o z_c} \cosh(\psi) \tag{2.20}$$

Thus, the acoustic power output of the primary source under the influence of the sound pressure field produced by the control source is

$$W_p = \frac{1}{2} Re\left\{ Q_p \left(Q_p \frac{\rho_o c_o}{S} + Q_c \frac{\rho_o c_o}{S} \gamma e^{-\psi} e^{-ik_o z_c} \cosh(\psi) \right)^* \right\} \tag{2.21}$$

Now consider the acoustic power output of the control source. The sound pressure at any point (z_s) on the finite size source can again be calculated by evaluating equations (2.6) and (2.18) at this location (note that this is equivalent to integrating the local acoustic intensity over the surface of the control source as the volume velocity is assumed contant over the face of the rectangular piston). The total acoustic pressure must then be found by integrating over the surface of the source. Thus, the total acoustic pressure "seen" by the control source is

$$p(z=z_c) = B\int_{z_c-L/2}^{z_c+L/2} Q_p\frac{\rho_o c_o}{S}e^{-ik_o z_s} + Q_c\frac{\rho_o c_o}{S}\gamma e^{-\psi}e^{-ik_o z_c}\cosh(\psi+ik_o z_s)\,dz_s$$

$$= Q_p\frac{\rho_o c_o}{S}\gamma e^{-ik_o z_c} + Q_c\frac{\rho_o c_o}{S}\gamma^2 e^{-\psi}e^{-ik_o z_c}\cosh(\psi+ik_o z_c) \qquad (2.22)$$

The acoustic power output of the control source, during operation of both the control and acoustic sources, is therefore

$$W_c = \frac{1}{2}Re\left\{ Q_c\left(Q_p\frac{\rho_o c_o}{S}\gamma e^{-ik_o z_c} + Q_c\frac{\rho_o c_o}{S}\gamma^2 e^{-\psi}e^{-ik_o z_c}\cosh(\psi+ik_o z_c)\right)^* \right\} \qquad (2.23)$$

The total acoustic power output of the system is given by the sum of equations (2.21) and (2.23). This sum can be used to determine the optimum control source volume velocity, which is that volume velocity will minimize the acoustic power output of the total (primary and control) acoustic system, as will be outlined in the following sections.

2.2.1 Solution for the optimum control source volume velocity - Idealized rigid termination

Consider firstly the idealized case of the duct termination at the primary source end being perfectly rigid. With this assumption, $\alpha=0$ and $\beta=0.5$. Substituting these values into equation (2.21), the primary source power output for this idealized case is

$$W_p = \frac{1}{2}|Q_p|^2\frac{\rho_o c_o}{S} + \frac{1}{2}\frac{\rho_o c_o}{S}\gamma\ Re\{Q_p(Q_c e^{-ik_o z_c})^*\} \tag{2.24}$$

For the control source, the acoustic power output is

$$W_c = \frac{1}{2}|Q_c|^2\frac{\rho_o c_o}{S}\gamma^2\cos^2(k_o z_c) + \frac{1}{2}\frac{\rho_o c_o}{S}\gamma\ Re\{Q_c(Q_p e^{-ik_o z_c})^*\} \tag{2.25}$$

Noting that $Q_p Q_c^*$ in equation (2.24) is the complex conjugate of $Q_c Q_p^*$ in equation (2.25), the total (real) acoustic power output of the active controlled system can be expressed as a quadratic fuction of complex control source volume velocity amplitude,

$$W_{tot} = Q_c^* a Q_c + Q_c^* b + b^* Q_c + c \tag{2.26}$$

where

$$a = \frac{1}{2}\frac{\rho_o c_o}{S}\gamma^2\cos^2(k_o z_c) \tag{2.27}$$

$$b = \frac{1}{2}\frac{\rho_o c_o}{S}\gamma Q_p\cos(k_o z_c) \tag{2.28}$$

$$c = \frac{1}{2}\frac{\rho_o c_o}{S}|Q_p|^2 \tag{2.29}$$

This equation is identical in form to that describing the control of two free field monopole sources, investigated by Nelson et al (1987). The optimum control source volume velocity is found by differentiating the equation with respect to this quantity, and setting the gradient equal to zero. Doing this, the optimum control source volume velocity is found to be

$$Q_{c,opt} = -a^{-1}b \tag{2.30}$$

2.2.2. Solution for the optimum control source volume velocity - Generic termination

Consider now the case of some generic primary source termination described by α and β. For this more general case, the total acoustic power output of the controlled system can again be written as a quadratic function of control source volume velocity

$$W_{tot} = Q_c^* Re\{a\} Q_c + Re\{b_1 Q_c\} + Re\{b_2 Q_c^*\} + c \tag{2.31}$$

where

$$a = \frac{1}{2}\frac{\rho_o c_o}{S}\gamma^2\left(e^{-\psi}e^{-ik_o z_c}\cosh(\psi+ik_o z_c)\right)^* \tag{2.32}$$

$$b_1 = \frac{1}{2}\frac{\rho_o c_o}{S}\gamma\left(Q_p e^{-ik_o z_c}\right)^* \tag{2.33}$$

$$b_2 = \frac{1}{2}\frac{\rho_o c_o}{S}\gamma Q_p\left(e^{-\psi}e^{-ik_o z_c}\cosh(\psi)\right)^* \tag{2.34}$$

$$c = \frac{1}{2}\frac{\rho_o c_o}{S}|Q_p|^2 \tag{2.35}$$

Note here that this is a "non-symmetric" equation, as b_1 and b_2 are not complex conjugates, as opposed to the "symmetric" equation (2.26). The implications of this will be discussed later in this chapter.

The optimum control source volume velocity can again be determined by differentiating the real part of equation (2.31) with respect to this quantity, and setting the gradient equal to zero. This produces

$$Q_{c,opt} = -\frac{1}{2}Re\{a\}^{-1}(b_1^* + b_2) \tag{2.36}$$

2.3. EXPERIMENTAL VERIFICATION OF MODEL

2.3.1. Experimental procedure

Experimental work was undertaken to verify the active noise control model developed in the previous section. The work was conducted in a duct 215 mm x 215 mm square in cross section, terminated anechoically at one end and closed at the other end by the

primary source (a 200 mm diameter circular speaker) mounted in the plane of the duct cross section. The anechoic wedge was 1.2 meters long, constructed of rockwool, and was found to produce a standing wave ratio for primary excitation of less than 0.5 dB. The control source was located in one of the duct walls with its centre 1.25m from the primary source. The control source was a 100 mm diameter circular speaker, which was approximated in the theoretical analysis as a square speaker of equal area (89mm x 89 mm).

To verify the previously described model of active noise control in a duct, it was necessary to measure both the net power flow down the anechoically terminated duct and the contributions from each source.

The acoustic power flow propagating down the duct was calculated by measuring the standing wave downstream of the sources:

$$W_{tot} = \frac{S}{\rho_o c_o} p_{\min} p_{\max} \tag{2.37}$$

Note that if the duct is anechoically terminated, then downstream from the control source there should not be a standing wave, so that $p_{min} = p_{max}$.

Measuring the power contributions from each source required a more sophisticated approach. Attempting to measure (the changes in) acoustic power radiation by measuring the electrical power supplied to the source is extremely difficult, as the electrical power (in watts) is several orders of magnitude larger than the acoustical power (in microwatts). What is required is a means of directly measuring the active

acoustic power output, which is equal to the product of the cone volume velocity and the in-phase part of the acoustic pressure adjacent to the cone. The acoustic pressure in the duct adjacent to the cone was measured by using a suitably located microphone. The volume velocity of the speaker cone was determined by enclosing the back of the speaker in a small box, measuring the pressure p_i in the box, and using the following expression for the acoustic impedance of a small volume (Bies and Hansen, 1988):

$$Z_v = \frac{p_i}{Q} = -i\frac{\rho_o c_o^2}{V\omega} \tag{2.38}$$

where p_i is the acoustic pressure measured inside the box, V is the volume of the box, and ω is the angular frequency. The phase between the cone volume velocity and the acoustic pressure in the duct at the cone face is 270 degrees greater than the measured phase between the acoustic pressure in the speaker box and the acoustic pressure in the duct (as there is a 90 degree phase difference between acoustic pressure and acoustic volume velocity in the box, and a 180 degree phase difference between the acoustic volume velocity on the top and bottom of the speaker cone).

Accurate measurement of the phase difference between the acoustic volume velocity and pressure at the speaker cone face is essential when measuring acoustic power output. In practice it was found that the phase was uniform throughout the small enclosure. However, phase varied quite dramatically as the microphone was moved away from the front of the speaker cone. It is crucial that the microphone be positioned as close to the cone as possible for accurate measurements. Also, pressure varied across the face of the speaker, even at frequencies whose wavelengths were

much greater than the speaker diameter. Figures 2.4 and 2.5 show the amplitude and phase variation across one diameter of the primary source (200mm speaker) mounted externally to the duct. Figures 2.6 and 2.7 show the same plots for the control source. In viewing these it can be seen that there is a significant phase and amplitude variation across the speakers, especially near the edges. This is not surprising, as the cone radius is actually approximately 10mm shorter than the overall speaker radius, with the outer 10mm being a flexible rubber strip. In the center region, however, the phase and amplitude are reasonably constant.

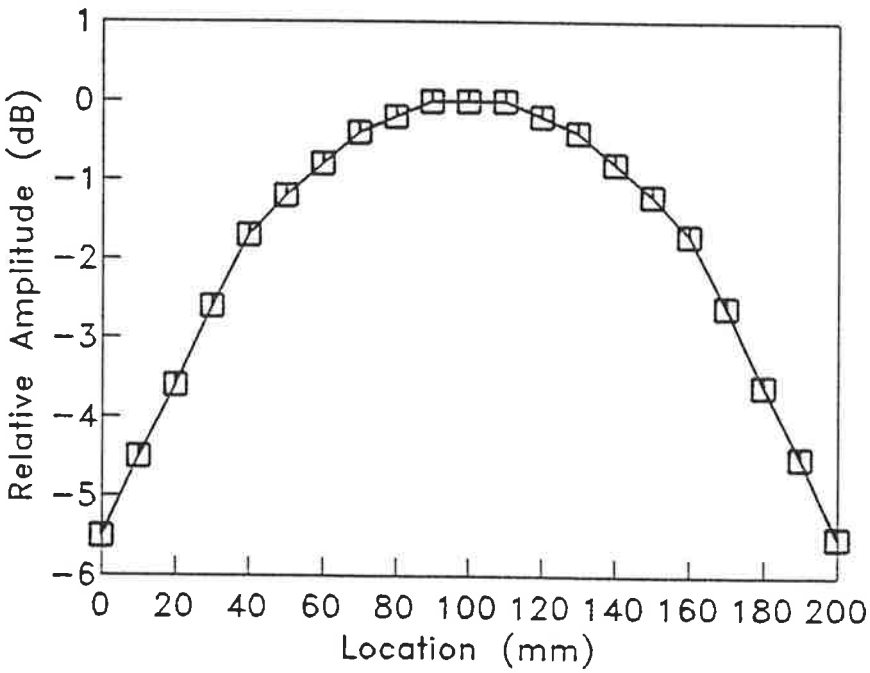

2.4 Sound pressure amplitude variation across the face of the primary source.

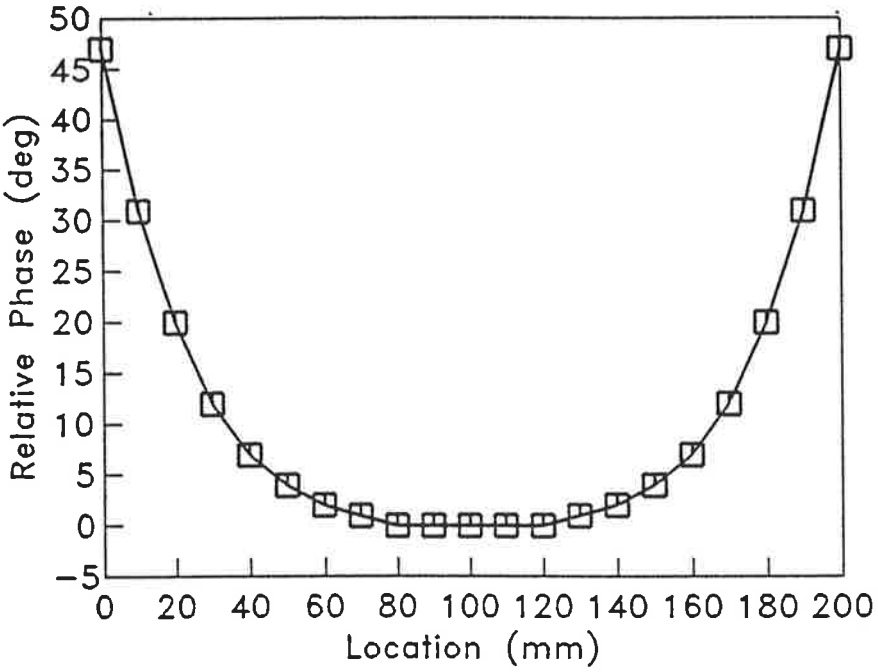

2.5 Sound pressure phase variation across the face of the primary source.

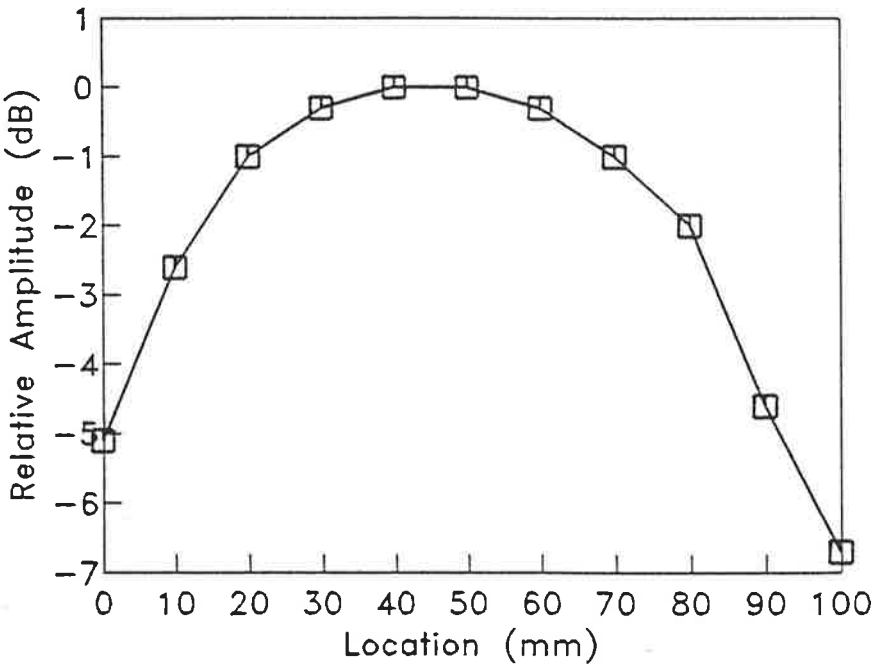

2.6 Sound pressure amplitude variation across the face of the control source.

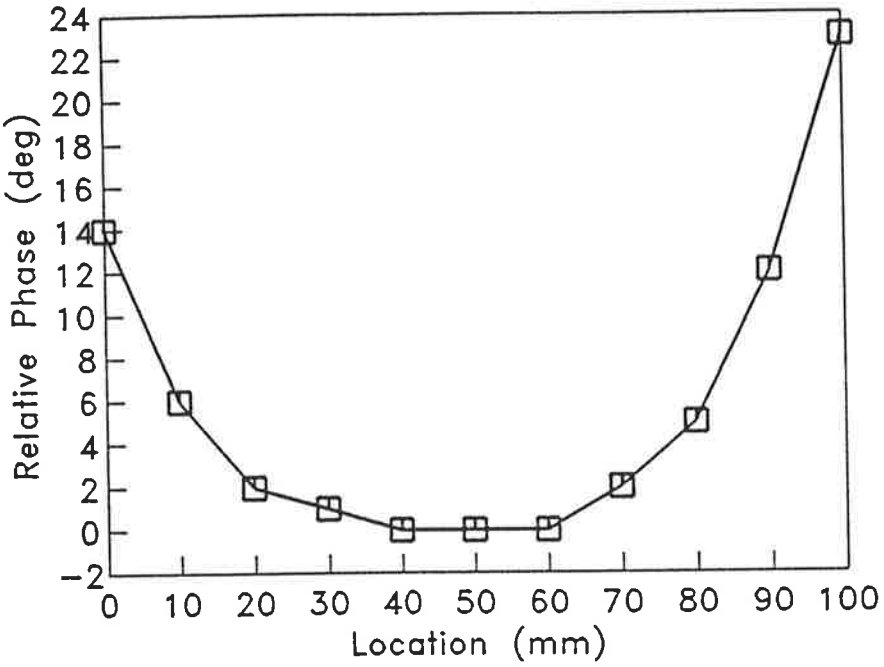

2.7 Sound pressure phase variation across the face of the control source.

The microphone was positioned near the centre of the speaker face at a location that produced an "average" pressure magnitude for the cone area of the speaker, as determined by traversing across its face. The accuracy of the microphone position was determined by driving only one source at a time, measuring the resulting pressure distribution in the duct, and comparing the power flow determined from equation (2.45) to that determined from the measured volume velocity and acoustic pressure at the speaker cone face. (It should be noted that in the case of the primary source, only one measurement, downstream, was required while for the control source(s) measurements upstream and downstream were required to find the total power flow). This was done iteratively until the two measured acoustic powers, at the source and downstream, matched.

Two frequencies, 400 Hz and 500 Hz, were chosen for the experimental tests, as these satisfied several criteria as follows;

(i) they were below the duct plane wave cut off frequency of 800 Hz,

(ii) they were below the frequency at which the larger primary source speaker cone exhibits higher order modes (found experimentally to be above 500 Hz);

(iii) they were sufficiently high that the acoustic termination at the end of the duct performed satisfactorily;

(iv) they are center frequencies of one third octave bands which is convenient from an instrumentation viewpoint.

At both of these frequencies the values of α and β were determined by examining the standing wave in the region between the two sources, as outlined in section (2.1). It was found that these values were close to those expected for a rigid termination, typically $\alpha = 0.002$ (vs. 0.0 for a rigid termination), and $\beta = 0.48$ (vs. 0.5 for a rigid termination). This slight variation, however, was enough to alter the results from what would be expected from the idealized assumption, as will be outlined later in this chapter.

For clarity, sound power data are plotted as micro-watts rather than dB as this allows simpler representation of negative power values which correspond to energy absorption rather than radiation.

2.3.2. Results

The first variable to be examined was the effect which varying the volume velocity of the control source, for a fixed primary source volume velocity and drive source phase difference, had upon the source acoustic power flows. Figure 2.8 illustrates both the theoretical and experimental primary source acoustic power flows, plotted against the (scalar) ratio of the control source to primary source volume velocity magnitudes (the source phase difference for these points was 4.0°, measured as the phase difference between the acoustic pressure in the control source and primary source speaker enclosures). The figure shows good agreement between analytical predictions and

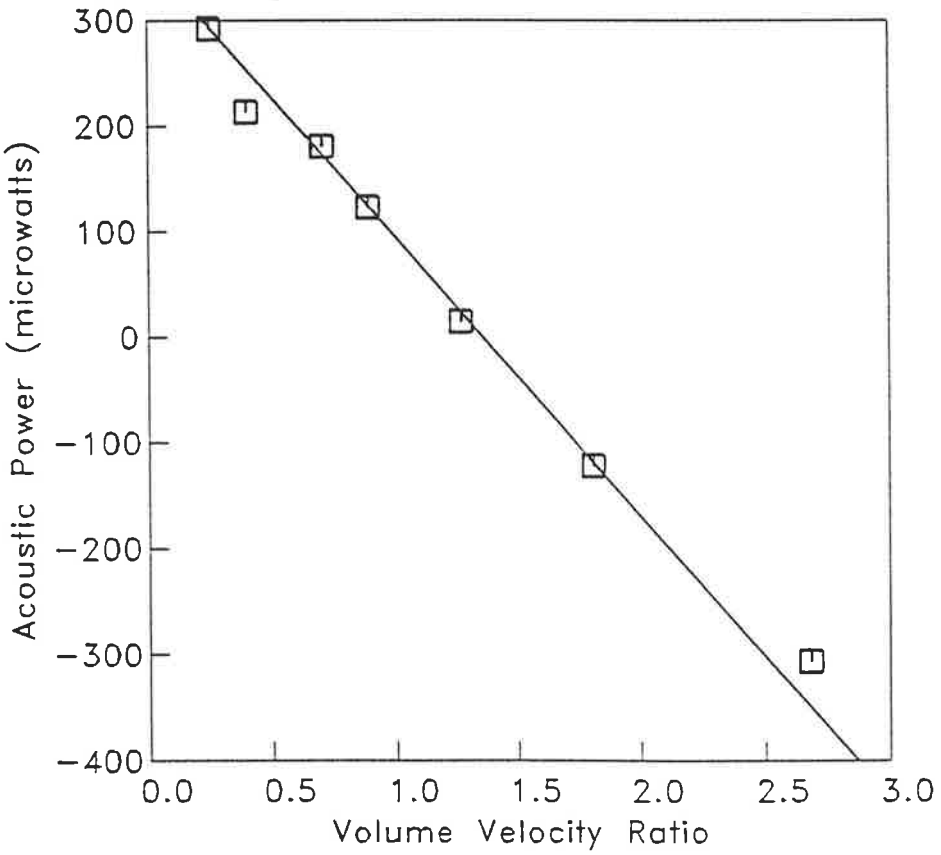

2.8 Effect of varying volume velocity ratio on primary source power output, 400 Hz. —— = theory, ⊡ = experiment.

measurement and indicates that, for this particular ambient temperature, driving signal relative phase angles, and source configuration, the primary source will begin to absorb sound power when the ratio of control source to primary source volume velocity amplitudes exceeds 1.2.

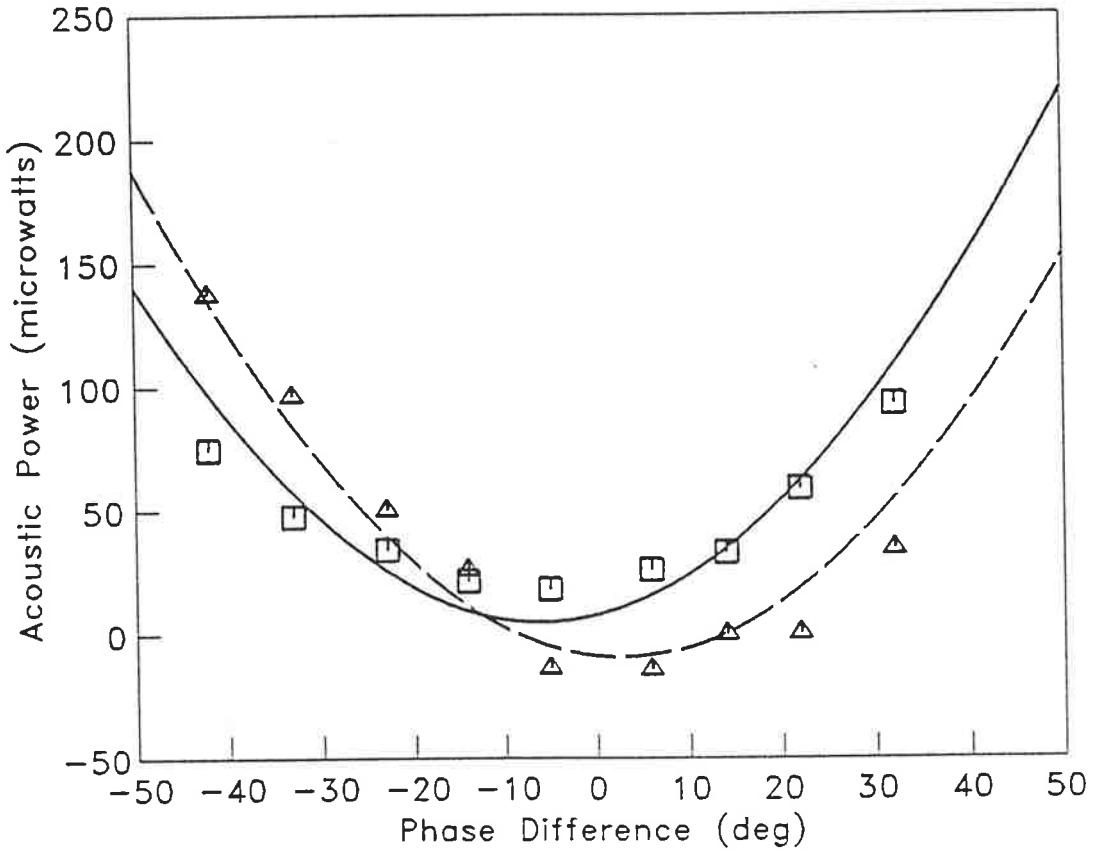

2.9 Effect of varying source driving phase difference on acoustic power output, 400 Hz. —— = primary source theory, ☐ = primary source experiment, — — = control source theory, △ = control source experiment.

In Figure 2.9 the variation in both primary source and control source acoustic power output is shown as a function of the phase difference (∠control - ∠primary) between the primary and control source driving signals (measured as the phase difference of the acoustic pressures in the speaker enclosures), for a primary source volume velocity of 200 $\mu m^3 s^{-1}$, and a control source volume velocity of 265 $\mu m^3 s^{-1}$. The total sound power radiated downstream is shown in Figure 2.10 (with only the primary source

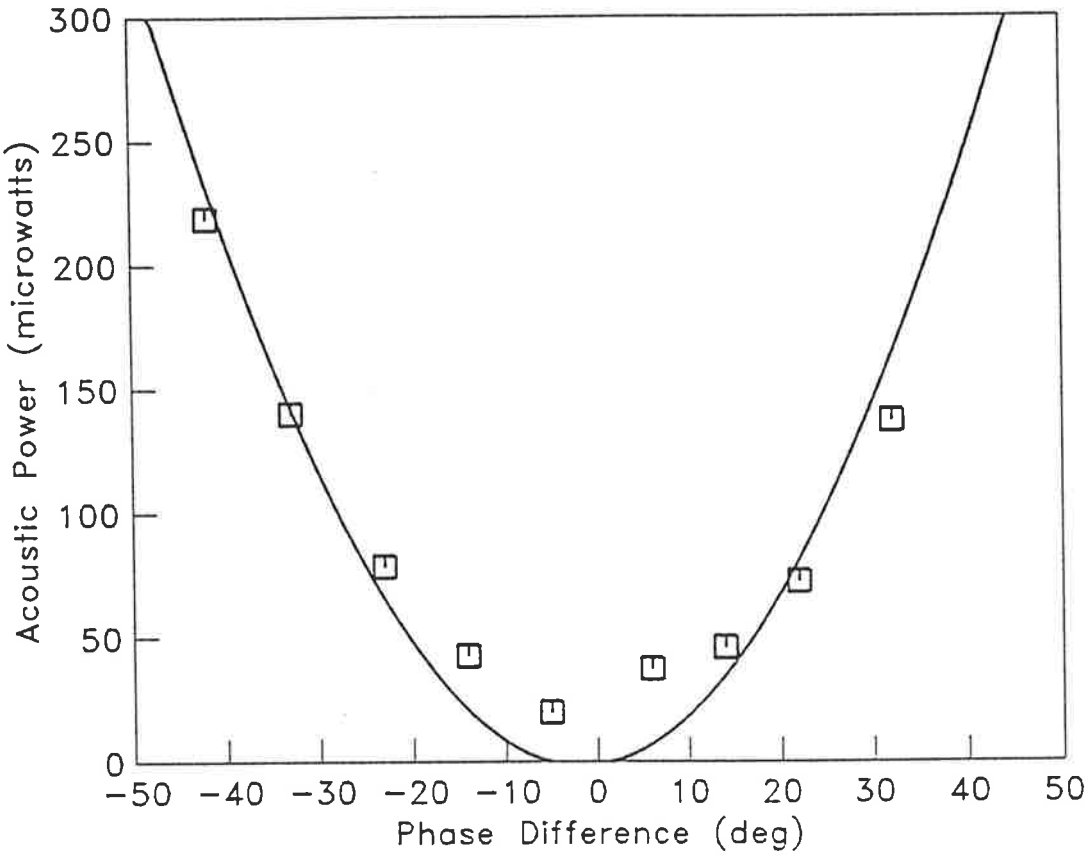

2.10 Effect of varying phase difference on total system acoustic power output, 400 Hz. —— = theory, ⊡ = experiment.

operating the sound power output was 370μW). In Figure 2.9 it can be seen that for this particular arrangement, there is no phase angle where the primary source will absorb energy; however the control source will absorb energy when the phase angle between the primary and control source driving signals is between -3 and 13 degrees. Measurements of control source power flow made at phase angles close to and within this range were subject to error because the measured phase angle between the control source volume velocity and surface acoustic pressure was in the range of 269-271 degrees, where small errors in phase angle measurement lead to large errors in power flow predictions (as the results are dependent upon the cosine of the phase angle).

Despite this, the agreement between theory and experiment is good.

These trends are also evident for the same experimental arrangement operating at 500 Hz, shown in figures 2.11 and 2.12. Here it can be seen that under optimum controlled conditions the primary source is producing a small amount of acoustic power, and the control source is absorbing it (note that the initial primary source power output was 21 μW). As with the 400 Hz case, there is good agreement between the experiment and theory.

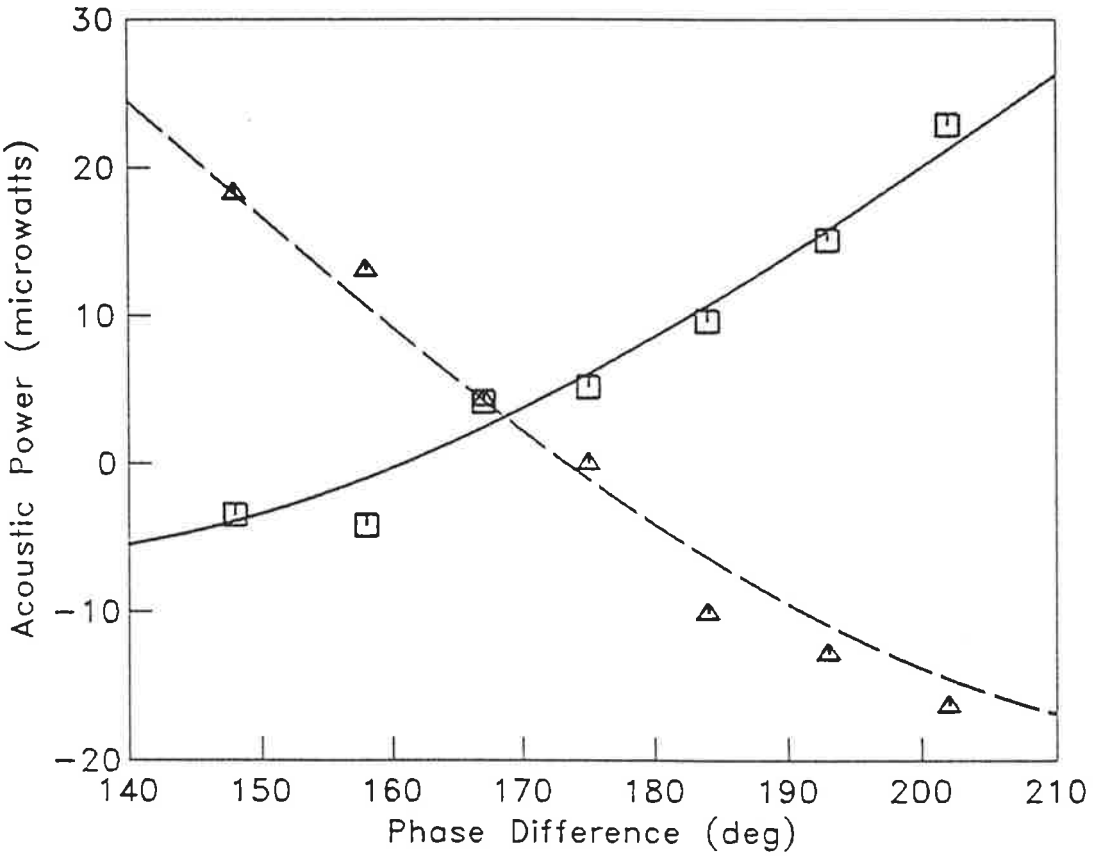

2.11 Effect of varying source driving phase difference on acoustic power output, 500 Hz. —— = primary source theory, ⊡ = primary source experiment, — — = control source theory, △ = control source experiment.

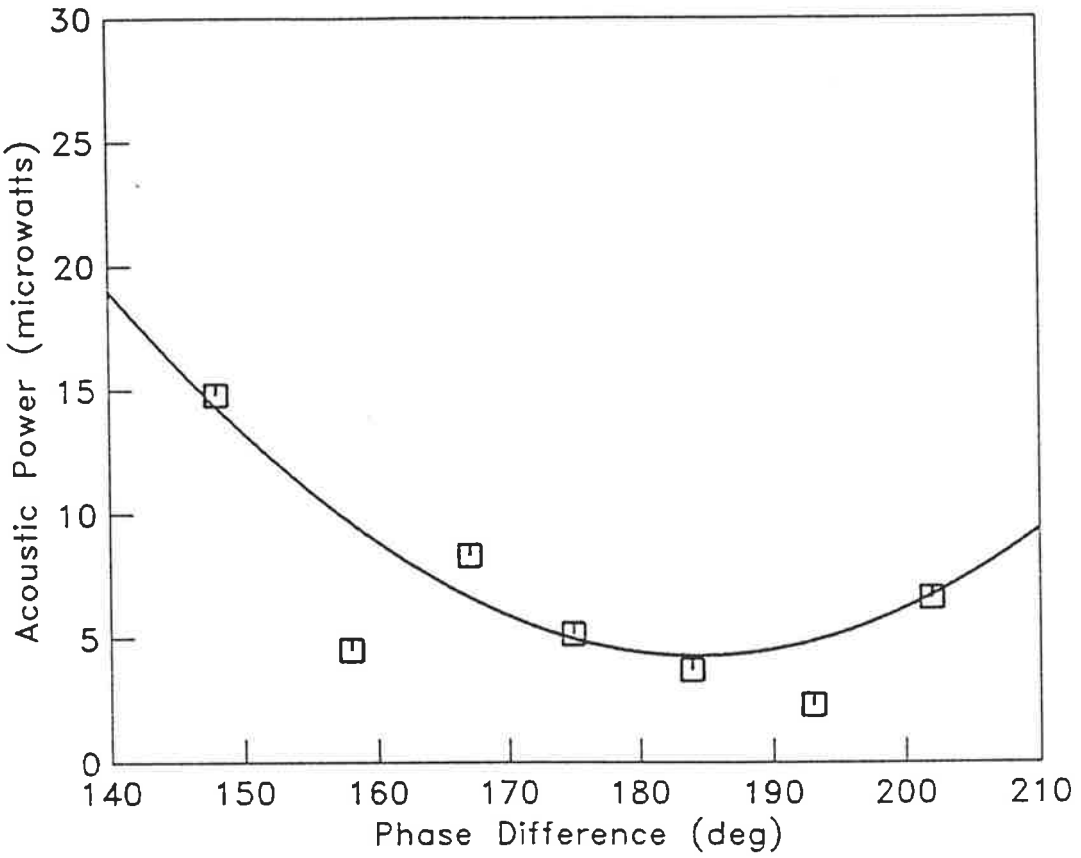

2.12 Effect of varying phase difference on total system acoustic power output, 500 Hz. —— = theory, ⊡ = experiment.

The measurements show that the active (or real) acoustic power output of the primary source is affected by operation of the control source, and that near optimum control the primary source power output is greatly reduced. Measurement of the total primary source impedance revealed little change in the magnitude of the reactive (or imaginary) component before and after operation of the control source, suggesting that the reduced active power is not re-routed into non propagating modes in the near field of the source (reactive power). Rather, it is simply not produced.

Although the primary source is unloaded by the control source, and is either producing very little (real) power or absorbing it, there is a large standing wave present between

the primary and control sources. The stored energy represented by this standing wave is a result of the finite time it takes for the unloading to occur. This duct section is acting like an "acoustic capacitance", storing that energy which is emitted during that time period.

2.4. ACTIVE CONTROL OF CONSTANT PRESSURE SOURCES

The previous sections have considered the acoustic power output of a constant volume velocity primary noise source being actively attenuated by the addition into the acoustic system of a constant volume velocity control source. This presents a good approximation of a primary noise source such as a reciprocating compressor. However, aerodynamic sources, such as a fan, are better modelled as constant pressure sources (Bies and Hansen, 1988). It will be useful here to modify the previous analysis to consider this type of primary source, and then use this to examine the differences in source acoustic power flow between the constant volume velocity and constant pressure sources under active control later in this chapter.

With a constant pressure source, the magnitude of the acoustic pressure at its face will remain constant before and after the application of active control. From equation (2.6), the initial acoustic pressure is

$$p_p(z=0) = Q_p \frac{\rho_o c_o}{S} \tag{2.39}$$

From equation (2.20), the acoustic pressure at the face of the primary source after the application of active control is

$$p(z=0) = Q_p' \frac{\rho_o c_o}{S} + Q_c \frac{\rho_o c_o}{S} \gamma e^{-\psi} e^{-ik_o z_c} \cosh(\psi) \tag{2.40}$$

where the primed primary source volume velocity under active controlled conditions, Q_p', is different than the initial primary source volume velocity operating alone, Q_p (note that the control source is still considered to be a constant volume velocity source, approximating a loudspeaker).

Equating the primary source face pressure before the application of active control, given in equation (2.39), with that after the application of active control, given in equation (2.40), enables the determination of the controlled primary source volume velocity

$$Q_p' = Q_p - Q_c \gamma e^{-\psi} e^{-ik_o z_c} \cosh(\psi) \tag{2.41}$$

Thus, the primary source acoustic power output under the action of active noise control is

$$W_p = \frac{1}{2} Re\{Q_p' P_p^*\} \tag{2.42}$$

$$= \frac{1}{2} Re\left\{ \left(Q_p - Q_c \gamma e^{-\psi} e^{-ik_o z_c} \cosh(\psi) \right) Q_p^* \frac{\rho_o c_o}{S} \right\} \tag{2.43}$$

Consider now the acoustic power output of the (constant volume velocity) control source. The pressure at the face of this source can be determined by substituting the

final primary source volume velocity into equation (2.22)

$$p(z=z_c) = Q_p' \frac{\rho_o c_o}{S} \gamma e^{-ik_o z_c} + Q_c \frac{\rho_o c_o}{S} \gamma^2 e^{-\psi} e^{-ik_o z_c} \cosh(\psi + ik_o z_c) \tag{2.44}$$

Expanding Q_p' using equation (2.41), the acoustic pressure at the face of the control source is found to be

$$p(z=z_c) = Q_p \frac{\rho_o c_o}{S} \gamma e^{-ik_o z_c} + Q_c \frac{\rho_o c_o}{S} \gamma^2 e^{-\psi} e^{-ik_o z_c} \left(\cosh(\psi + ik_o z_c) - \frac{\rho_o c_o}{S} e^{-ik_o z_c} \cosh(\psi) \right) \tag{2.45}$$

Thus, the control source acoustic power output is

$$W_c = \frac{1}{2} Re\left\{ Q_c \left(Q_p \frac{\rho_o c_o}{S} \gamma e^{-ik_o z_c} + Q_c \frac{\rho_o c_o}{S} \gamma^2 e^{-\psi} e^{-ik_o z_c} \left(\cosh(\psi + ik_o z_c) - e^{-ik_o z_c} \cosh(\psi) \right) \right)^* \right\} \tag{2.46}$$

Combining equations (2.43) and (2.45), the total system acoustic power output can be expressed as a quadratic function similar to equation (2.31),

$$W_{tot} = Q_c Re\{a\} Q_c^* + Re\{Q_c b_1\} + Re\{Q_c b_2\} + c \tag{2.47}$$

where

$$a = \left(\frac{1}{2} \frac{\rho_o c_o}{S} \gamma^2 e^{-\psi} e^{-ik_o z_c} \left(\cosh(\psi + ik_o z_c) - e^{-ik_o z_c} \cosh(\psi) \right) \right)^* \tag{2.48}$$

$$b_1 = \left(\frac{1}{2} Q_p \frac{\rho_o c_o}{S} \gamma e^{-ik_o z_c} \right)^* \tag{2.49}$$

$$b_2 = \frac{1}{2} \frac{\rho_o c_o}{S} \gamma e^{-\psi} e^{-ik_o z_c} \cosh(\psi)\ Q_p^* \tag{2.50}$$

$$c = \frac{1}{2} |Q_p|^2 \frac{\rho_o c_o}{S} \tag{2.51}$$

Differentiating equation (2.46) with respect to the control source volume velocity, and setting the gradient equal to zero, produces the optimum control source volume velocity equal to

$$Q_{c,opt} = -\frac{1}{2} Re\{a\}^{-1} (b_1^* + b_2^*) \tag{2.52}$$

2.5. ALTERNATIVE MODELLED SOURCE ARRANGEMENT

Pressure cancellation on the face of both the primary and control sources of a monopole system during active noise control has been considered by previous investigators (Elliott and Nelson, 1986, Sha and Tian, 1987). However, they have

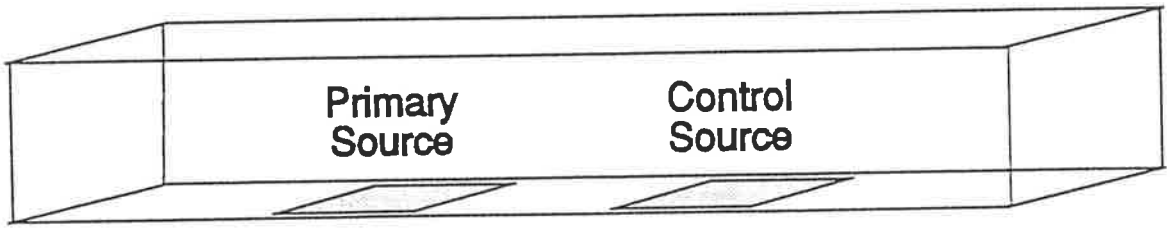

2.13 Alternative modelled source arrangement.

modelled the primary source as extending along the axis of the duct, as shown in Figure 2.13, instead of in the cross-sectional plane. With this arrangement an incident plane wave will have a phase variation across the face of both the control and primary sources. Because of this, these models will give differing indications as to the potential of an active noise control system to work in the many of practical duct sound source configurations such as compressors or fans, as these sources are almost universally mounted in the plane of the duct cross section. In the following section a model of active noise control similar to the constant volume source model of section 2.2 will be developed for this geometry. This model will be used later in this chapter to examine the differences in predicted trends.

Equation (2.6) describes the acoustic pressure field generated by the primary source mounted on the end of an infinite duct. This can be modified for the doubly infinite geometry of figure 2.13 as

$$p(z) = Q_p \frac{\rho_o c_o}{2S} e^{-ik_o z} \tag{2.53}$$

For the case considered here, the primary source now has a finite length along the duct axis. Therefore, the total acoustic pressure at any location z must be the sum of contributions integrated across the face of the source. Again, modelling the source as a rectangular piston of dimensions (B x L), assuming that the velocity distribution across the face of the source is uniform, and considering only the plane wave mode, this integral is

$$p(z) = B \int_{z_o-L/2}^{z_o+L/2} u_p \frac{\rho_o c_o}{2S} e^{-ik_o z_s} \, dz_s \tag{2.54}$$

Evaluating this produces

$$p(z) = Q_p \frac{\rho_o c_o}{2S} \gamma e^{-ik_o z_o} \tag{2.55}$$

Note that, as the primary source and control source are identically mounted, this expression can describe the sound pressure field of either the primary or control sources.

Consider now the acoustic pressure on the face of these sources operating in the presence of the other's sound field. For the primary source, the pressure is

$$p(0) = \int_{-L/2}^{L/2} Q_p \frac{\rho_o c_o}{2S} \gamma e^{-ik_o z} dz + \int_{z_c-L/2}^{z_c+L/2} Q_c \frac{\rho_o c_o}{2S} \gamma e^{-ik_o z} dz \tag{2.56}$$

$$= Q_p \frac{\rho_o c_o}{2S} \gamma^2 + Q_c \frac{\rho_o c_o}{2S} \gamma^2 e^{-ik_o z_c} \tag{2.57}$$

Thus, the acoustic power output of the primary source is

$$W_p = \frac{1}{2}Q_p\frac{\rho_o c_o}{2S}\gamma^2 Q_p^* + \frac{1}{2}Re\left\{Q_p\left(Q_c\frac{\rho_o c_o}{2S}\gamma^2 e^{-ik_o z_c}\right)^*\right\} \tag{2.58}$$

Using a similar analysis, the power output of the control source is found to be

$$W_c = \frac{1}{2}Q_c\frac{\rho_o c_o}{2S}\gamma^2 Q_c^* + \frac{1}{2}Re\left\{Q_c\left(Q_p\frac{\rho_o c_o}{2S}\gamma^2 e^{-ik_o z_c}\right)^*\right\} \tag{2.59}$$

Noting that $Q_p Q_c^*$ in equation (2.58) is the complex conjugate of $Q_p^* Q_c$ in equation (2.59), the total acoustic power flow, found by combining equations (2.58) and (2.59), can be written as a quadratic function of the control source volume velocity

$$W_{tot} = Q_c^* a Q_c + Q_c^* b + b^* Q_c + c \tag{2.60}$$

where

$$a = \frac{1}{2}\frac{\rho_o c_o}{2S}\gamma^2 \tag{2.61}$$

$$b = \frac{1}{2}Q_p\frac{\rho_o c_o}{2S}\gamma^2\cos(k_o z_c) \tag{2.62}$$

$$c = \frac{1}{2} Q_p Q_p^* \frac{\rho_o c_o}{2S} \gamma^2 \tag{2.63}$$

Differentiating equation (2.60) with respect to the control source volume velocity, and setting the gradient equal to zero, produces the optimum control source volume velocity of

$$Q_{c,opt} = -a^{-1} b = -Q_p \cos(k_o z_c) \tag{2.64}$$

It should be noted that the volume velocity of equation (2.64) is the one which will minimize the total acoustic power output of the system, propagating both upstream and downstream in the duct. It is sometimes desireable to simply stop the acoustic power flow in one direction, irrespective of what changes occur in acoustic power flow in the other direction. This is the concept employed by Trinder and Nelson (1983) in their acoustic virtual earth technique. In this, the acoustic pressure on the face of the control source was minimized, thereby stopping any acoustic power flow past the control source in the infinitely extending downstream duct section. This is equivalent to minimizing

$$p(z=z_c) = Q_p \frac{\rho_o c_o}{2S} \gamma e^{-ik_o z_c} + Q_c \frac{\rho_o c_o}{2S} \gamma \tag{2.65}$$

Here, the optimum control source volume velocity is

$$Q_{c,opt} = -Q_p e^{-ik_o z_c} \tag{2.66}$$

The difference between the total power optimum control source volume velocity, given

in equation (2.64), and the pressure optimum control source volume velocity, given in equation (2.66), is that the power optimum minimizes only the in-phase (with the source volume velocity) component of the sound pressure, whilst the other minimizes the total sound pressure. This difference has a marked effect upon the final (controlled) sound pressure distribution. Figures 2.14 and 2.15 show the final sound

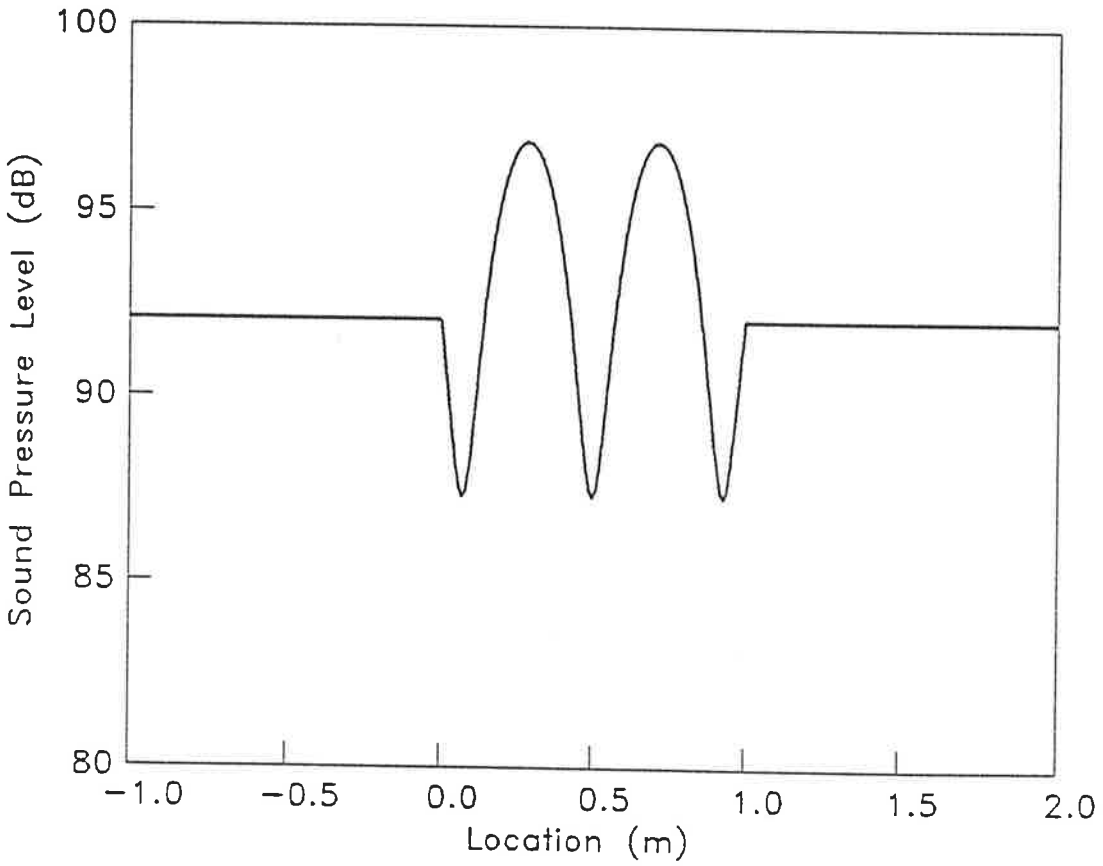

2.14 Sound pressure distribution for minimizing the total acoustic power output of the alternative modelled source arrangement, 400 Hz. The primary source is at 0.0, the control source at 1.0.

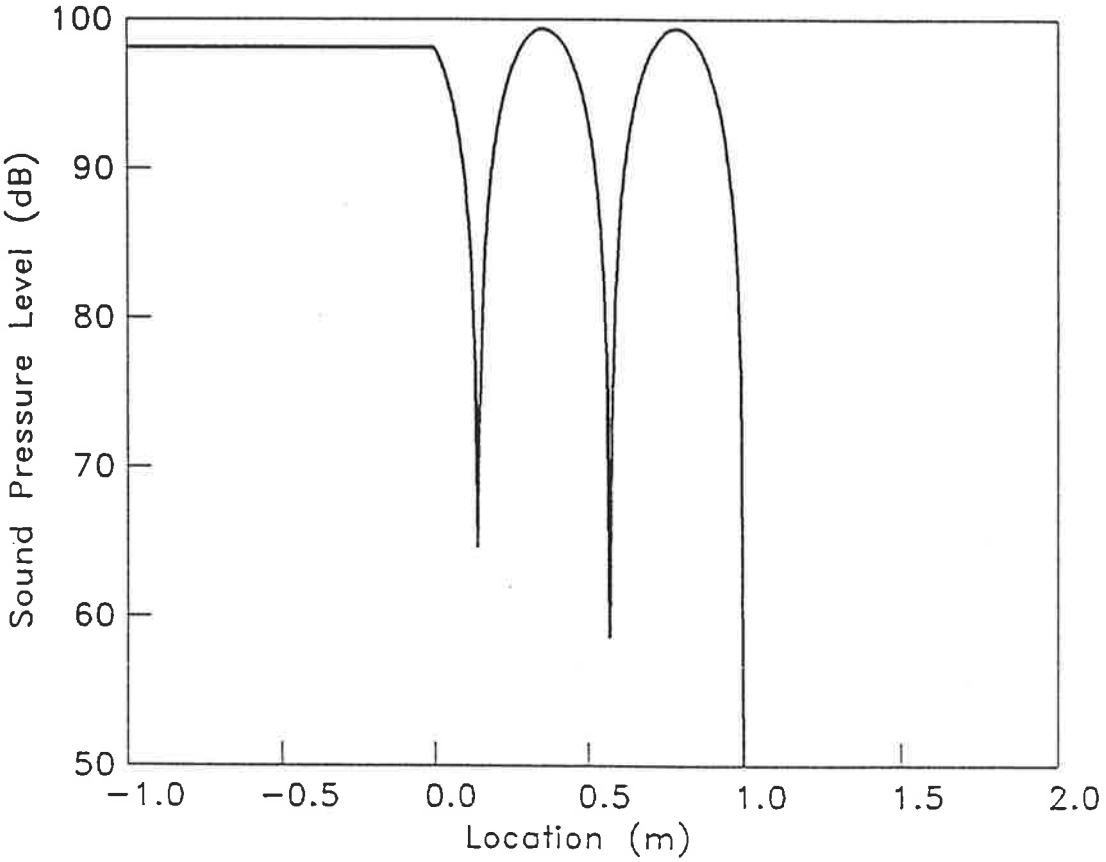

2.15 Sound pressure distribution for minimizing the downstream propagating acoustic power of the alternative modelled source arrangement, 400 Hz. The primary source is at 0.0, the control source at 1.0.

pressure distribution for two identical systems, where figure 2.14 has had the total acoustic power output minimized, and figure 2.15 has had the pressure at the control source minimized. The system shown here is operating at 400 Hz, and the sources are separated by 1 meter. Clearly, the downstream power flow of the pressure minimized case is substantially less than for the power minimized, but the upstream radiated acoustic power is increased as a result.

2.6. THE EFFECT OF PRIMARY SOURCE TYPE ON THE MECHANISMS OF ACTIVE NOISE CONTROL

Two types of primary noise source have been considered so far in this chapter; a constant volume velocity source, and a constant pressure source. It was shown experimentally in section 2.3 that, for the constant volume velocity primary source, sound power attenuation was achieved principally by an unloading mechanism, reducing the radiation impedance seen by the source. This section will examine the mechanisms at work in the control of a constant pressure source, then constrast the two arrangements. The primary source termination will be idealized here as rigid (α_t=0.0, β_t=0.5) for simplification. The section which follows this one will examine the effects of this assumption.

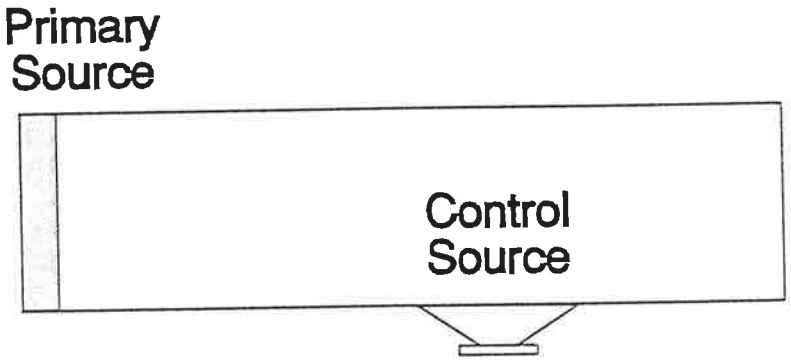

2.16 Terminated duct arrangement.

The arrangement of the system to be considered here is shown in figure 2.16. The primary source is taken to be a constant pressure source, terminating one duct end, and operating at 400 Hz. A control source, taken here to be a constant volume velocity

source, is located in the wall of the duct 1 meter downstream of the primary source. Figure 2.17 illustrates the acoustic power flow out of each source when the control source is operating at the optimum volume velocity amplitude, as the phase difference between the two sources (∠control - ∠primary) is varied. Figure 2.18 depicts the associated total system sound power attenuation in dB (note that the initial primary source acoustic power output was 371 μW). In viewing the data of figure 2.17, it is evident that the acoustic power output of the primary source is greatly reduced, in fact being equal to zero at the optimum phase difference. Thus, the mechanism here would

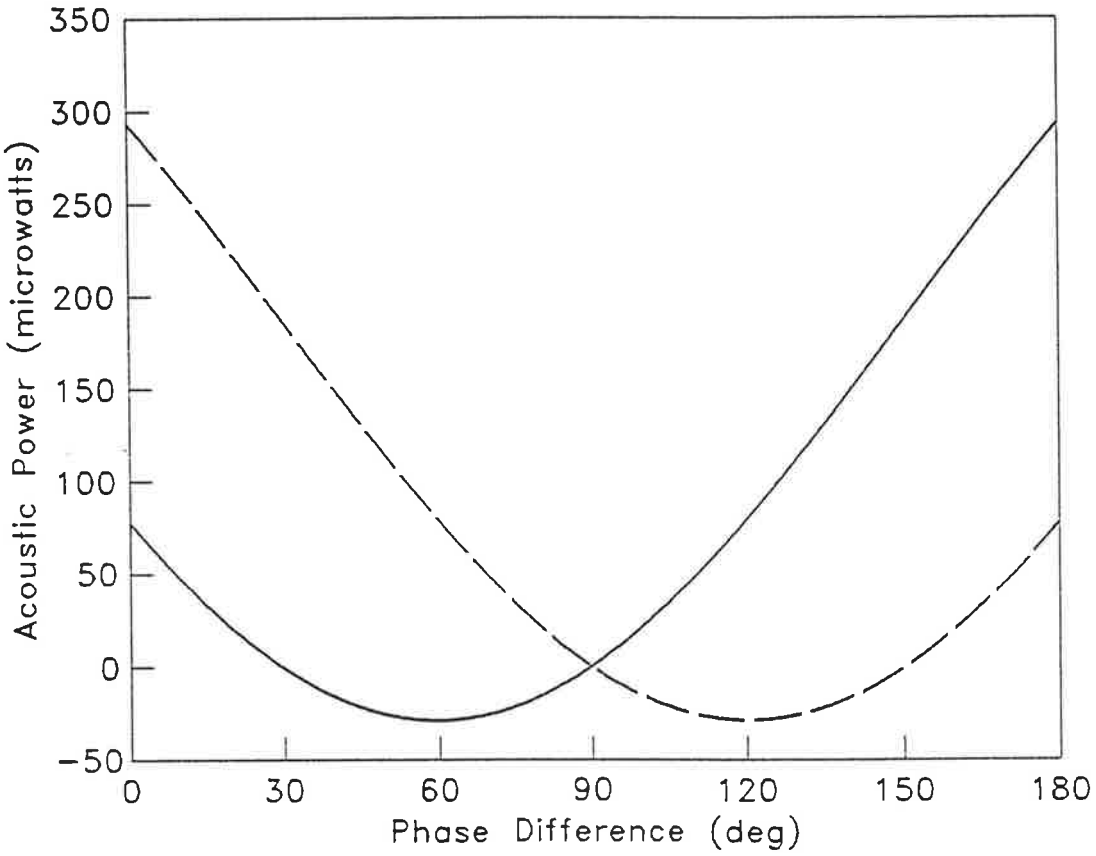

2.17 Source acoustic power output for a constant pressure primary source, 400 Hz, control source 1 meter downstream. —— = primary source, — — = control source.

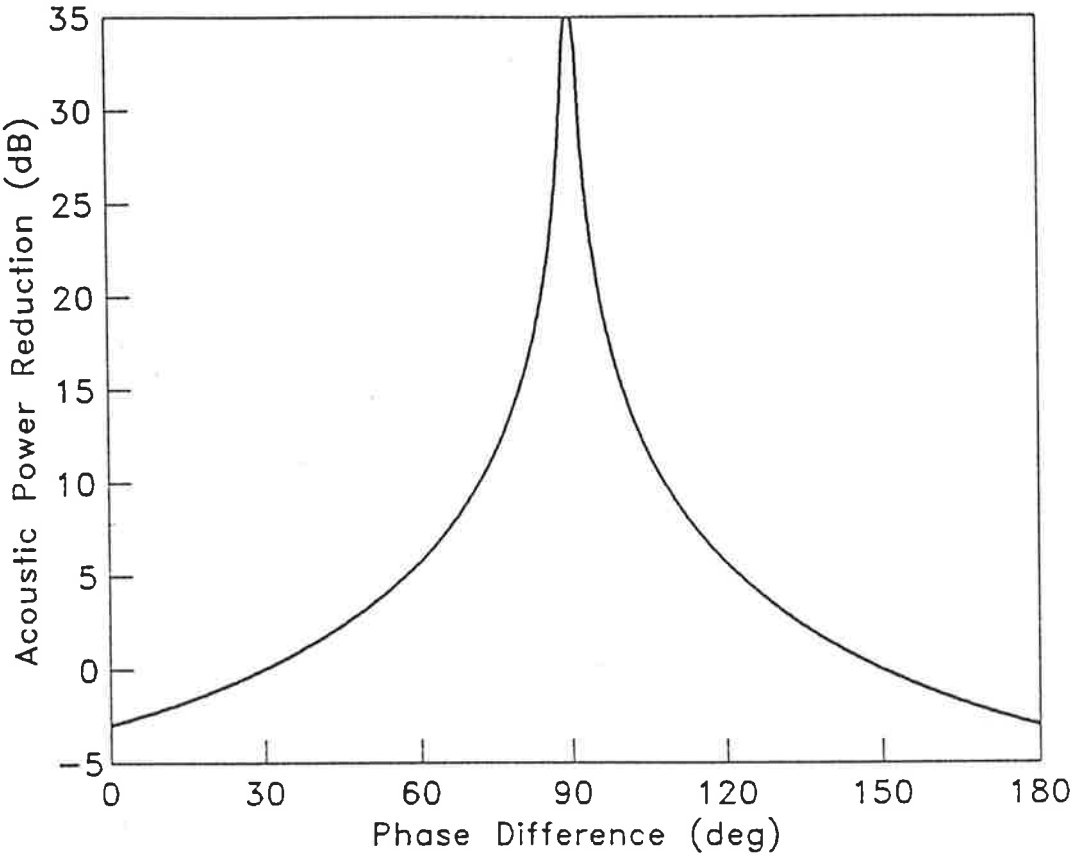

2.18 Reduction in total system acoustic power output for a constant pressure primary source, 400 Hz, control source 1 meter downstream.

again appear to be one of source unloading; that is, the radiation impedance of the noise source must be significantly altered.

As the primary source here is constant pressure, the volume velocity must be reduced to achieve sound power attenuation. Alternatively, as the control source is constant volume velocity, the sound pressure at its face must be reduced. This is shown to be the case in figures 2.19 and 2.20, which illustrate the in-phase primary source volume velocity and the in-phase control source face pressure associated with the power flows

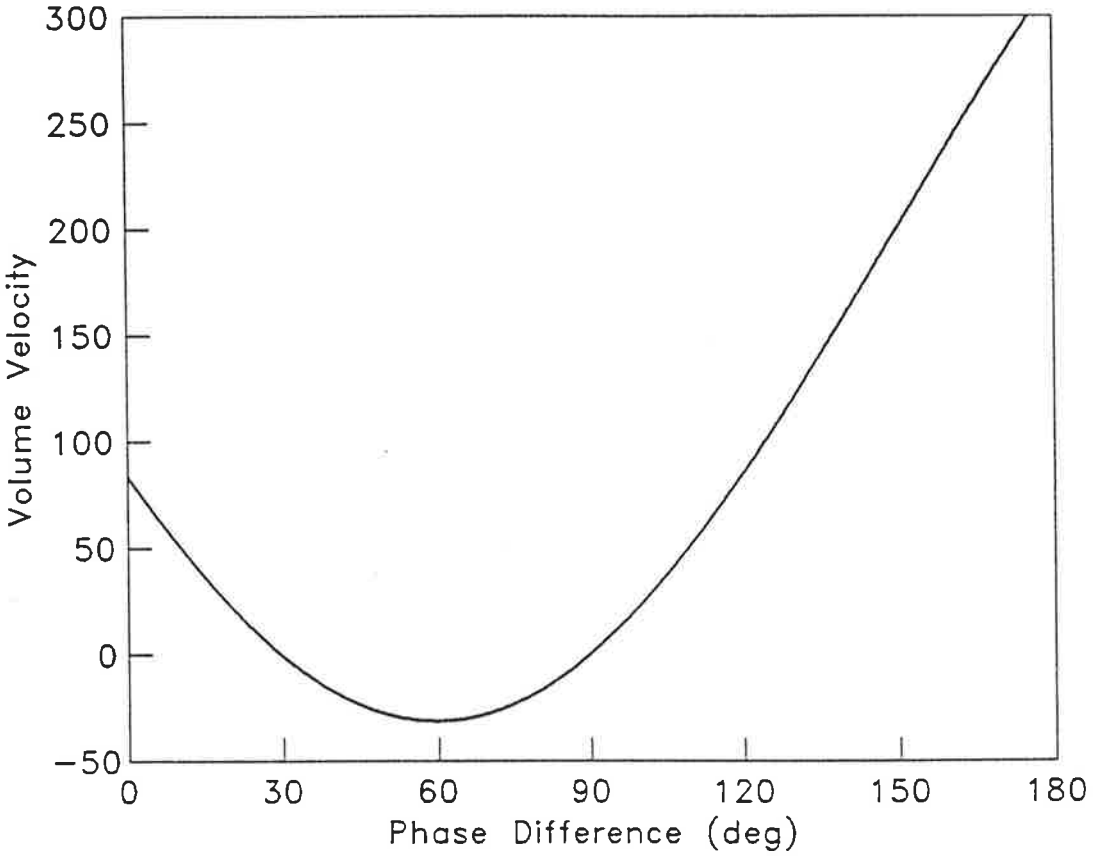

2.19 In-phase component of primary source volume velocity for a constant pressure primary source / constant volume velocity control source system, 400 Hz, control source 1 meter downstream of the primary source.

of figures 2.17 and 2.18. Therefore, as radiation impedance is defined as the ratio of sound pressure to volume velocity (see equation (2.21)), it can be surmized that for a constant pressure source, the acoustic power output is reduced by an increase in the radiation impedance, which causes a suppression in source volume velocity and an associated reduction in source acoustic power output as acoustic power is linearly proportion to radiation impedance, but proportion to volume velocity squared (note that constant pressure sources are assumed to have negligible internal (mechanical) impedance, which enables this to occur). Alternatively, if the noise source is a

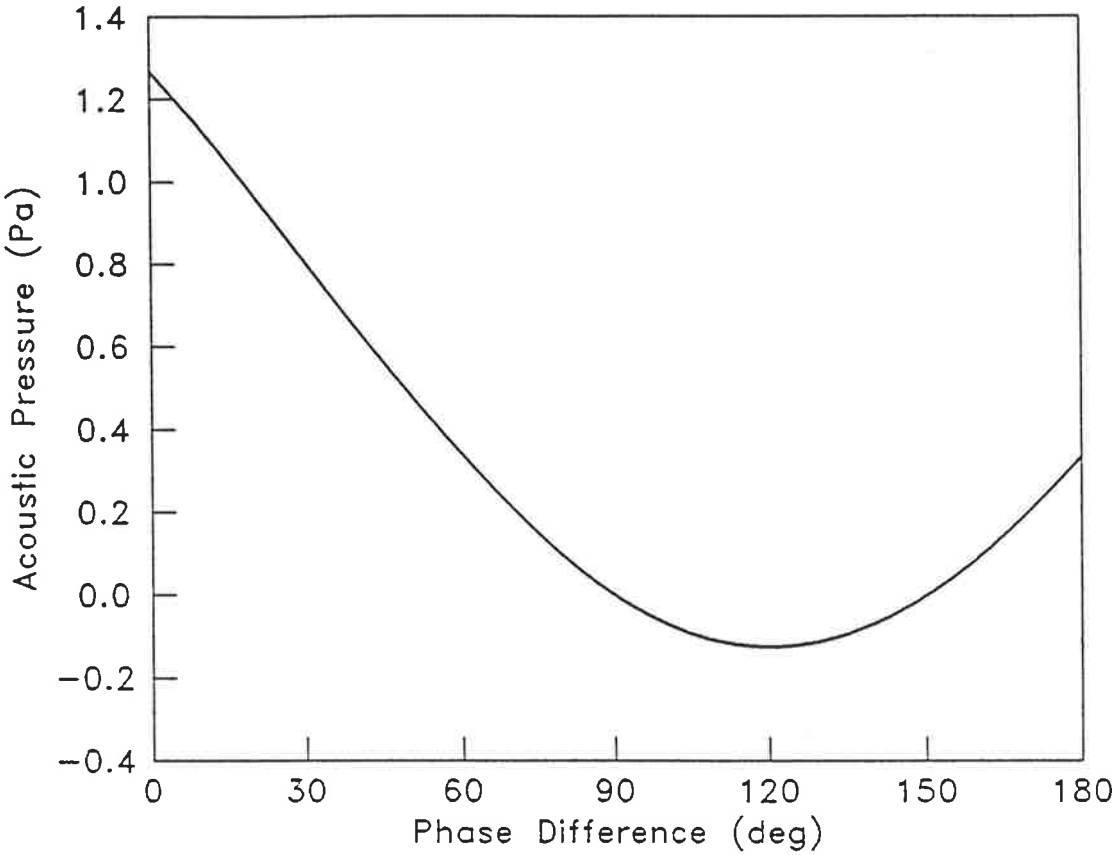

2.20 In-phase component of control source pressure for a constant pressure primary source / constant volume velocity control source system, 400 Hz, control source 1 meter downstream of the primary source.

constant volume velocity source, fluid unloading causes a reduction in source radiation impedance, which in turn reduces the in-phase sound pressure on the face of the source, and the radiated power power. It is interesting to note that these different mechanisms lead to different optimal phase differences between the primary and control sources when a constant volume velcity control source (such as a speaker) is used to control either a constant pressure, or constant volume velocity, primary source. Figure 2.21 illustrates the effect which phase difference has on the total power attenuation for the physical arrangement described previously, when the primary source

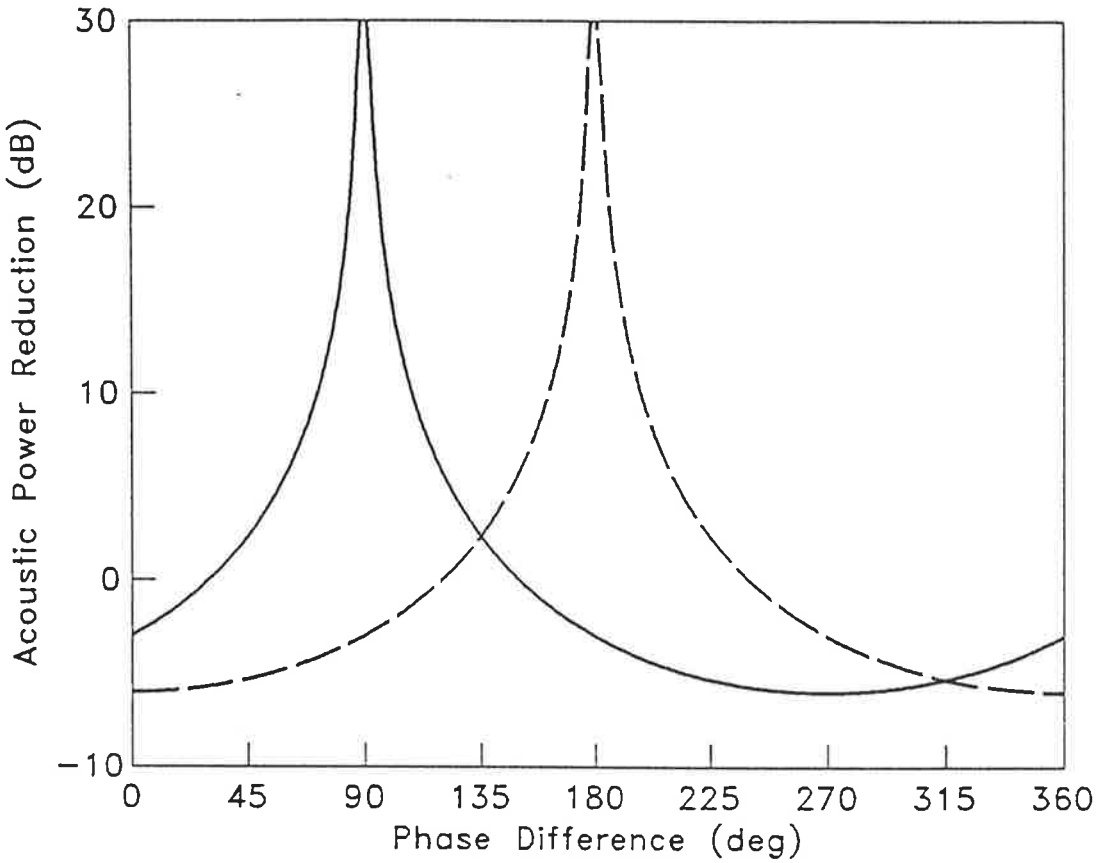

2.21 Effect of phase difference on total acoustic power reduction, 400Hz, control source 1 meter downstream of the primary source. —— = constant pressure primary source,— — = constant volume velocity primary source.

is either a constant pressure or constant volume velocity type (the control source volume velocity amplitudes are fixed at the optimum value for these plots). Note that the optimum phase difference for the constant pressure source is 90°, while for the constant volume velocity source it is the more commonly cited 180°. This difference arises from the different ways the source impedance is changed. For a constant pressure source, control is achieved by a change in source volume velocity, while for a constant volume velocity source it is achieved by a reduction in source face sound pressure. As these quantities (pressure and velocity) are out of phase by 90° in the

duct, for a constant volume velocity source to control a constant pressure source the phase difference should be ±90°. However, for two constant volume velocity sources, the phase difference should either be 0° or 180°.

2.7. THE EFFECT OF SOURCE LOCATION AND DUCT TERMINATION ON ACOUSTIC POWER FLOW ATTENUATION

The previous sections in this chapter have developed analytical models describing the active control of plane wave sound propagation in an infinitely extending duct for the both constant pressure and constant volume velocity sources. Using these, the mechanisms of this form of active noise control, namely changing of noise source impedances, have been demonstrated. Using these models, this section aims to examine the effect which source location has upon the levels of total acoustic power attenuation that can be achieved. Coupled to this is the effect which the impedance of the duct termination has upon this parameter.

To facilitate this examination, it is necessary to first derive an expression for the total system acoustic power output under optimally controlled conditions. Consider firstly the case of a constant volume velocity primary source being controlled by a constant volume velocity control source, using the semi-infinite geometry of figure 2.16. For this arrangement, the total acoustic power flow was expressed as a quadratic function of control source volume velocity in equation (2.31), which was solved for the optimum control source volume velocity in equation (2.36). Substituting this value back into equation (2.31), the expression for the minimum acoustic power output is found to be

$$W_{\min} = c - \frac{1}{4}(b_1^* + b_2)^* Re\{a\}^{-1}(b_1^* + b_2) \tag{2.67}$$

Expanding this using equations (2.32) - (2.35), it is found that the ratio of controlled (residual) acoustic power flow, W_{min}, to the initial uncontrolled acoustic power flow, W_{unc}, is

$$\frac{W_{\min}}{W_{unc}} = 1 - \frac{1}{2}\left(\frac{1 + \frac{1}{2}e^{-2\pi\alpha}(\cosh(2\pi\alpha) - \cos(2\pi\beta) - 2\cos(2k_o z_c + 2\pi\beta)) + \cos(2k_o z_c)}{1 - e^{-2\pi\alpha}\cos(2k_o z_c + 2\pi\beta)} \right) \tag{2.68}$$

Note that the acoustic power attenuation in dB is

$$\Delta W = -10 \log_{10}\left(\frac{W_{\min}}{W_{unc}} \right) \tag{2.69}$$

Consider firstly the case where the primary source termination is rigid, with α_1=0.0 and β_1=0.5. Substituting these values into equation (2.68), it is found that the sound power attenuation, as a function of source location, is

$$1 - \frac{1}{2}\left(\frac{2 + 2\cos(2k_o z_c)}{1 + \cos(2k_o z_c)} \right) = 0 \tag{2.70}$$

That is, the total acoustic power flow can be completely suppressed (theoretically) regardless of control source location. The control source volume velocity required to do this, found by expanding equation (2.36) using equations (2.32) - (2.35), is

$$Q_c = -\frac{Q_p}{\gamma}\left(\frac{e^{-ik_o z_c}+e^{ik_o z_c}(e^{-\psi}\cosh(\psi))^*}{1-e^{-2\pi\alpha}\cos(2k_o z_c+2\pi\beta)}\right) \tag{2.71}$$

Substituting in the rigid termination boundary conditions, this is simplified to

$$Q_c = -\frac{Q_p}{\gamma\ \cos(k_o z_c)} \tag{2.72}$$

Thus, although it is theoretically possible to completely supress the total system acoustic power output with the control source at any location, clearly it is most efficient to place the control source at a half-wavelength interval from the noise source (note that if the control source is placed at an odd quarter wavelength from the primary source, an infinite volume velocity would be required to achieve total control).

One additional point that should be noted from the result of equation (2.72) is the effect which size has upon the volume velocity required to achieve maximum noise control. Whilst from equation (2.68) it can be deduced that the control source size (theoretically) has no influence upon the levels of control which can be achieved, as the size of the source begins to approach ½ wavelength of the frequency of sound of interest, the volume velocity required to achieve control increases dramatically.

Consider now the effect of slightly relaxing the rigid termination boundary conditions. Figure 2.22 depicts the power attenuation which can be achieved for a boundary defined by α_1=0.002, β_1=0.47, plotted as a function of control source / primary

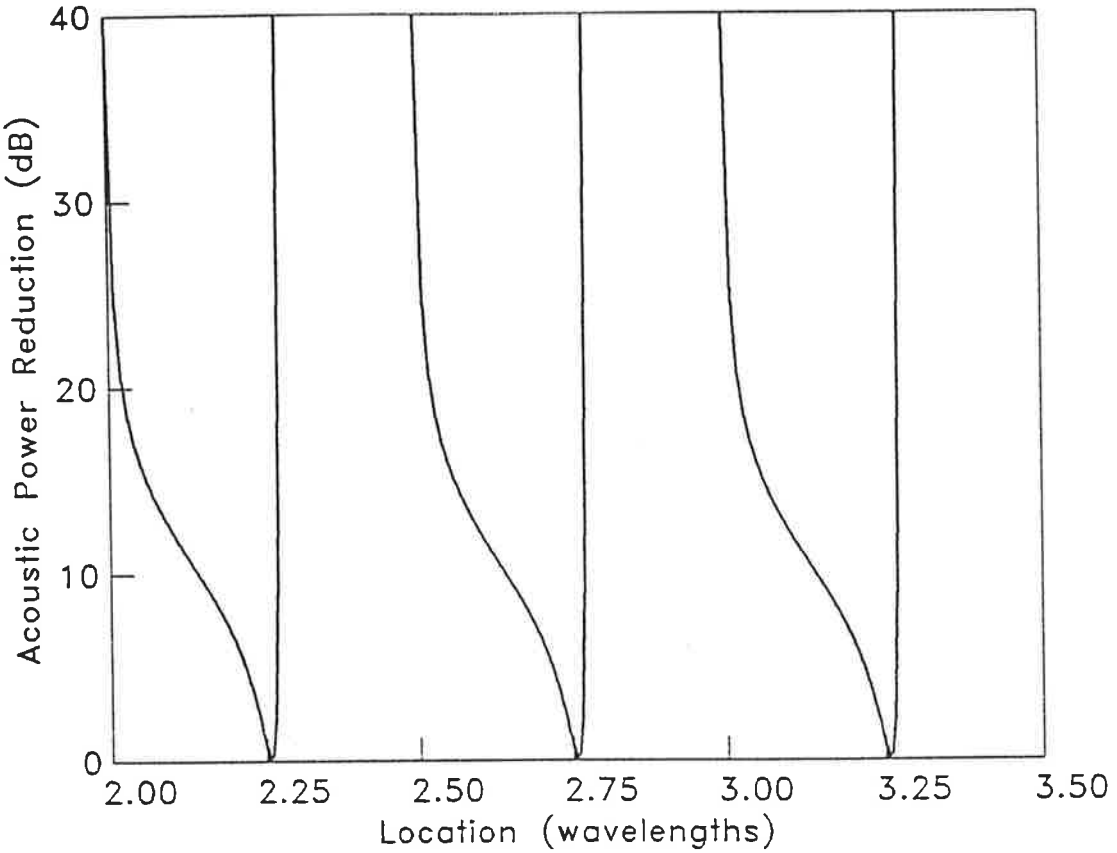

2.22 Total acoustic power reduction as a function of primary source/control source separation distance, 400 Hz, with the primary source termination defined by α=0.002, β=0.47.

source separation distance expressed in wavelengths. Plotted in figure 2.23 is the associated volume velocity ratio (defined as the ratio of control source to primary source volume velocity magnitudes), with some experimentally measured points. In viewing this data, it is evident that significant levels of acoustic power attenuation can still be achieved at ½ wavelength intervals, but that the attenuation that can be achieved at odd quarter wavelengths has been significantly reduced. Also, the volume velocities required to achieve the maximum levels of control away from the optimum have been reduced.

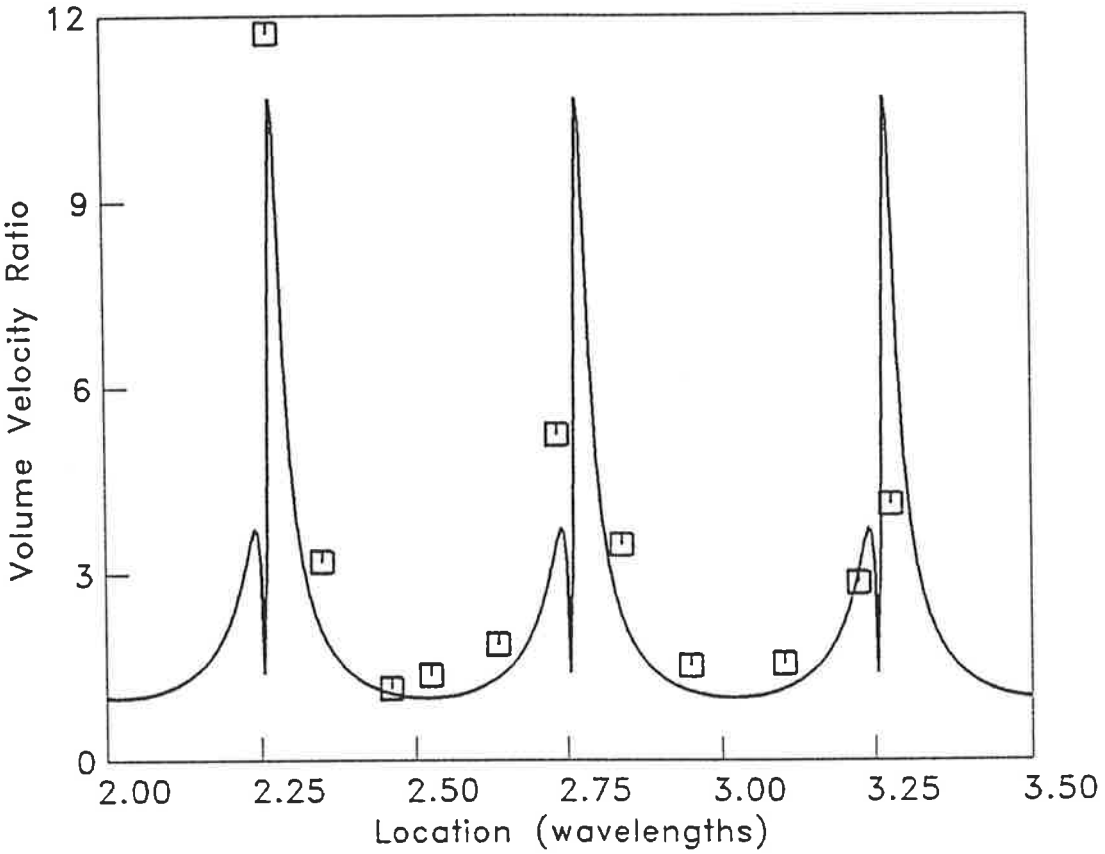

2.23 Volume velocity ratio required to achieve maximum total acoustic power reduction as a function of primary source/control source separation distance, 400 Hz, with the primary source termination defined by α=0.002, β=0.47. ——= theory, ☐ = experiment.

The next case to consider is the use of a constant volume velocity source to control the sound power output of a constant pressure primary source. For this arrangement, the total acoustic power flow was expressed as a quadratic function of control source volume velocity in equation (2.47), which was solved for the optimum control source volume velocity in equation (2.52). Substituting this value back into equation (2.31), the expression for the minimum acoustic power output is found to be

$$W_{min} = c - \frac{1}{4}(b_1 - b_2)Re\{a\}^{-1}(b_1 - b_2)^* \tag{2.73}$$

Expanding this by using equations (2.48) - (2.51), it is found that the ratio of controlled (residual) acoustic power flow, W_{min}, to the initial uncontrolled acoustic power flow, W_{unc}, is

$$\frac{W_{min}}{W_{unc}} = 1-\frac{1}{2}\left(\frac{1+\frac{1}{2}e^{-2\pi\alpha}(\cosh(2\pi\alpha)-\cos(2\pi\beta)+2\cos(2k_oz_c+2\pi\beta))-\cos(2k_oz_c)}{1-\cos(2k_oz_c)}\right) \tag{2.74}$$

Consider firstly the case where the primary source termination is rigid, with $\alpha_1=0.0$ and $\beta_1=0.5$. Substituting these values into equation (2.74), it is found that the sound power attenuation, as a function of source location, is

$$1-\frac{1}{2}\left(\frac{2-2\cos(2k_oz_c)}{1-\cos(2k_oz_c)}\right) = 0 \tag{2.75}$$

Therefore, as with the constant volume velocity case, when the primary source termination is perfectly rigid, it is (theoretically) possible to completely suppress the total system acoustic power output with any control source location. Expanding equation (2.52) using equations (2.48) - (2.51), the control source volume velocity required to do this is

$$Q_c = -\frac{Q_p}{\gamma}\left(\frac{e^{-ik_oz_c}-\frac{1}{2}e^{ik_oz_c}(1-e^{-2\psi^*})}{\sin^2(k_oz_c)}\right) \tag{2.76}$$

Substituting the boundary conditions for the rigidly terminated primary source end into equation (2.76), the optimum control source volume velocity for this simplified model is found to be

$$Q_c = \frac{iQ_p}{\gamma \sin(k_o z_c)} \tag{2.77}$$

It is interesting to contrast this optimum control source volume velocity result with that obtained for the similar constant volume velocity primary source case, given in equation (2.72). Whereas the most efficient control source placement for the constant

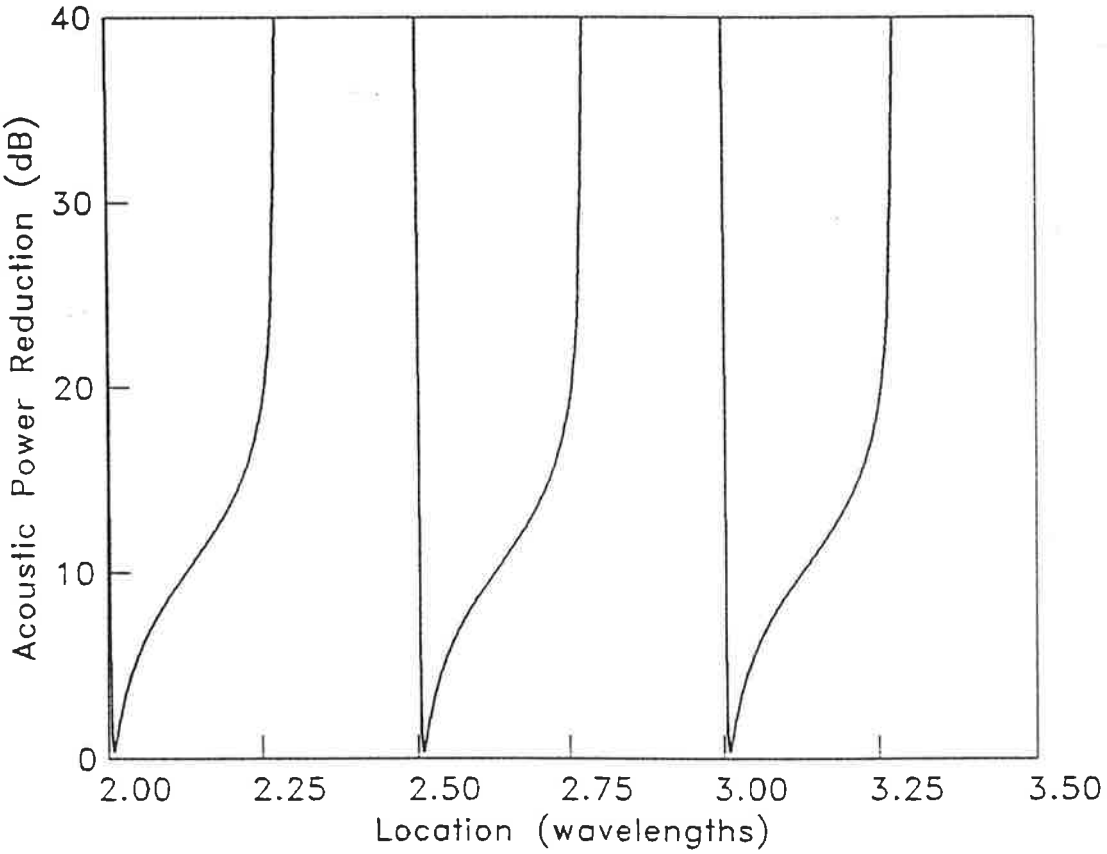

2.24 Total acoustic power reduction as a function of primary source/control source separation distance, 400 Hz, constant pressure primary source, with the primary source termination defined by α=0.002, β=0.47.

volume velocity case was at half wavelength intervals, the most efficient control source placement for the constant pressure case was at odd quarter wavelength intervals. Also, the phase difference between the primary and control sources for the constant pressure case is modulated, as a function of the separation distance, between ±90° by the presence of the imaginary term. Finally, note that, as with the constant volume velocity case, the control source size does influence the optimum control source volume velocity; as the size of the source approaches ½ wavelength of the frequency of interest, the required volume velocity increases dramatically.

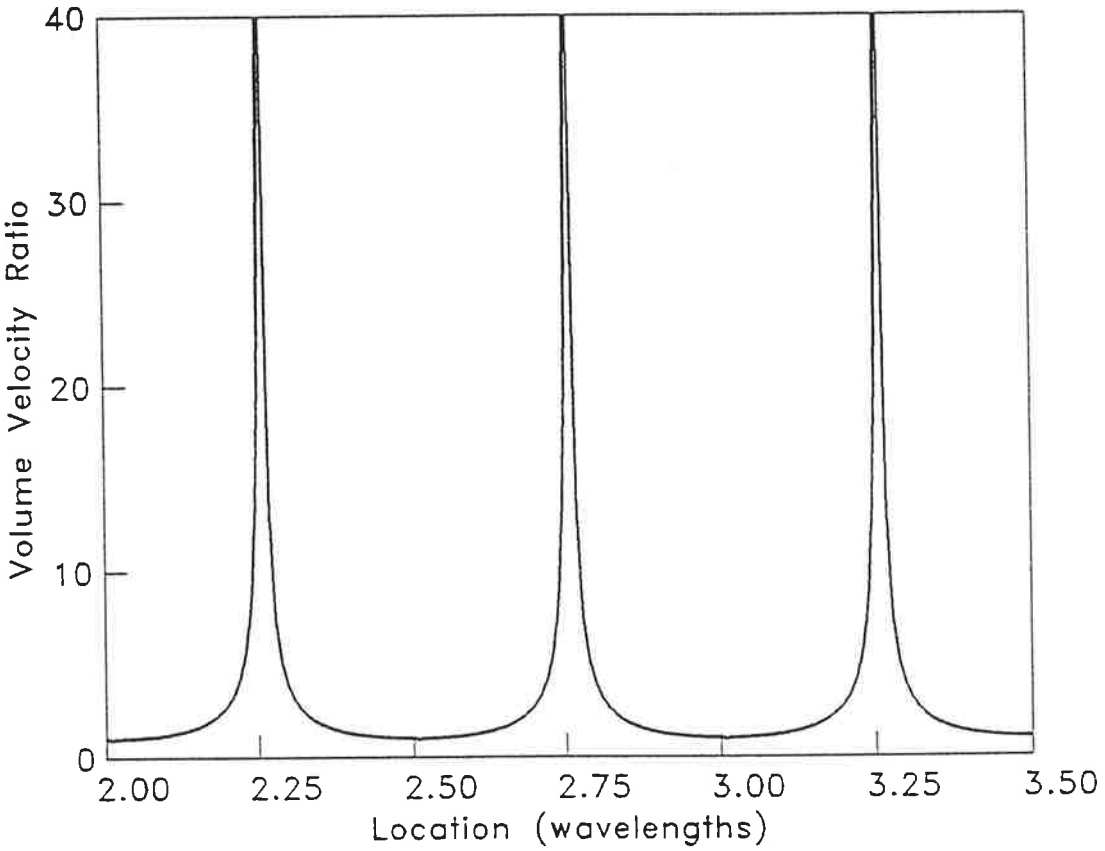

2.25 Volume velocity ratio required to achieve maximum total acoustic power reduction as a function of primary source/control source separation distance, 400 Hz, constant pressure primary source, with the primary source termination defined by α=0.002, β=0.47.

Consider now the effect of slightly relaxing the rigid termination boundary conditions. Figure 2.24 depicts the total acoustic power attenuation which can be achieved for a boundary defined by α_t=0.002, β_t=0.47, plotted as a function of control source / primary source separation distance expressed in wavelengths. Plotted in figure 2.25 is the associated control source volume velocity required to achieve this control. As can be seen, the optimum control source location is just before each half wavelength interval, where significant levels of acoustic power attenuation can still be achieved. At odd quarter wavelengths, however, very little acoustic power attenuation is possible.

The final case to consider here is the alternative constant volume velocity primary source arrangement shown in figure 2.13. For this arrangement, the total acoustic power flow was expressed as a quadratic function of control source volume velocity in equation (2.60), which was solved for the optimum control source volume velocity in equation (2.64). Substituting this value back into equation (2.60), the expression for the minimum acoustic power output is found to be

$$W_{min} = c - b^* a^{-1} b \tag{2.78}$$

Expanding this using equations (2.61) - (2.63), it is found that the ratio of controlled (residual) acoustic power flow, W_{min}, to the initial uncontrolled acoustic power flow, W_{unc}, is

$$\frac{W_{min}}{W_{unc}} = 1 - \cos^2(k_o z_c) \tag{2.79}$$

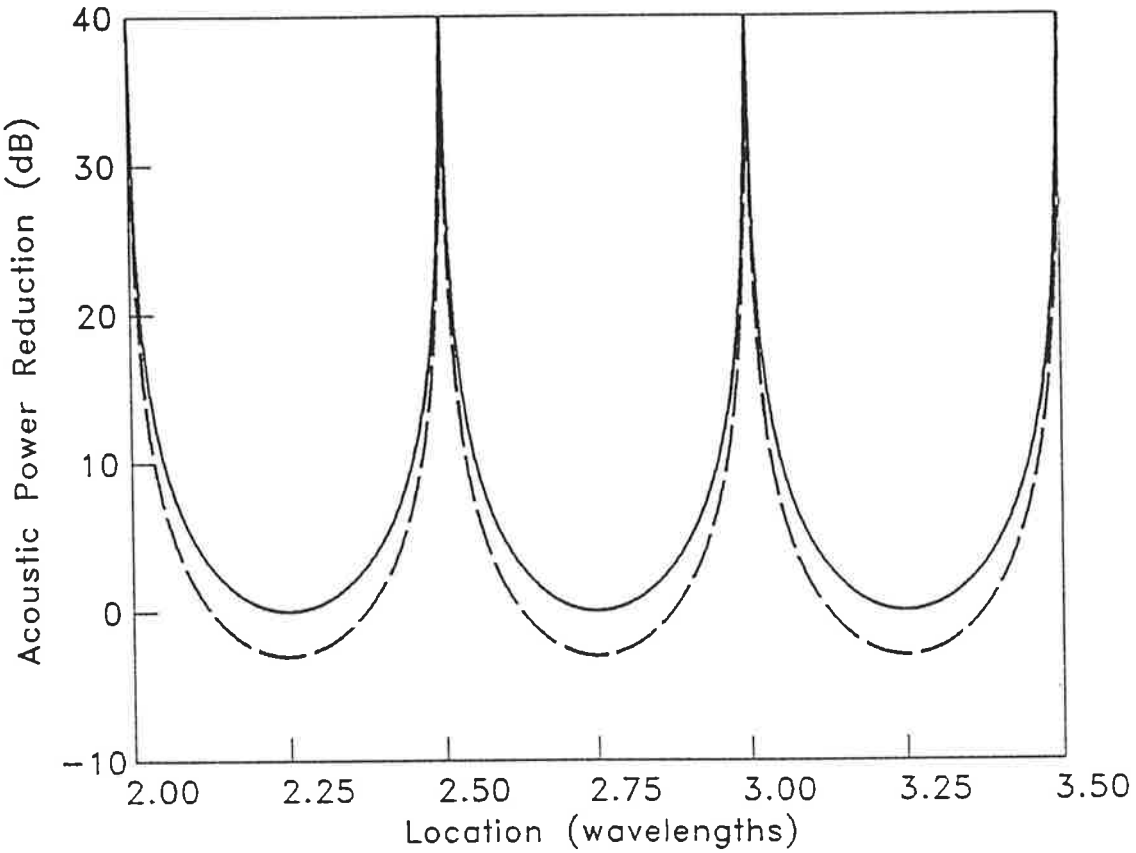

2.26 Total acoustic power reduction as a function of primary source/control source separation distance, 400 Hz, for the alternative modelled source arrangement. —— = total power optimization, — — = downstream power optimization.

Figure 2.26 illustrates the acoustic power attenuation that can be achieved for such a system plotted as a function of source separation distance expressed in wavelengths. Figure 2.27 depicts the associated control source / primary source volume velocity amplitude ratio and phase difference. Comparing these plots to those of the similar, rigidly terminated duct, shown in figures 2.22 and 2.23, it shows that many of the trends are, in fact, the same; namely, the optimum source separation distance is at ½ wavelength intervals, with the worst results achieved at odd ¼ wavelength intervals.

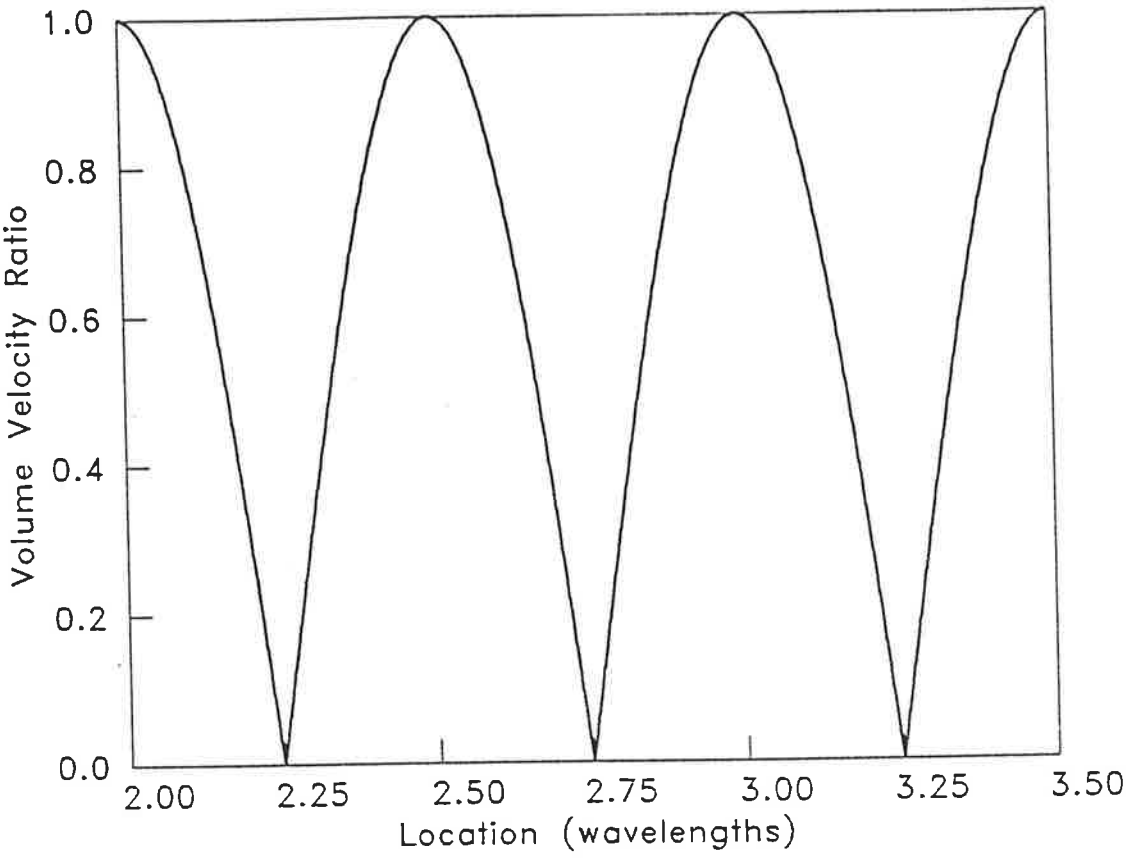

2.27 Volume velocity ratio required to achieve maximum total acoustic power reduction as a function of primary source/control source separation distance, 400 Hz, for the alternative modelled source arrangement.

This system, however, will always be a symmteric one due to the lack of a phase and amplitude modified reflected wave. This means that absorption will never be an optimal control mechanism, only suppression will be. Consider the data shown in figures 2.28 and 2.29, which illustrates the acoustic power output of the primary and control sources around the optimum phase difference of 180° for two constant volume velocity source separated by 1 meter and operating at 400 Hz. The data shown in figure 2.28 is for the doubling infinite arrangement of figure 2.13 (where both the primary and control sources are mounted in the wall of an infinite duct), and the data

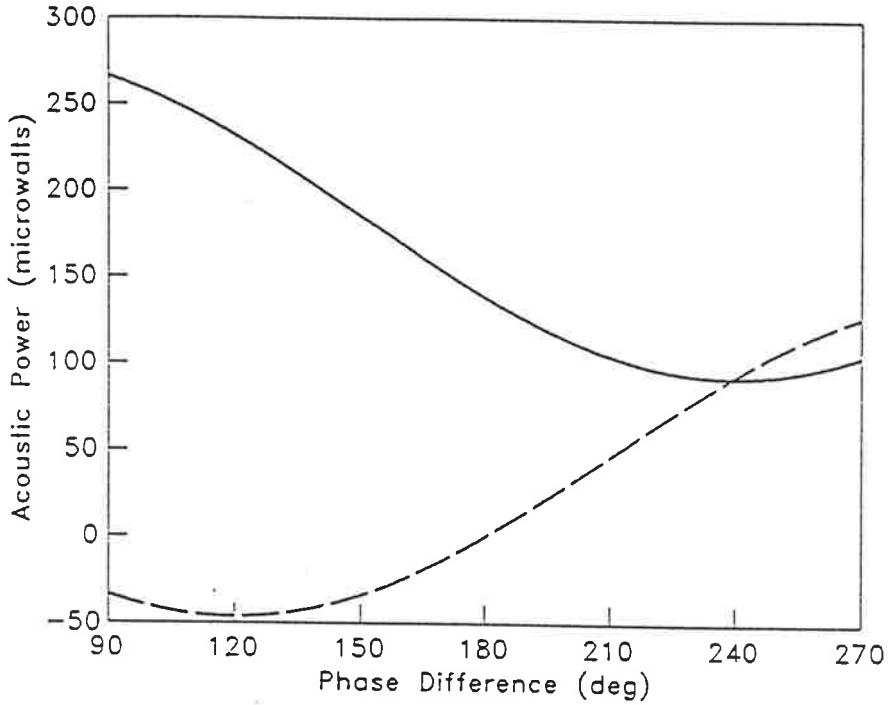

2.28 Source acoustic power output as a function of source phase difference for the alternative modelled source arrangement, 400 Hz, with a source separation distance of 1 meter. —— = primary source, — — = control source.

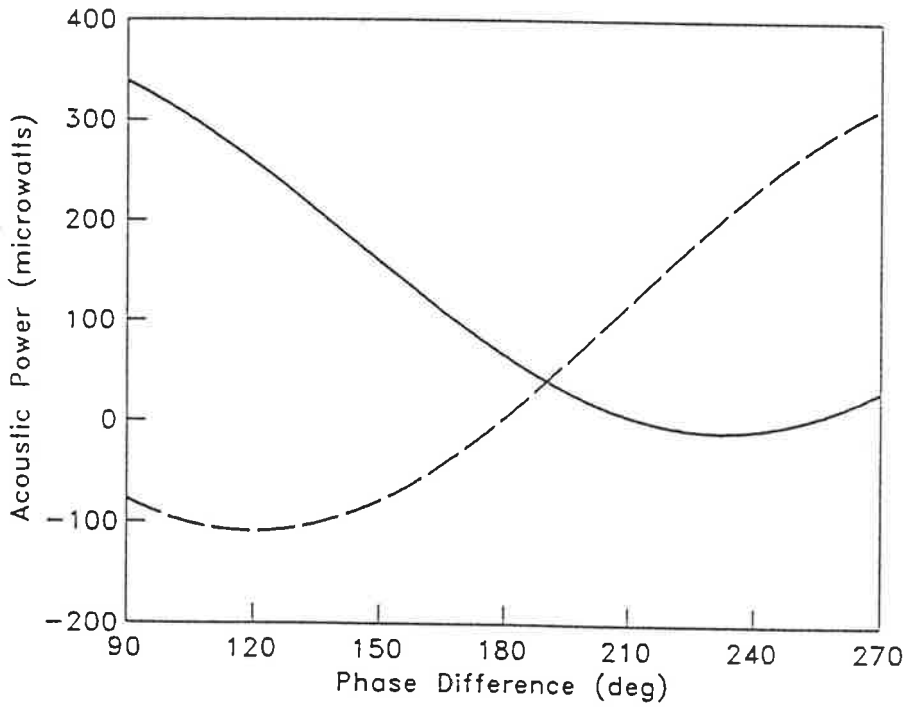

2.29 Source acoustic power output as a function of source phase difference for a primary source termination defined by α=0.05, β=0.45, 400 Hz, with a source separation distance of 1 meter. —— = primary source, — — = control source.

in figure 2.29 is for the terminated arrangement of figure 2.16, with the termination conditions defined by α_t=0.05, β_t=0.45. For the doubly infinite case, optimal control is achieved when the control source is producing zero acoustic power (at an operating phase difference of 180°). For the other case, however, optimal control is achieved when the control source is, in fact, absorbing 29 μW of the residual 96 μW acoustic power produced by the primary source (at an operating phase difference of 169.6°).

2.8. SUMMARY

Results discussed in this chapter show conclusively that the mechanism of active noise control in a duct cannot be properly understood if the (primary) sound source is omitted from consideration. This is in contrast to many of the previous models, which concentrate on analysing the interaction between an assumed plane wave propagating down the duct and a control source or sources. These models are limited in control mechanism to absorption, or reflection of the plane wave back upstream to be dissipated by viscous losses of some form.

Noise reduction in a duct by active control is not simply a cancellation phenomenon. While it may be viewed that pressure cancellation in front of the source is a mechanism of control, which reduces the acoustic impedance at that point and causes a reflection of the incident propagating plane wave, it is not a case of the control source(s) reflecting the energy back upstream where it is magically dissipated. Rather, one of two or a combination of two physical processes occurs. Firstly, the primary and control sources mutually alter each other's radiation impedances so as to reduce the acoustic output of both sources. For a constant volume velocity source, this means

a reduction in radiation impedance, which is achieved by a reduction in in-phase acoustic pressure on the face of the source. For a constant pressure source, this means an increase in radiation impedance associated with a decrease in source volume velocity (note that as acoustic power is linearly proportional to radiation impedance, but proportional to volume velocity squared, this will result in a reduction in acoustic power output). Secondly, the control source(s) may absorb all or part of the primary source acoustic energy.

It was further shown that the ability of the active system to provide global control is greatly influenced by a number of geometric and acoustic variables. The location of the single control source in the duct relative to the primary source plays an important part in determining the maximum possible acoustic power attenuation which could be achieved, along with the control source volume velocity required required to achieve this control. If the primary source end duct termination is close to a rigid termination, the control source should be located in the vicinity of an integer number of half wavelengths from the primary source for the best results. Clearly then, for a single control source, the optimum location is frequency dependent, and any given location will produce good results at some frequencies, and poor results for others. Also, the size of the control source relative to the wavelength of the frequency of interest is important; as the axial length of the source becomes large, the volume velocity required by the control source to achieve the maximum possible acoustic power attenuation greatly increases.

CHAPTER 3.
GENERAL ANALYTICAL MODELS FOR AIDING THE DESIGN OF ACTIVE SYSTEMS TO CONTROL SOUND RADIATED BY VIBRATING STRUCTURES INTO FREE SPACE AND INTO ENCLOSED SPACES

3.1 INTRODUCTION

As mentioned in the introduction chapter 1, it has thus far proved, in general, impossible to directly determine the optimal locations of the control sources and error sensors during the design of an active noise control system to reduce sound radiated by vibrating structures, for two reasons. Firstly, the maximum level of achievable sound power attenuation is not a linear function of control source location. Secondly, the optimum error sensor locations are dependent upon the control source locations. It is therefore necessary to use a numerical search routine to optimize the arrangement of the control sources and error sensors.

To implement a numerical search routine, it must be possible to predict the effect which applying a control disturbance at a given location(s) has upon the acoustic power flow. This means that either an analytical or numerical model of the structural / acoustic system must be developed which allows calculation of the sound field generated by a particular vibration or acoustic control source. The sound field generated by the primary excitation force must either be calculated (from a knowledge of the primary forcing function) or, if available, test data for the sound field generated by the system to be controlled could be used. As

referenced in the introduction chapter 1, there has been a body of research concerned with this type of modelling for controlling sound radiation from vibrating structures, both into free space and into weakly coupled enclosures. The majority of these models are based on quadratic optimization theory, and are specific to their individual topics. They can be generalized, however, to enable inference of control mechanisms to be made, and the effects which system parameters have upon these mechanisms, to be determined for a wide range of structural radiation problems, thus allowing a more generalized design methodology to be developed.

This chapter develops generalized models which can be implemented in a numerical search routine to determine the optimum control source and error microphone locations for the control of both periodic sound radiation from planar surfaces into free space, and periodic sound transmission into weakly coupled enclosures. The models allow the use of either acoustic or vibration control sources. Quadratic optimization theory is initially used to formulate the equations required for the numerical search routines. Problems with this approach are then discussed, and an improved technique based on multiple regression is then presented.

The models developed in this chapter will be verified experimentally in the subsequent 2 chapters, for the cases of controlling periodic sound radiation from a vibrating rectangular panel into free space, and the control of periodic sound transmission into a weakly coupled cylindrical cavity. They will also form the basis for a thorough analytical study of the effect of system variables on the performance of active systems for controlling periodic sound radiation from a vibrating panel into free space, conducted in the next chapter.

3.2. ERROR CRITERIA

When designing an active system to provide global control of sound radiation from a vibrating structure, it is the minimization of the acoustic power flow which is of interest, and the chosen error criterion must therefore be a measure of this quantity. Hence the models must be developed to allow examination of the acoustic power flow, under both the primary excited and controlled conditions. For radiation into free space from a planar structure, the quantity to be minimized (and thus the error criterion) is the total radiated sound power (Deffayet and Nelson, 1988), defined in the farfield of the radiating structure as

$$W_{tot} = \int_0^{2\pi} \int_0^{\pi/2} \frac{|p(\vec{r})|^2}{2\rho_o c_o} |\vec{r}|^2 \sin\theta \, d\theta \, d\phi \qquad (3.1)$$

For minimizing sound transmission through a structure into a (weakly) coupled acoustic enclosure, it is the minimization of acoustic potential energy in the enclosure which becomes the error criterion. The acoustic potential energy is given by (Nelson et al, 1987a; Pan et al, 1990):

$$E_p = \left(\frac{1}{2\rho_o c_o^2} \right) \int_V |p(\vec{r})|^2 \, d\vec{r} \qquad (3.2)$$

To minimize either of these quantities it must be possible to calculate the sound pressure amplitude squared at any point $\vec{r}=\vec{r}(r,\theta,\phi)$ during the application of active control. Being a linear system, the sound pressure at any location can be considered as the sum of the primary generated and control disturbance generated sound pressures as follows:

$$p(\vec{r}) = p_p(\vec{r}) + p_c(\vec{r}) \qquad (3.3)$$

where the subscripts $_p$ and $_c$ denote primary and control sources, respectively. Thus, the sound pressure amplitude squared at any point is:

$$|p(\vec{r})|^2 = p_c(\vec{r})\ p_c(\vec{r})^* + p_p(\vec{r})\ p_c(\vec{r})^* + p_c(\vec{r})\ p_p(\vec{r})^* + p_p(\vec{r})\ p_p(\vec{r})^* \qquad (3.4)$$

where * denotes the complex conjugate.

In the following two sections the equations necessary to determine the sound pressures at any point will be developed in a form amenable to solution by quadratic optimization theory. The above error criteria will then be considered further in light of these equations.

3.3. MODELLING OF RESPONSE UNDER PRIMARY EXCITATION

Before studying the effect of applying active noise control, it is first necessary to determine the response of the structural or coupled structural/acoustic system under the action of the primary exciting force. As the analytical approaches used in modelling periodic sound radiation from a vibrating planar surface into free space and periodic sound transmission into a coupled structural/acoustic enclosure are different, they will be presented separately. (It should be noted that throughout this chapter harmonic time dependence of the form $e^{i\omega t}$ is assumed.)

3.3.1. Primary excitation: radiation into free space from a vibrating planar surface

The problem considered here of sound radiation into free space from a vibrating planar surface will be formulated in terms of the velocity distribution on the surface, although acceleration or displacement could equally well be used. The purpose of the analysis is to develop an expression for the acoustic pressure generated by the vibrating structure, in terms of the surface velocity distribution, at some point in its far field. It will be assumed that the primary excitation is an acoustic field on the other side of the surface which excites it into vibration. This is the most general case, which can be specialized for particular forcing functions, such as point or distributed forces.

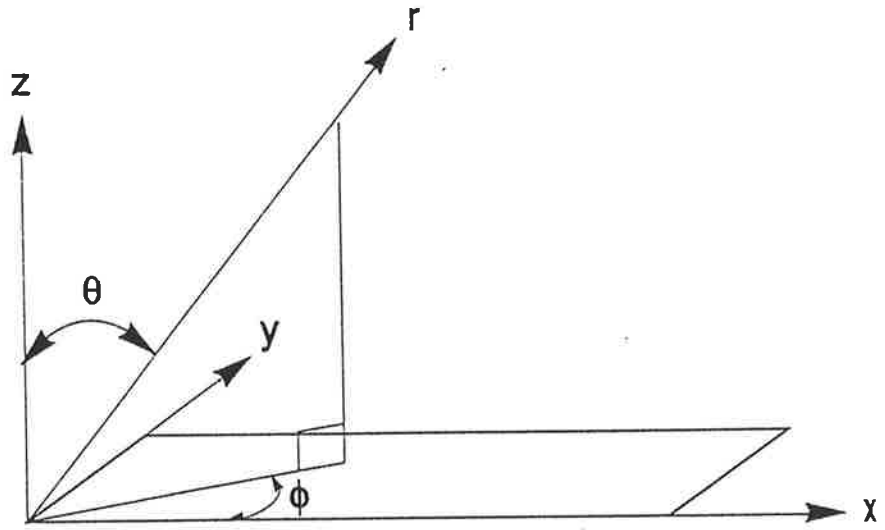

Figure 3.1 Arbitrary vibrating structure radiating into free space.

For the arbitrary structure shown in Figure 3.1, the velocity v at any point $\vec{x}=\vec{x}(x,y)$ under primary excitation pressure p is governed by the equation (Pope, 1971):

$$v(\vec{x}) = i\omega \int_S G_s(\vec{x}|\vec{x}')\, p(\vec{x}')\, d\vec{x}' \qquad (3.5)$$

where ω is the frequency of interest in rad s^{-1}, $p(\vec{x}')$ is the forcing function at point $\vec{x}'$ expressed in terms of pressure, and $G_s(\vec{x}\,|\,\vec{x}')$ is the Green's function of the structure given by:

$$G_s(\vec{x}\,|\,\vec{x}') = \sum_{j=1}^{\infty} \frac{\psi_j(\vec{x})\ \psi_j(\vec{x}')}{M_j\ Z_j} \qquad (3.6)$$

where $\psi_j(\vec{x})$ is the jth mode shape of the structure evaluated at point $\vec{x}$, and M_j is the modal mass of the jth mode, defined as:

$$M_j = \int_S m(\vec{x})\,\psi_j^2(\vec{x})\ d\vec{x} \qquad (3.7)$$

where $m(\vec{x})$ is the surface density at point $\vec{x}$:

$$m(\vec{x}) = \rho_s(\vec{x})\,h(\vec{x}) \qquad (3.8)$$

$\rho_s(\vec{x})$ and $h(\vec{x})$ are respectively the density and thickness of the structure at $\vec{x}$, and Z_j is the square of the mass normalized impedance of the jth structural mode at frequency ω:

$$Z_j = (\omega_j^2 + i\eta_j\omega_j\omega - \omega^2) \qquad (3.9)$$

where ω_j is the resonance frequency of the jth structural mode, and η_j is its associated loss factor. As an alternative to the preceding analysis, if the primary excitation force were unknown or difficult to calculate, measured values of the velocity distribution of the radiating surface could be used. Typically, the measured data would be modally decomposed, and the complex modal amplitudes used in the analysis that follows. While

the modal decomposition is not strictly necessary, providing that the radiation transfer function at each measured point on the surface can be calculated, it is a convenient way of expressing the data.

To continue, for an analytical study it is convenient to expand the velocity at point $\vec{x}$ in terms of the normal modes of vibration of the structure:

$$v(\vec{x}) = \sum_{j=1}^{\infty} v_j \psi_j(\vec{x}) \qquad (3.10)$$

where v_j is the velocity amplitude (complex) of the jth structural mode. If the expanded form of equation (3.10) is substituted into equation (3.5), and the infinite sum is approximated by a sum over m structural modes (the exact number of which is dependent upon the system response at the frequency of interest), the response of the structure under primary excitation can be expressed in matrix form as:

$$[V_p] = [Z_I]^{-1} [\Gamma_p] \qquad (3.11)$$

where $[V_p]$ is the (mx1) matrix of complex modal velocity amplitudes, whose jth element is v_j, $[\Gamma_p]$ is the (mx1) matrix of (modal) generalized forces whose jth element is defined as:

$$\gamma_j = \int_S \psi_j(\vec{x}') \, p(\vec{x}') \, d\vec{x}' \qquad (3.12)$$

and $[Z_I]$ is the (mxm) diagonal matrix of modal impedances, whose (j,j)th element is:

$$z_{I(j,j)} = M_j Z_j \qquad (3.13)$$

Once the structure is set into motion, the resulting sound pressure it radiates to some location $\vec{r}$ in its far field can be found from the equation (Fahy, 1985):

$$p_p(\vec{r}) = i2\rho_o\omega \int_S v(\vec{x})\ G_a(\vec{x}|\vec{r})\ d\vec{x} \qquad (3.14)$$

where the (far field) free space Green's function is given by:

$$G_a(\vec{x}|\vec{r}) = \frac{1}{4\pi R} \exp(-ikR) \qquad (3.15)$$

where k is the wavenumber at the frequency of interest, ρ_o is the density of the medium and R is the distance from the point $\vec{x}$ on the structure to the location $\vec{r}$ in the medium. Note that equation (3.14) is simply the Rayleigh integral.

If the velocity amplitude is again expanded in terms of the normal modes of vibration, and the infinite sum approximated by a summation over m structural modes, equation (3.14) can be expressed in matrix form as:

$$p_p(\vec{r}) = [Z_{rad}]^T [V_p] \qquad (3.16)$$

where $[Z_{rad}]$ is the (mx1) modal radiation transfer vector, whose jth element is (Fahy, 1985):

$$z_{rad_j} = \frac{i\rho_o\omega}{2\pi R} \exp(-ikR) \int_S \psi_j(\vec{x})\ d\vec{x} \qquad (3.17)$$

3.3.2 Primary excitation: Transmission into a coupled enclosure

In this case, the purpose of the analysis is to derive an expression for the sound pressure in the enclosure as a function of the exterior excitation pressure or alternatively as a function of the structural velocity distribution. If the fluid medium of interest is air (as is considered here), weak coupling can normally be assumed and the formulation of the response of a coupled structural/acoustic system can be developed using modal coupling theory (Pope, 1971) (weak coupling assumes the *in vacuo* mode shapes of the structure and the mode shapes of a rigidly enclosed acoustic space can be used to determine the coupled system response). The difference in formulation to that for radiation into free space is due to the coupling of the structural vibration modes with the interior cavity modes.

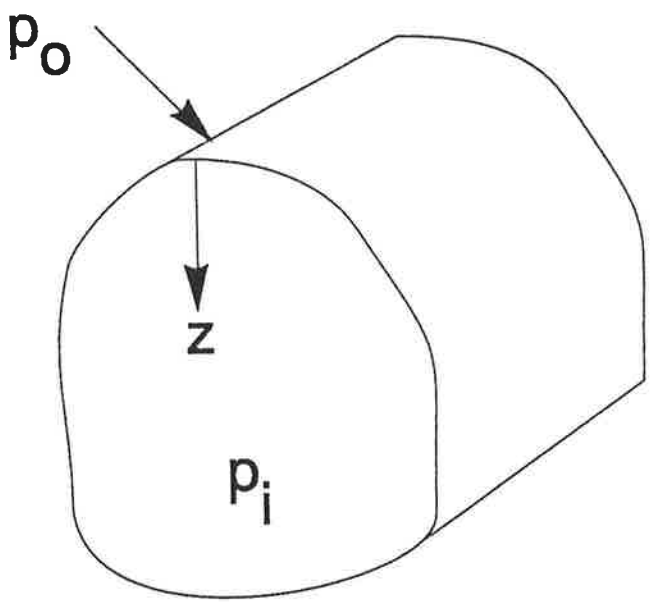

Figure 3.2 Arbitrary vibrating structure radiating into an enclosed space.

Referring to figure 3.2, the velocity at any point $\vec{x}$ on the vibrating structure is governed by the equation (Pope, 1971):

$$v(\vec{x}) = i\omega \int_S G_s(\vec{x}|\vec{x}')\,(p_e(\vec{x}') - p_i(\vec{x}'))\,d\vec{x}' \qquad (3.18)$$

where p_e and p_i are respectively the external and internal acoustic pressures, and $\vec{x}'$ is a point on the structure.

The interior pressure field induced by the vibration of the structure is defined by:

$$p_i(\vec{r}) = i(\rho_o c_o)^2 \omega \int_A G_a(\vec{x}|\vec{r})\, v(\vec{x})\, d\vec{x} \qquad (3.19)$$

where $G_a(\vec{x}|\vec{r})$ is the Green's function of the interior space and is given by:

$$G_a(\vec{x}|\vec{r}) = \sum_{\imath=1}^{\infty} \frac{\phi_\imath(\vec{x})\,\phi_\imath(\vec{r})}{M_\imath(\kappa_\imath^2 - k^2)\,c_o^2} \qquad (3.20)$$

k is the wave number of the sound in the cavity, $\phi_\imath(\vec{r})$ is the $\imath$th acoustic mode shape evaluated at point $\vec{r}$ in the cavity and $\phi_\imath(\vec{x})$ is the $\imath$th acoustic mode shape evaluated at location $\vec{x}$ on the panel. $M_\imath$ is the modal mass of the $\imath$th acoustic mode, given by:

$$M_\imath = \int_V \rho_o\, \phi_\imath^2(\vec{r})\, d\vec{V} \qquad (3.21)$$

and, as damping is included, $\kappa_\imath$ is the $\imath$th complex eigenvalue of the cavity, where the cavity has a wall admittance β such that:

$$\nabla^2\phi_\imath + \kappa_\imath^2\phi_\imath = 0 \quad \text{in the cavity} \qquad (3.22)$$

$$\frac{\partial\phi_\imath}{\partial z} + ik\beta\phi_\imath = 0 \quad \text{on the structure/fluid boundary} \qquad (3.23)$$

where z denotes the direction normal to the surface. (Here continuity of the surface and particle velocities at the structure/fluid boundary is assumed, and positive z is defined as pointing into the acoustic enclosure). It should be noted that while the inclusion of acoustic damping in this manner is not mathematically rigorous (as the Green's function assumes a rigid walled boundary condition), it is commonly done with little error provided that the magnitude of the damping is not sufficient to alter the rigid walled mode shapes significantly (Fahy, 1985).

The pressure $p_i(\vec{x}')$ at the inner surface of the enclosure can be expressed in terms of the *in vacuo* structural mode shape functions according to:

$$p_i(\vec{x}') = \sum_{j=1}^{\infty} m(\vec{x}')\, \dot{v}_j\, \psi_j(\vec{x}') \qquad (3.24)$$

Substituting this expression into the original governing equations, it can be shown (in Appendix 1 at the end of this thesis and in Pope, 1971) that, for the r^{th} structure mode:

$$\left\{ i\,(\rho_o c_o)^2\, S^2 \omega \left\{ \sum_{l=1}^{\infty} \frac{B_{l,r}\, B_{l,r}}{M_l Z_l} \right\} + i\, \frac{M_r Z_r}{\omega} \right\} v_r + \sum_{j=1,\neq r}^{\infty} i\,(\rho_o c_o)^2\, S^2 \omega \left\{ \sum_{l=1}^{\infty} \frac{B_{l,r}\, B_{l,j}}{M_l Z_l} \right\} v_j = -\gamma_{r,p} \qquad (3.25)$$

where S is the surface area of the structure, and $B_{l,j}$ is the coupling coefficient between the lth acoustic mode and jth structural mode, defined as:

$$B_{\imath,j} = \frac{1}{S} \int_S \psi_j(\vec{x})\ \phi_\imath(\vec{x})\ d\vec{x} \tag{3.26}$$

and

$$Z_\imath = (\kappa_\imath^2 - k^2)\ c_o^2 \tag{3.27}$$

Thus, if the infinite sums over j and $\imath$ are replaced with a summation over n acoustic modes and m structural modes, the response of the structure to the external exciting pressure (primary source) can be represented in matrix form as:

$$[V_p] = [Z_I]^{-1}\,[\Gamma_p] \tag{3.28}$$

where $[Z_I]$ is the (mxm) structural modal input impedance matrix, whose terms are:

$$\text{diagonal: } z_{j,j} = \left[i(\rho_o c_o)^2\, S^2 \omega \sum_{\imath=1}^{n} \frac{B_{\imath,j} B_{\imath,j}}{M_\imath Z_\imath} \right] + \frac{iM_j Z_j}{\omega} \tag{3.29}$$

$$\text{off-diagonal: } z_{m,n} = i(\rho_o c_o)^2\, S^2 \omega \sum_{\imath=1}^{n} \frac{B_{\imath,m} B_{\imath,n}}{M_\imath Z_\imath} \tag{3.30}$$

and $[\Gamma_p]$ is the (mx1) matrix of modal generalized forces, whose jth element is:

$$\gamma_j = \int_S \psi_j(\vec{x}')\ p(\vec{x}')\ d\vec{x}' \tag{3.31}$$

As in the previous section, if measured surface velocity data are used, it is not strictly necessary to perform a modal decomposition on the data to determine the interior sound pressures. It is, however, a suitable means of expressing the analytical problem as well as useful in providing intuitive information about optimal actuator / sensor arrangements.

Expanding the pressure in terms of the (cavity) acoustic modes, and the velocity in terms of the *in vacuo* structural modes, the induced acoustic pressure amplitude for the ith acoustic mode is:

$$p_i = \frac{i(\rho_o c_o)^2 S \omega}{M_i Z_i} \sum_{j=1}^{\infty} v_j B_{i,j} \qquad (3.32)$$

Again, approximating the infinite sums with summations over n acoustic modes and m structural modes, equation (3.32) can be written in matrix form as:

$$[P_{n,p}] = [Z_a] [V_p] \qquad (3.33)$$

where $[P_{n,p}]$ is the (nx1) matrix of (complex) acoustic pressure modal amplitudes, and $[Z_a]$ is the (nxm) matrix of modal internal radiation transfer functions, whose terms are:

$$z_{a_{n,m}} = \frac{i(\rho_o c_o)^2 S \omega}{M_n Y_n} B_{n,m} \qquad (3.34)$$

From this, the sound pressure at any point in the enclosure (under primary excitation) can be found using:

$$p_p(\vec{r}) = [\Phi]^T [P_{n,p}] \qquad (3.35)$$

where $[\Phi]$ is the (nx1) vector of acoustic mode shape functions evaluated at point $\vec{r}$.

3.4. MODELLING OF RESPONSE UNDER CONTROL SOURCE EXCITATION

Once the primary excited response of the structural or coupled structural/acoustic system has been characterized in terms of the normal modes of vibration, the effect of applying the

control sources can be considered. As stated previously, either vibration or acoustic sources may be used effectively to control sound radiation from vibrating structures. Vibration control sources affect the structural velocity distribution, whereas it is assumed here that the effect of acoustic control sources on the structural velocity distribution is negligible.

Before formulating the equations which will enable assessment of the achievable noise attenuation for a particular arrangement of the control sources and error sensors, the response of the structural or coupled structural/acoustic system due to the application of active control sources must be analysed. To do this, the use of vibration and acoustic control sources will be considered separately.

3.4.1. System response using vibration control sources

The response of the structural or coupled structural/acoustic system under the action of the vibration control (point) force(s) operating alone may be formulated using the approach outlined in the previous section.

The modal velocity amplitudes for a given forcing function may be determined for the case of radiation into free space from equation (3.11), and for the case of transmission into a coupled enclosure from equation (3.28), where the forcing function is included in the generalized force matrix. For a point control force at location $\vec{x}$, the jth modal generalized force is:

$$\gamma_{j,c} = \int_A \psi_j(\vec{x}') \; f \; \delta(\vec{x}' - \vec{x}) \; d\vec{x}' \qquad (3.36)$$

where the subscript c refers to the control source contribution, f is the complex amplitude of the control force, and $\delta(\vec{x}' - \vec{x})$ is a Dirac delta function. If L control sources are used, the total generalized force can be found from the superposition of the individual forcing functions:

$$\gamma_{j,c_{tot}} = \sum_{i=1}^{L} \int_A \psi_j(\vec{x}') \; f_i \; \delta(\vec{x}' - \vec{x}_i) \; d\vec{x}' \qquad (3.37)$$

If m structural modes are considered, the modal generalized force (for the application of vibration control sources) can be re-expressed as a product of two sub-matrices:

$$[\Gamma_c] = [\Psi_c] \; [F_c] \qquad (3.38)$$

where $[\Gamma_c]$ is the (mx1) modal generalized force matrix for the control sources, $[\Psi_c]$ is the (mxL) matrix of m structural mode shape functions evaluated at the L control source locations, and $[F_c]$ is the (Lx1) matrix of complex control force amplitudes.

For the case of radiation into free space, the sound pressure produced at some point in the farfield due to the vibration control sources operating alone is found by combining equations (3.11), (3.16), and (3.38):

$$\begin{aligned} p_c(\vec{r}) &= [Z_{rad}]^T \; [Z_I]^{-1} \; [\Gamma_c] \\ &= [Z_{rad}]^T \; [Z_I]^{-1} \; [\Psi_c] \; [F_c] \end{aligned} \qquad (3.39)$$

For transmission into a coupled enclosure, the internal sound pressure at location $\vec{r}$ is found by combining equations (3.28), (3.33), (3.35), and (3.38):

$$p_c(\vec{r}) = [\Phi]^T [Z_A] [Z_I]^{-1} [\Gamma_c]$$

$$= [\Phi]^T [Z_A] [Z_I]^{-1} [\Psi_c] [F_c] \qquad (3.40)$$

3.4.2. System response using acoustic control sources

As acoustic control sources have a negligible effect upon the structural velocity distribution, the previously outlined structural and coupled structural/acoustic analysis is not needed; only the acoustic environment needs to be considered.

Firstly, consider the case of periodic sound radiation into free space. If monopole sound sources are used as control sources, the sound pressure radiated by each can be determined by considering the Green's function of the source and its mirror image (due to reflection by the radiating surface), defined in equation (3.15):

$$p_c(\vec{r}) = i \rho_o \omega Q G_a(\vec{x}_s|\vec{r}) + i \rho_o \omega Q G_a(\vec{x}_i|\vec{r}) \qquad (3.41)$$

where Q is the volume velocity of the source, and subscripts $_s$ and $_i$ denote the location of the source and the mirror image, respectively. This can be expanded to:

$$p_c(\vec{r}) = \frac{i\rho_o \omega Q}{4\pi} \left(\frac{\exp(-ikR_s)}{R_s} + \frac{\exp(-ikR_i)}{R_i} \right) \qquad (3.42)$$

If L control sources are used, the superposition of the sound pressures radiated by each of the sources is given by:

$$p_c(\vec{r}) = \sum_{j=1}^{L} \frac{i\rho_o \omega Q_j}{4\pi} \left(\frac{\exp(-ikR_{j,s})}{R_{j,s}} + \frac{\exp(-ikR_{j,i})}{R_{j,i}} \right) \qquad (3.43)$$

This can be expressed in matrix form as:

$$p_c(\vec{r}) = [Z_{mono}]^T [Q_c] \qquad (3.44)$$

where $[Z_{mono}]$ is the (Lx1) control source radiation transfer function vector, whose jth element is:

$$z_{mono_j} = \frac{i\rho_o\omega}{4\pi} \left(\frac{\exp(-ikR_{j,s})}{R_{j,s}} + \frac{\exp(-ikR_{j,i})}{R_{j,i}} \right) \qquad (3.45)$$

and $[Q_c]$ is the (Lx1) matrix of complex control source volume velocities.

Consider the case of sound transmission into an enclosure. If monopole sound sources are used as control sources inside the enclosure, the sound pressure at any point $\vec{r}$' in the enclosure due to one control source is given by:

$$p_c(\vec{r}') = i\rho_o\omega \, Q \, G_a(\vec{r}|\vec{r}') \qquad (3.46)$$

where $G_a(\vec{r}|\vec{r}')$ is the Green's function of the acoustic space, as defined in equation (3.20). If L control sources are used, the superposition of the sound pressures radiated by the sources is given by:

$$p_c(\vec{r}') = \sum_{j=1}^{L} i\rho_o\omega \, Q_j \, G_a(\vec{r}|\vec{r}_j') \qquad (3.47)$$

This can also be expressed in the matrix form as:

$$p_c(\vec{r}') = [Z_{mono}]^T [Q_c] \qquad (3.48)$$

where the jth element of the control radiation transfer matrix, $[Z_{mono}]$, is:

$$z_{mono_j} = i\rho_o\omega \, G_a(\vec{r}|\vec{r}') \qquad (3.49)$$

3.5. DETERMINATION OF THE OPTIMUM CONTROL SOURCE AMPLITUDES AND PHASES USING QUADRATIC OPTIMIZATION THEORY

When assessing the performance achievable using a given arrangement of the control sources and error sensors for an active noise control system, two criteria must be considered; how much control can be achieved using the given active source placement, and how close to this value will be the actual attenuation if the sound field is minimized at the given error sensing locations. As the acoustic pressure at any point $\vec{r}$ is a linear function of control force or volume velocity, quadratic optimization theory can be used as a mathematical tool in the assessment of both of these criteria. This involves expressing the square of the radiated acoustic pressure amplitude as a quadratic function of the variable of interest (control force or volume velocity), differentiating with respect to that variable, and setting the result equal to zero to find the optimum value of the variable. For a given control source arrangement, this procedure can be used either to determine the required control source volume velocities or forces to achieve a minimum sound pressure at a number of specified error sensing locations, or, alternatively, to determine the required control source volume velocities or forces to minimize the total radiated sound power or acoustic potential energy. Using the control forces or volume velocities so determined, the effectiveness of the specified source arrangement can be evaluated by comparing the achievable reduction of total radiated sound power or acoustic potential energy with the desired reduction. The effectiveness of the specified error sensor arrangement can be evaluated by comparing the reduction in sound power or acoustic potential energy achieved

by minimizing the sum of the squared sound pressures at each error sensor with the maximum reduction achievable with the given control source arrangement.

The problem of minimizing the sound pressure at a discrete point or points will be considered first. From equation (3.4) it can be deduced that the total sound pressure squared at any point in the acoustic field is a quadratic function of the pressure produced by the control source(s). Assuming that the acoustic control sources have an infinite internal impedance (constant volume velocity sources), or that the vibration control sources have a negligible internal impedance (constant force sources), equation (3.4) can be re-expressed in terms of the complex forces for the vibration control sources, or in terms of the complex source volume velocities for acoustic control sources. The preceeding assumptions are usually closely approximated by common acoustic sources and vibration sources such as electro-magnetic, magnetostrictive, piezoelectric ceramic, or electro-dynamic actuators. The assumptions imply that for the case of vibration control sources, the force output of the primary and control sources is unaffected by the other forces acting on the panel. For acoustic control sources, the assumption is that the primary and control source volume velocities are unaffected by the presence of other sound fields.

Consider firstly the sound pressure produced by the primary noise source operating alone. For the case of sound radiation into free space, this is found by combining equations (3.11) and (3.16):

$$p_p(\vec{r}) = [\, Z_{rad} \,]^T [\, V_p \,] = [\, Z_{rad} \,]^T [\, Z_I \,]^{-1} [\, \Gamma_p \,] \quad (3.50)$$

For the case of sound transmission into a coupled enclosure, the primary source sound pressure is found by combining equations (3.28), (3.33), and (3.35):

$$p_p(\vec{x}) = [\Phi]^T [Z_A] [V_p]$$

$$= [\Phi]^T [Z_A] [Z_I]^{-1} [\Gamma_p] \qquad (3.51)$$

Consider now the use of vibration control sources. For radiation into free space, the sound pressure produced at some point in the farfield due to the control sources operating alone is given in equation (3.39). For transmission into a coupled enclosure, it is given in equation (3.40). Using these equations and equations (3.50) and (3.51), the quadratic function of equation (3.4) can be re-expressed in terms of the control force input matrix, and expanded to include $\imath$ sensing locations:

$$\sum_{i=1}^{\imath} p_i^2 = [F_C]^H[a][F_C] + [F_C]^H[b] + [b]^H[F_C] + [c] \qquad (3.52)$$

where p_i^2 is the squared sound pressure amplitude at the i^{th} sensing location, and ^{H} denotes the hermitian of the matrix (transpose of the complex conjugate). For radiation into free space:

$$[a] = [\Psi_C]^H \{[Z_I]^{-1}\}^H [A] [Z_I]^{-1} [\Psi_C] \qquad (3.53)$$

$$[A] = [Z_r]^* [Z_r]^T \qquad (3.54)$$

$$[b] = [\Psi_C]^H \{[Z_I]^{-1}\}^H [A] [V_p] \qquad (3.55)$$

$$[c] = [V_p]^H [A] [V_p] \qquad (3.56)$$

where $[Z_r]$ is the (1 x $\imath$) column vector of modal radiation impedance transfer vectors, $[Z_{rad}]$, (defined in equation (3.17)) to the $\imath$ error sensing locations.

For transmission into an enclosure, the same equations apply, with the exception that [A] is now equal to:

$$[A] = [Z_A]^H [\Phi_e]^* [\Phi_e]^T [Z_A] \qquad (3.57)$$

where $[\Phi_e]$ is the (1 x n) column vector of acoustic mode shape function vectors, $[\Phi]$, (defined after equation (3.35)) evaluated at the $\imath$ error sensing locations.

The quadratic function given in equation (3.52) has a unique (global) pressure minimum. The "optimum" control force matrix which will produce this minimum for a given actuator position is (Nelson et al, 1985, 1987):

$$[F_c]_{opt} = -[a]^{-1} [b] \qquad (3.58)$$

producing the minimum sum of the squared error location sound pressures:

$$\sum_{i=1}^{\imath} p_i^2 \Big|_{min} = [c] - [b]^H [a]^{-1} [b] \qquad (3.59)$$

A similar solution can be found for acoustic control sources. For radiation into free space, the sound pressure at any point in the farfield due to the acoustic control sources acting alone is given by equation (3.44). For sound transmission into a coupled enclosure, the sound pressure at any point in the acoustic space due to the interior acoustic control sources acting alone is given by equation (3.48). It should be noted that these equations differ only in the elements of the control source radiation transfer matrix. Using the above mentioned equations, and equations (3.50) and (3.51), the quadratic function of equation (3.4) can be re-expressed in terms of the control source volume velocity matrix:

$$\sum_{i=1}^{\imath} p_i^2 = [Q_c]^H [a] [Q_c] + [Q_c]^H [b] + [b]^H [Q_c] + [c] \qquad (3.60)$$

where:

$$[a] = [Z_m]^* [Z_m]^T \tag{3.61}$$

$$[b] = [Z_m]^* [Z_r]^T [V_p] \tag{3.62}$$

$$[c] = [V_p]^H [Z_r]^* [Z_r]^T [V_p] \tag{3.63}$$

and $[Z_m]$ is the $(1 \times \imath)$ column vector of control source radiation transfer vectors, $[Z_{mono}]$, (defined in equation (3.45)) to the $\imath$ error sensing locations. As stated previously, the only difference between the expressions for sound radiation into free space and sound transmission into an enclosure are the elements of $[Z_m]$.

Following the same procedure as used for vibration control sources, the "optimum" control source volume velocity matrix is (Nelson et al, 1985, 1987):

$$[Q]_{opt} = -[a]^{-1} [b] \tag{3.64}$$

producing the minimum sum of squared error location sound pressures:

$$\sum_{i=1}^{\imath} p_i^2 \Big|_{min} = [c] - [b]^H [a]^{-1} [b] \tag{3.65}$$

The procedure for calculating the control source volume velocity or force matrix that minimizes the acoustic power related functions outlined in the previous section is much the same as that outlined for minimizing the sound pressure at a discrete point or points. The difference is that the matrices [a], [b], and [c] must be modified to include the surface integration necessary in sound power calculations. For radiation into free space, the modification is:

$$[a_{opt}] = \int_0^{2\pi} \int_0^{\pi/2} \frac{[a]}{2\rho_o c_o} |\vec{r}|^2 \sin\theta \, d\theta \, d\phi \tag{3.66}$$

The same relationship applies for [b] and [c].

For control of sound transmission into an enclosure, these become:

$$[a_{opt}] = \int_V \frac{[a]}{2\rho_o c_o^2} d\vec{x} \qquad (3.67)$$

Again, the same relationships hold for [b] and [c].

It should be noted that the "optimal" control forces or volume velocities that produce a pressure minimum at the acoustic "error" sensing locations are not necessarily optimal from the standpoint of minimizing the radiated acoustic power error criteria.

3.6. OPTIMIZATION OF THE CONTROL SOURCE / ERROR SENSOR PLACEMENT AND PROBLEMS WITH THE QUADRATIC OPTIMIZATION THEORY APPROACH

Equations (3.52) and (3.60), formulated using quadratic optimization theory, allow the determination of the control forces or volume velocities, for a given control source arrangement, which minimize the sound pressure at a point or points. Using the integrations of equations (3.66) and (3.67), the forces or volume velocities that minimize the total radiated sound power or acoustic potential energy can also be found. Knowing these forces or volume velocities, numerical integration can then be used to find the actual decrease in the acoustic power flow quantities for a given control source or control source / error

microphone arrangement. This procedure can be used to assess the performance of a given arrangement of control sources and error sensors.

Increasing the number of control sources will generally increase the levels of acoustic power flow reduction that can be achieved. This is not, however, a linear process. Often a few strategically placed control sources will provide levels of sound attenuation comparable to a large array of "randomly placed" sources. (Note that this is different from modal control, where it is often stated that one control source is needed per mode (albeit for mathematical simplicity (Meirovitch et al, 1983)); as will be shown in chapter 4, for a lightly damped structure, even a single control source can often provide substantial levels of sound attenuation.) If the complexity of the electronic control system required to drive the specified number of sources and sensors and the practicality of providing the control effort (in terms of force or volume velocity) is incorporated into the assessment criteria, then it will usually be concluded that the former (sparse) control source arrangement is superior.

However, for a given number of control sources it is often difficult to determine the optimum placement. This must be done on a "trial and error" basis using a numerical search routine (such as described in Press et al, 1986), using the previously discussed maximum acoustic power flow reductions as error criteria. This highlights one problem associated with the previously outlined analytical approach; that is, the extensive computational requirements for assessing the quality of a given control source placement. For free space radiation four numerical integrations are required, while for enclosure transmission six numerical integrations are required. The integrals of equations (3.66) and (3.67) are not

only a large computational load, but may also be difficult to evaluate for multiple control sources.

Once the control source arrangement has been specified, the problem remains of determining the optimum number and location of error sensors. Generally, there must be at least as many error sensors as control sources to satisfy observability / controllability requirements. More error sensors result in the achievable sound power or potential energy reduction being closer to the maximum achievable with the particular control source arrangement. However, as with the control sources, this is not a linear process. It is often more efficient (when the electronic controller performance is taken into consideration) to use a few optimally placed error sensors than a random array. If the number of error sensors is specified, then their optimum locations can be found using a numerical search routine, again a time consuming process using standard quadratic optimization theory.

With these limitations, it is clear that an alternative procedure is needed for the formulation of a practical design methodology.

3.7. DETERMINATION OF THE OPTIMUM CONTROL SOURCE AMPLITUDES AND PHASES USING MULTIPLE REGRESSION

One alternative method to quadratic optimization, which can overcome these problems, is multiple regression. This is a generalized linear least-squares technique, where several independent variables are used to predict the dependent variable of interest. Here the dependent variable of interest is the 180° inverse of the primary sound field (which will

provide the greatest level of acoustic power flow attenuation), while the independent variables are the control source transfer functions and volume velocities or forces.

Referring to equations (3.1) and (3.2), it can be concluded that minimization of the acoustic power error criterion, used for determining the maximum possible attenuation with a given control source arrangement, is equivalent to minimizing the average squared sound pressure over a hemisphere enclosing the source for free-field radiation, or the average square sound pressure in the enclosed volume for the case of sound transmission into an enclosure.

The power related error criterion using a finite number of points is thus equivalent to minimizing:

$$\sum_{i=1}^{N} \left[p_{p,i} + p_{c,i} \right]^2 \qquad (3.68)$$

where the number of points N should be chosen so that equation (68) is representative of the radiated acoustic power or acoustic potential energy as the case may be. For vibration control sources, the control generated sound pressure at any point i can be expressed as:

$$p_{c,i} = [Z_{vt,i}]^T [F] \qquad (3.69)$$

where:

$$[Z_{vt,i}]^T = [Z_{rad}]^T [Z_I]^{-1} [\Psi_c] \qquad (3.70)$$

for free space radiation, and

$$[Z_{vt,i}]^T = [\Phi]^T [Z_a] [Z_I]^{-1} [\Psi_c] \qquad (3.71)$$

for transmission into an enclosure.

For acoustic control sources, $p_{c,i}$ is defined by equations (3.44) or (3.48). The primary generated sound pressure can either be calculated using the previously outlined analytical methods, or measured *in situ*.

Substituting these relations into equation (3.68), and introducing a measurement error, σ, the optimization criterion for vibration control sources is that the following expression should be minimized:

$$\sum_{i=1}^{N} \left(\frac{p_{p,i} + \sum_{j=1}^{L} z_{vt_{j,i}} f_j}{\sigma_i} \right)^2 \qquad (3.72)$$

and for acoustic control sources, the following should be minimized:

$$\sum_{i=1}^{N} \left(\frac{p_{p,i} + \sum_{j=1}^{L} z_{mono_{j,i}} q_j}{\sigma_i} \right)^2 \qquad (3.73)$$

where the subscripts $_{j,i}$ denote the transfer function between the jth control source and the ith measurement point. Expressions (3.72) and (3.73) can be written in matrix form. For vibration control sources, expression (3.72) becomes:

$$| [Z_v][F] - [-P_p] | \qquad (3.74)$$

and for acoustic control sources, expression (3.73) becomes:

$$| [Z_{mn}][Q] - [-P_p] | \qquad (3.75)$$

where the matrix elements are given by:

$$-P_{p_i} = \frac{-p_{p,i}}{\sigma_i} \tag{3.76}$$

$$z_{v_{i,j}} = \frac{z_{vt_{i,j}}}{\sigma_i} \tag{3.77}$$

$$z_{mn_{i,j}} = \frac{z_{mono_{i,j}}}{\sigma_i} \tag{3.78}$$

Equations (3.74) and (3.75) can be solved by various methods, such as by the use of singular value decomposition, or by using one of many commercially available multiple regression software packages. The control forces and/or control volume velocities that result are those which are optimal (those which minimize the power flow) for the given control source positions. Note also that a combination of acoustic and vibration control sources can be optimized in the same manner.

The level of power attenuation achieved using active noise control can be estimated as:

$$\Delta W = -10 \log_{10} \left[\frac{\sum_{i=1}^{N} (p_{p,i} + p_{c,i})^2}{\sum_{i=1}^{N} (p_{p,i})^2} \right] \tag{3.79}$$

From equations (3.74) and (3.75), it can be seen that the control source sound pressure, $p_{c,i}$, desired is actually the estimated inverse of the primary source sound pressure, $-p_{p,i}$. Therefore, equation (3.79) can be written as:

$$\Delta W = -10 \log_{10} \left[\frac{\sum_{i=1}^{N} (p_{p,i} - p'_{p,i})^2}{\sum_{i=1}^{N} (p_{p,i})^2} \right] \qquad (3.80)$$

where ' denotes estimate. For periodic sound, the mean (complex) sound pressure is zero (for both the real and imaginary parts). Thus, equation (3.80) can be expressed as:

$$\Delta W = -10 \log_{10} \left[\frac{\sum_{i=1}^{N} (p_{p,i} - p'_{p,i})^2}{\sum_{i=1}^{N} (p_{p,i} - \bar{p}_{p,i})^2} \right] \qquad (3.81)$$

The denominator of equation (3.81) is equivalent to the sum of the squares of the measured dependent variable, SS_p, while the numerator is equivalent to the sum of squares of the residuals, SS_{res} (Tabachnick and Fidell, 1989). Using this, the estimated acoustic power reduction for the given control source arrangement can be written:

$$\Delta W = -10 \log_{10} \left[\frac{SS_{res}}{SS_p} \right] \qquad (3.82)$$

$$= -10 \log_{10} (1 - R^2) \qquad (3.83)$$

where R is the multiple correlation coefficient (Tabachnick and Fidell, 1989). Therefore, the multiple correlation coefficient can be used to estimate the acoustic power reduction under optimum control for a given control source arrangement. As the number of measurement points increases, so does the accuracy of the estimate. For a very large number of points, this method becomes equivalent to the integration methods of the previous section for determining the optimum control source volume velocities or forces for a given control source and error sensor arrangement. The main advantages of this method

are the speed of calculation, and the ability to easily incorporate combined vibration and acoustic control sources. This makes it well suited to practical implementation in a multi-dimensional optimization routine. It should be noted that this technique is also suitable for determining the control source volume velocities or forces which minimize the sum of the squared sound pressure at a specific point or points. In this case, only the error sensing locations would be used as measurement points in the equations.

One point to note concerning the implementation of the outlined multiple regression routine is that the majority of terms (acoustic pressures, forces, volume velocities, and impedances) are complex, and therefore cannot be directly incorporated into a commercial package. Rather, the real and imaginary components of the acoustic pressure at each location must be considered separately, doubling the size of the problem. Consider, for example, equation (3.77). For one pressure point and one control source, this can be written as

$$(z_{vR} + iz_{vI})\ (F_R + iF_i) = (-P_{pR} - i\ P_{pI}) \qquad (3.84)$$

where the subscripts $_R$ and $_I$ refer to real and imaginary components, respectively. Equation (3.84) can be written in a matrix form suitable for implementation as

$$\begin{bmatrix} z_{vR} & -z_{vI} \\ z_{vI} & z_{vR} \end{bmatrix} \begin{bmatrix} F_R \\ F_I \end{bmatrix} = \begin{bmatrix} -P_{pR} \\ -P_{pI} \end{bmatrix} \qquad (3.85)$$

Thus, to implement the multiple regression routine with complex numbers, the problem can be separated into real and imaginary components as in equation (3.85), and the problem simply becomes twice as big.

There is one other advantage to using multiple regression which will become apparent in the next chapter (chapter 4). It will be shown there that the optimum error microphone locations are at the points of minimum sound pressure in the optimally controlled residual sound field. These points can be determined directly using a commercial multiple regression package. These packages usually produce, as part of their output data, a vector of residuals. These residuals are the difference between the measured quantity (pressure here), and the value predicted by the regression equation. The point of minimum acoustic pressure in the residual sound field will be the point with the smallest residual value.

3.8. SUMMARY

Analytical models have been presented that allow the assessment of the optimum performance acheivable with a particular physical arrangement of control sources and error sensors for actively controlling sound radiation from vibrating structures. The analytical techniques can be used with either acoustic or vibration control sources, and for either transmission into an enclosure or sound radiation into free space. Only the transfer functions change. The required terms can be determined analytically for simple systems, or numerically or experimentally for more complex ones. The models can be used to formulate the error criteria for use in a multi-dimensional optimization routine for determination of the "best" control source / error sensor location(s).

CHAPTER 4.

THE ACTIVE CONTROL OF SOUND RADIATION FROM A RECTANGULAR PANEL INTO FREE SPACE

4.1 INTRODUCTION

In the previous chapter (3), generalized analytical models were developed that could be implemented in a numerical search routine to optimize the physical control system parameters for controlling periodic sound radiation from planar surfaces into free space and for controlling sound transmission into weakly coupled enclosed spaces. This chapter is concerned with the first of these models, examining the active control of periodic sound radiation from a planar surface into free space.

There are three aims to the work presented in this chapter. The first is to provide experimental data to verify the analytical models presented in chapter 3 concerned with applying active control to attenuate periodic sound radiation from a planar surface into free space. The second aim is to use the analytical models to examine the important physical noise control mechanisms, which are still not fully understood (Thomas et al, 1990). The third aim is to analytically examine the effects which physical system variables, such as control source and error sensor type and location, structure size, damping, and modal density, have upon the ability of the active system to attenuate the total radiated sound power. This third aim will lead to the development of a methodology for designing the physical part (arrangement of control sources and error sensors) of active noise control systems for this class of structural radiation problem.

To achieve these aims, the control of periodic sound radiation from a baffled, rectangular panel will be studied. This chapter first summarizes the equations necessary to specialize the generalized models of chapter 3 to this application. Following this, the physical control mechanisms will be outlined to provide a basis from which to view the experimental model verification and analytical studies, presented in the sections which follow.

4.2. EQUATIONS FOR THE RECTANGULAR PANEL

The general equations for modelling periodic sound radiation from a planar, vibrating structure into free space have been presented in the previous chapter. These same models will need to be specialized for a study of the active control of periodic sound radiation from a baffled rectangular panel. The following is a summary of the equations which are required for this application.

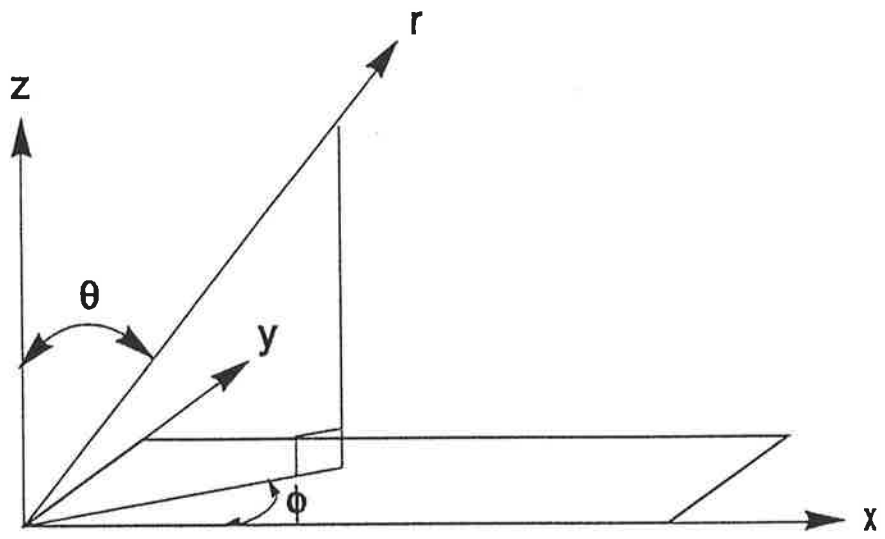

Figure 4.1 Panel geometry.

What is required initially is the mode shape function of the rectangular panel, which when referenced (x=y=0) to the panel lower left corner, is for mode number m,n:

$$\Psi_{mn} = \sin\left(\frac{m\pi x}{L_x} \right) \quad \sin\left(\frac{n\pi y}{L_y} \right) \qquad (4.1)$$

where L_x, L_y are the panel dimensions (the panel geometry is outlined in Figure 4.1).

The resonance frequencies (in radians per second) of these panel modes are found from the equation (Junger and Feit, 1982):

$$\omega_{mn} = \left(\frac{D}{\rho_s h} \right)^{0.5} \quad \left(\left(\frac{m\pi}{L_x} \right)^2 + \left(\frac{n\pi}{L_y} \right)^2 \right) \qquad (4.2)$$

where the bending stiffness, D, is given by:

$$D = EI = \frac{E\, h^3}{12\ (1-\nu)^2} \qquad (4.3)$$

and ρ_s is the structural material density, h is the panel thickness, E the modulus of elasticity, and ν the Poisson's ratio.

Using the mode shape of equation (4.1), the modal mass for mode (m,n) is:

$$M_{mn} = \int_S \rho_s h\, \Psi_{mn}^2\, dS = \rho_s h\, A / 4 \qquad (4.4)$$

where A is the panel area.

Finally, the sound pressure due to structural mode Ψ_{mn} at a point (r,θ,ϕ) in the farfield of the panel can be approximated by (Wallace, 1972):

$$p_{mn} = \frac{i\,\tilde{v}_{mn}\,k\,\rho_o c}{2\,\pi\,r}\,\exp(-ikr)\,\frac{L_x\,L_y}{mn\pi^2}\left[\frac{(-1)^m\exp(-i\alpha)-1}{\left(\frac{\alpha}{m\pi}\right)^2-1}\right]\cdot$$

$$\left[\frac{(-1)^n\exp(-i\beta)-1}{\left(\frac{\beta}{n\pi}\right)^2-1}\right] \qquad (4.5)$$

where

$$\alpha = k\,L_x\,\sin\theta\,\cos\phi \qquad (4.6)$$

$$\beta = k\,L_y\,\sin\theta\,\sin\phi \qquad (4.7)$$

$\tilde{v}_{mn}$ is the modal velocity amplitude, k is the acoustic wavenumber, and ρ_0 is the density of the fluid medium (air is being considered here). Note also that harmonic time dependence of the form ($e^{i\omega t}$) is assumed here.

4.3 OVERVIEW OF PHYSICAL NOISE CONTROL MECHANISMS

When the noise source to be quietened is a vibrating structure, either acoustic or vibration control sources can be used effectively in an active noise control system. Similar to the case of controlling plane wave sound propagation in an air handling duct, discussed in chapter 2, acoustic control sources provide a reduction in the total acoustic power flow by reducing the radiation impedance "seen" by both the vibrating structure and control source(s).

However, the physical noise control mechanisms involved when vibration control sources are used are more complex than those at work with the use of acoustic control sources. When vibration sources are used to control sound radiation from a vibrating structure, there are two

possible mechanisms by which attenuation of acoustic power flow can be achieved. The first is an increase in the input impedance of the primary offending structural modes, resulting in a decrease in their amplitude (modal control). The second is an alteration in the relative amplitudes and phases of the structural modes (modal rearrangement). This has two possible effects; the overall vibration levels of the structure can be reduced, and/or the radiation efficiency of the structure can be reduced. These two mechanisms, modal control and modal rearrangement, can coexist, and do so in varying degrees for the same structure when vibration control sources are attached at different locations.

These noise control mechanisms will be discussed in more depth in the sections that follow.

4.4 EXPERIMENTAL VERIFICATION OF ANALYTICAL MODELS

4.4.1 Experimental Arrangement

Experiments were conducted to verify the theory outlined in the preceding sections for the case of sound pressure minimization at a single point in the far field of the noise source using both acoustic and vibration control sources. The tests were undertaken in an anechoic chamber using a rectangular steel panel of (x,y) dimensions 380mm x 300mm mounted in a heavy steel frame. Two panel thicknesses, 2mm and 9.5mm, were used in the experiments. The steel panel was placed in the center of a large, rigid wooden baffle of dimensions 4.8m x 2.4m x 19mm thick as shown in figure 4.2. Simply supported boundary conditions were implemented by using thin shim spring steel strips. One edge of each strip was attached to an edge of the panel by glue and small set screws while the other edge was bolted to the heavy steel frame. This approach

gives a good approximation to the simply supported boundary condition as the shim is stiff for in-plane motion but flexible for rotation (Ochs and Snowden, 1975).

The panel was excited by a non-contacting electro-magnetic exciter (primary source) located 3mm from the plane of the panel, adjacent to the panel centre at the rear. This driver consisted of a copper coil wound around an iron core (connected to the driving amplifier) surrounded by a permanent magnet. When a vibration control source was used, the control force was applied using an electrodynamic shaker connected to the panel with a 6mm diameter by 250mm long aluminium rod as shown in figure 4.3. When acoustic control was used, each control source consisted of a horn driver attached to a 30 mm diameter tube with a 90 degree bend and a flare to 50mm at the open end, as shown in figure 4.4. This allowed the sound delivery to be positioned 20mm away from the face of the panel with the minimum possible interference to the acoustic field.

The panel response was measured by using 17 accelerometers placed in two lines along the panel. Modal decomposition of the panel response was conducted by fitting the simply supported mode shape functions to the data, using a method similar to that described in (Moore, 1979; Silcox and Lester, 1982). The radiated sound field was measured using a Bruel and Kjaer one-inch microphone mounted on an arm attached to a turntable. This rotated through 180° such that the microphone traversed a horizontal arc of 1.8m radius around the panel center (using the criteria in Beranek (1986, p.100), this is in the farfield, as will be evident by the uniformity of the radiation patterns to be presented), in a plane perpendicular to the plane of the panel, allowing the panel sound radiation directivity to be measured in one horizontal plane

with a single microphone. The measurements were recorded as a polar plot using a Bruel and Kjaer level recorder.

	0.38m x 0.3m x 1.96mm panel		0.38m x 0.3m x 9.5mm panel	
Mode	Theoretical Resonance (Hz)	Experimental Resonance (Hz)	Theoretical Resonance (Hz)	Experimental Resonance (Hz)
(1,1)	86.3	88	418.5	444
(2,1)	185.8	187	900.6	920
(1,2)	245.9	244	1191.9	1196
(2,2)	345.4	343	1674.0	1688
(3,1)	351.6	349	1703.9	1692
(3,2)	511.1	-	2477.4	-
(1,3)	511.9	501	2481.0	2456
(4,1)	583.6	581	2828.8	2796
(2,3)	611.3	595	2963.0	2928
(4,2)	743.0	732	3602.2	-

Table 4.1. Theoretical and experimental resonance frequencies.

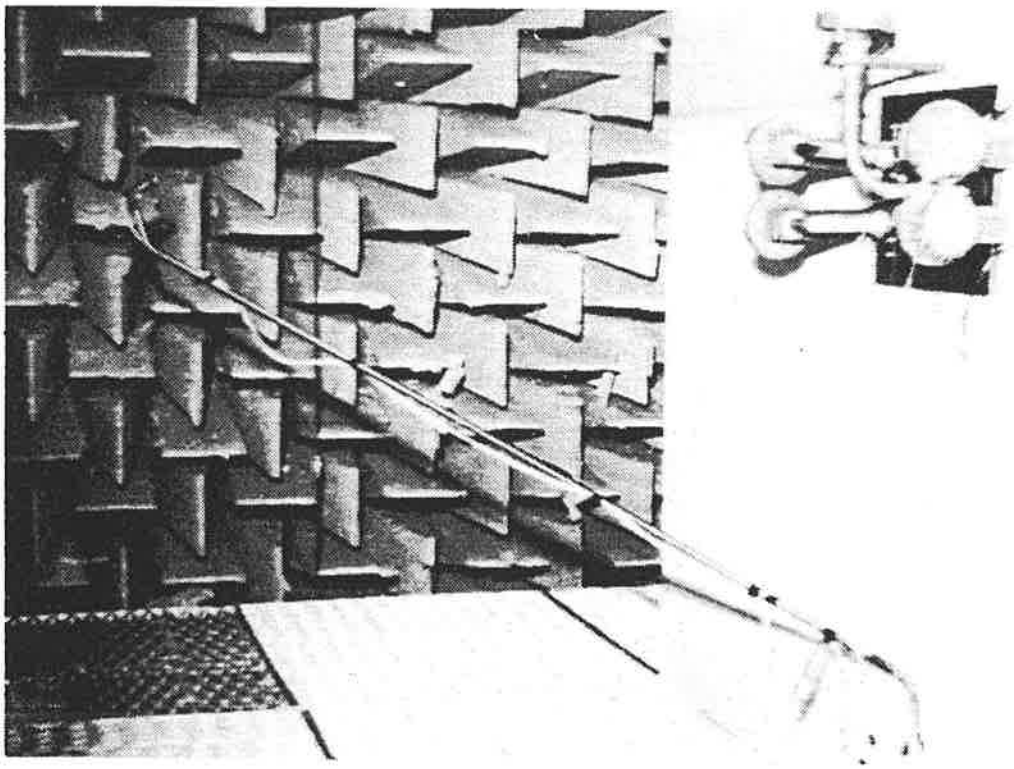

Figure 4.2 Experimental arrangement.

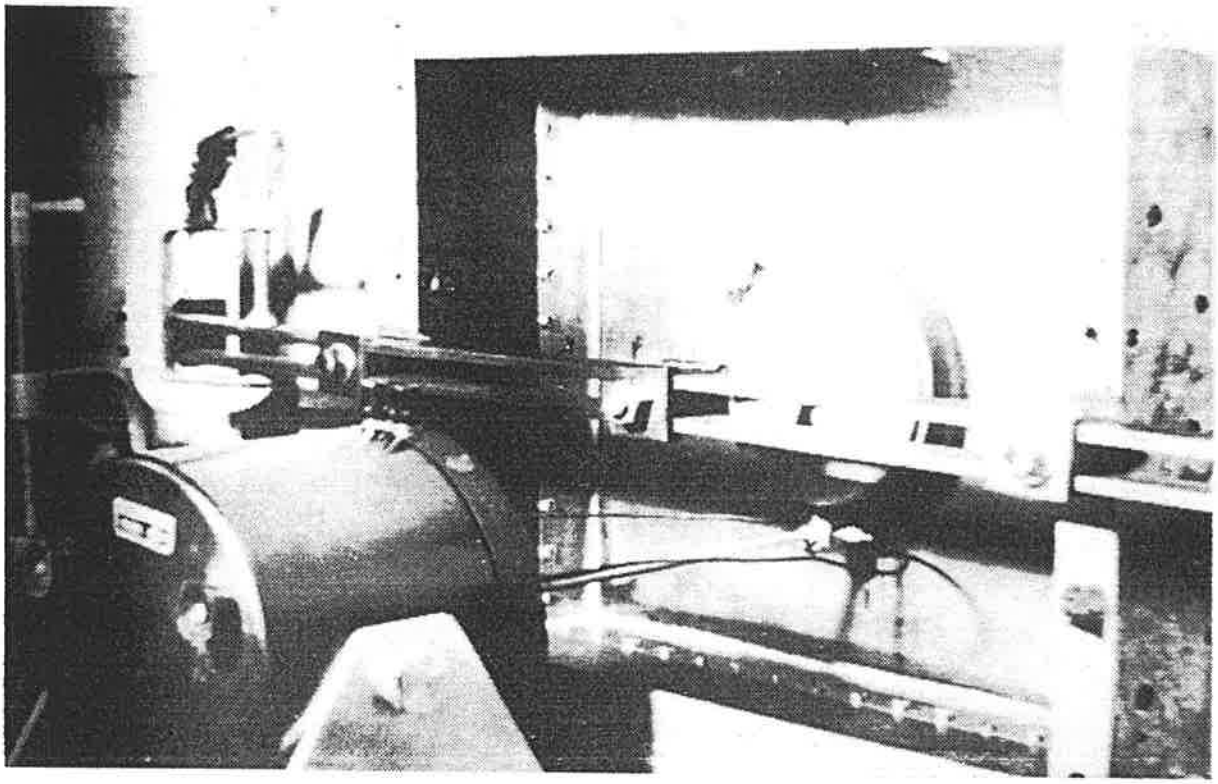

Figure 4.3 Vibration control arrangement.

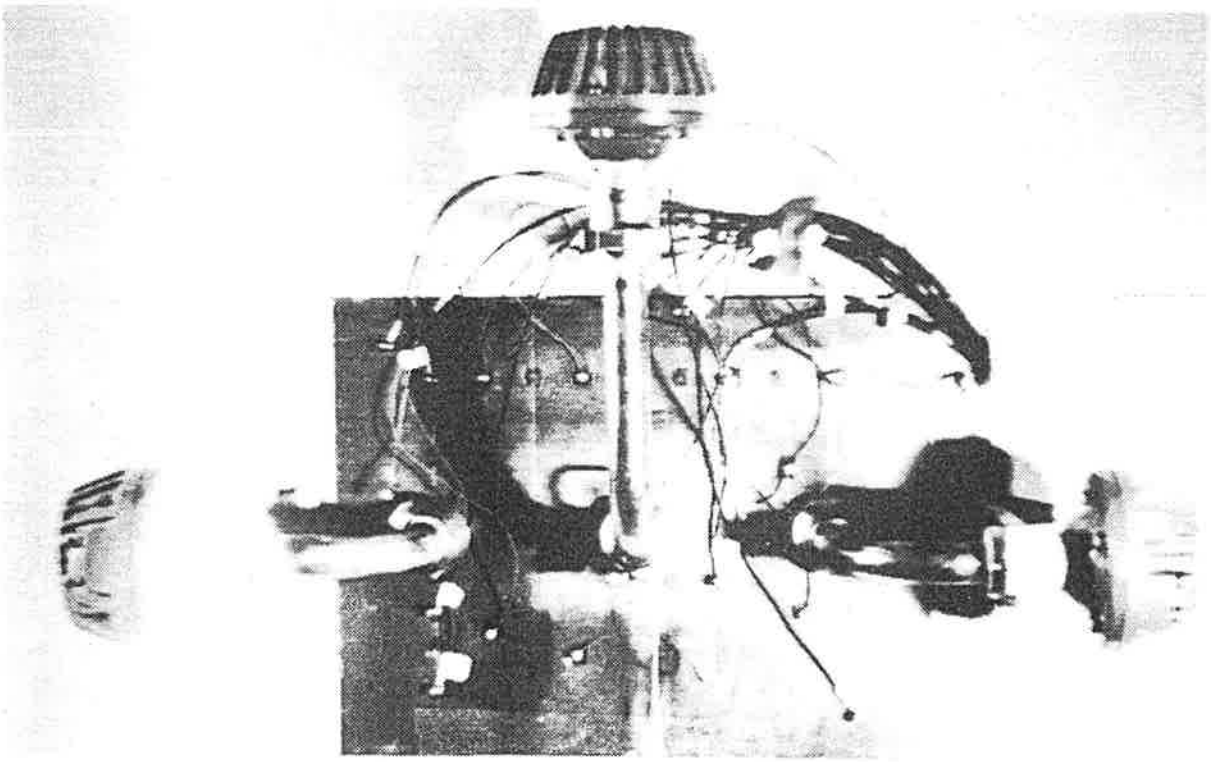

Figure 4.4 Acoustic control arrangement.

The electromagnetic exciter was driven by a pure tone reference signal. The same reference signal was used to drive the control source (vibrational or acoustic) after being fed through a separate power amplifier and manually operated phase shifter. With both the primary exciter and control source(s) operating simultaneously, the amplitude and phase of the driving signal to the control exciter was adjusted to produce a minimum sound pressure level at a particular position of the traversing microphone. The residual panel radiation field and plate response were then measured.

The theoretical sound pressure distributions were calculated using the analytical models of chapter 3, specialized by using the equations of section 4.2. The electro-magnetic actuator was modelled as a point force input at the panel center. This introduced some error into the results, as the forcing function contains a permanent distributed magnetic force component, as will be described later in this chapter. For the particular control source arrangement, the sound pressure level at the error microphone position was minimized using equation (3.58) for vibration control sources or equation (3.64) for acoustic control sources. The theoretical sound pressure plots were calculated from equation (3.16) for the primary source disturbance, and for the controlled sound field by evaluating equation (3.52) for vibration control sources, or equation (3.60) for acoustic control sources, at all points. The theoretical primary source structural modal amplitudes were calculated from equation (3.11) and the controlled results (for vibration sources) from adding to this the results obtained for the modal generalised force of equation (3.38). The theoretical resonance frequencies for the dominant structural modes used in these calculations are shown in Table 4.1, compared with the experimentally measured values. The modal loss factors of the panel were determined by examination of the resonance peaks (as the resonances are well spaced and the panel is lightly damped) on a spectrum

analyser. For convience, the average value of 0.039 so determined was used for all panel modes.

For ease of comparison, the theoretical results were normalized to best fit the experimental data. This was done by first matching the experimental and primary sound pressure fields by adding or subtracting some constant value from each of the theoretically calculated data points. This same value was then added or subtracted from the theoretical controlled levels, allowing a direct assessment of the ability of the theoretical model to predict the residual controlled sound field. (This procedure was necessary as it was not possible to measure the input force of the electromagnetic shaker, hence draw a comparison between predicted and measured primary source sound fields. However, as it is the ability to predict sound attenuation which is of interest here, this is not considered detrimental to the analysis.) Further, for the theoretical results presented, the sound pressure reduction at the error microphone was limited to a value comparable to that achieved experimentally, and not reduced to the maximum level theoretically possible, to better simulate the practical system. This was done by first completely analytically minimising the error location sound pressure(s) using equation (3.58) or (3.64), and then decreasing the amplitude of the complex control force or volume velocity (maintaining the optimum phase) until the desired levels of attenuation were reached. Finally, note that all of the radiation plots to be shown are in the centerline of the plate.

4.4.2 Vibration Control Sources

Initially, vibration control was applied to the 2mm thick panel, vibrating at 338 Hz, at a location of (x=0, y=-70)mm relative to the panel center. This frequency is slightly below the (2,2) and

(3,1) mode resonances, as shown in Table 3.1 (note that the (1,1) mode is the fundamental vibration mode of the panel). A plot of the theoretical and measured primary radiated and controlled residual sound pressure levels achieved by minimizing the sound pressure at an azimuthal angular location of 90° is given in Figure 4.5.

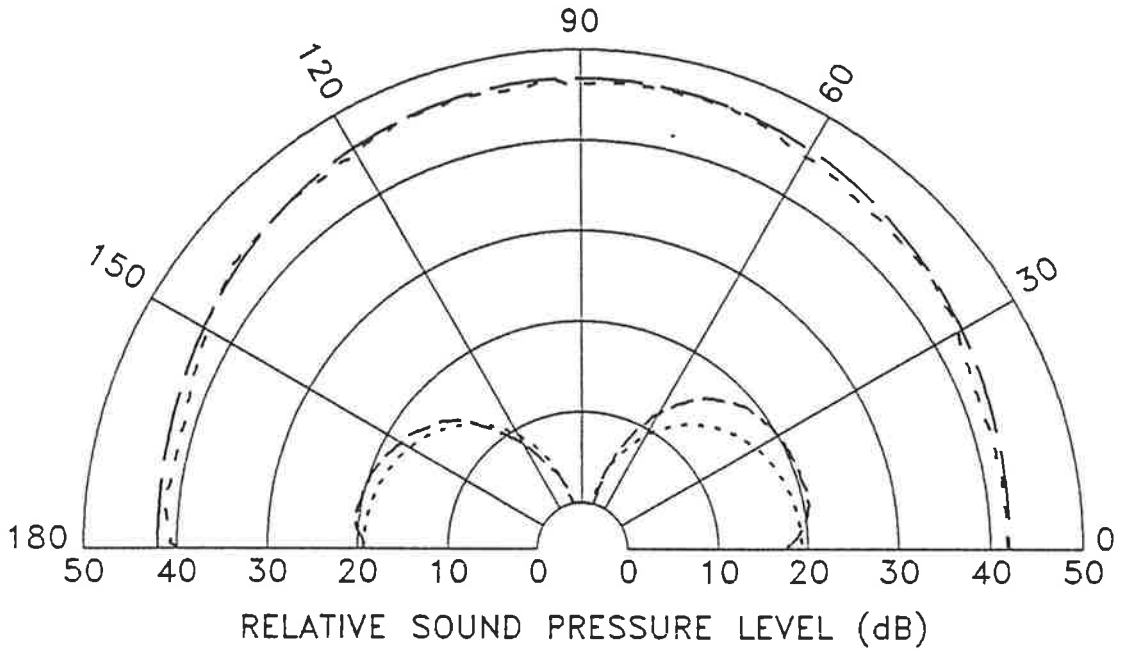

Figure 4.5 Radiation pattern from 2mm panel, 338 Hz, vibration control at (0,-70) mm, error sensor at 90°,—— = theoretical primary, - - = measured primary, - - - = theoretical controlled, — — = measured controlled.

In viewing figure 4.5, it can be seen that the general agreement between theory and experiment is good. There are two main sources of experimental error, however. The first is the mass loading effect caused by the asymmetric placement of the accelerometers. This has the effect of slightly skewing the radiation plot. The second source of error is the distributed nature of the primary forcing function, which has the effect of slightly reducing the levels of attenuation achieved. This effect will be discussed in more detail later.

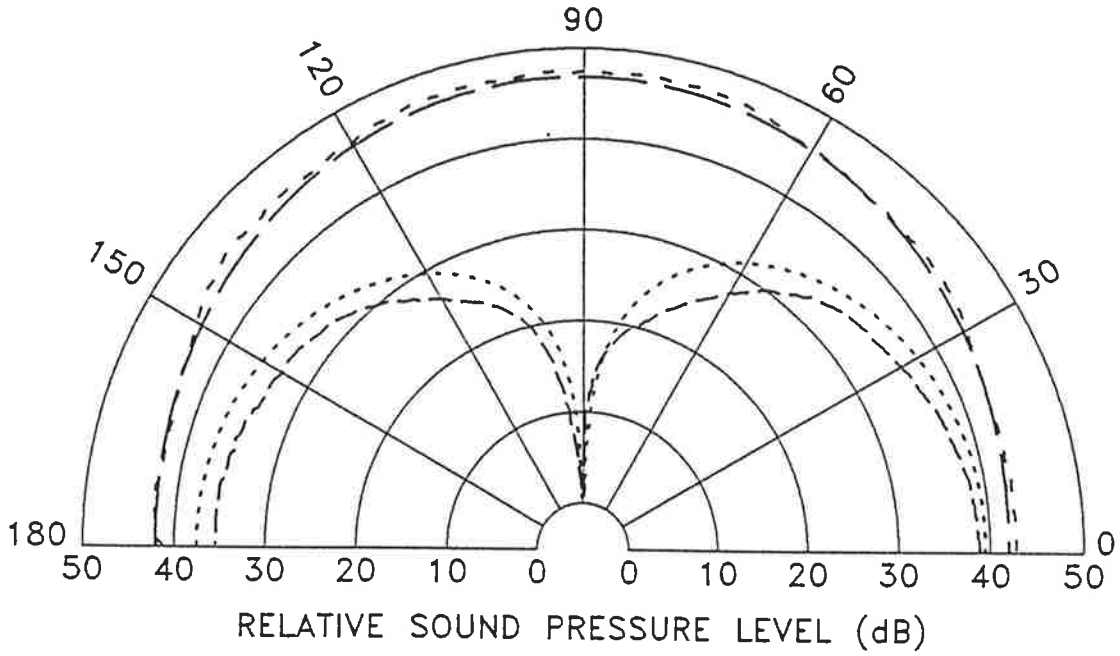

Figure 4.6 Radiation pattern from 2mm panel, 338 Hz, vibration control at (-150,0) mm, error sensor at 90°, ——= theoretical primary, - - = measured primary, - - - = theoretical controlled, — — = measured controlled.

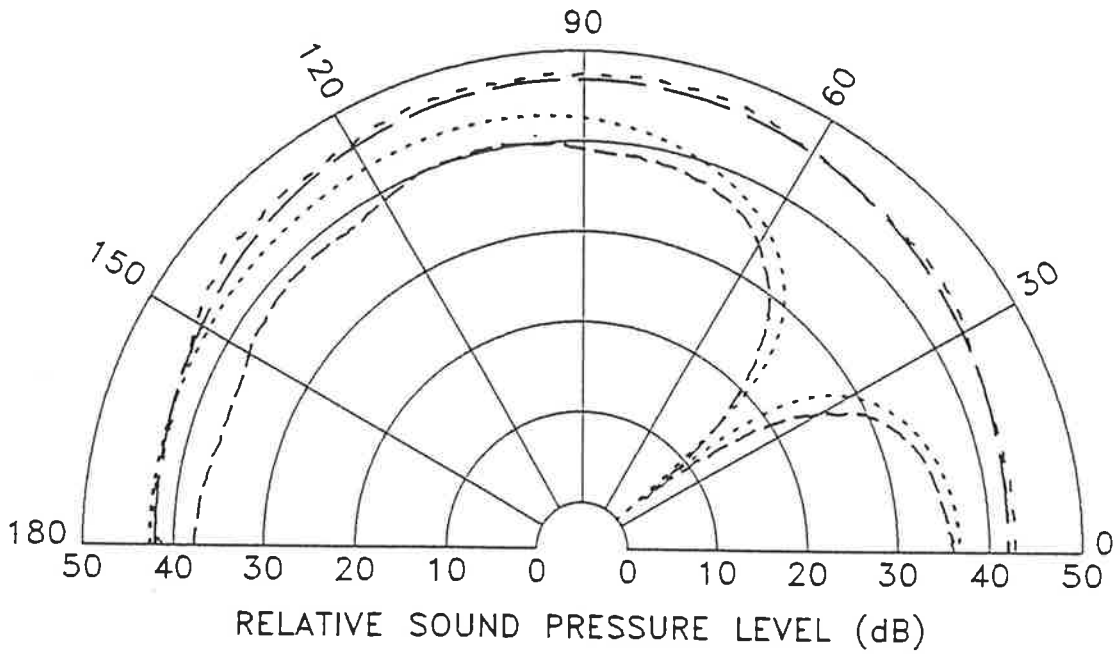

Figure 4.7 Radiation pattern from 2mm panel, 338 Hz, vibration control at (-150,0) mm, error sensor at 40°, ——= theoretical primary, - - = measured primary, - - - = theoretical controlled, — — = measured controlled.

Next, the vibration control source was moved to an (x,y) position of (-150,0) mm relative to the panel center. Plots of the theoretical and measured primary radiated and residual controlled sound fields generated by minimizing the sound pressure at an azimuthal angular location of 90° and 40°, are given in figures 4.6 and 4.7, respectively. In viewing these figures, it is again clear that the agreement between theory and experiment is good. However, a notable feature of both plots is that there is a 2 to 3 dB difference between the theoretical and measured residual sound fields, with the amplitudes of the measured residual sound fields being less than those predicted theoretically. This error is due predominantly to the distributed nature of the primary forcing function, as will be discussed shortly.

It is clear from viewing figures 4.5, 4.6, and 4.7 that significant levels of reduction in the total radiated sound power have been achieved, with the vibration control source at two different locations. As outlined in section 4.3, there are two possible mechanisms of control when vibration sources are used; modal control, where the amplitudes of the dominant radiating panel modes are reduced, and modal rearrangement, where the relative amplitudes and phases of the dominant panel modes are altered so as to reduce the overall radiation efficiency of the panel. These two mechanisms can coexist, and do so in varying degrees, for any given location of the vibration control application. It is useful, therefore, to examine the panel modal amplitudes associated with the radiation plots of figures 4.5 and 4.6.

Consider first the modal amplitudes resulting from the application of vibration control at (x=0, y=-70)mm, with the sound pressure minimized at 90° (associated with the radiation plot of figure 4.5), shown in figure 4.8. In viewing these it is clear that the principal mechanism here is one of modal amplitude control, where the amplitudes of the primary offending panel modes are

significantly reduced. The effect upon the modal amplitudes of applying vibration control at (x=-150, y=0)mm, and minimizing the sound pressure at 90° (corresponding to the radiation plot of

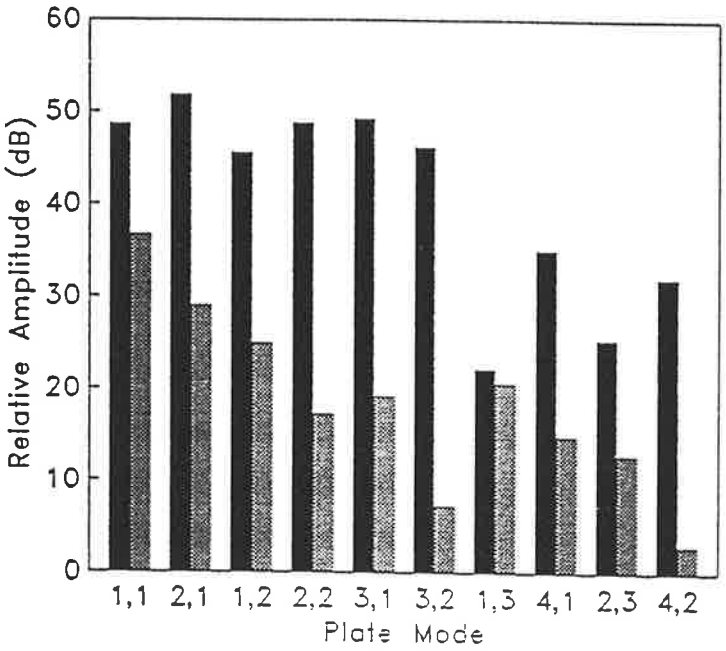

Figure 4.8 Measured modal amplitudes from 2mm panel, vibration control at (0,-70) mm, error sensor at 90°, ■ = primary, ▒ = controlled.

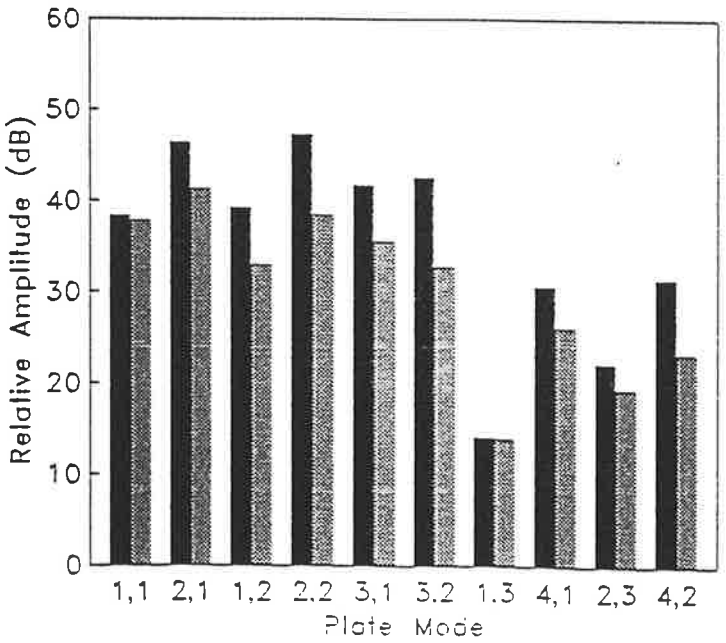

Figure 4.9 Measured modal amplitudes from 2mm panel, vibration control at (-150,0) mm, error sensor at 90°, ■ = primary, ▒ = controlled.

figure 4.6), shown in figure 4.9. In viewing figure 4.9, it can be seen that the amplitudes of the panel modes have not been reduced markedly. This is especially true of the (1,1) mode, which is one of the dominant radiators. To achieve the levels of radiated sound pressure (hence power) attenuation seen in figure 4.6, rearrangement of the modal phases must be the principal mechanism at work.

Before considering the theoretical results for the two cases, it will be useful to consider the effect of using a distributed primary source in the experiment, rather than a point force as modelled. The action of the permanent magnetic force will tend to increase the input impedance of the panel modes for which it is not anti-symmetrically located (there is no nodal line passing through the center of action of the magnetic force). For the results considered here it will be worst for the (1,1) mode, as the magnet is situated over its antinode. Thus, the (1,1) mode will have an increased input impedance, making it more resistant to change under the action of the vibration control source. Thus, if the amplitude of the mode should go up, it will go up less than expected if the primary excitation were a point force; if it should go down, it will go down less than expected.

Consider now the theoretical results for the case of vibration control applied at (x=0, y=-70)mm, with the sound pressure minimized at 90°, shown in figure 4.10. The analytical models predict that control should be achieved by a reduction in the panel modal amplitudes. Comparing this result to the corresponding experimental case of figure 4.8, it can be seen that experimentally the (1,1) mode has not decreased as much as predicted, owing to the distributed nature of the primary force. This accounts for the 2-3 dB error in the radiation plot of figure

4.5, where the measured residual field is greater than that predicted theoretically. Despite this slight error, the agreement is good.

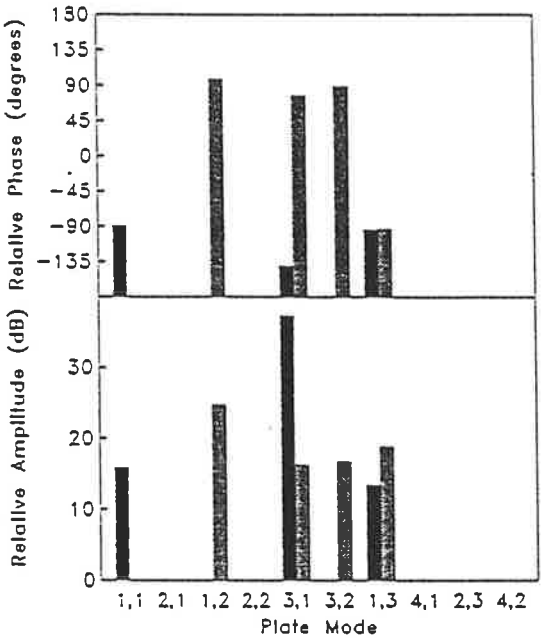

Figure 4.10 Theoretical modal amplitudes and phases for 2mm panel, vibration control at (0,-70) mm, error sensor at 90°, ■ = primary, ▩ = controlled.

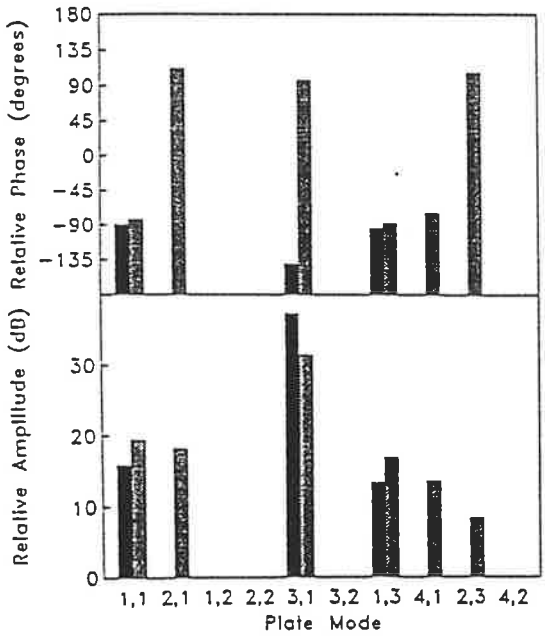

Figure 4.11 Theoretical modal amplitudes and phases for 2mm panel, vibration control at (-150,0) mm, error sensor at 90°, ■ = primary, ▩ = controlled.

Consider now the theoretical results for the case of applying vibration control at (x=-150, y=0)mm and minimizing the sound pressure at 90°, shown in figure 4.11. It can be seen that theoretically, the amplitude of the (3,1) mode should be reduced, but that the amplitude of the (1,1) mode should be increased. Here it is the mechanism of rearrangement of the amplitudes and phases of the panel modes which is providing sound control. Comparing this to the associated experimental result of figure 4.9, it can be seen that while the mechanism is still mainly one of modal amplitude and phase rearrangement, the predicted increase in the amplitude of the (1,1) mode did not eventuate. This is again due to the influence of the distributed nature of the primary source, and accounts for the 2-3 dB error in the experimental radiation plots of figures 4.6 and 4.7, where the measured sound pressure level is less than that theoretically predicted. Despite this, the principal theoretical features can be seen clearly in the experimental data.

To better understand how the modal amplitude and phase rearrangement mechanism provides global farfield sound attenuation, it is useful to consider the theoretical primary and controlled surface velocity amplitudes and phases associated with the modal plot of figure 4.11. These amplitudes and phases are shown in figures 4.12 - 4.15. Comparing the primary and controlled velocity distribution plots of figures 4.12 and 4.13, it can be seen that the surface velocity does decrease under the action of active vibration control, but only by approximately 2 dB. This is not, however, enough to account for the large reduction in the radiated sound pressure.

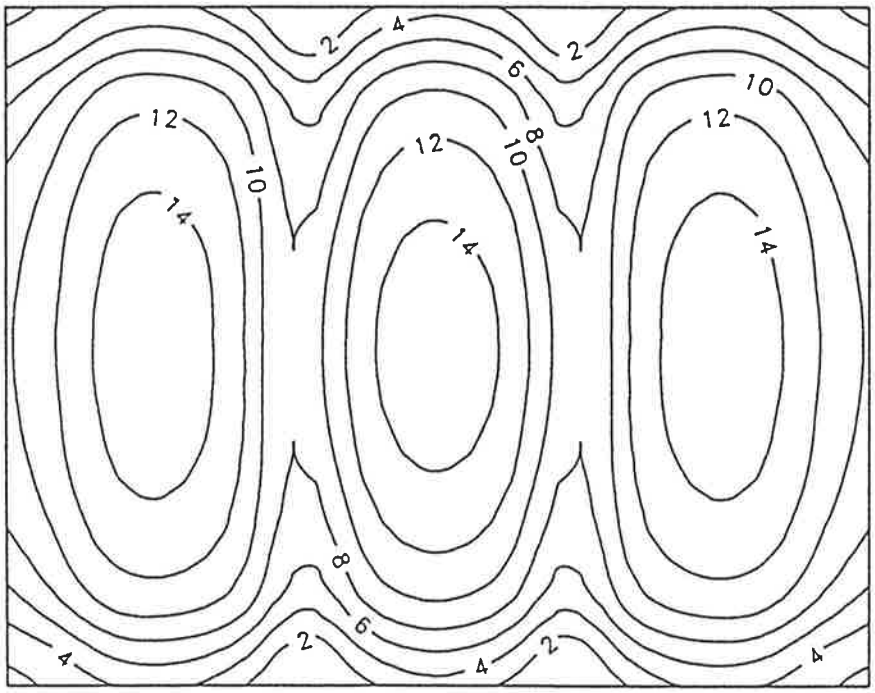

Figure 4.12 Theoretical primary mean square velocity levels (dB) for 2mm panel, 338 Hz.

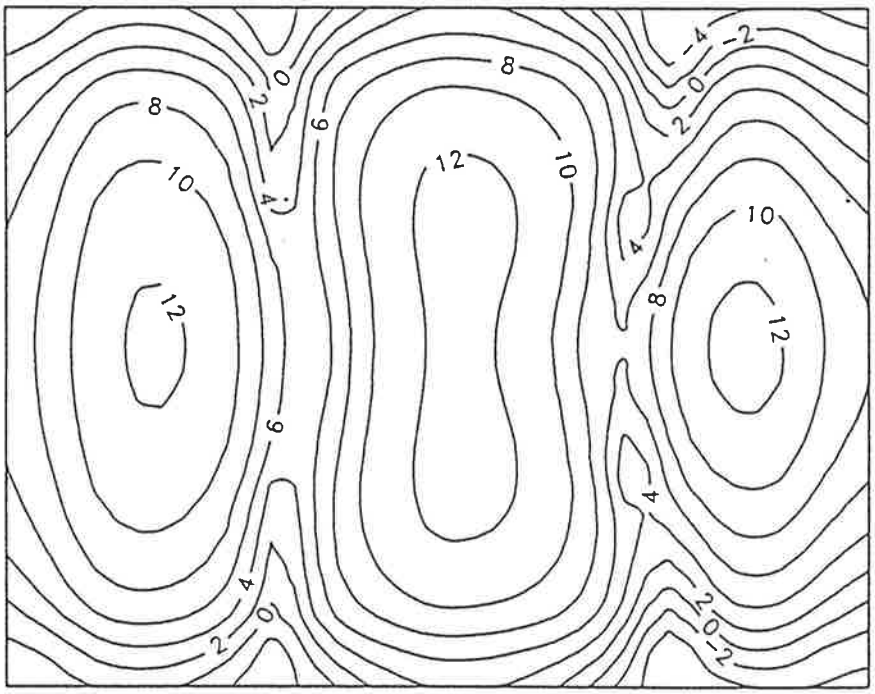

Figure 4.13 Theoretical controlled mean square velocity levels (dB) for 2mm panel, 338 Hz, vibration control at (-150,0) mm, error sensor at 90°.

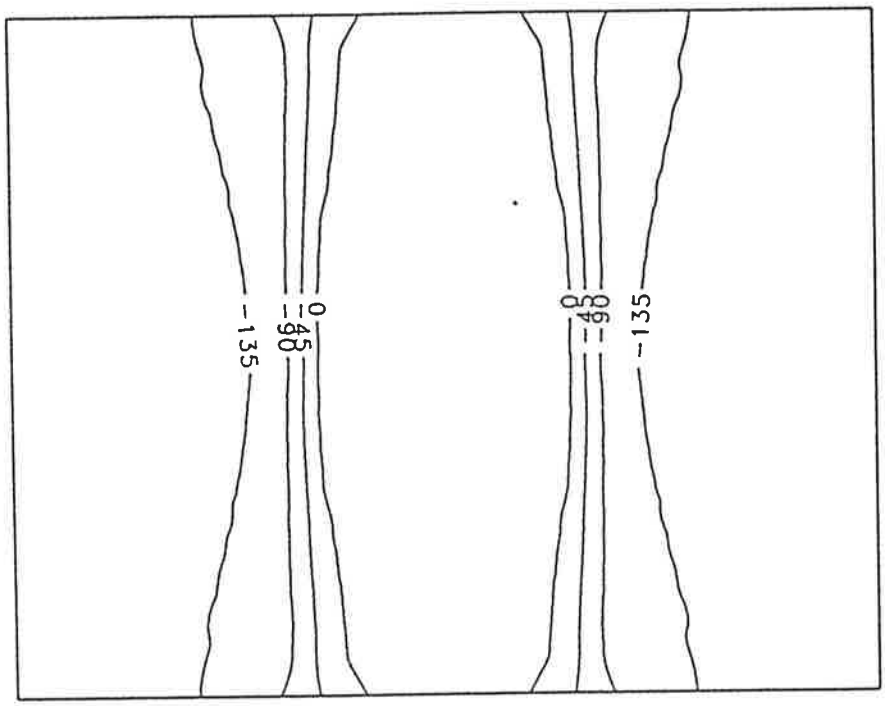

Figure 4.14 Theoretical primary phasing (deg) for 2mm panel, 338 Hz.

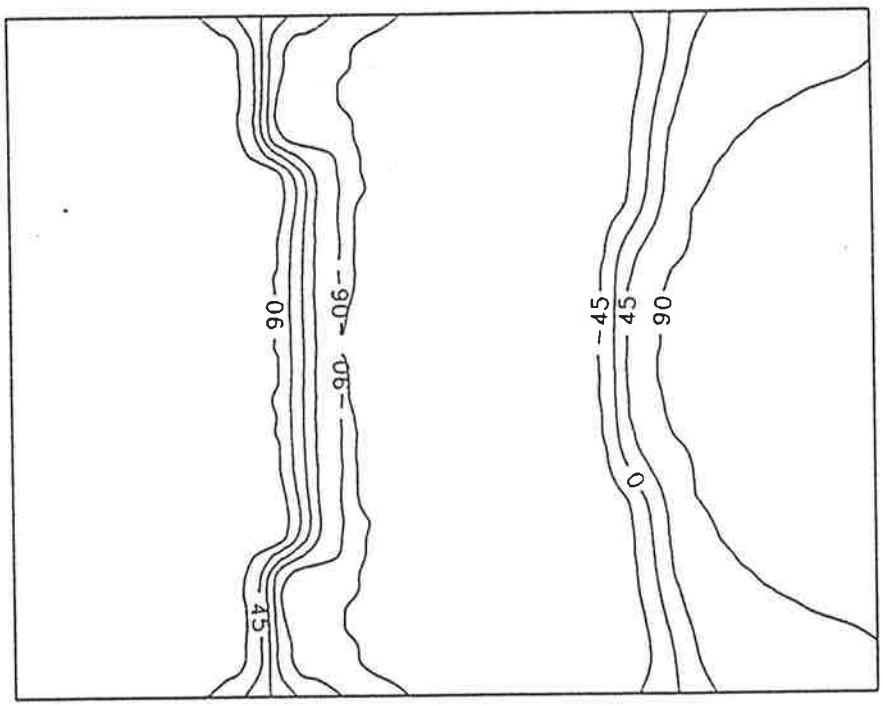

Figure 4.15 Theoretical controlled phasing (deg) for 2mm panel, 338 Hz, vibration control at (-150,0) mm, error sensor at 90°.

When this result is viewed in light of the change in the phasing of the surface velocity, found by comparing the primary phasing of figure 4.14 with the controlled phasing of figure 4.15, the total effect can be deduced. Under the action of vibration control the "high velocity" center region of the panel, which is approximately 180° out of phase with each side, has increased in size relative to the two edge regions. Thus the center region has become more of an acoustic sink, reducing the overall radiation efficiency of the panel.

Two other vibration control cases will be considered experimentally here. The first is the effect of increasing the panel thickness from 2mm to 9.5mm, altering the excitation frequency from 338 to 1707 Hz, and applying vibration control at (x=0, y=-70)mm while minimizing the sound pressure at 90°. This result, comparable to the thin plate test of figure 4.5, is shown in figure 4.16. In viewing this result, it can be deduced that there is a significant interference problem, possibly arising from the higher frequency, shorter wavelength sound field being more affected by reflection from foreign objects and the floor grating in the anechoic room. Despite this, there is general agreement between the shapes of the theoretical and measured plots.

Finally, the use of a (25 x 30)mm piezoelectric ceramic patch as a control source was considered. For this test, conducted on the 9.5mm plate vibrating at 1685 Hz, the primary force was moved to a position of (x=-126, y=0)mm and the control force was mounted in the panel center. The sound pressure was then minimized at an azimuthal angular location of 40°. A comparison of the experimental results with those obtained theoretically by modelling the piezoelectric patch as a point force is shown in figure 4.17. The general agreement is good, even though this is an extremely simplified analytical model.

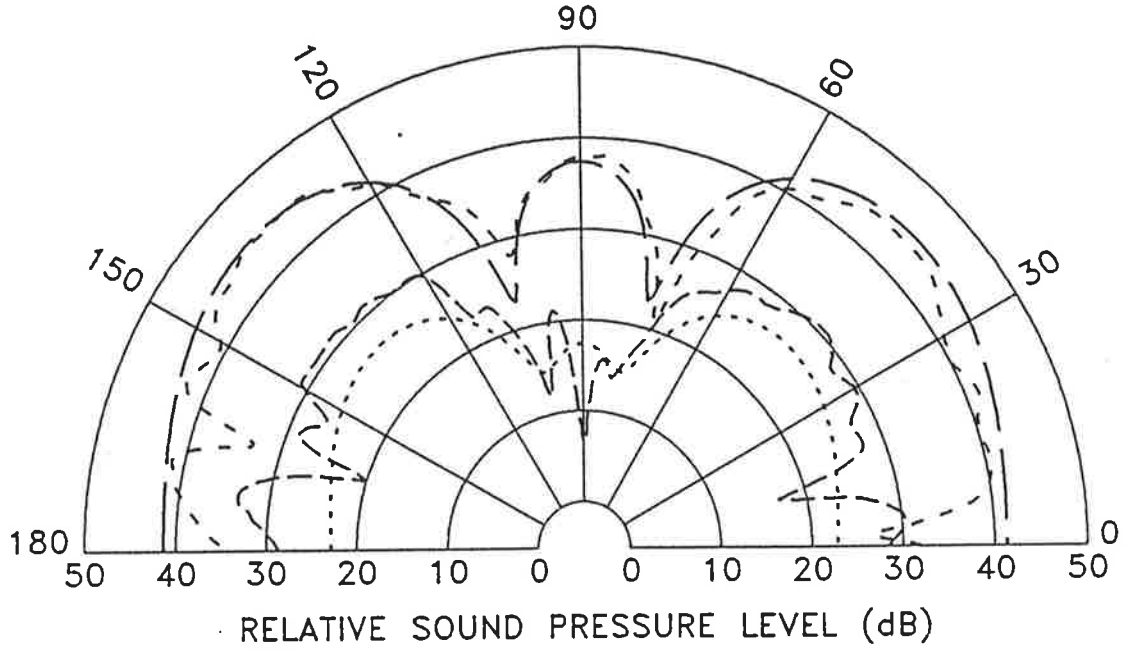

Figure 4.16 Radiation pattern from 9.5mm panel, 1707 Hz, vibration control at (0,-70) mm, error sensor at 90°, ——= theoretical primary, - -= measured primary, - - - = theoretical controlled, — —= measured controlled.

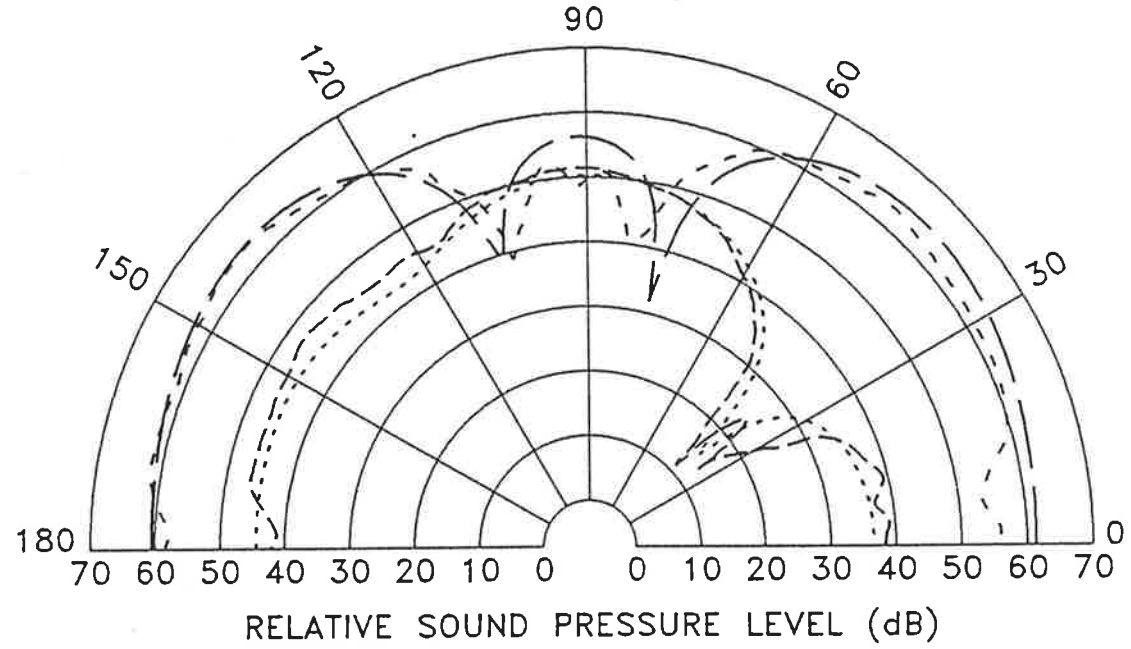

Figure 4.17 Radiation pattern from 9.5mm panel, 1707 Hz, piezoelectric ceramic actuator control at (0,0) mm, error sensor at 90°, ——= theoretical primary, - -= measured primary, - - - = theoretical controlled, — —= measured controlled.

4.4.3 Acoustic Control Sources

The use of acoustic control sources was examined next. Initially a single horn driver, discharging at the panel center, was used to control the acoustic pressure radiated from the 2mm thick panel vibrating at 338 Hz. The comparison between theory and experiment for the cases of minimizing the sound pressure at angular locations of 90° and 40° is shown in figures 4.18 and 4.19, respectively. In viewing these it can be seen that the general agreement between theory and experiment is good, although diffraction around the horn driver has slightly altered the acoustic field, introducing an interference pattern into the result.

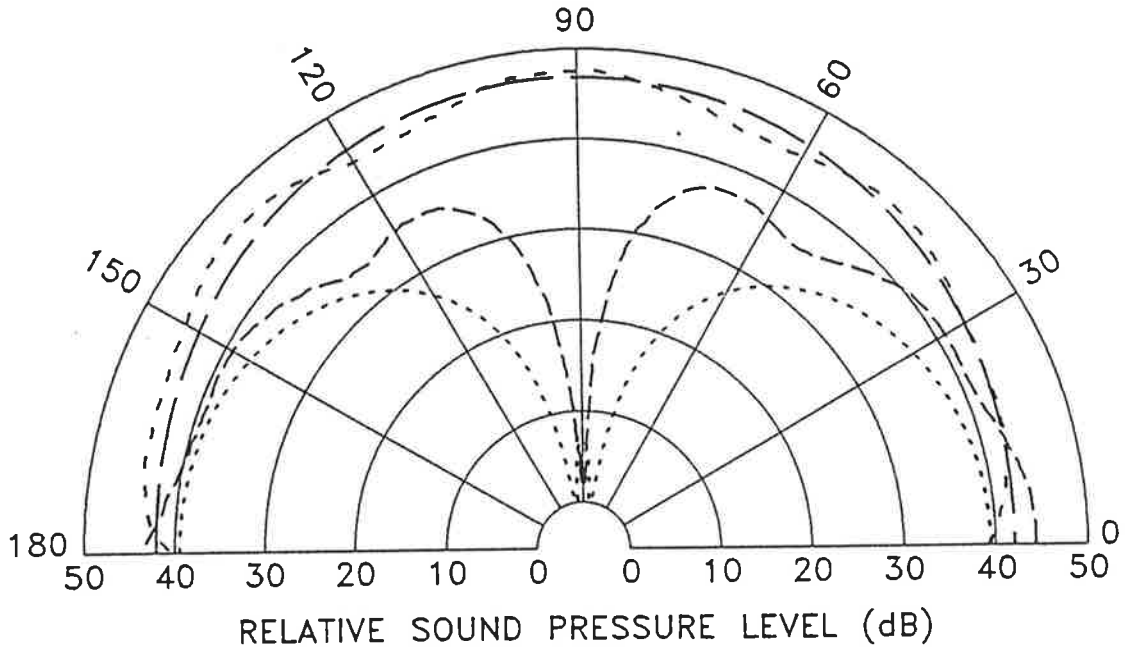

Figure 4.18 Radiation pattern from 2mm panel, 338 Hz, acoustic control at (0,0) mm, error sensor at 90°, ——= theoretical primary, - -= measured primary, - - -= theoretical controlled, — —= measured controlled.

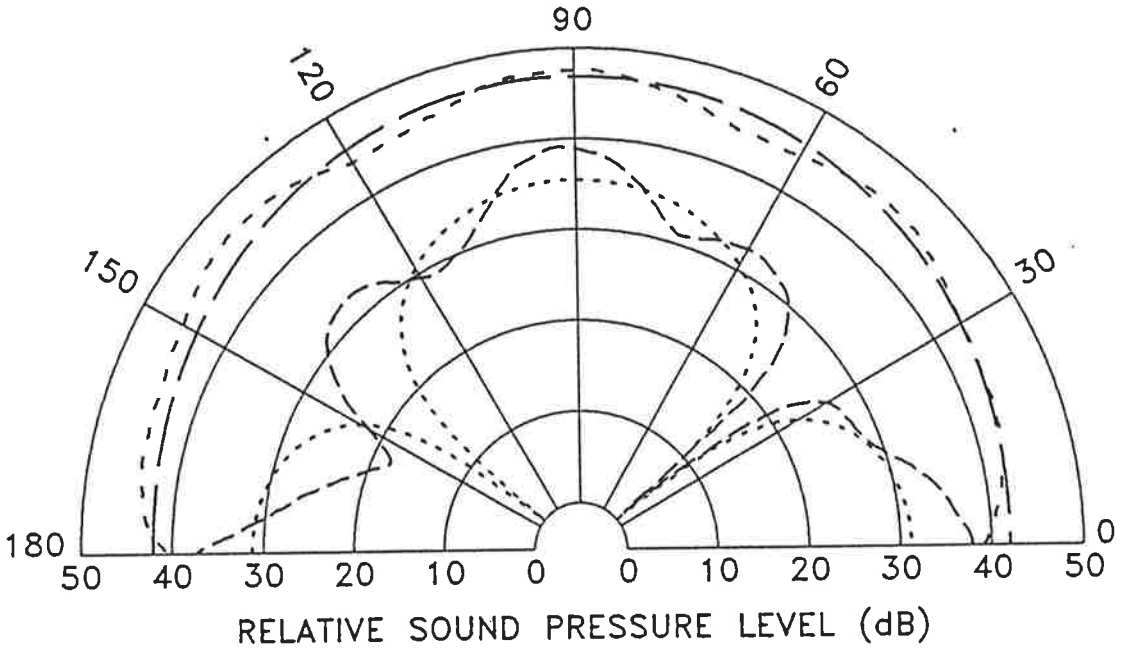

Figure 4.19 Radiation pattern from 2mm panel, 338 Hz, acoustic control at (0,0) mm, error sensor at 40°, ——= theoretical primary, - -= measured primary, - - - = theoretical controlled, — —= measured controlled.

Next, the panel thickness was increased to 9.5mm, the frequency of excitation to 1707 Hz, and the tests repeated. The primary sound field for these tests is shown in figure 4.20, with the residual sound fields corresponding to pressure minimization at 90° and 40° shown in figures 4.21 and 4.22, respectively. Here again the general agreement is good, although the diffraction problem is again evident, especially in figure 4.22.

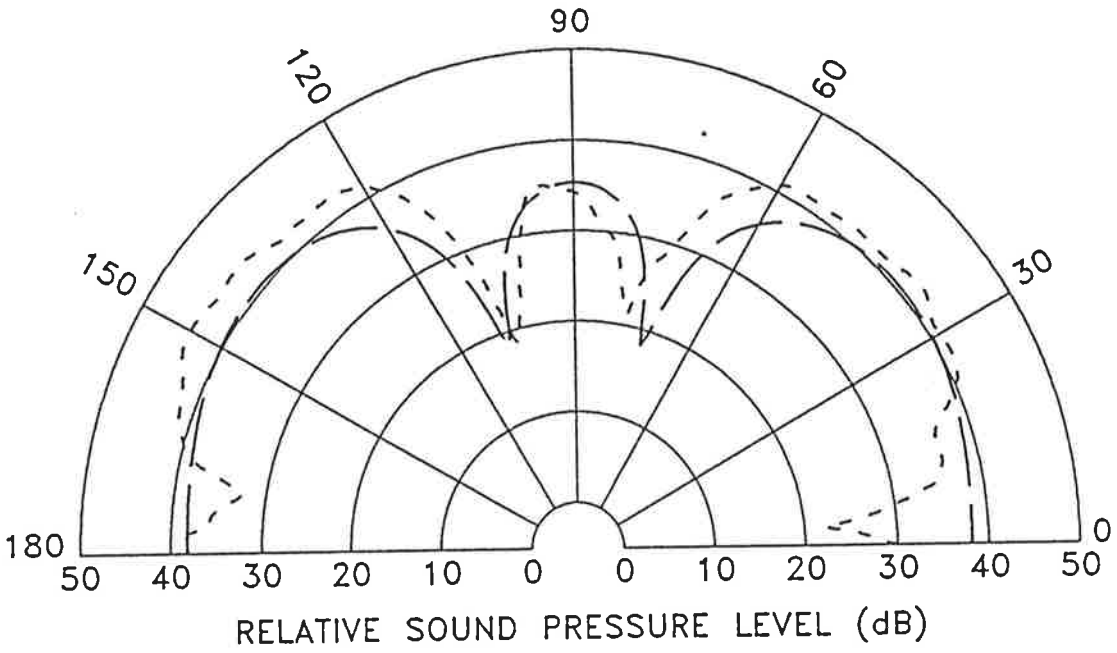

Figure 4.20 Primary source radiation pattern for 9.5mm panel, 1707 Hz, ——= theoretical, - -= measured.

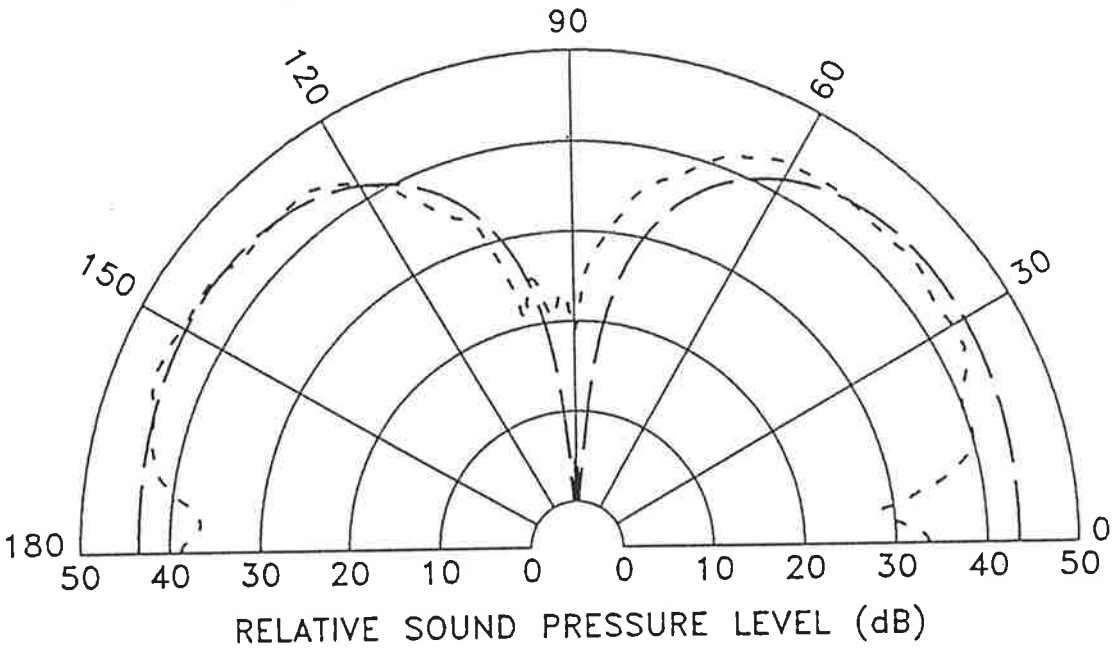

Figure 4.21 Controlled radiation pattern from 9.5mm panel, 1707 Hz, acoustic control at (0,0) mm, error sensor at 90°, ——= theoretical, - -= measured.

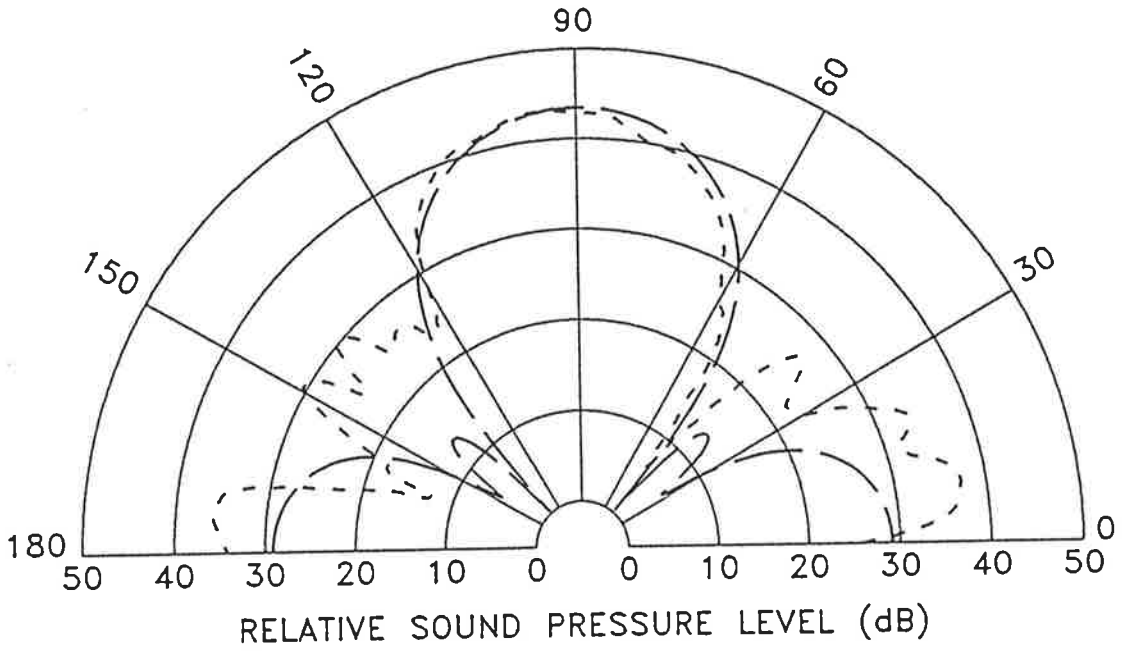

Figure 4.22 Controlled radiation pattern from 9.5mm panel, 1707 Hz, acoustic control at (0,0) mm, error sensor at 40°, ——= theoretical, - -= measured.

Finally, 2 more horn drivers were added, at (x=±100, y=0)mm. The magnitude of each of these was constrained to be equal, with the relative phases varying 0°/180°/0° across the panel. The residual sound fields resulting from minimizing the sound pressure at angular locations of 90° and 40° are shown in figures 4.23 and 4.24, respectively. Here the interference pattern has become markedly worse, owing to the introduction of two new horn drivers. However, the average amplitudes of the predicted and measured residual sound fields match quite well.

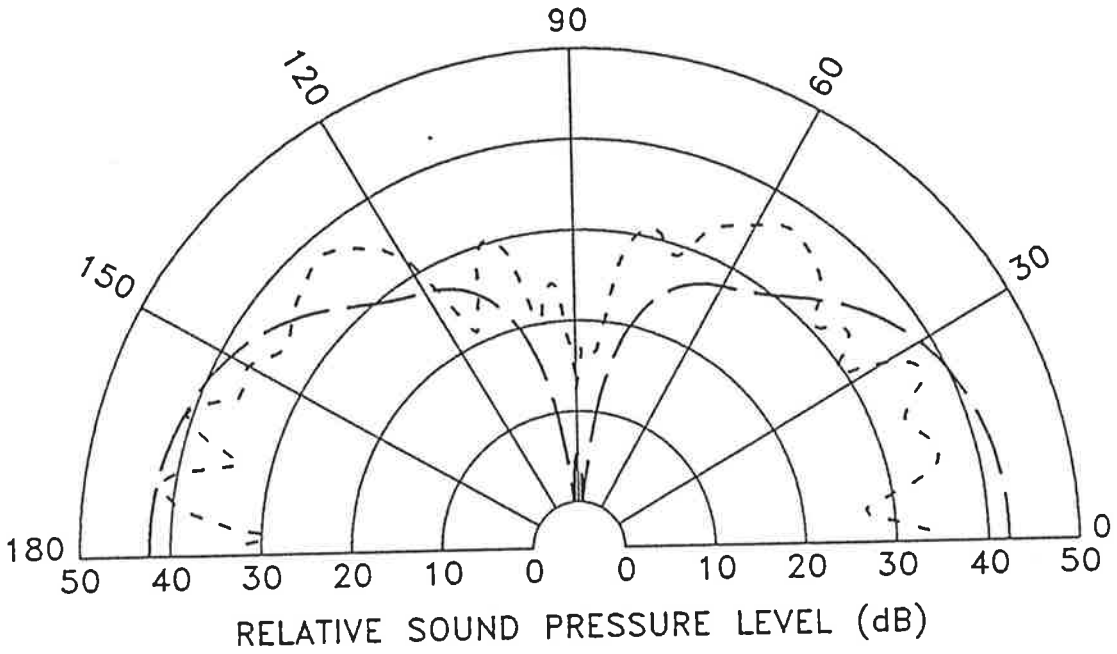

Figure 4.23 Controlled radiation pattern from 9.5mm panel, 1707 Hz, 3 acoustic controls at (0,0), (±100,0) mm, error sensor at 90°, ——= theoretical, - -= measured.

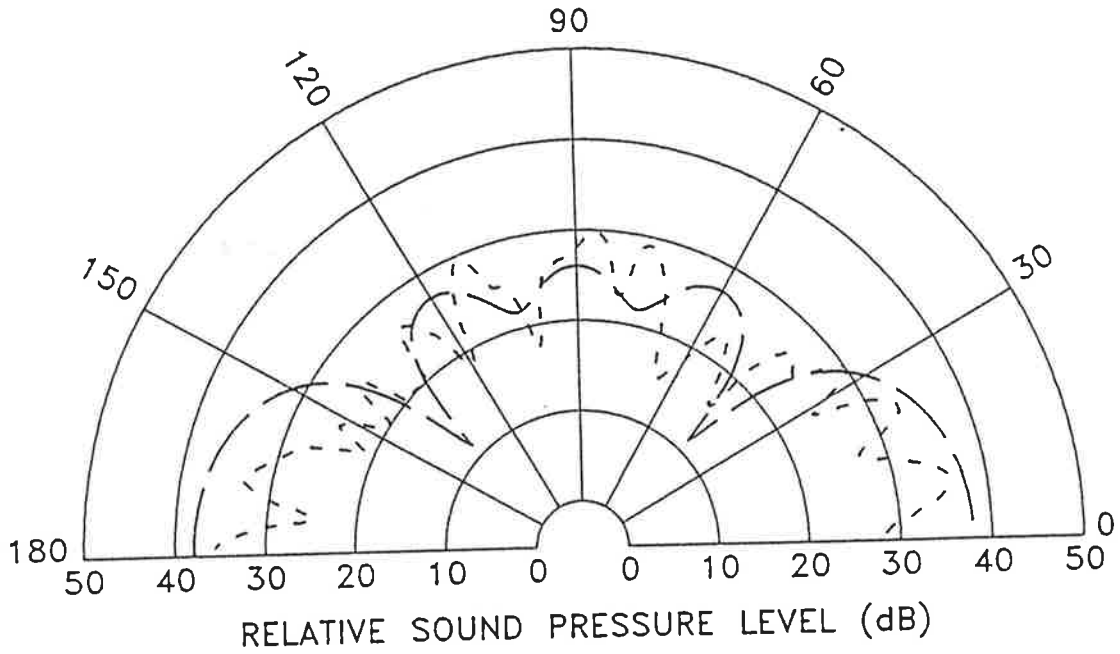

Figure 4.24 Controlled radiation pattern from 9.5mm panel, 1707 Hz, 3 acoustic controls at (0,0), (±100,0) mm, error sensor at 40°, ——= theoretical, - -= measured.

4.4.4. Discussion of results

The experimental work outlined in the previous section demonstrates the ability of the analytical models presented in Chapter 3 to predict the effect of applying active noise control, via either vibration or acoustic sources, to attenuate periodic sound radiation from a baffled, vibrating panel into free space. The experimental results (and the corresponding analytical models) were limited to a relatively simple single control source / single error sensor arrangement for ease of evaluation of the theory presented. However, the models can be extended to multiple source / multiple sensor arrangements.

It was shown that vibration sources provide global sound control by modifying the velocity distribution of the vibrating panel. This modification can have two effects; a reduction in the amplitudes of the primary offending structural modes, and/or an alteration in the relative amplitudes and phases of the structural modes. The first of these two effects provides sound control by reducing the velocity of the panel, the second by reducing the overall radiation efficiency of the panel. The results presented here show that, for a given panel and primary exciting force, the employment of these two mechanisms can be combined in varying degrees at any given vibration control application point. Also, a single vibration control source can utilize effectively either or both of these mechanisms in some instances. Further, it was shown that a single vibration control source can provide global sound control when the primary radiated sound field is simple (unlobed) or complex (lobed) in nature.

It is interesting to consider that a single vibration control source can reduce the amplitudes of a number of structural modes simultaneously, without causing an increase in the amplitudes of

other structural modes for this particular arrangement. This can be explained by considering that for a lightly damped, mechanically excited panel there will be regions where the majority of the transfer functions between the control force and the radiating section of the dominant structural modes will be in phase. In these regions, a single vibration source can effectively control the acoustic radiation from all of the in-phase modes simultaneously to some degree, dependent upon the relative vibration amplitudes of the modes. Conversely, it is the use of a control source at locations on the panel where the transfer functions between the control force and the radiating section of the dominant structural modes are out of phase which results in the structural modal rearrangement control mechanism being important in providing sound attenuation.

It was demonstrated in Chapter 2, both analytically and experimentally, that acoustic sources provide global noise control in active systems for controlling plane wave sound propagation in air handling ducts by reducing the radiation impedance seen by both the primary and control noise source. This mechanism has also been demonstrated analytically for the case of controlling free field sound radiation from monopole sources (Nelson et al, 1987). It can be deduced that the same mechanism is at work here in light of there being a negligible reduction in volume velocity for both the primary and control noise sources. This was an explicit assumption in the analytical models developed in chapter 3. Also, measurements of the panel velocity levels during the experimental investigations of acoustic active control (not presented) confirm this to be the case.

It was shown in the results that the primary excitation radiation pattern has a significant influence upon the number of acoustic control sources required to provide global sound control.

This has been discussed previously for acoustic wavelengths much longer than the panel dimensions (Deffayet and Nelson, 1988). It was seen that where the radiation pattern is largely uniform (unlobed), a single acoustic control source can provide global sound control. For a more complex radiation pattern, however, multiple sources are required.

4.5. ANALYTICAL STUDY OF SYSTEM VARIABLES - USE OF VIBRATION CONTROL SOURCES

When the noise source targeted for active control is a vibrating structure, a small number of vibration sources may be used to provide global sound attenuation. As outlined before, these can achieve noise reduction in two different ways; the amplitude of the primary radiating structural modes can be reduced (modal control), and/or the relative amplitudes and phases of the structural modes can be altered (modal rearrangement). For the case of a simply supported panel the relative phase rearrangement is in the time domain, as the spatial phases remain fixed due to the boundary constraints. The relative phase difference between the modes is achievable (although not immediately obvious) because of the damping inherent in the panel and because of the relative phase difference between the primary and control source excitation. This latter mechanism can result in a reduction in the radiated sound power by causing a reduction in the structure's overall velocity levels, and/or by reducing its radiation efficiency. The first of the two mechanisms is most likely to occur when the system is radiating at a frequency near a structural resonance; the second is most likely to occur when the panel response is forced (that is, the excitation frequency is not close to any of the panel resonance frequencies). Each of these mechanisms is affected differently by various structural / acoustic parameters. The aim of this section is to investigate analytically these effects.

What will be examined first is the "base case" of controlling sound radiation from a lightly damped ($\eta = 0.04$), mechanically excited panel using a single vibration control source. Included in this examination will be a study of the effect of control source and error sensor location. Following this, several structural / acoustic and geometric parameters will be varied to examine the influence which they have on both the physical mechanisms at work, and on the ability of the control source to achieve significant levels of sound power attenuation.

4.5.1. Examination of the base case

The base case panel, shown in figure 4.25, is 0.38 x 0.30 meters on edge, and 2mm thick. It is excited in the four corners by point forces, at x = ±0.171, y = ±0.135, with all forces equal in amplitude and phase (note that all coordinate locations are given relative to the panel center). This is similar to the form of excitation that may be found on a rotating machinery cover plate. The excitation frequency is 350 Hz, which lies slightly below the fourth and fifth panel modes, the (2,2) and (3,1) modes, as shown in Table 4.2. This frequency was chosen for its ability to readily demonstrate all control mechanisms, as will be shown. The control source is a single point force that can be applied to any location on the panel.

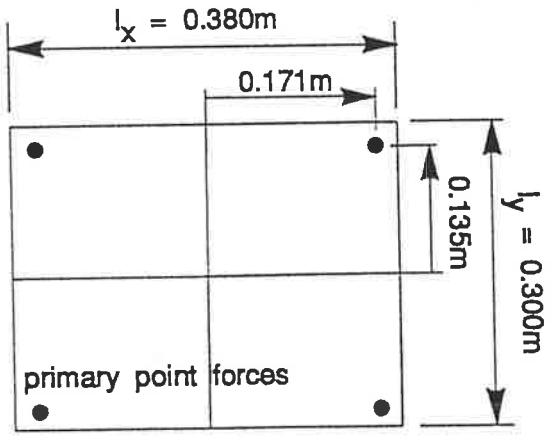

Figure 4.25 Base case panel geometry.

		0.38m x 0.3m x 2mm panel		1.075m x 0.8485m x 4mm panel (from section 4.5.4)	
Mode	Resonance (Hz)	Radiation Efficiency ($\times 10^{-3}$)	k/k_b	Radiation Efficiency ($\times 10^{-3}$)	k/k_b
(1,1)	88.1	421.4	0.481	1297.8	1.359
(2,1)	189.6	52.1	0.328	1156.2	0.927
(1,2)	250.9	33.2	0.285	889.0	0.805
(2,2)	352.4	2.4	0.240	484.0	0.680
(3,1)	358.7	33.1	0.238	371.3	0.674
(3,2)	521.6	3.0	0.198	112.0	0.559
(1,3)	522.3	37.4	0.197	150.2	0.558
(4,1)	595.5	11.3	0.185	82.6	0.523
(2,3)	623.8	5.1	0.181	85.1	0.511
(4,2)	758.4	0.6	0.164	51.6	0.463

Table 4.2. Resonance frequencies and radiation efficiences of simulation panels. k_b is the structural wavenumber, $k_b = \sqrt{\left(\frac{m\pi}{l_x}\right)^2 + \left(\frac{n\pi}{l_y}\right)^2}$

The effect which location of the source has upon the level of attenuation of radiated sound power that can "ideally" be achieved is shown in figure 4.26 (note here that "ideally" refers to the maximum sound power attenuation that can be achieved with the specified control source arrangement assuming that the error sensor arrangement was capable of measuring total radiated sound power, as opposed to the attenuation that can be achieved by minimizing the sound pressure at a point or points). The figure shows the optimal achievable sound power attenuation as a function of control source location on the panel. Here three optimum control source locations can be seen, on the (y=0) centerline, at the two edges and in the middle. The fact that there is not a single optimum location has implications for the form of search routine used to determine the control source placement. If a gradient-based method is used, the starting point will determine which optimum is arrived at. One possible means of overcoming this

problem is to consider "control effort", or the amount of force required to achieve the maximum levels of sound power attenuation. The usefulness of this, however, is very much case dependent.

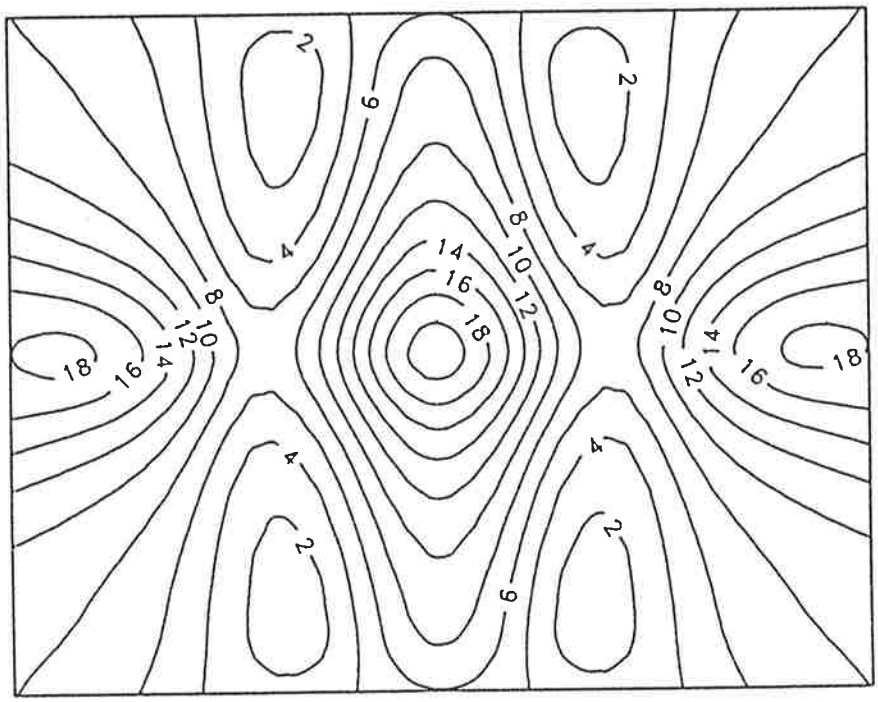

Figure 4.26 Maximum achievable levels of sound power attenuation (dB) as a function of the vibration source location on the panel, 0.38 x 0.3 x 0.002 m, with light damping and harmonic excitation at 350 Hz.

As outlined earlier, there are two possible mechanisms which can provide radiated sound power attenuation when active vibration control sources are used; modal amplitude reduction and modal relative phase rearrangement. These two mechanisms can coexist, and do so in varying degrees for the same structure when a vibration control source is attached at different locations. Therefore, it is possible that the different optimum control source locations produce control in different ways.

The effect of controlling the panel radiation at the optimum location of (0.17,0.0) upon the amplitudes and relative phases of the first 10 panel modes is shown in figure 4.27 (note that the phases are referenced to motion of the panel center). Here it can be seen that the amplitudes of the nearly-resonant (3,1) mode and the (1,1) mode are substantially reduced. These two modes, based on their velocity levels and radiation efficiencies at this frequency, have the greatest potential for sound power generation. Their reduction will cause a significant reduction in the total radiated sound power, which is the primary control mechanism producing the 19.9 dB attenuation achieved here.

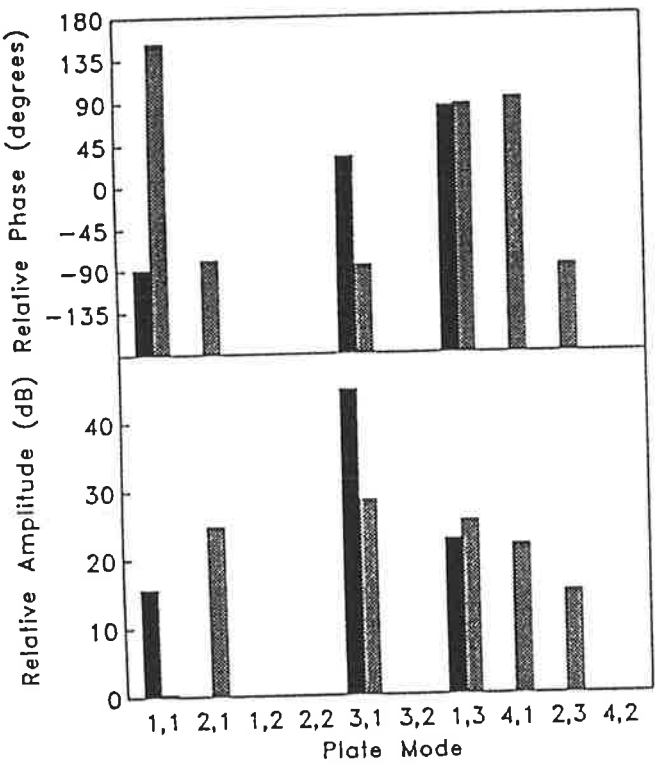

Figure 4.27 Comparison of modal velocity levels on the lightly damped panel, 0.38 x 0.3 x 0.002 m, harmonically excited at 350 Hz, before and after control, ▬ = primary excitation, ▒ = vibration control at (0.17, 0.0).

One additional point to note concerning figure 4.27 is the lack of excitation of any even numbered modes under the primary forcing function. This is due solely to the symmetric nature of the primary forcing function.

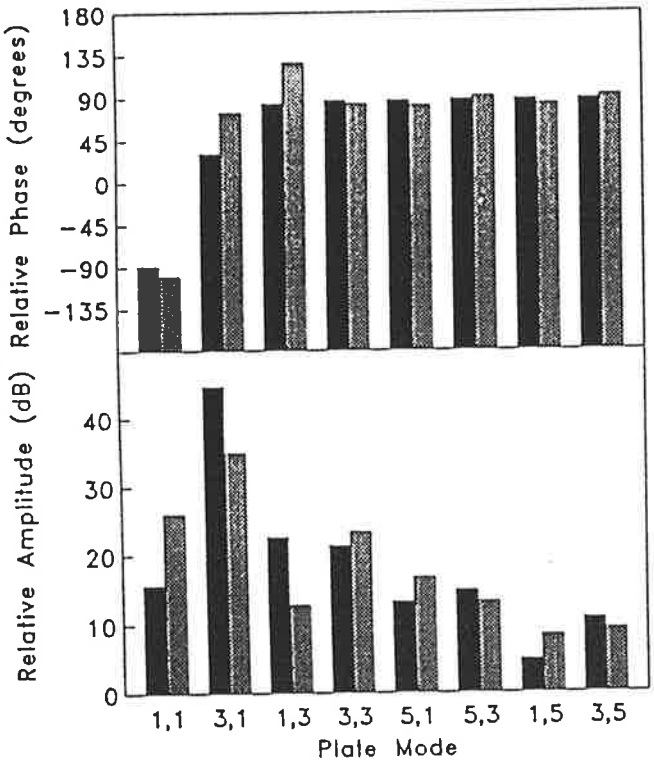

Figure 4.28 Comparison of modal velocity levels on the lightly damped panel, 0.38 x 0.3 x 0.002 m, harmonically excited at 350 Hz, before and after control, ▬ = primary excitation, ▩ = vibration control at (0.0, 0.0).

The effect which using a vibration source at (0.0,0.0) to control sound power radiation has upon the first 8 non-zero amplitude panel modes is shown in figure 4.28. Here the nearly resonant (3,1) mode, as well as the (1,3) mode, both have a reduction in amplitude of approximately 10 dB. This would appear to be offset, however, by an increase in the amplitude of the (1,1) mode of approximately 10 dB. Just in viewing these results, it would seem unlikely that the 22.7 dB reduction in radiated sound power would be achieved only by a reduction in the modal vibration amplitudes of the radiating modes. However, it can be seen in figure 4.28 that the relative

amplitudes and phases of the modes (and thus the overall radiation efficiency of the panel) have changed significantly and this is responsible for the extent of the sound power reduction achieved.

As mentioned previously, this alteration can have two possible effects; the total panel velocity levels can decrease, and/or the radiation efficiency of the panel can be reduced. The uncontrolled and controlled panel velocities and phases for the case being considered here are shown in figures 4.29 to 4.32. A comparison of the mean square panel velocity levels before and after control, shown in figures 4.29 and 4.30, depicts an overall reduction in amplitude of approximately 6 dB. This is because the reduction in amplitude of the (3,1) and (1,3) modes is greater than the increase in amplitude of the (1,1) mode. This, however, is not enough to account for the 22.7 dB of radiated sound power attenuation. The remainder of the sound attenuation must therefore be due to modal rearrangement.

To examine this possibility, consider first the radiation characteristics of the two dominant radiating structural modes. At these low frequencies, the (3,1) mode will be principally edge radiating, while the (1,1) mode will radiate everywhere on the panel. Therefore, for rearrangement of the (1,1) and (3,1) modes to provide sound attenuation, the edges of the (3,1) mode should be out of phase with the (1,1) mode, and be of greater amplitude than the (1,1) to compensate for its reduced radiating area. From figure 4.28, this is exactly what happens. This is modal rearrangement. A comparison of the panel phases, illustrated in figures 4.31 and 4.32, shows that under modal rearrangement the "edges" become reduced in size, while the out of phase "center" region expands. The resulting drop in radiation efficiency is largely responsible for the radiated sound power attenuation.

It should be noted that in both of the examined control source positions, the force required to achieve maximum control is less than any single primary force (of which there are four). For the control source placed at (0.17,0.0), it is approximately 64% of a single primary control source, and approximately 23% of this value when the control source is placed at (0.0,0.0).

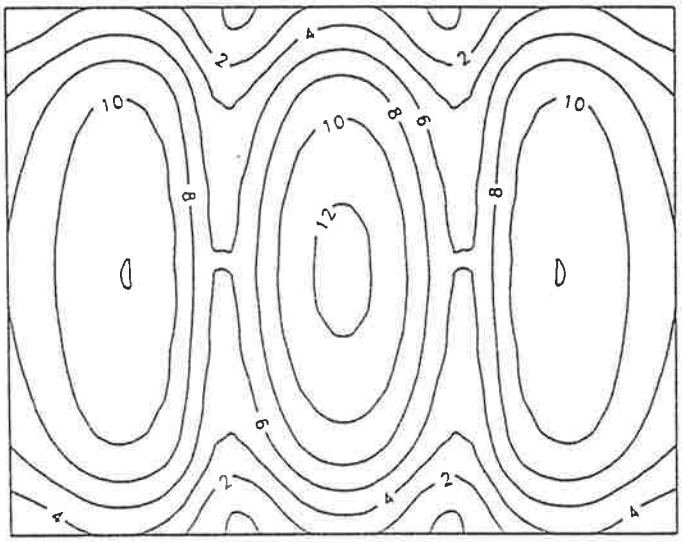

Figure 4.29 Primary excitation mean square velocity levels (dB) on the (0.38 x 0.3 x 0.002m) panel surface for harmonic excitation at 350 Hz and light damping.

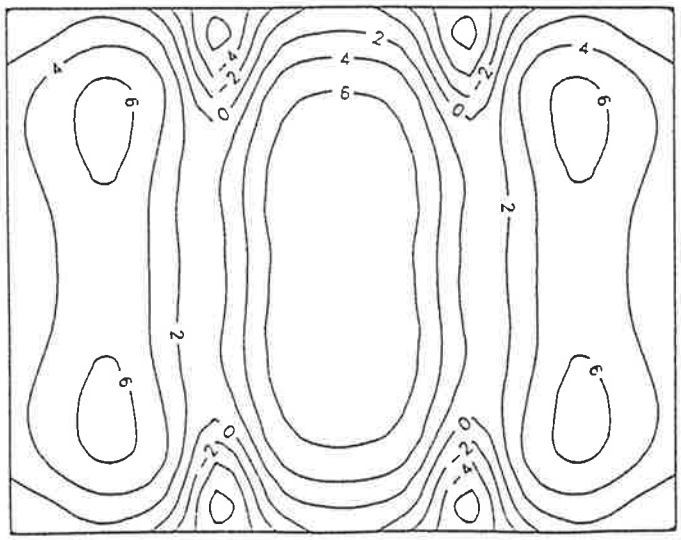

Figure 4.30 Controlled mean square velocity levels (dB) on the (0.38 x 0.3 x 0.002m) panel surface for harmonic excitation at 350 Hz and light damping. vibration control at (0.0, 0.0).

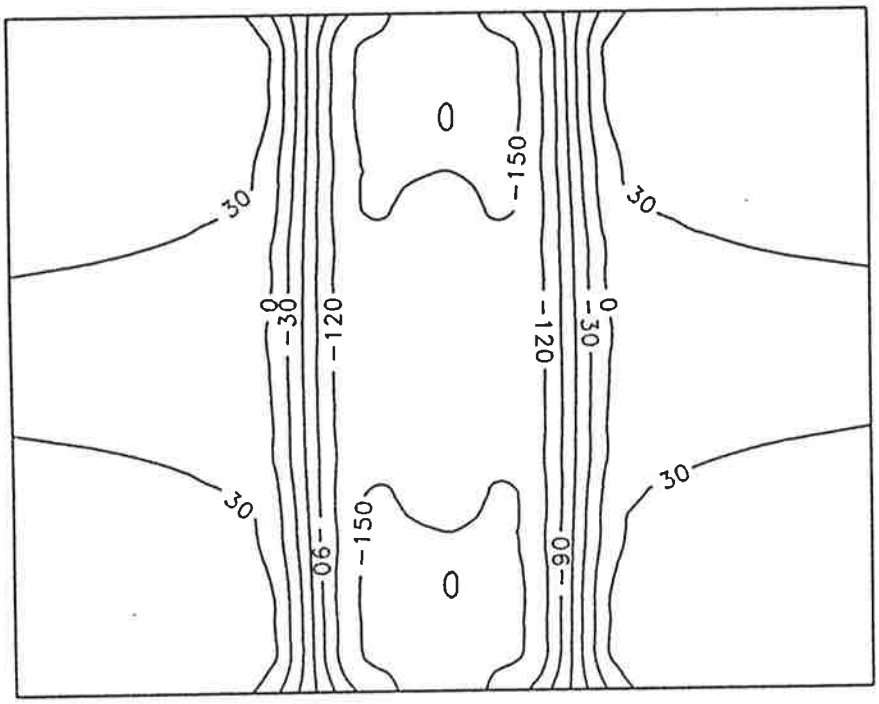

Figure 4.31 Relative phases (degrees) of the panel surface velocity under primary excitation only for the lightly damped panel, 0.38 x 0.3 x 0.002m, harmonically excited at 350 Hz.

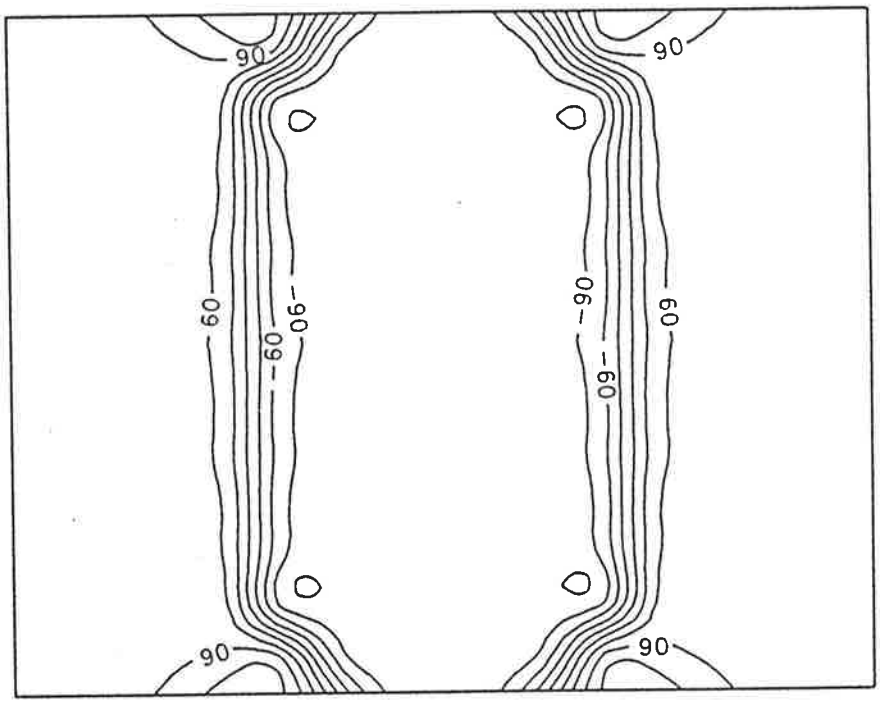

Figure 4.32 Relative phases (degrees) of the panel surface velocity under controlled conditions for the lightly damped panel, 0.38 x 0.3 x 0.002m, harmonically excited at 350 Hz, vibration control at (0.0, 0.0).

It is interesting to note the differences in phasing between the primary radiating structural modes at the two control source locations in light of the differences in the control mechanisms. At the (0.17,0.0) position, the transfer function between the control source and the radiating section of the two dominant modes, the (3,1) and (1,1), are in phase. Therefore, a single control source can reduce both of their amplitudes simultaneously. This produces the reduction in radiated sound power. At the (0.0,0.0) location, however, the (3,1) and (1,1) transfer functions are out of phase. Therefore, the amplitudes of these cannot be reduced simultaneously. A decrease in one will cause an increase in the other. Hence, sound power attenuation must come as a result of balancing the modes in such a way that the total radiation efficiency is reduced.

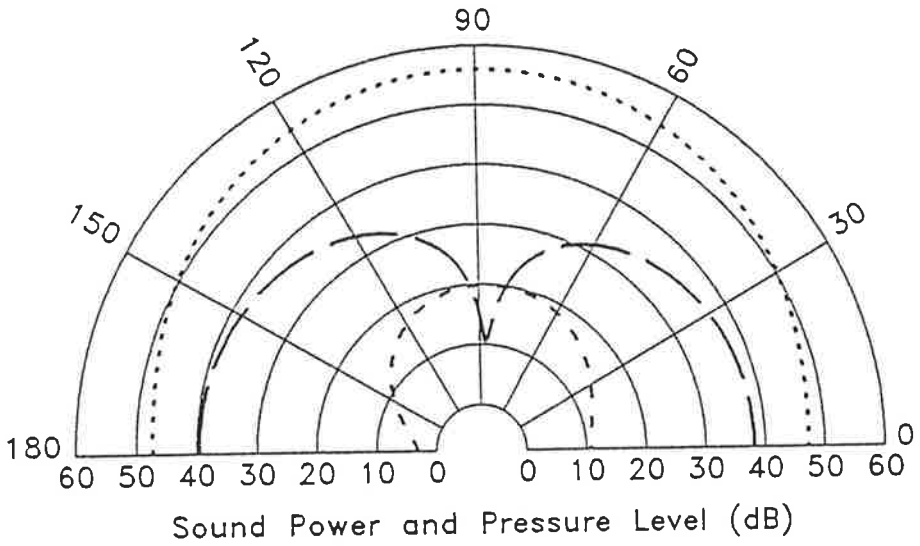

Figure 4.33 Sound pressure levels (dB) before control and after "ideal" control as a function of azimuthal angle in a horizontal plane normal to the mid point of the panel surface; and the maximum achievable reductions (dB) in radiated sound power as a function of angular location of a single error microphone in the same plane. The panel size is 0.38 x 0.3 x 0.002m, lightly damped, harmonically excited at 350 Hz, and the single vibration control source is located at (0.17, 0.0), · · · · = primary radiated, —— · = residual radiated, - - - = sound power reduction for a given single error microphone placement.

From figure 4.26, it is clear that the choice of control source location will determine the maximum sound power attenuation possible under ideal conditions. The placement of the error sensor (providing feedback of the residual sound field) will determine how close to this value the achievable level of attenuation is. The influence of the angular location of a single microphone error sensor located at a radius of 1.8 meters (the sound pressure is minimized at this location), upon the sound power attenuation possible when the control source is located at (0.17,0.0) is shown in figure 4.33, plotted with both the primary radiated sound pressure field and the residual controlled sound pressure field under "ideal" control (maximum achievable control of total radiated sound power for the specified control source arrangement, which is 19.9 dB in this case). Note that this radius will be used for all radiation plots throughout this section (4.5) and the one that follows (4.6), unless otherwise stated. As can be seen, the location of the error microphone greatly influences the maximum achievable level of sound power reduction. The optimum angular location is at the point of minimum sound pressure in the controlled residual sound field. In this case, the residual sound field is dominated by the (2,1) panel mode, so the optimum error microphone angular location is nearly normal to the panel center. (This point will be discussed further for the case of multiple control sources / error microphones in a later section). Minimization of the sound pressure at this location results in the maximum possible sound power attenuation of 19.9 dB being achieved.

A similar plot for the control source located at (0.0,0.0) is given in figure 4.34. As discussed earlier, the action of the control force causes the panel to radiate like a longitudinal quadrupole, a fact borne out by the controlled radiation plot in figure 4.34. Again the optimum error microphone angular location is at the point(s) of minimum sound pressure in the ideally controlled sound fields.

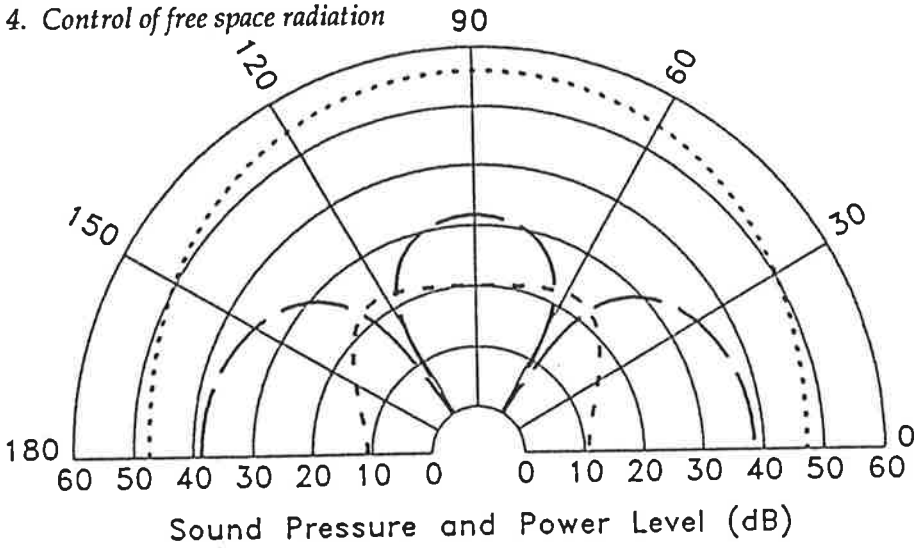

Figure 4.34 Sound pressure levels (dB) before control and after "ideal" control as a function of azimuthal angle in a horizontal plane normal to the mid point of the panel surface; and the maximum achievable reductions (dB) in radiated sound power as a function of angular location of a single error microphone in the same plane. The panel size is 0.38 x 0.3 x 0.002m, lightly damped, harmonically excited at 350 Hz, and the single vibration control source is located at (0.0, 0.0), ----- = primary radiated, - - - = residual radiated, —— ·= sound power reduction for a given single error microphone placement.

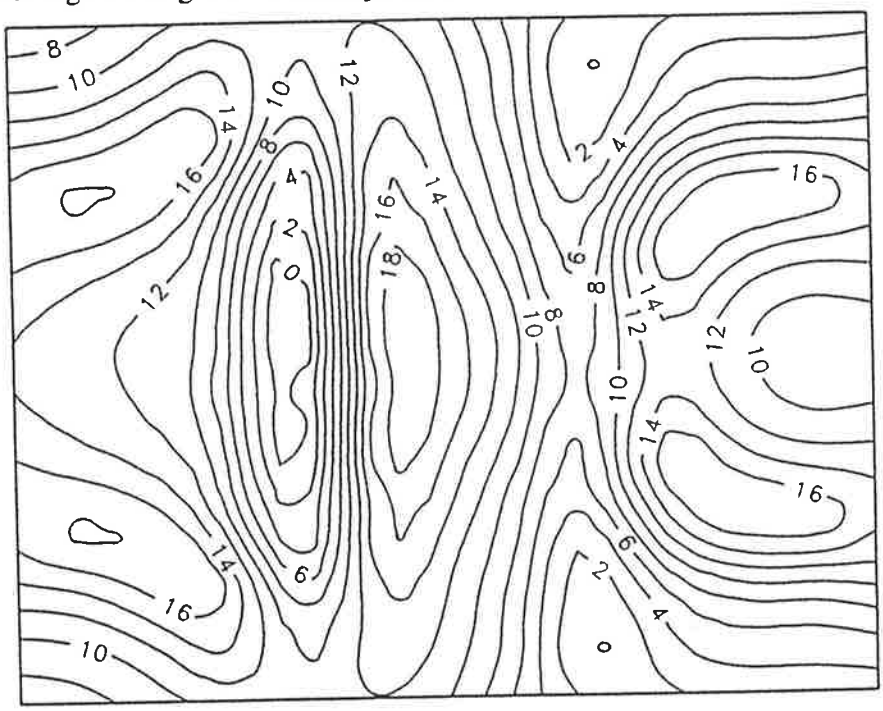

Figure 4.35 Maximum achievable reductions in radiated sound power (dB) as a function of location on the lightly damped, harmonically excited (350 Hz), 0.38 x 0.3 x 0.002m panel of the point at which the panel velocity is minimized for a vibration control source location of (0.17, 0.0).

When using vibration sources to control structural sound radiation, it may be possible to use a vibration sensor, such as an accelerometer, to provide an error signal. The reduction in radiated sound power achieved by minimizing the vibration at a single point on the panel when the control source is located at (0.17,0.0) is shown in figure 4.35, where the maximum achievable reduction in sound power under control is shown as a function of location of the vibration error sensor (or minimization point) on the panel. Here there are areas where the sound power attenuation approaches the maximum achievable level of 19.9 dB. This is not surprising, as the primary control mechanism here is a reduction in the modal amplitudes of the offending structural modes.

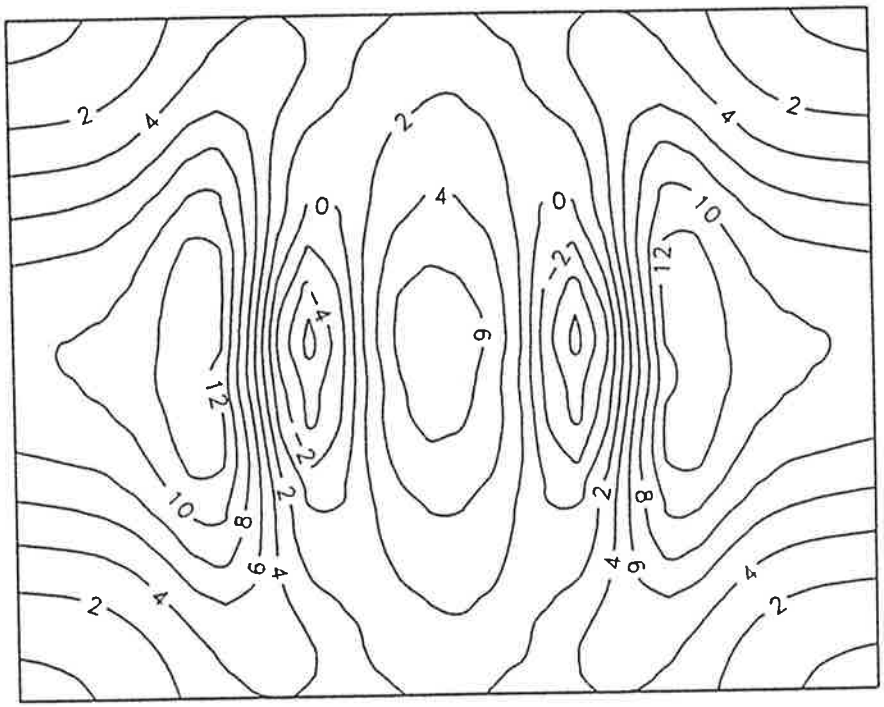

Figure 4.36 Maximum achievable reductions in radiated sound power (dB) as a function of location on the lightly damped, harmonically excited (350 Hz), 0.38 x 0.3 x 0.002m panel of the point at which the panel velocity is minimized for a vibration control source location of (0.0, 0.0).

A similar plot for the control source located at (0.0,0.0) is given in figure 4.36. Here, the achievable sound power attenuations are well below the maximum 22.7 dB possible under ideal conditions. This reflects the fact that control is achieved primarily by a reduction in the panel radiation efficiency, not by a reduction in panel velocity level. It is likely that more vibration sensors would not improve this result because the overall vibration levels are not reduced under control.

The preceding results will constitute a base case for the use of a vibration control source. In the following sections several geometric and structural / acoustic system parameters will be varied to study the effect which they have upon the control mechanisms and radiated sound power attenuation levels.

4.5.2. Effect of structural damping

The addition of structural damping to a mechanically excited panel has the effect of reducing the amplitudes of the resonant or nearly-resonant panel modes, but has little effect upon the off-resonant modes (Bies and Hansen, 1988). Based on the results of the previous section, this would appear to have the same effect as the first of the two vibration control mechanisms, modal vibration amplitude control. Therefore, it would be expected that if this were the principal mechanism by which sound power attenuation was produced with light structural damping, an increase in damping would greatly reduce the ability of the active source to achieve substantial levels of control.

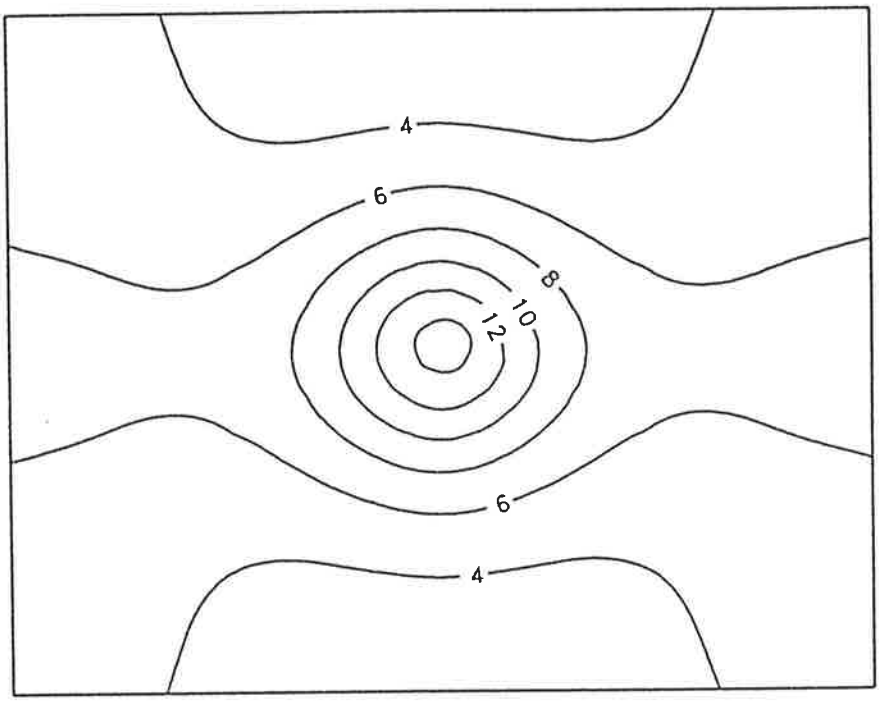

Figure 4.37 Maximum achievable levels of sound power attenuation (dB) as a function of the vibration source location on the panel, 0.38 x 0.3 x 0.002 m, with heavy damping and harmonic excitation at 350 Hz.

A plot of the maximum possible levels of sound power attenuation by application of a single vibration control at a given point for the previous panel with greatly increased damping (η = 0.4) is shown as a function of vibration control source location in figure 4.37. The previously seen optimum locations on the panel ends, where control was achieved primarily by a reduction in modal amplitudes, have been substantially reduced in terms of maximum possible sound power attenuation. The center optimum location, however, which achieved control principally by an alteration in the panel radiation efficiency, is still present with the level of reduction slightly smaller than with lower damping.

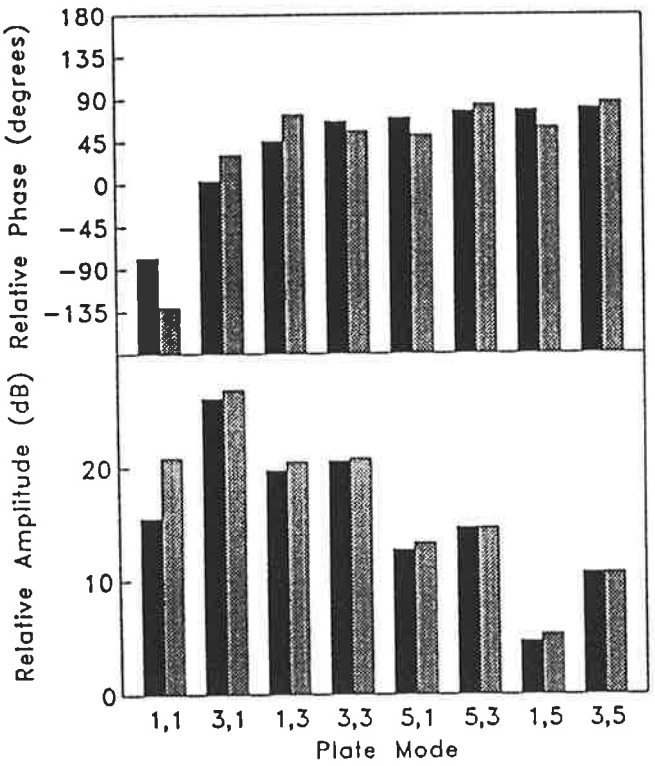

Figure 4.38 Comparison of modal velocity levels on the heavily damped panel, 0.38 x 0.3 x 0.002 m, harmonically excited at 350 Hz, before and after control, ▬ = primary excitation, ▒ = vibration control at (0.0, 0.0).

For this damped case, the effect which ideally controlling panel sound radiation by placing a control source at (0.0,0.0) has upon the amplitudes and phases of the first 8 non-zero amplitude panel modes is shown in figure 4.38. Comparing this with the previously considered lightly damped case, shown in figure 4.28, it can be seen that although the primary forcing function is unchanged, the amplitude of the nearly resonant (3,1) panel mode is greatly reduced under primary excitation. The amplitudes of all of the significant modes increase under the action of the control source, although there is a 16.3 dB reduction in the total radiated sound power.

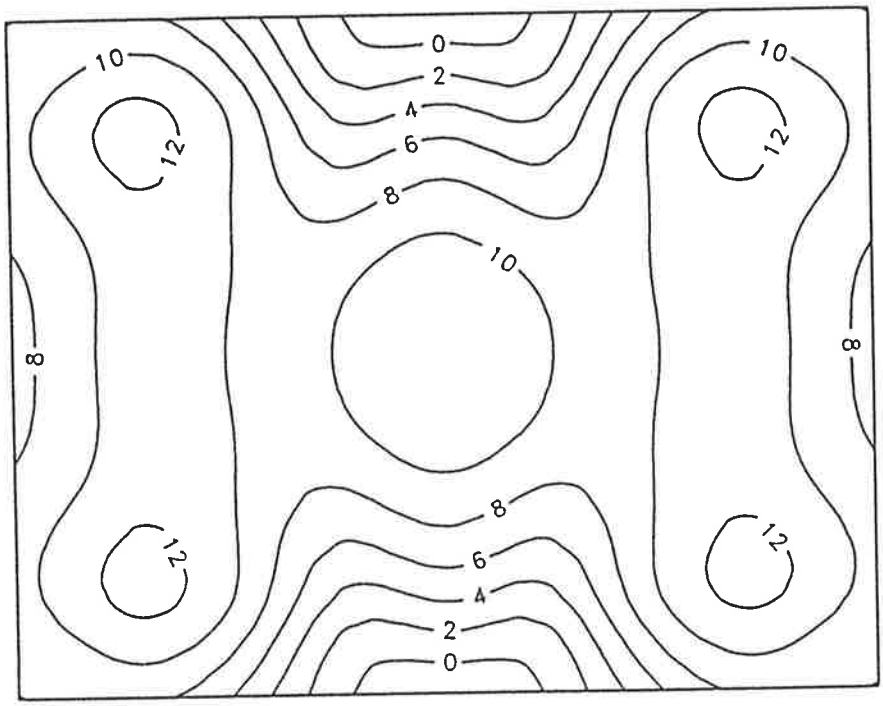

Figure 4.39 Primary excitation mean square velocity levels (dB) on the (0.38 x 0.3 x 0.002m) panel surface for harmonic excitation at 350 Hz and heavy damping.

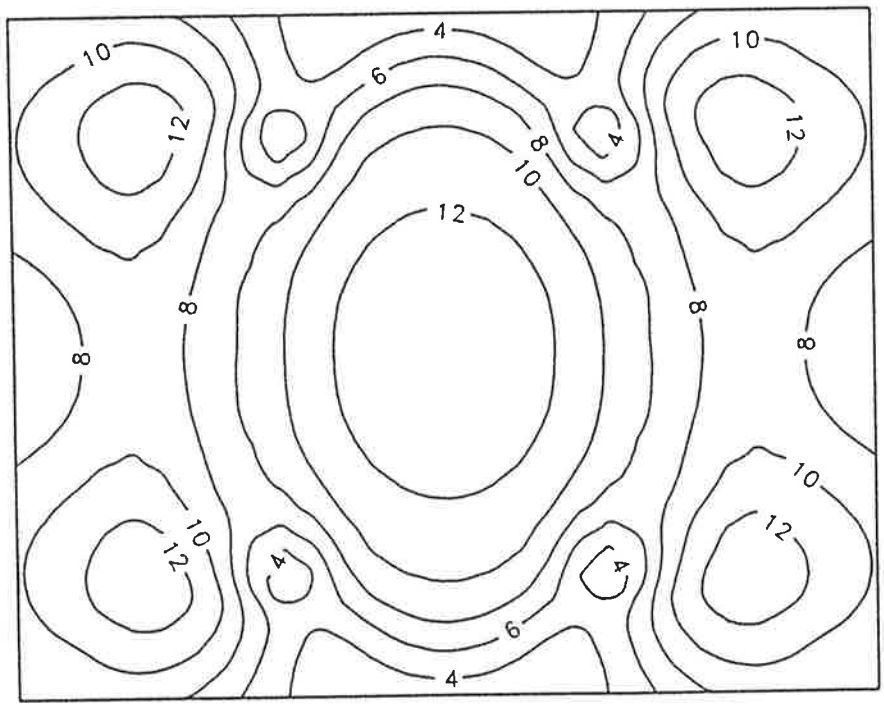

Figure 4.40 Controlled mean square velocity levels (dB) on the (0.38 x 0.3 x 0.002m) panel surface for harmonic excitation at 350 Hz and heavy damping, vibration control at (0.0, 0.0).

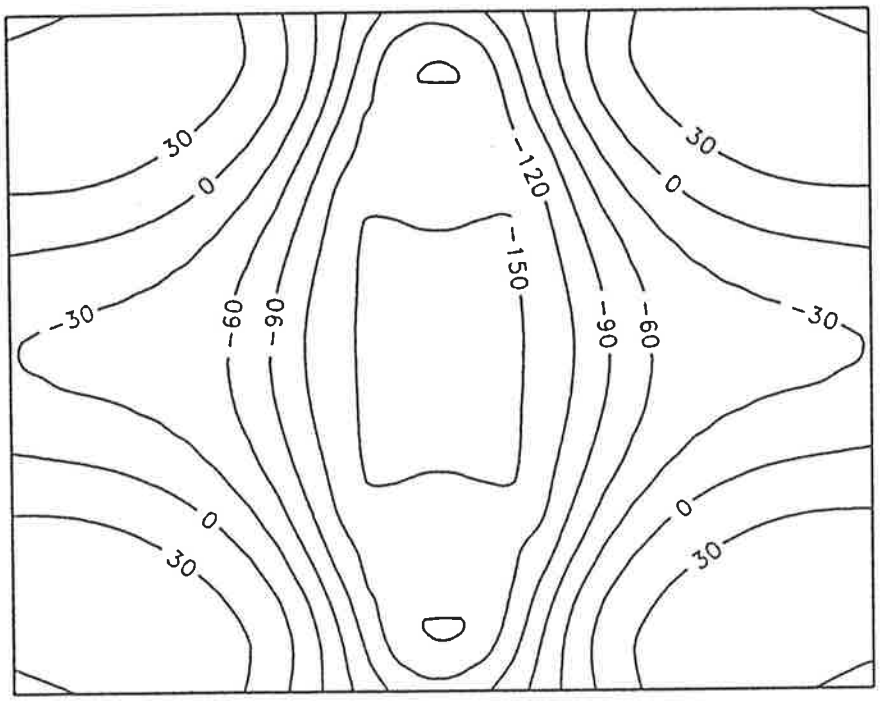

Figure 4.41 Relative phases (degrees) of the panel surface velocity under primary excitation only for the heavily damped panel, 0.38 x 0.3 x 0.002m, harmonically excited at 350 Hz.

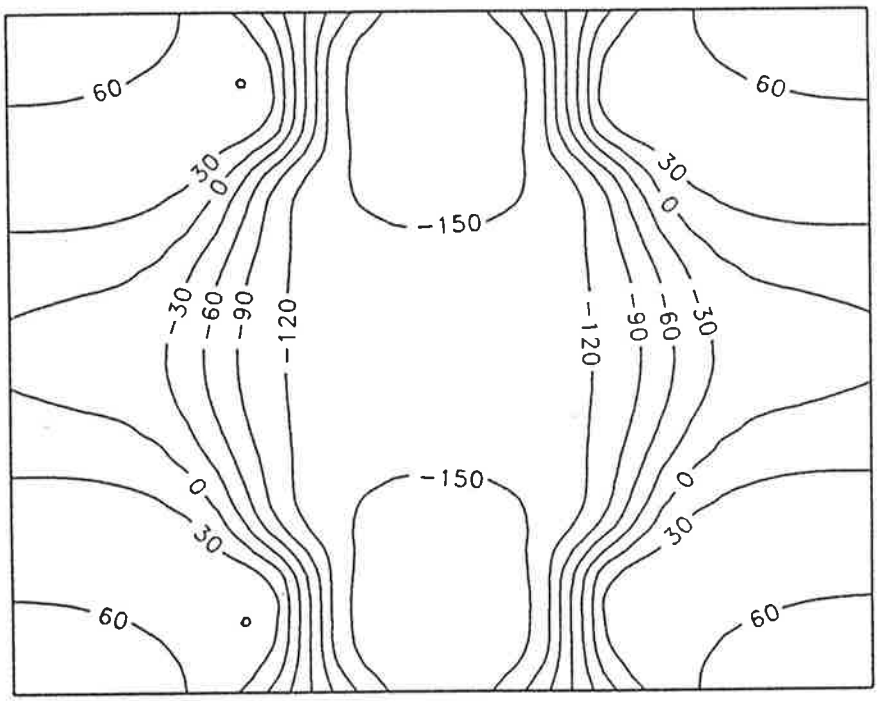

Figure 4.42 Relative phases (degrees) of the panel surface velocity under controlled conditions for the heavily damped panel, 0.38 x 0.3 x 0.002m, harmonically excited at 350 Hz, vibration control at (0.0, 0.0).

The panel velocities and phases before and after control are shown in figures 4.39 - 4.42. Comparing figures 4.39 and 4.40, it can be seen that the overall velocity levels under controlled conditions increase. Importantly here, the velocity level in the center region, and the area it encompasses, both increase. When this is viewed in light of the controlled phases, plotted in figure 4.42, it can be deduced that the center has become an acoustic sink. The panel is again radiating like a longitudinal quadrupole under controlled conditions, with the associated reduction in radiation efficiency. Thus in this case the sound power reduction is achieved solely by the modal phase rearrangement mechanism.

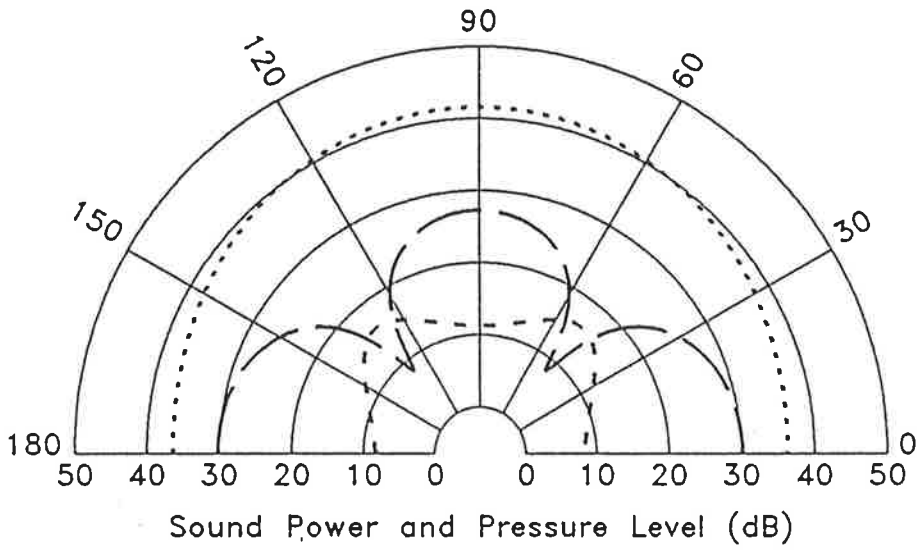

Figure 4.43 Sound pressure levels (dB) before control and after "ideal" control as a function of azimuthal angle in a horizontal plane normal to the mid point of the panel surface; and the maximum achievable reductions (dB) in radiated sound power as a function of angular location of a single error microphone in the same plane. The panel size is 0.38 x 0.3 x 0.002m, heavily damped, harmonically excited at 350 Hz, and the single vibration control source is located at (0.0, 0.0), ----- = primary radiated, - - - = residual radiated, —— · = sound power reduction for a given single error microphone placement.

As the controlled vibration characteristics are similar for both the lightly and heavily damped cases when the vibration source is attached at the panel center, it would be expected that the influence which the angular location of a single error microphone has upon the maximum achievable sound power attenuation would also be similar. This influence is shown in figure 4.43, again plotted with the primary radiated and ideally controlled sound fields. The results can be compared to figure 4.34, for the lightly damped case. Indeed, both the ideally controlled sound field, and the influence of error microphone placement, are similar for both the lightly and heavily damped cases.

One point of interest when comparing figures 4.34 and 4.43 is that both the controlled sound pressure levels and power reductions of the lightly damped case (figure 4.34) are reduced by approximately 6 dB from the heavily damped case (figure 4.43), yet the patterns are approximately the same. This attenuation "bias" is that portion of the control that resulted primarily from a reduction in the amplitude of the nearly-resonant (3,1) mode, seen by comparing the panel velocity plots of figures 4.29 and 4.30. The addition of the structural damping has removed this bias.

The final point to consider is the ability of a single vibration error sensor to produce sound power attenuation. The levels of maximum sound power attenuation which are possible as a result of minimizing the vibration at a single error sensor point on the heavily damped panel are plotted in figure 4.44 as a function of location of the minimization point. From the figure it can be deduced that the use of a vibration error sensor is in this case ineffective, regardless of where it is located. Indeed, minimizing the vibration level in the majority of locations will produce an increase, rather than a decrease, in the total radiated sound power level. This is not surprising,

however, as it has already been shown that optimum sound power attenuation with the control source located at (0.0,0.0) is achieved with an increase in the panel velocity levels and an alteration in the relative modal phasing, causing a reduction in the overall panel radiation efficiency.

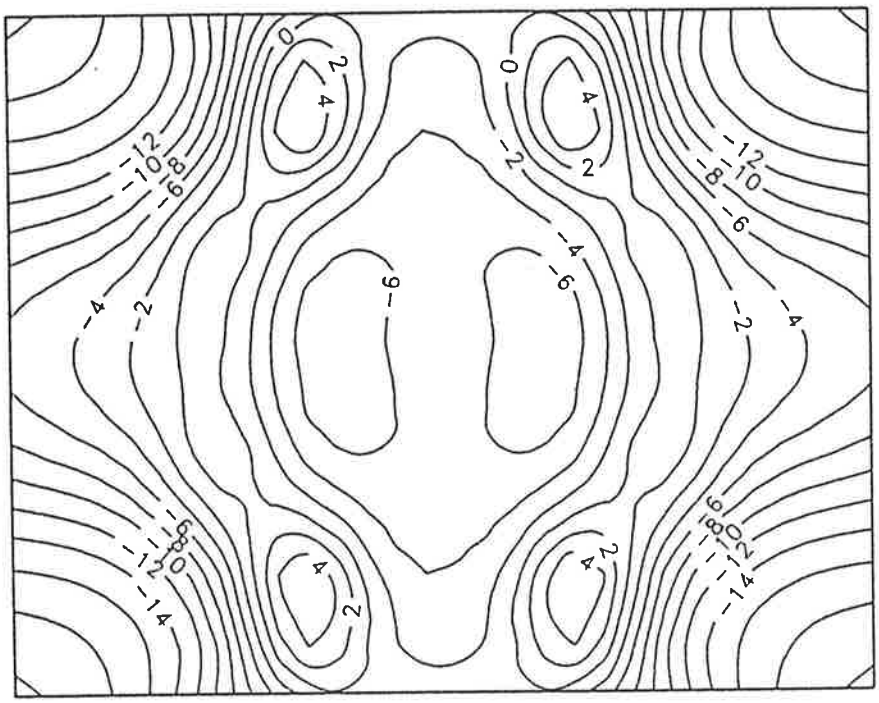

Figure 4.44 Maximum achievable reductions in radiated sound power (dB) as a function of location on the heavily damped, harmonically excited (350 Hz), 0.38 x 0.3 x 0.002m panel of the point at which the panel velocity is minimized for a vibration control source location of (0.0, 0.0).

4.5.3. Influence of modal density

The previously considered panels have a relatively low modal density. To determine whether or not a single vibration control source could produce significant levels of sound power attenuation with an increased modal density, the thickness of the original (lightly damped) panel was reduced from 2.0 mm to 0.5 mm, with the edge dimensions kept constant. Results

showing maximum possible sound power attenuation levels as a function of control source location on the 0.5 mm thick panel are given in figure 4.45. From this figure, it can be seen that there are areas on the panel where the application of a single vibration control source can produce significant levels of sound power attenuation, even with the increase in modal density.

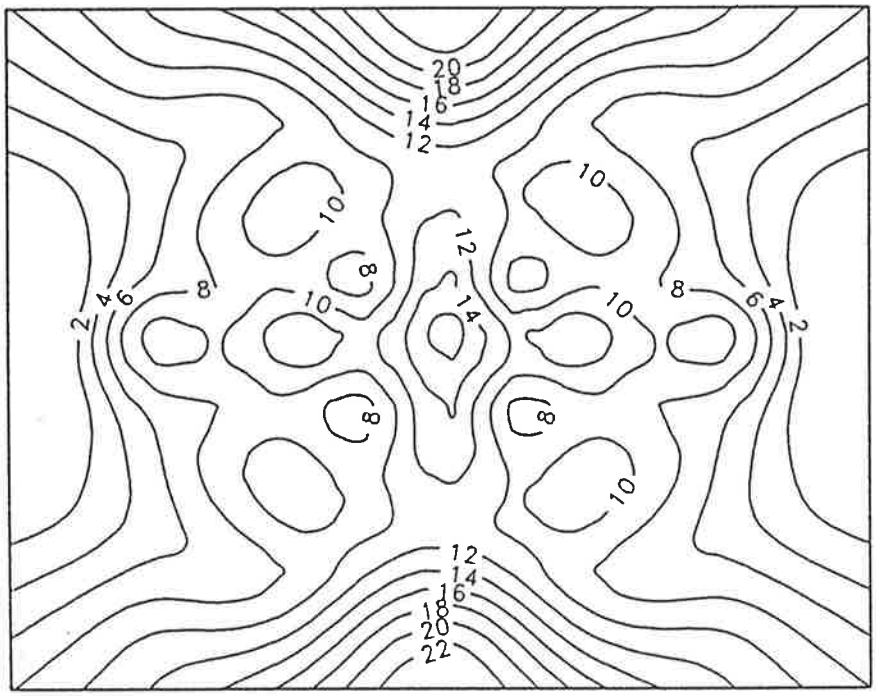

Figure 4.45 Maximum achievable levels of sound power attenuation (dB) as a function of the vibration source location on the panel, 0.38 x 0.3 x 0.0005 m, with light damping and harmonic excitation at 350 Hz.

The change in the velocity amplitudes and phases of the first 8 non-zero panel modes which result when vibration control is applied at (0.0,0.0) are illustrated in figure 4.46. There is an increase in the amplitude, and a change in phase, for many of these modes (note especially the efficient radiating (1,1), (3,1), and (1,3) modes). The associated panel velocities and phases before and after control are illustrated in figures 4.47 - 4.50. Comparing the before and after panel velocity levels shown in figures 4.47 and 4.48, it can be seen that the action of the control source increases the overall panel velocity levels. The key to the control mechanisms at work here, though, can be seen in the "before" and "after" phase plots of figures 4.49 and 4.50. The application of vibration control has caused the panel to "break up" into many small areas of in phase and out of phase vibration. The radiation efficiency of such a pattern is poor, resulting in the 19.3 dB attenuation in radiated sound power.

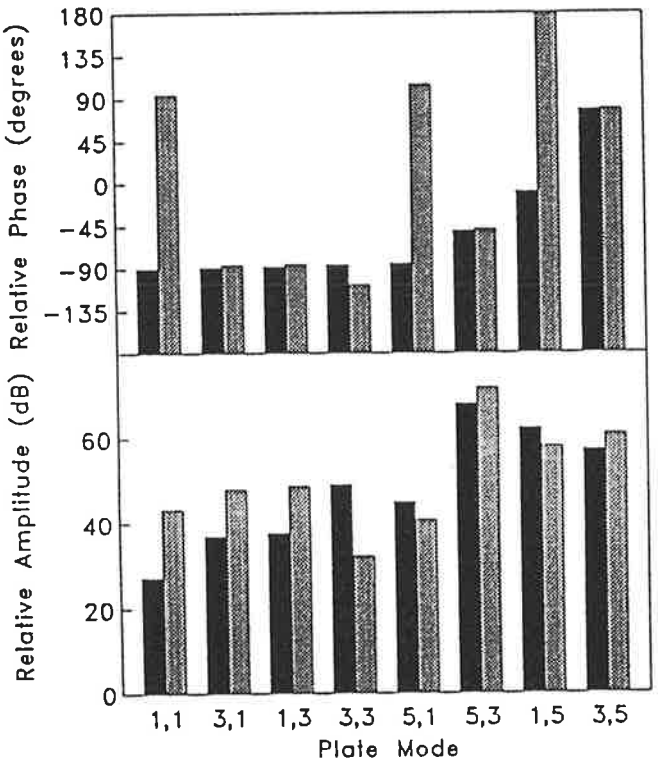

Figure 4.46 Comparison of modal velocity levels on the lightly damped panel, 0.38 x 0.3 x 0.0005 m, harmonically excited at 350 Hz, before and after control, ■ = primary excitation, ▒ = vibration control at (0.0, 0.0).

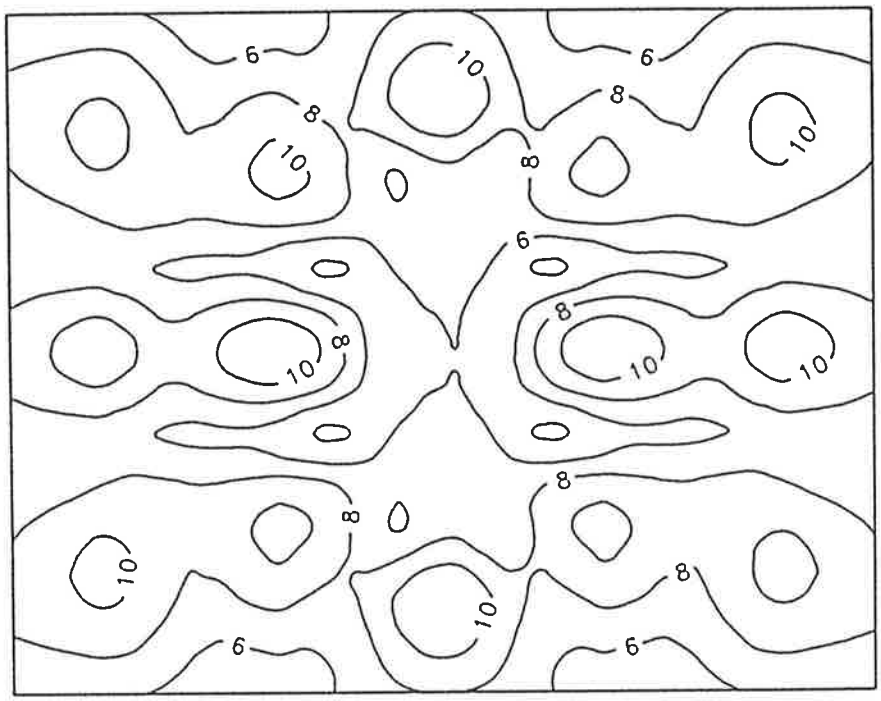

Figure 4.47 Primary excitation mean square velocity levels (dB) on the (0.38 x 0.3 x 0.0005m) panel surface for harmonic excitation at 350 Hz and light damping.

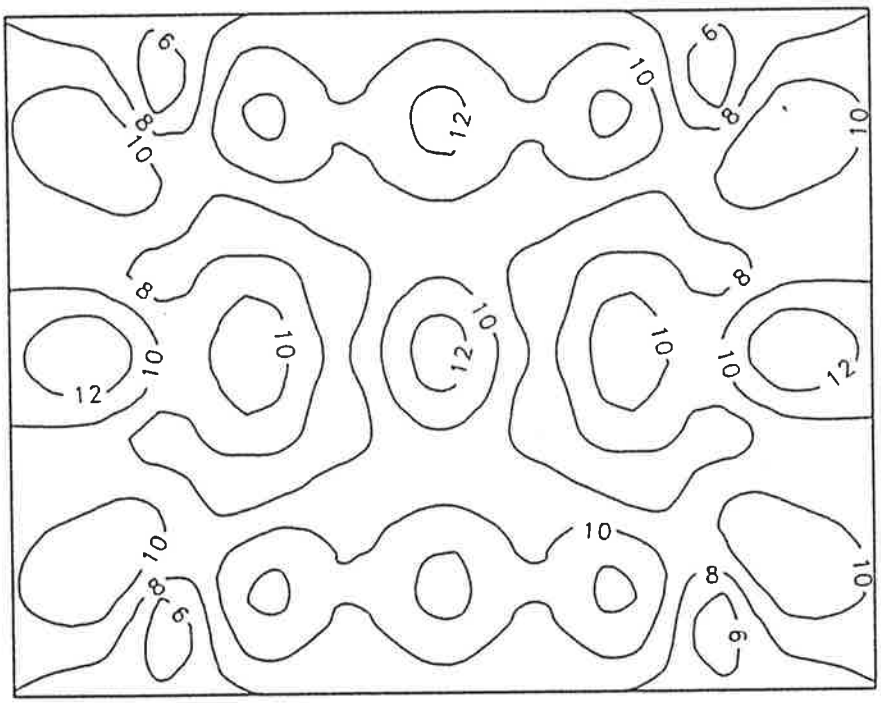

Figure 4.48 Controlled mean square velocity levels (dB) on the (0.38 x 0.3 x 0.0005m) panel surface for harmonic excitation at 350 Hz and light damping, vibration control at (0.0, 0.0).

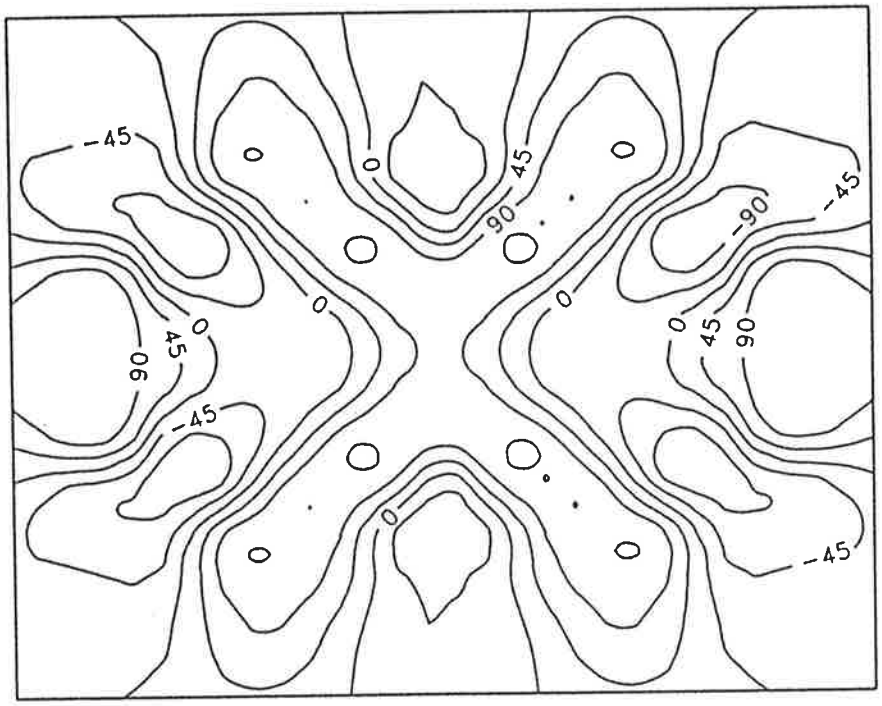

Figure 4.49 Relative phases (degrees) of the panel surface velocity under primary excitation only for the lightly damped panel, 0.38 x 0.3 x 0.0005m, harmonically excited at 350 Hz.

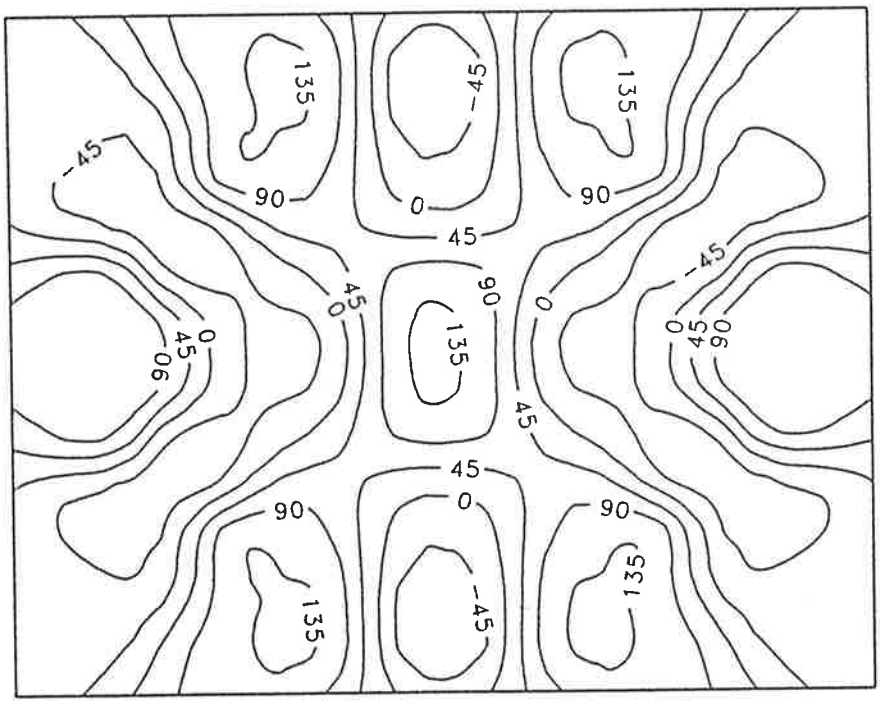

Figure 4.50 Relative phases (degrees) of the panel surface velocity under controlled conditions for the lightly damped panel, 0.38 x 0.3 x 0.0005m, harmonically excited at 350 Hz, vibration control at (0.0, 0.0).

4.5.4. Effect of panel size

As the modal phase rearrangement mechanism achieves sound power reduction by changing how the structure interacts with the (nearfield) acoustic space, it would seem reasonable to suggest that the size of the structure relative to the acoustic wavelength at the frequency of interest would have an influence upon the effectiveness of this mechanism. To examine this, the base case panel was extended proportionally in size (to keep the same mode order). The panel thickness was increased, and the material density decreased, to maintain the same modal density and modal overlap. The relationship between the the panel area, thickness, and material density required to do this is:

$$\frac{\rho_{s1}}{\rho_{s2}} = \left(\frac{h_2}{h_1} \right)^4 = \left(\frac{A_2}{A_1} \right)^{4/3} \qquad (4.8)$$

The final dimensions considered here are 1.075m x 0.8485m x 4mm, resulting in a panel size of approximately one wavelength across at the frequency of interest (350 Hz), in contrast to almost three for the original panel. It should be noted that these alterations have the effect of reducing the panel critical frequency (Bies and Hansen, 1988), and thus increasing all of the modal radiation efficiencies as shown in Table 4.2. This, too, will influence the results, as discussed shortly. The primary point forces were relocated (proportionally) to x = ±0.484m, y = ±0.382m. The maximum levels of sound power attenuation plotted as a function of control source position are given in figure 4.51 for this panel.

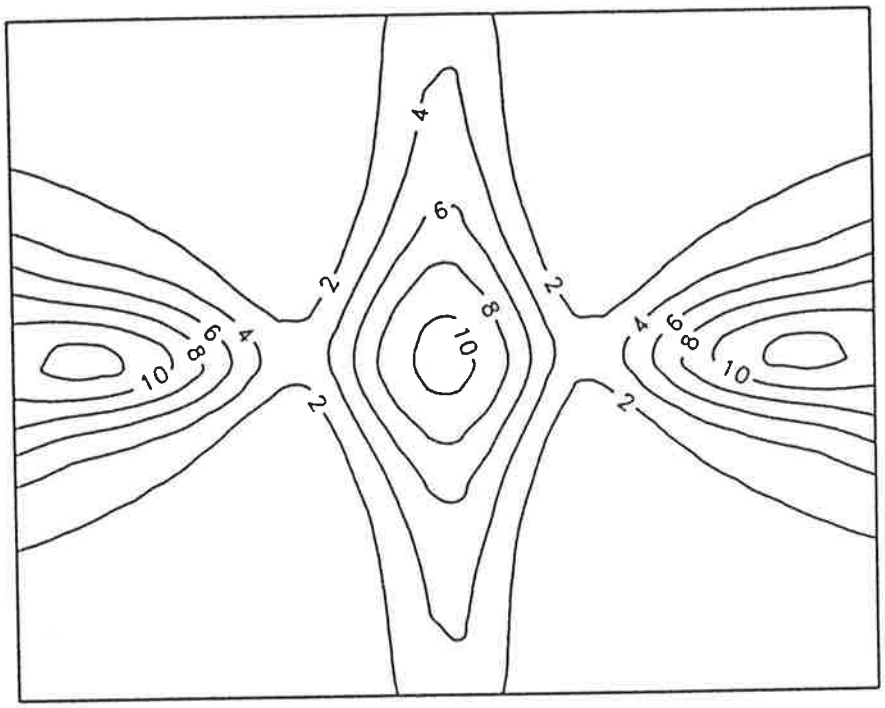

Figure 4.51 Maximum achievable levels of sound power attenuation (dB) as a function of the vibration source location on the panel, 1.075 x 0.8485 x 0.004 m, with light damping and harmonic excitation at 350 Hz.

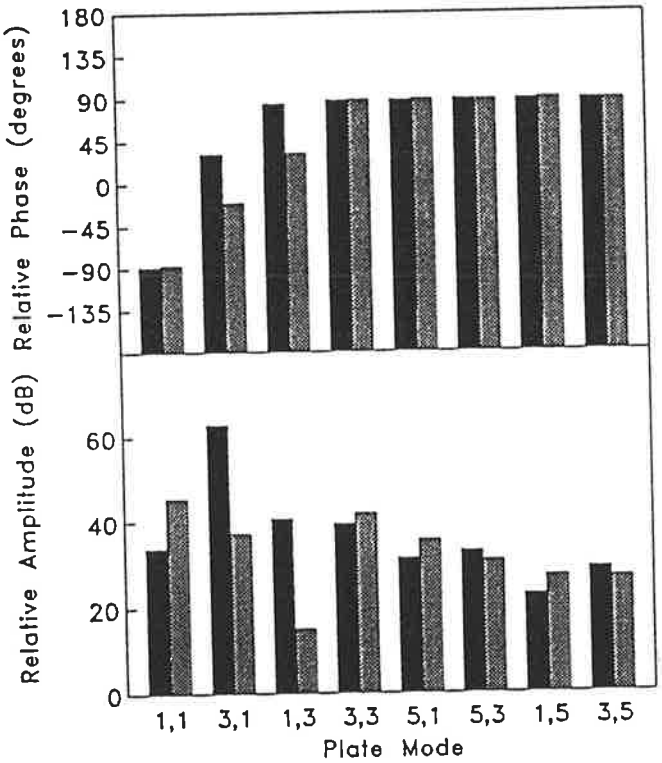

Figure 4.52 Comparison of modal velocity levels on the lightly damped panel, 1.075 x 0.8485 x 0.004 m, harmonically excited at 350 Hz, before and after control, ■ = primary excitation, ▒ = vibration control at (0.0, 0.0).

In comparing figure 4.51 to the base case figure 4.26, it is apparent that the pattern of optimal attenuation contours is similar, but that the levels of attenuation are significantly reduced. This reduction is due, in part, to the increase in radiation efficiency of the even indice panel modes, especially the (2,1) mode, as shown in Table 4.2. These modes are not excited by the primary disturbance, but will be excited by a non-symmetric placement of the control source. As these modes are now efficient radiators this will have a dterimental effect upon the levels of attenuation achieved.

Consider now the effect upon the modal amplitudes and phases of minimizing the radiated sound power caused by applying a control force at the panel center, which will not excite any of these even indice modes, shown in figure 4.52. It is clear that the amplitudes of the (3,1) and (1,3) modes have been reduced by an amount much greater than the increase in the (1,1) modal amplitude. This indicates that the principal mechanism of control has now changed from modal phase rearrangement to modal amplitude control, due to the increase in the size of the structure.

4.5.5. Effect of frequency upon modal rearrangement

It was shown in the base case examination that modal rearrangement was the principal mechanism by which sound power attenuation was achieved when a vibration control source was placed at the panel center. This was due to the fact that the two principal radiating modes, the (3,1) and (1,1), were out of phase at this point. At 350 Hz (the frequency examined in the base case) the (3,1) mode had not yet passed through resonance. When this does happen, the (3,1) and (1,1) modes will no longer be out of phase, but rather in phase. This should have a

significant effect upon the sound power attenuation achieved by applying vibration control at the panel center.

The effect of increasing the frequency to 400 Hz (above the (3,1) resonance of approximately 359 Hz) can be deduced by viewing figure 4.53 which shows the maximum sound power attenuation as a function of control source location. The optimum control source locations on the panel edges, where attenuation was achieved mainly through modal amplitude control, are still present. The optimum location in the panel center, however, where the principal mechanism was modal phase rearrangement, has disappeared. This is principally because the (3,1) and (1,1) modes are now in phase at this point. It is also partly due to the fact that the (3.1) modal amplitude under primary excitation has decreased, as it is further removed from its resonance frequency.

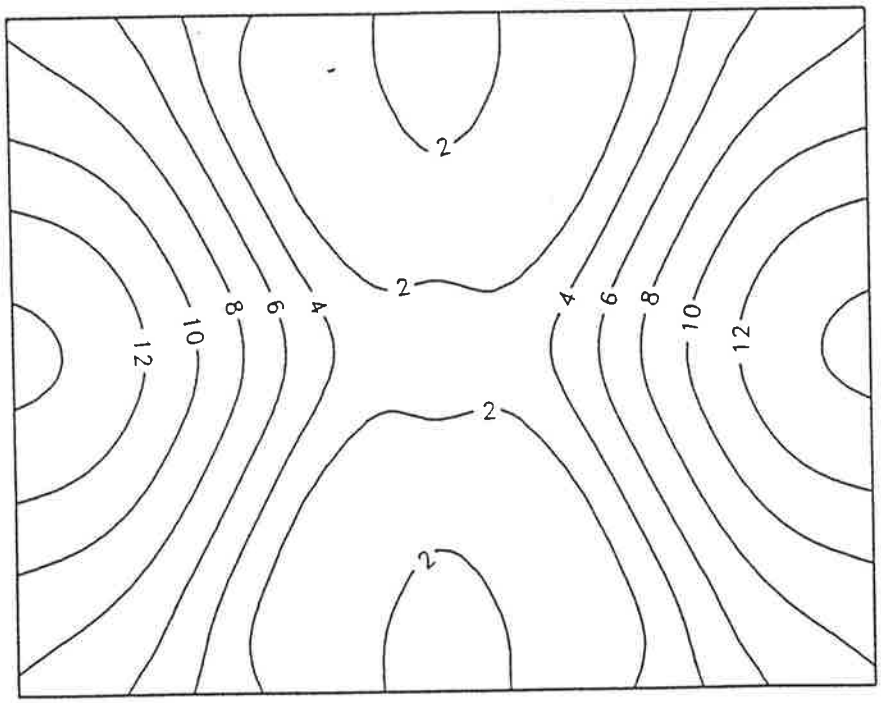

Figure 4.53 Maximum achievable levels of sound power attenuation (dB) as a function of the vibration source location on the panel, 0.38 x 0.3 x 0.002 m, with light damping and harmonic excitation at 400 Hz.

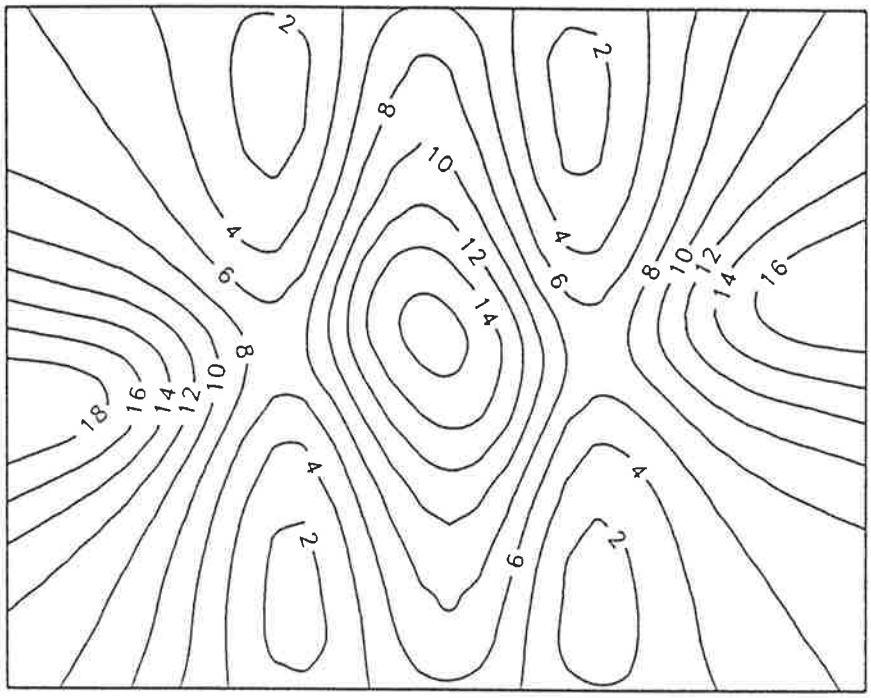

Figure 4.54 Maximum achievable levels of sound power attenuation (dB) as a function of the vibration source location on the panel, 0.38 x 0.3 x 0.002 m, with light damping and non symmetric primary harmonic excitation at 350 Hz.

4.5.6. Effect of a non-symmetric forcing function

The primary forcing functions of the previously examined cases are all symmetric with respect to the panel geometry. As a result, only odd-odd panel modes are excited under the action of the primary forcing function. Although these modes represent the dominant radiators at this frequency (350 Hz), a change in the nature of the primary forcing function may alter the results.

The effect which moving one of the four primary point forces by 10 mm in both the positive x and y directions (from (-0.171,-0.135) to (-0.161,-0.125)) has upon the maximum radiated sound power attenuations at any point can be found by comparing this case, shown in figure

4.54, with the base case of figure 4.26. Comparing these, it can be deduced that this shift produces a skew in the plot of maximum achievable power attenuation as a function of control source location, but no other significant result. This is not surprising, as the volumetric (3,1), (1,1), and (1,3) modes dominate the sound radiation in this frequency range.

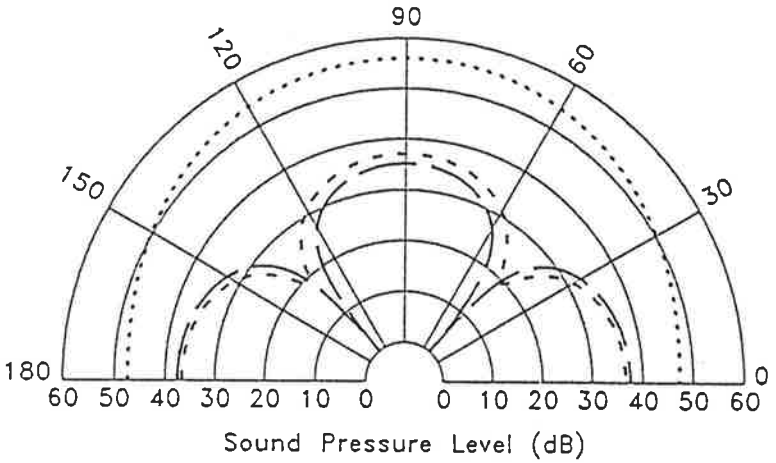

Figure 4.55 Sound pressure levels (dB) before and after control for the 0.38 x 0.3 x 0.002m lightly damped panel excited harmonically at 350 Hz for two cases of control by a single vibration control source at (0.0, 0.0); one with the sound field minimized at the error microphone location (the optimum location for this source location) and the second with the sound field only reduced by 30 dB at the error microphone location. ····· = primary radiated, —— · = residual with maximum pressure reduction, - - - = residual with 30 dB pressure reduction.

4.5.7. Effect of reduced sound pressure attenuation at the error microphone

Thus far it has been assumed that it is possible to completely minimize the sound pressure at the error microphone position. In theory, this means perfect cancellation. In practice, however, such levels of reduction are not achievable by the electronic control systems. For periodic sound attenuation, reductions at a point of the order of 30 dB are more reasonable. The effect

which this will have upon the total radiated sound power attenuation needs to be considered. This can be done theoretically by using equation (3.58) to first find the complex control force which will provide the maximum levels of sound attenuation, then reduce the control force while maintaining the optimal phase (between the complex components).

Figure 4.55 depicts the primary radiated sound field for the base case 2 mm panel, and two residual sound fields produced by minimizing the sound pressure at an azimuth angle of 50° (near an optimum location) at a radius of 1.8 meters. One residual sound field is produced by perfect cancellation at the error microphone location, the other by only a 30 dB reduction at this point. The two residual sound field patterns are similar in shape, with the 30 dB case slightly greater in the front lobe, and slightly less on the sides. In fact, the 30 dB case has produced a sound power attenuation level of 20.8 dB, while the perfect cancellation case has achieved 22.1 dB of sound power control. Thus, the global effect of reduced control at the error microphone location is minimal, as the dramatic pressure reductions at this location are due only to local cancellation.

4.5.8. Tolerance to phase error

When the noise source is periodic in nature, it may be advantageous to implement the electronic control system in the frequency domain. Unless the sampling rate of the controller is synchronized with the (acoustic) frequency of interest, there will be phase errors associated with the bandwidth of the bins of the Fourier transform. If a frequency domain scheme is to be viable, the effect of phase errors on the sound power reduction must be known.

The effect which holding the optimum control force amplitude (found from equation (3.58)) fixed, but deviating the phase (for the complex force), of the control source vibration signal has upon the maximum levels of sound power attenuation is shown in figure 4.56, and upon the levels of sound pressure reduction at the error microphone in figure 4.57.

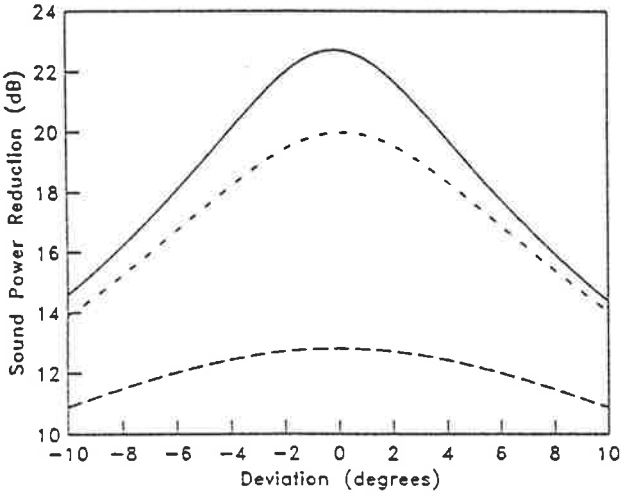

Figure 4.56 Maximum achievable sound power reduction (dB) as a function of phase error in the signal used to drive the control source for a lightly damped panel (0.38 x 0.3 x 0.002m) harmonically excited at 350 Hz, ——— = vibration control at (0.0, 0.0), - - - = vibration control at (0.17, 0.0), — — — = acoustic control at (0.0, 0.0, 0.02).

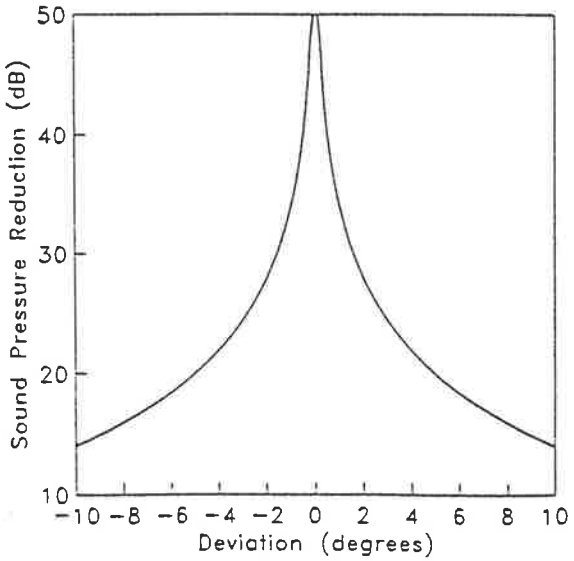

Figure 4.57 Maximum achievable sound pressure reduction (dB) at the error microphone as a function of phase error in the signal used to drive the control source for a lightly damped panel (0.38 x 0.3 x 0.002m) harmonically excited at 350 Hz, ——— = vibration control at (0.0, 0.0), - - - = vibration control at (0.17, 0.0), — — — = acoustic control at (0.0, 0.0, 0.02).

In comparing these, it is obvious that the pressure reduction at the error microphone is much more sensitive to phase errors than the overall reduction in radiated sound power. This further indicates that the dramatic levels of sound pressure reduction possible at the error microphone are due to local cancellation. It would also appear from figure 4.56 that the modal rearrangement mechanism, which is dominant when the control source is placed at (0.0,0.0), is more sensitive to phase errors than the modal control mechanism, which is dominant when the control source is placed at (0.17,0.0).

4.6. ANALYTICAL STUDY OF SYSTEM VARIABLES - USE OF ACOUSTIC CONTROL SOURCES

It was shown theoretically and experimentally in chapter 2, and theoretically elsewhere(Nelson et al, 1987), that acoustic control sources provide global sound power attenuation by a reduction in the radiation impedance of both the primary and control noise sources. Under the action of active control, each source either emits a greatly reduced level of sound power, or becomes an acoustic sink (using the "absorbed" acoustic energy to help overcome the mechanical input impedance of the source).

For the analytical models presented here, it will be assumed that the fluid reaction force on the panel is negligible. Therefore, the action of the active acoustic source has a negligible influence upon the primary excited panel velocity distribution. This assumption was found to be valid experimentally for the case being considered here, where the fluid medium is air.

4.6.1. Examination of the base case

The use of a single acoustic point source, located 20mm from the surface of the same mechanically excited panel considered in section 4.4.1, will be examined as a base case here (note that this radial distance will be used throughout this section unless otherwise specified). The effect which the control source location has upon the level of total radiated sound power attenuation is shown in figure 4.58, where the maximum achievable sound power attenuation is plotted as a function of acoustic control source location in a plane 20mm in front of the panel surface. For the case considered here the wavelength of sound in air is approximately 2.5 to 3 times the panel dimensions.

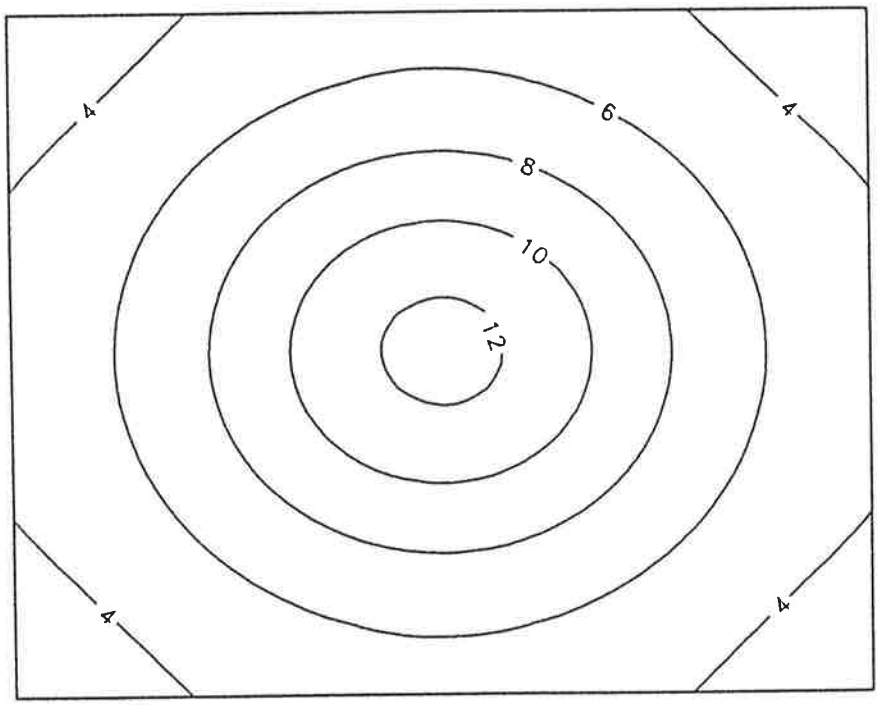

Figure 4.58 Maximum levels of sound power attenuation (dB) as a function of location of an acoustic control source in a plane parallel to the panel surface and 0.02m from it. The panel is lightly damped, 0.38 x 0.3 x 0.002m, and is harmonically excited at 350 Hz.

In viewing figure 4.58, it can be seen that the optimum control source location is at the panel center, with locations corresponding to similar levels of attenuation forming concentric rings about this. This pattern results from the fact that the panel is radiating, under primary excitation, in a monopole-like fashion. This radiation pattern is concentric about the panel center, due to the symmetric nature of the primary forcing function. The control of the total radiated sound power for this case becomes similar to the minimization of the total radiated sound power from two freefield acoustic point sources having a separation distance much less than a wavelength of sound (Nelson et al, 1987).

As described in the previous section, the placement of the active control source(s) will set the maximum levels of total radiated sound power attenuation. The placement of the error sensors will determine how close to this upper bound the maximum levels achievable by the electronic control system are. When acoustic control sources are used, the error sensor is constrained to being acoustic in nature (such as a microphone), as there is a negligible change in the panel velocity distribution during the application of active control.

The influence of the angular location of a single error microphone (at which the sound pressure is minimized) upon the maximum achievable of reduction in total radiated sound power, for the use of an acoustic control source located at the panel center, is shown in figure 4.59. It is plotted with both the primary radiated sound field and the optimally controlled residual sound field. As with the use of vibration control sources, it can be seen that the optimum error sensing angular location is at the point of minimum sound pressure in the optimally controlled residual sound field.

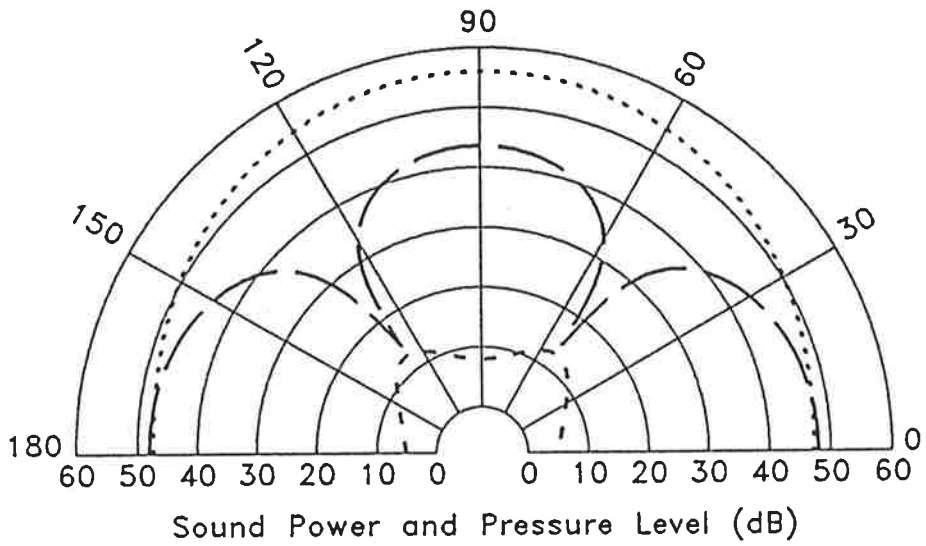

Figure 4.59 Sound pressure levels (dB) before control and after "ideal" control as a function of azimuthal angle in a horizontal plane normal to the mid point of the panel surface; and the maximum achievable reductions (dB) in radiated sound power as a function of angular location of a single error microphone in the same plane. The panel size is 0.38 x 0.3 x 0.002m, lightly damped, harmonically excited at 350 Hz, and the single acoustic control source is located at (0.0, 0.0, 0.02), ----- = primary radiated, ——— · = residual radiated, - - - = sound power reduction for a given single error microphone placement.

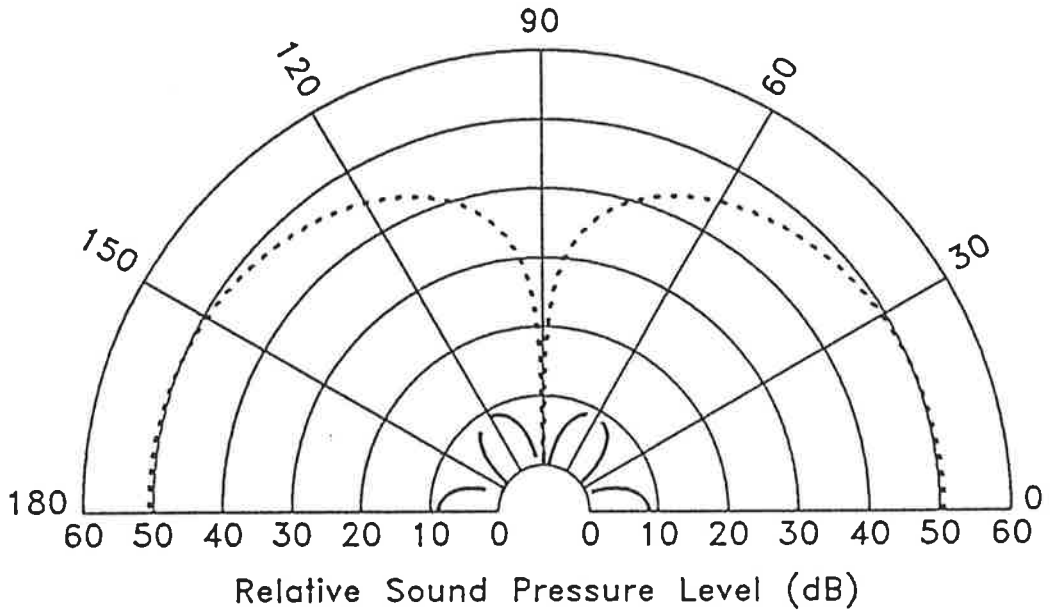

Figure 4.60 Sound pressure levels (dB) before and after "ideal" control for the 0.38 x 0.3 x 0.002m lightly damped panel excited harmonically at 200 Hz by an antisymmetric primary force and controlled by two acoustic sources at (±0.2, 0.0, 0.02m), - - - - - = primary radiated, —— · = residual radiated.

It should be noted that this trend exists for multiple control sources as well as for single control sources. Figure 4.60 shows the primary radiated and optimally controlled residual sound fields for the case of the base 2mm panel excited antisymmetrically (the primary point forces at x = +0.171 180° out of phase with those at x = -0.171) at 200 Hz, controlled by 2 acoustic sources at (x,y,z) = (±0.20, 0, 0.02) meters relative to the plate surface. Here it can be seen that there are 3 pressure minima, at azimuth angles of 30°, 90°, and 150°. To practically implement this two control source system a minimum of 2 error microphones are required to satisfy the observability / controllability constraints. Figure 4.61 shows the maximum achievable levels of

sound power reduction for a given microphone position pairing, calculated at a radius of 1.8 meters. Here it can be seen that the optimum locations are at the pairings of residual acoustic pressure minima, (30°, 90°), (30°, 150°), and (90°, 150°), a result similar to that for the single control source case. It is possible to nearly achieve the maximum possible sound power reduction (43.3 dB) with this control source arrangement by minimizing the sound pressure at two locations corresponding to any one of the preceding pairs.

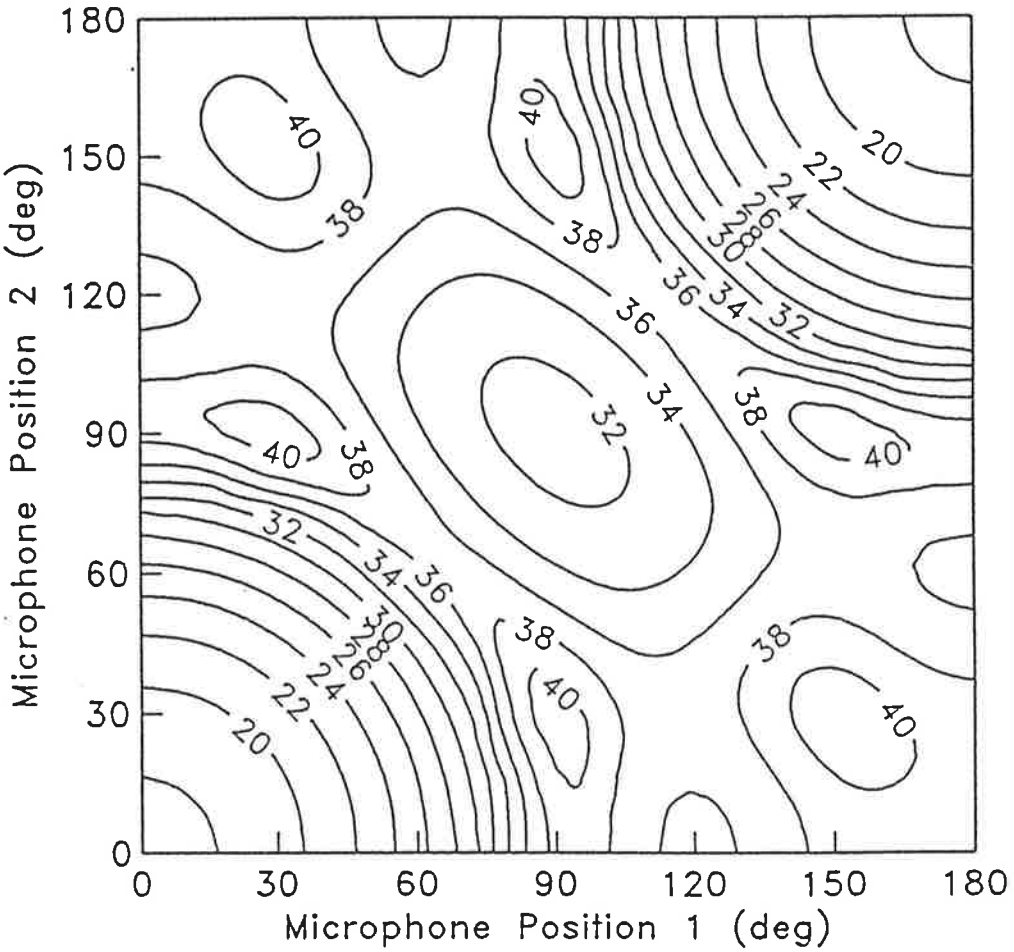

Figure 4.61 Maximum achievable levels of sound power attenuation (dB) as a function of angular location in a horizontal plane normal to the mid point of the panel surface of two error microphones for the lightly damped 0.38 x 0.3 x 0.002m lightly damped panel harmonically excited at 200 Hz by an antisymmetric primary force and controlled by two acoustic sources at (±0.2, 0.0, 0.002m).

4.6.2. Effect of panel / control source separation distance

The effect on the maximum achievable sound power reduction of moving an acoustic control source, located at the panel center (the optimal location here), normally outwards from the panel surface is shown in figure 4.62. The pattern is that of the absolute value of a sinc function, rotating through one cycle for a distance corresponding to one acoustic wavelength at the frequency of interest (the wavelength is equivalent to a full cycle, approximately one meter in this case). Thus at a wavelength from the noise radiating surface, the acoustic control source is completely ineffective. This is the same result as that derived previously (Nelson et al, 1987) for the separation of two freefield point sources, further supporting the fact that the same physical mechanism (a mutual reduction in the radiation impedances of both the primary and control noise sources) is at work in both cases.

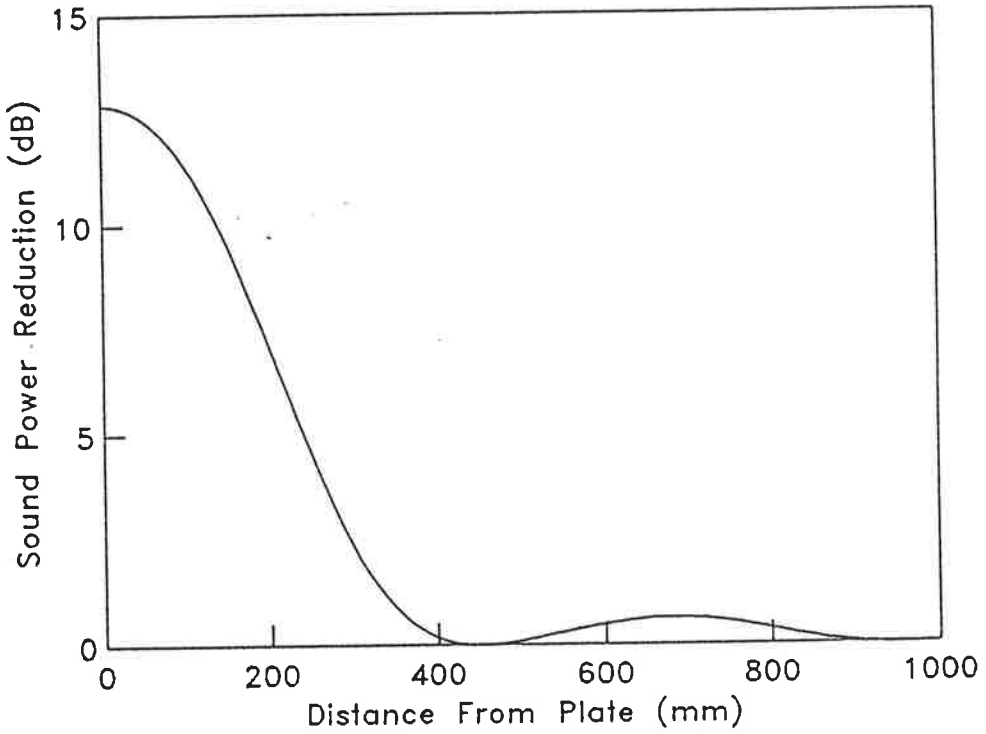

Figure 4.62 Maximum achievable reduction in sound power (dB) radiated by the 0.38 x 0.3 x 0.002m lightly damped panel harmonically excited at 350 Hz for an acoustic control source located on an axis normal to the panel center as a function of axial distance of the control source from the panel center.

4.6.3. Effect of panel size

For the base case, only the odd-odd panel modes were excited, due to the nature of the primary forcing function, and this coupled with the small plate size compared to a wavelength of sound resulted in the panel radiation pattern being largely monopole-like (see Figure 4.59). If the panel dimensions were increased, this sound radiation pattern would significantly alter, reflecting more the velocity distribution of the dominant structural mode(s). This would be expected to influence the optimum location of the acoustic control source(s), and the maximum levels of sound power attenuation that can be achieved for the same number of control sources.

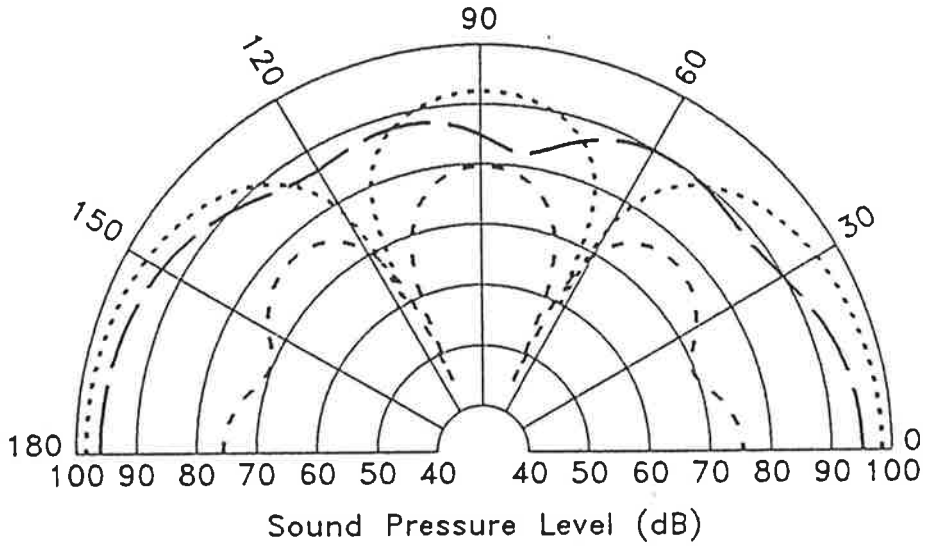

Figure 4.63 Sound pressure levels (dB) as a function of azimuthal angle in a horizontal plane normal to the mid point of the panel surface before and after "ideal" control for the 1.075 x 0.8485 x 0.004m lightly damped panel harmonically excited at 350 Hz and controlled by one acoustic source at (0.0, 0.0, 0.02) or three at (0.0, 0.0, 0.02), (±0.3, 0.0, 0.02), ····· = primary radiated, —— ·= 1 acoustic control, - - - ·= 3 acoustic controls.

To study this effect, the panel dimensions were again increased to 1.075m x 0.8485m x 4mm, in accordance with equation (4.8) in section 4.5.4. This resulted in the panel dimensions approximating one wavelength of sound and the critical frequency of the panel dropping by a factor of 4, making the panel a much more efficient sound radiator. The primary excited radiation pattern, shown in figure 4.63, now has three main lobes, as opposed to the single lobe for the smaller panel shown in figure 4.34.

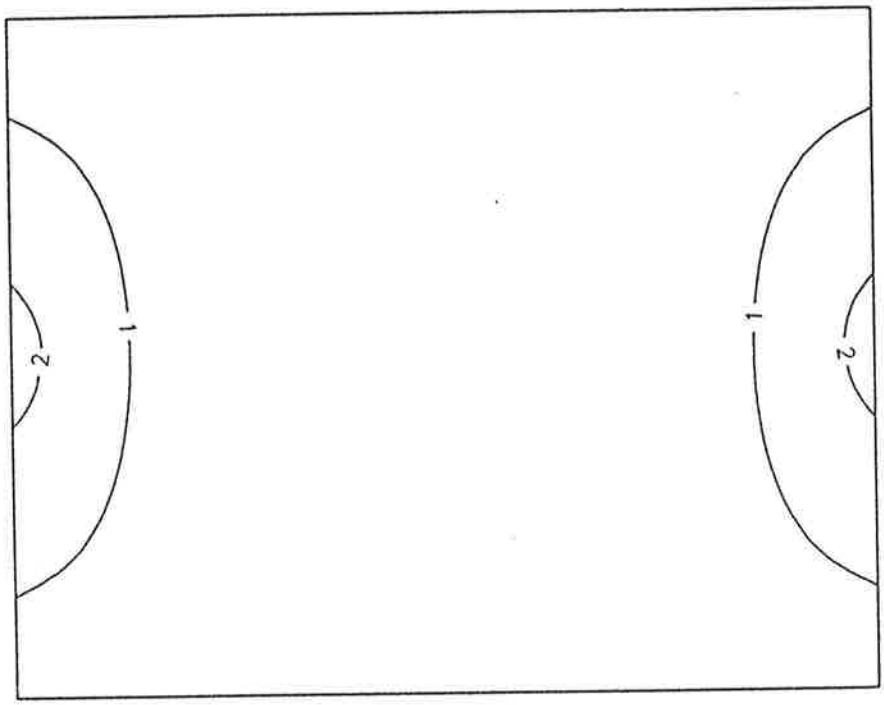

Figure 4.64 Maximum achievable levels of sound power attenuation (dB) as a function of the acoustic control source location in a plane parallel to the panel surface and 0.02m from it, 1.075 x 0.8485 x 0.004 m panel with light damping and harmonic excitation at 350 Hz.

The maximum levels of sound power attenuation for a single control source, plotted as a function of control source location in a plane parallel to the plane of the panel and 20mm from it, are shown in figure 4.64 for this enlarged panel. The two main points of interest are the greatly reduced levels of attenuation, and the change in optimum control source location. These changes have occurred because the separation distance between the radiating edges, and the length of these edges, have increased. If the acoustic control source is placed in the center of the panel, it would be approximately one half of a wavelength from the radiating edges. At this separation distance the amount of acoustic power control is small, as evidenced by the similar effect of increasing the normal separation distance between the control source and panel surface, as illustrated in figure 4.62. Also, the radiating edge itself is nearly one wavelength long. Therefore, the acoustic field generated by a source placed at its center (on the x-axis here) would have a phase variation along the edge of nearly 180° in each direction, greatly reducing the attenuation that can be achieved. Thus the best control that can be achieved is 2.6 dB, and this is achieved with the control source located at one of the panel edges.

This effect is similar to the effect of control source length on the attenuation of plane wave propagation in ducts, discussed in chapter 2. In the latter case, there is a phase variation across the face of the source as the plane wave propagates downstream. This phase variation causes a reduction in the ability of the source to control the propagation, a reduction proportional to a sinc function rotating through one cycle for a distance of one acoustic wavelength. Near a source length of one half of a wavelength or greater, the achievable sound power reduction drops off markedly.

The addition of a second acoustic control source does help this problem. The optimal location for the first and second control sources is now on each plate edge and the x-axis (that is, ±0.51, 0.0). This provides a 7.4 dB sound power attenuation level, as opposed to the 2.6 dB level for the optimally placed single source (at one edge of the panel).

The further addition of a third acoustic control source greatly improves these results. The optimum locations here are (±0.30,0.0) and (0.0,0.0). The sound power attenuation that can be achieved is 14.8 dB. Figure 4.63 shows the residual sound field for this case, as well as for the optimized case of a single control source at one of the panel edges.

It is interesting to note that for 3 acoustic control sources, the optimal locations for two of them are not on the edges, as might be expected from the single and double source cases. If the three control sources are placed in that arrangement (one at the center and one at each edge of the panel), the maximum possible level of sound power reduction is 9.9 dB, almost 5 dB short of the optimum. This is also in contrast to the base case panel, where the optimal locations for three control sources are at the edges and center, corresponding to a maximum achievable sound power attenuation of 27.5 dB. Clearly, the panel size compared to a wavelength of sound affects the optimal control source location not only for a single source but also for multiple sources. It also affects the maximum achievable reduction in radiated sound power.

4.6.4. Effect of modal density and structural damping

As in section 4.5.3, the modal density of the panel was increased, by decreasing its thickness to 0.5mm, to examine the effect of variations in this parameter. The levels of maximum achievable attenuation plotted as a function of control source location for this case are given in figure 4.65. This can be compared to the base case plot of figure 4.58.

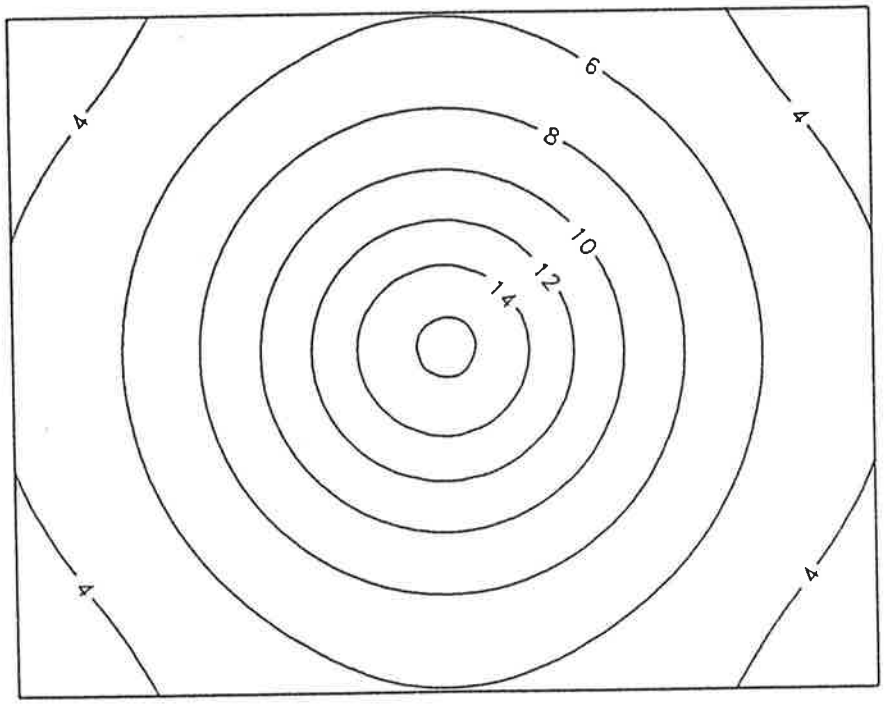

Figure 4.65 Maximum achievable levels of sound power attenuation (dB) as a function of the acoustic control source location in a plane parallel to the panel surface and 0.02m from it, 0.38 x 0.3 x 0.0005 m panel with light damping and harmonic excitation at 350 Hz.

In comparing figures 4.65 and 4.58, it can be seen that the patterns are the same in both cases, but that the levels of attenuation which can be achieved for the higher modal density case are

greater than those achieved for the lower modal density case. The reason for this can be deduced by comparing the primary source radiation plot for the high modal density case, shown in figure 4.54, with the similar plot for the low modal density case, shown in figure 4.34. The increase in modal density has produced a more uniform (monopole-like) radiation pattern, as the influence of the (3,1) modal radiation has been reduced. As the radiation patterns of the primary and control sources are more similar, the levels of sound power attenuation that can be achieved are increased.

The structural damping was also increased, to $\eta = 0.4$, to examine the influence of this parameter. The results were very similar to those found by increasing the modal density, as the radiation pattern also becomes more uniform with increased damping.

4.6.5. Effect of a non-symmetric primary forcing function

As discussed in sections 4.6.1, 4.6.4, and 4.6.5, the effect which the location of the acoustic control source has upon the achievable reduction of total radiated sound power, is influenced by the radiation pattern produced by the panel under the action of the primary forcing function. The cases examined thus far have all had a symmetric primary forcing function, which produces a symmetric primary radiated sound field.

To study the effect of altering this symmetric nature, one of the primary forces was shifted by 10mm in both the x and y directions (identical to the case described in section 4.5.6). The influence of this move can be seen by comparing the plots of maximum achievable sound power attenuation for the symmetric case, shown in figure 4.58, with the non-symmetric case,

shown in figure 4.66. By altering the symmetry of the primary radiated sound field, the levels of maximum achievable sound power attenuation for a given control source location have been slightly reduced. Also, the pattern has been slightly skewed, similar to the results obtained for the use of vibration sources, described in section 4.5.6.

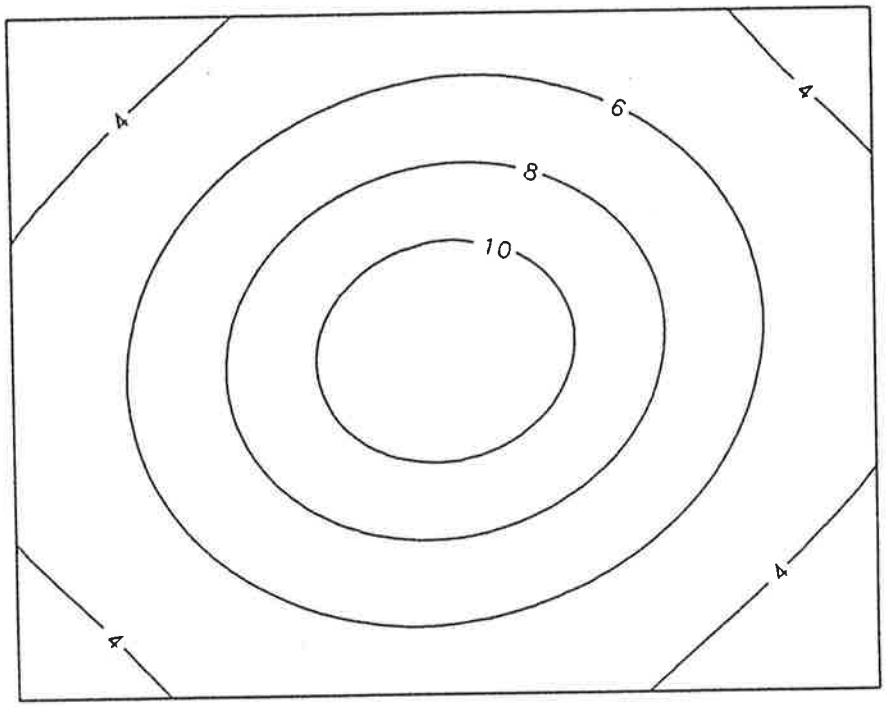

Figure 4.66 Maximum achievable levels of sound power attenuation (dB) as a function of the acoustic control source location in a plane parallel to the panel surface and 0.02m from it, 0.38 x 0.3 x 0.0005 m panel with light damping and non symmetric primary harmonic excitation at 350 Hz.

4.6.6. Effect of reduced attenuation at the error microphone

As mentioned in the previous section, the results thus far have assumed that "perfect" cancellation can be achieved by the electronic control system at the error sensing location. In

practice, however, a 30 dB reduction in sound pressure at the error microphone would be more realistic. The effect which this reduced sound pressure reduction has on the acoustic power flow attenuation must be known.

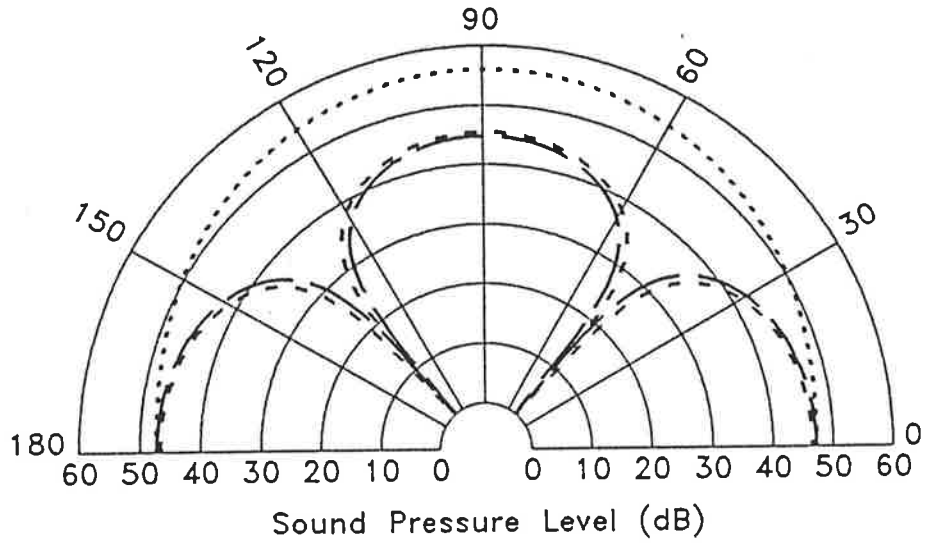

Figure 4.67 Sound pressure levels (dB) before and after control for the 0.38 x 0.3 x 0.002m lightly damped panel excited harmonically at 350 Hz for two cases of control by a single acoustic control source at (0.0, 0.0, 0.02); one with the sound field minimized at the error microphone location (the optimum location for this source location) and the second with the sound field only reduced by 30 dB at the error microphone location. ----- = primary radiated, ——— · = residual with maximum pressure reduction, - - - · = residual with 30 dB pressure reduction.

Figure 4.67 illustrates a comparison of the residual sound fields when a single control source, located in the center of the base case panel, is tuned to completely minimize the sound pressure at an azimuth angle location of 20°, at a radius of 1.8 meters, and then tuned to reduce the pressure levels by only 30 dB. The difference between the sound fields is minimal. In fact, complete local pressure cancellation at the error microphone achieves an overall acoustic power reduction of 12.8 dB, while a reduction of only 30 dB in sound pressure level at the error microphone achieves an acoustic power reduction of 12.6 dB. Clearly, the final dramatic level of sound pressure reduction at the error microphone is due only to local cancellation.

One further interesting point to note is that with decreased pressure reduction at the error microphone, the actual pressure minimum is not at the error microphone, but next to it. This has also been noted experimentally.

4.6.7. Phase error tolerance

As discussed in section 4.5.8, it is important to know the phase tolerance of the system when implementing the electronic control system in the frequency domain. Figures 4.56 and 4.57 show the influence of phase errors on both the sound power attenuation and the reduction in sound pressure at the error microphone, located at an azimuth angle of 50°, at a radius of 1.8 meters. As with the vibration control sources, the sound power attenuation is reasonably tolerant, while the sound pressure reduction at the error microphone is intolerant. Again, this is due to local cancellation at the error sensing location.

4.7. SUMMARY OF ANALYTICAL MODELLING

Vibration and acoustic control sources can both be used effectively in systems to actively attenuate the sound power radiated from a vibrating surface into free space. Acoustic control sources achieve this attenuation by reducing the radiation impedance seen by both the primary and control sound sources. For vibration control sources, there are two basic physical mechanisms; modal amplitude control and modal phase rearrangement. The relative importance of these (in terms of overall sound power reduction) is greatly influenced by a variety of geometric and structural / acoustic parameters.

For vibration control sources applied to a lightly damped panel, where the panel dimensions are smaller than approximately one acoustic wavelength at the frequency of interest, both vibration control source mechanisms may provide global sound power attenuation. Here the location of the control source has a significant influence on both the levels of attenuation achieved, and the physical means by which this occurs. An increase in structural damping, which tends to reduce the amplitudes of the resonant or near-resonant modes, increases the importance of the modal phase rearrangement mechanism. So too does an increase in the modal density. In contrast, an increase in the panel dimensions relative to the acoustic wavelength results in an increase in the importance of the modal amplitude control mechanism.

As for vibration control sources, the location of the acoustic control source(s) has a significant influence upon the levels of sound power attenuation optimally possible. For a relatively small plate radiating in a monopole-like fashion, a single acoustic control source can achieve substantial levels of sound power attenuation. Panels with less uniform radiation patterns

require a greater number of sources. The physical size of the panel affects both the number of acoustic control sources required to achieve attenuation, and the optimum (relative) locations of the sources. These sources should also be placed as close as possible to the vibrating structure, as a distance from the radiating surface of approximately one half wavelength or greater will achieve very little reduction in the total radiated sound power level.

It has also been shown that the placement of the error sensor, whether it is a microphone or accelerometer, has a significant influence upon the levels of sound power attenuation achievable by using a closed loop control system. When microphones are used, the optimum placement is at the points of minimum optimally controlled residual sound pressure. The optimum placement of an accelerometer is less straightforward, requiring a more thorough investigation. It is apparent, however, that if an accelerometer is to be effective in providing feedback for system optimization, the mechanism of modal amplitude control must be capable of providing the required sound power reduction.

Finally, it has been shown that the maximum levels of global sound power attenuation achieved by reducing local sound pressure levels at an error microphone are relatively tolerant to both phase errors and reduced levels of performance of the electronic controller, resulting in higher sound pressure levels at the error microphone location.

4.8. GENERAL DESIGN PROCEDURE

Chapter 3 presented analytical models that could be used in the design of systems to actively control sound radiation from vibrating structures. This chapter has considered only the problem

of sound radiation from a planar surface into free space. The previous three sections have endeavoured to demonstrate the influence which several geometric and structural / acoustic parameters have on the performance of the active noise control system. These influences must be understood if the design is to be optimized.

Keeping the previously outlined results in mind, what will presented here is a series of 4 steps that may be undertaken to optimize the arrangement of the control sources and error sensors of active systems to control freefield structural sound radiation. It is not intended to be taken as the only way to design such a system, but rather a chronological progression that will aid the exercise.

4.8.1. Characterization of the system

Before beginning the design process, the system, and its response under primary excitation, must be characterized. The minimum requirement here is that the primary sound field (amplitude and relative phase) on a test surface surrounding the structure in the farfield be measured at the frequency of interest using an appropriate measurement location distribution similar to that used when sound intensity is used to estimate sound power. If vibration control sources are to be used, the structural response must also be measured and decomposed into its individual contributing modes. This measurement includes an experimental modal analysis, and the use of these results to determine the sound field radiated by each mode at the frequency of interest.

4.8.2. Selection of control source type

As demonstrated in the previous sections, the use of either acoustic or vibration control sources can produce significant levels of reduction in the overall sound power radiated by a vibrating structure into free space. The mechanisms by which they achieve this attenuation, and the influence which various geometric and structural / acoustic parameters have upon the magnitudes of these reductions, are different for the two control source types. In choosing the control source type for a particular application, the following points should be remembered.

Acoustic control sources are the easier of the two types with which to design a system. No information about the structural response is required, only measurements of the primary radiated sound field at the frequency of interest are necessary, and this is a very distinct advantage for the free space radiation problem. One disadvantage is that the system is constrained to using an acoustic error sensor (such as a microphone) to provide feedback to the electronic control system. Another disadvantage is that the levels of sound attenuation that can be attained per source may be less than those attained with a vibration control source, especially if the panel dimensions are approximately equal to, or larger than, the acoustic wavelength at the frequency of interest, or if the panel is near resonance. Acoustic control sources can also be more obtrusive than some vibration sources, such as peizoelectric actuators.

Conversely, vibration control sources are more difficult to use than acoustic control sources for system design. A detailed description of the structural response, and also the resulting sound radiation field, must be known if an optimized design is to be undertaken. However, if this can be done, vibration control sources may exhibit an increased level of performance (on a per

source basis) over acoustic control sources. The final system may also be more compact and unobtrusive for vibration control sources, especially if piezoelectric actuators and vibration error sensors can be used.

4.8.3. Optimization of control source location

Once the system has been characterized, and the type and number of control sources chosen, the next step is to optimize the location of the control sources. This can be a particularly difficult exercise, as it is, in general, impossible to directly determine the optimum source locations due to it not being a linear function of sound power attenuation. Therefore, a numerical search routine is required to optimize the control source locations. What is required for this is a means to estimate of the maximum possible sound power attenuation for a given control source arrangement. As described in chapter 3, multiple regression is a relatively easy technique to use for this task.

One other problem with the use of a numerical search routine is that there may be local optima (minima) in the error surface, as demonstrated in the previous two sections. In this case, the starting point(s) for the search algorithm will influence the final result. The designer must be aware of this, restarting the procedure at several locations or using a random search technique to determine the optimal starting location if it is not possible to choose a starting point based on "common sense". Such common sense guidelines would include initial placement of the control sources as close as possible to the antinodes of the modes contributing most to the sound radiation, and also placement of the vibration control sources in the least stiff parts of the structure so that control effort is minimized.

4.8.4. Error sensor location and type

Once the control source location has been selected, the final step is to select the type and location of the error sensor(s). Regardless of the control source type, microphones sampling the far field will always be effective (provided there are no background noise problems from other sources). They should be placed at the location of greatest pressure difference between the primary radiated and ideally controlled residual sound fields. If multiple regression is used to place the control source(s), this location for the error sensor(s) can be determined directly by an inspection of the residuals vector, as described in chapter 3.

If vibration control sources are used, and if the principal mechanism is modal amplitude control, vibration sensors may be used to provide system feedback. The optimum sensor location is harder to specify in general, but if the primary mechanism is modal amplitude control the vibration sensor should be placed at the location of greatest difference between the primary and "ideally" controlled vibration levels.

4.9. SUMMARY

It has been shown analytically and experimentally that either vibration or acoustic control sources may be used effectively to control freefield sound radiation from a vibrating structure. The analytical models presented in chapter 3, specialized for the case of controlling sound radiation from a baffled, rectangular panel, have been shown to be able to predict the effect which applying active control has upon the structural / acoustic system.

It has been shown that acoustic and vibration control sources achieve sound attenuation by different physical noise control mechanisms. Acoustic sources provide global sound attenuation by reducing the radiation impedance of both the primary and control noise sources. Vibration control sources can provide control in two different ways; by a reduction in the amplitude of the primary offending mode or modes (modal amplitude control), or by altering the relative phases and amplitudes of the modes (modal phase rearrangement). This modal phase rearrangement mechanism effectively reduces the radiation efficiency of the radiating structure.

The location of the control source(s) has been shown to have a significant effect upon the levels of sound power attenuation that can be achieved. So too do other geometric variables such as the size of the structure relative to the acoustic wavelength at the frequency of interest and the location of the system error sensor. Structural / acoustic variables such as damping, modal density, and the characteristics of the primary forcing function also affect the final results, and the mechanisms by which the attenuation is achieved.

The results also indicate that for the control of total radiated sound power, the phase accuracy requirement for the signal generated by the electronic controller is not nearly as critical as it is for minimizing sound pressure at a particular location. This has important consequences for the detailed design of the digital electronic controller, in particular the number of bits necessary to obtain good results.

Based on the analytical models presented in chapter 3, and the study of the effects of various system parameters undertaken here, a general procedure has been formulated to assist in the design of systems to actively control harmonic freefield sound radiation from planar structures.

CHAPTER 5.

DEMONSTRATION OF GENERALIZED FORMULATION FOR MODELLING OF ACTIVE CONTROL OF SOUND TRANSMISSION INTO A COUPLED CYLINDRICAL ENCLOSURE

5.1 INTRODUCTION

In chapter 3, a generalized analytical formulation was presented which was suitable for modelling the active control of sound transmission into a weakly coupled enclosure. The purpose of this chapter is to demonstrate the use of this formulation for modelling the active control of sound transmission into a cylindrical enclosure using vibration (point) control sources. A thorough investigation of the effects of various structural / acoustic and geometric variables, as was undertaken in the previous chapter, will *not* be undertaken here. The work presented here will be limited to a demonstration of the ability of the analytical model to predict the effect of the application of the active control force for two simple, but fundamentally different, cases.

The use of vibration point sources to control sound transmission into a cylindrical enclosure has been treated both theoretically and experimentally before (Fuller and Jones, 1987; Jones, 1987). The previous analytical formulations, however, have used classical shell theory , and not modal coupling theory as will be used here. A modal coupling formulation has the advantage of being applicable (in theory) to any weakly coupled enclosure, not simply those with a regular geometry. It has been used in the past to analytically examine the effect of applying a vibration

force to control sound transmission through a rectangular panel into a rigid rectangular cavity (Pan et al, 1990), the results of which have been verified experimentally (Pan and Hansen, 1990). It has not, however, been used previously to examine the control of sound transmission into a cylindrical enclosure.

The first section of this chapter will specialize the previous general formulation for the cylindrical enclosure system. Following this some theoretical and experimental results will be given.

5.2 SPECIALIZATION OF ANALYTICAL MODEL FOR THE CYLINDRICAL ENCLOSURE SYSTEM

The modal coupling theory used in the formulation presented in chapter 3 utilizes the *in vacuo* mode shape of the structure, and the rigid walled mode shape of the enclosed space, to determine the response of the coupled system. For the circular cylinder shown in figure 5.1, which is assumed to be simply supported on the ends, the *in vacuo* structural mode shape function is:

$$\Psi_{MN}(z,\theta) = \sin \frac{M\pi z}{L} \left[\cos N\theta + \sin N\theta\right] \qquad (5.1)$$

where M,N are the axial and circumferential modal indices, respectively, and L is the length of the cylinder (note that capital letters will be used to denote the modal indices of the cylinder structure). Note that both sine and cosine functions are required to define the circumferential placement of the structural modes.

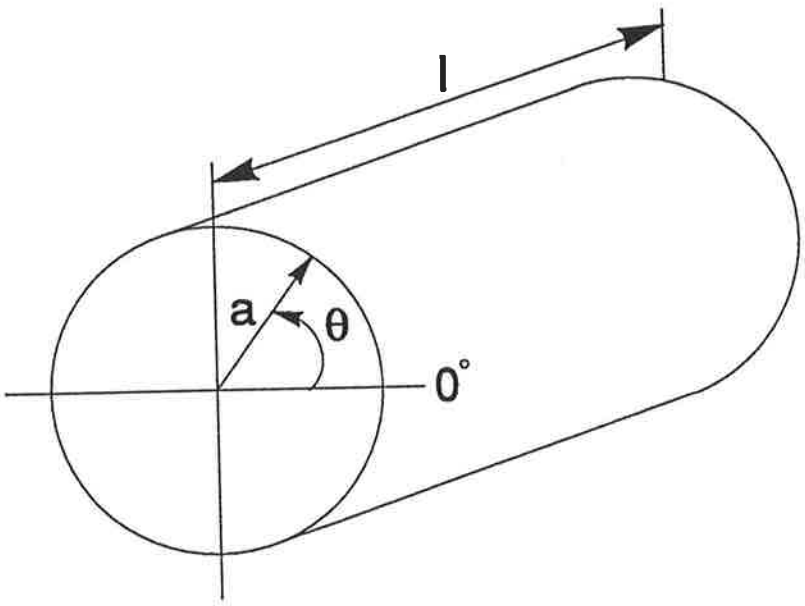

Figure 5.1. Cylinder geometry.

The resonance frequencies of associated with these mode shape functions can be found from the characteristic equation (Leissa, 1973):

$$(\Omega^2)^3 - (K_2 + \tilde{h}\,\Delta K_2)(\Omega^2)^2 + (K_1 + \tilde{h}\,\Delta K_1)(\Omega^2) - (K_o + \tilde{h}\,\Delta K_o) = 0 \qquad (5.2)$$

where

$$\Omega^2 = \frac{\rho_s (1-\nu^2)}{E} a^2 \omega_{MN}^2 = \frac{a^2 \omega_{MN}^2}{c_s} \qquad (5.3)$$

$$\tilde{h} = \frac{h^2}{12\, a^2} \qquad (5.4)$$

ρ_s is the structure material density, ν the Poisson's ration, E the modulus of elasticity, c_s the speed of sound in the material, h the thickness, and ω_{MN} the resonance frequency in rad s^{-1} of the (M,N)th mode. The constants K_o, K_1, and K_2 in equation (5.2) are from Donnell-Mustari shell theory, defined as (Leissa, 1973):

$$K_o = 0.5\,(1-\nu)\,\left[\,(1-\nu^2)\,\lambda^4 + \tilde{h}\,(N^2+\lambda^2)^4\,\right]$$

$$K_1 = 0.5\,(1-\nu)\,\left[\,(3+2\nu)\,\lambda^2 + N^2 + (N^2+\lambda^2)^2 + \frac{(3-\nu)}{(1-\nu)}\,\tilde{h}\,(N^2+\lambda^2)^3\,\right]$$

$$K_2 = 1 + 0.5\,(3-\nu)\,(N^2+\lambda^2) + \tilde{h}\,(N^2+\lambda^2)^2 \qquad (5.5)$$

where $\lambda = \dfrac{M\pi a}{L}$ (5.6)

ΔK_o, ΔK_1, and ΔK_2 are the modifying constants of Goldenveizer - Novozhilov / Arnold - Warburton, defined as (Leissa, 1973)

$$\Delta K_o = 0.5\,(1-\nu)\,\left[\,4(1-\nu^2)\,\lambda^4 + 4\lambda^2 N^2 + N^4 - 2(2-\nu)(2+\nu)\,\lambda^4 - 8\lambda^2 N^4 - 2N^6\,\right]$$

$$\Delta K_1 = 2(1-\nu)\,\lambda^2 + N^2 + 2(1-\nu)\,\lambda^4 - (2-\nu)\,\lambda^2 N^2 - 0.5\,(3+\nu)\,N^4$$

$$\Delta K_2 = 2(1-\nu)\,\lambda^2 + N^2 \qquad (5.7)$$

Goldenveizer - Novozhilov / Arnold - Warburton shell theory was chosen based on its previously demonstrated ability to accurately predict the modal response of a thin, circular finite length shell of the type considered in a later section of this chapter (Pope et al, 1980, 1982).

The cubic characteristic equation (5.2) has 3 roots, corresponding to 3 resonance frequencies, associated with motion predominantly in each of the radial, tangential, and axial directions. The

first root is the one associated with the predominantly radial response (Junger and Feit, 1986), and will be the only one used here as it is the flexure of the cylinder which is responsible for the interior sound generation.

The modal mass associated with each structural mode (assuming the structure has uniform material properties) is found from:

$$M = \rho_s \int_S \Psi_{MN}^2(x) \, dS = \frac{\rho_s \, h \, A}{4} \epsilon_N \qquad (5.8)$$

$$\text{where } \epsilon_N = \begin{cases} 2 & N = 0 \\ 1 & N > 0 \end{cases}$$

For the rigid walled circular enclosure, the mode shape function is:

$$\Phi_{qns}(r, \theta, z) = J_n(\gamma_{ns} r/a) \cos(n(\theta-\theta')) \cos(\frac{q\pi z}{L}) \qquad (5.9)$$

where q is the axial modal indice, n is the circumferential modal indice, J_n is a Bessel function of the first kind of order n, γ_{ns} is the value of the sth zero of the derivative of the Bessel function of order n:

$$J_n'(\gamma_{ns}) = 0$$

and (θ-θ') describes the circumferential placement of the mode (note that lower case letters will be used to denote the acoustic modal indices). The resonance frequencies of the acoustic modes are found from:

$$f_{qns} = \frac{c_o}{2\pi} (\gamma_{ns}^2 + (\frac{q\pi}{L})^2)^{0.5} \text{ Hz} \qquad (5.10)$$

The modal mass of the these is:

$$M_{qns} = \rho_o \int_V \Phi^2_{qns}(x)\, dV$$

$$= \rho_o \left[\frac{\gamma_{ns}^2 - n^2}{2\, M_{ns}^2} \right] \frac{J_n^2(\gamma_{ns})\, \pi\, a^2 L}{2}\, \epsilon_q\, \epsilon_n \qquad (5.11)$$

where $\epsilon_q,\ \epsilon_n = \begin{cases} 2 & q,n = 0 \\ 1 & q,n > 0 \end{cases}$

The modal coupling factor β, which describes the ability of a given structural mode to excite a given interior acoustic mode, for the structural mode shape functions of equation (5.1) and the acoustic mode shape functions of equation (5.9), is found from (Pope et al, 1980, 1982):

$$\beta_{MN,qns} = \frac{1}{S} \int_S \Psi_{MN}(x)\, \Phi_{qns}(x)\, dS$$

$$= \frac{J_n(\gamma_{ns})}{2\, L} \frac{\epsilon_n\, \kappa_m\, (1-(-1)^{M+q})}{(\kappa_m^2 - \kappa_q^2)} \quad n=N,\ \frac{(M+q)}{2} \neq \text{integer}$$

$$= 0 \quad \text{otherwise} \qquad (5.12)$$

where $\kappa_m = \frac{M\pi}{L}$, $\kappa_q = \frac{q\pi}{L}$

Equations (5.1) - (5.12) can be used in the generalized formulation for modelling the active control of sound transmission into weakly coupled enclosures, presented in chapter 3, to study the specific problem of active control of sound transmission into cylindrical enclosures. With this the interior sound pressure levels under primary excitation can be calculated from equation (3.35), and the controlled interior sound pressure levels at any interior point from equation (3.52) using the optimum control force derived from equation (3.58). The following section will present some initial theoretical models, with experimental verification, to demonstrate the ability

of the analytical model to predict the residual sound fields under the action of active vibration sources.

5.3 PRELIMINARY RESULTS FOR THE USE OF MODAL COUPLING THEORY TO DESCRIBE THE RESIDUAL SOUND FIELD IN A CYLINDRICAL ENCLOSURE UNDER THE ACTION OF ACTIVE VIBRATION SOURCES

The experimental and analytical work presented here is concerned with the use of vibration sources to control sound transmission into the cylindrical enclosure system of figure 5.2. The radius of the structure is 0.254m, the length is 1.2m, and the wall thickness 1.6mm. The structure is fabricated from aluminium, with a longitudinal wave speed of 5150 ms^{-1}, and density of 2700 kgm^{-3}. The cylinder has two rigid end caps, constructed from 19mm particle board. Two vibration sources were available for use, midway along the cylinder length and at 45° and 180° around the circumference. Two microphone error sensing points were available for use, midway along the length at a radius of 0.232m, and at an angular location of 135° and 180°. 72 points in the primary and residual radiated sound fields were measured at the cylinder midsection, at a radii of 0.038, 0.130, and 0.232m in 15° increments. All tests were conducted in an anechoic chamber.

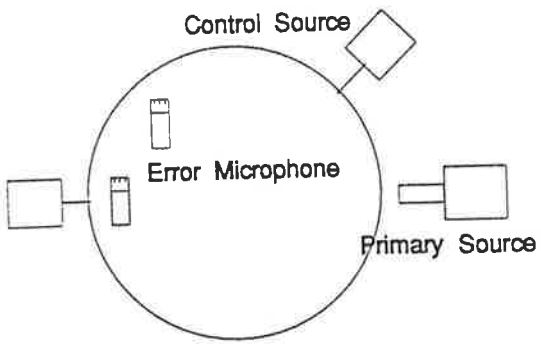

Figure 5.2. Experimental cylinder arrangement.

The primary sound field was generated with a pair of in-phase horn drivers located midway along the cylinder length at 0°, placed 50mm from the cylinder surface. For the purposes of the analytical study, these were modelled as a single monopole source.

In the analytical formulation presented in chapter 3, the primary forcing function is expressed as a modal generalized force:

$$\gamma_{MN} = \int_S p(x)\ \Psi_{MN}(x)\ dS \qquad (5.13)$$

Neglecting the radiation reaction force as a second order effect, the pressure, p(x), at any point can be taken as the blocked pressure, $p_{bl}(x)$, at that point:

$$p(x) = p_{bl}(x) = p_i(x) + p_s(x) \qquad (5.14)$$

where $p_i(x)$ is the incident pressure, and $p_s(x)$ is the scattered pressure. For a monopole source located at a position (r_o, z_o, θ_o) relative to the cylinder origin, these terms are (Fuller, 1987):

$$p_i(r,z,\theta) = \frac{i\ p_o}{2} \sum_{n=0}^{\infty} \epsilon_n \cos\left(n(\theta-\theta_o)\right) \cdot \int_{-\infty}^{\infty} J_n(\zeta r)\ H_n(\zeta r_o)\ e^{-i\alpha(z_o-z)}\ d\alpha \qquad (5.15)$$

$$p_s(r,z,\theta) = \frac{-i\ p_o}{2} \sum_{n=0}^{\infty} \epsilon_n \cos\left(n(\theta-\theta_o)\right) \cdot \int_{-\infty}^{\infty} \frac{J_n'(\zeta r)\ H_n(\zeta r_o)\ H_n(\zeta r)\ e^{-i\alpha(z_o-z)}}{H_n'(\zeta r)} \qquad (5.16)$$

where $\zeta = (k^2 - \alpha^2)^{1/2}$, and H_n is a Hankel function of the first kind of order n.

Equations (5.14), (5.15), and (5.16) are substituted into equation (5.13) and evaluated numerically to determine the modal generalized force.

Two discrete frequency cases are examined in the theoretical and experimental work. The first frequency was close to a structure controlled modal resonance ((1,2) structural mode, experimentally resonant at 258 Hz, and theoretically resonant at 270 Hz), where the majority of the coupled structural / acoustic system energy is contained in the shell. The other frequency was close to an acoustic cavity controlled modal resonance ((0,2,1) acoustic mode, experimentally resonant at 669 Hz, and theoretically resonant at 656 Hz), where the majority of the coupled structural / acoustic system energy is contained in the acoustic space. The first 100 structural and 100 acoustic modes were used in the calculations, as the use of the modes included in the range has been found previously to be able to accurately model the interior sound field (theoretically the sum of an infinite number of modal contributions) (Pope et al, 1980).

For ease of comparison, the theoretical results presented were normalized to best fit the experimental data. This involved matching the levels of the theoretical and experimental primary sound pressures by adding to, or subtracting from, all theoretical data points the same constant value. This same value was then added or subtracted from the theoretical controlled levels, allowing a direct assessment of the ability of the theoretical model to predict the residual controlled sound field. Further, for the theoretical results presented, the sound pressure reductions at the error microphones were limited to 35 dB, rather than the maximum theoretically possible, to better simulate a practical system.

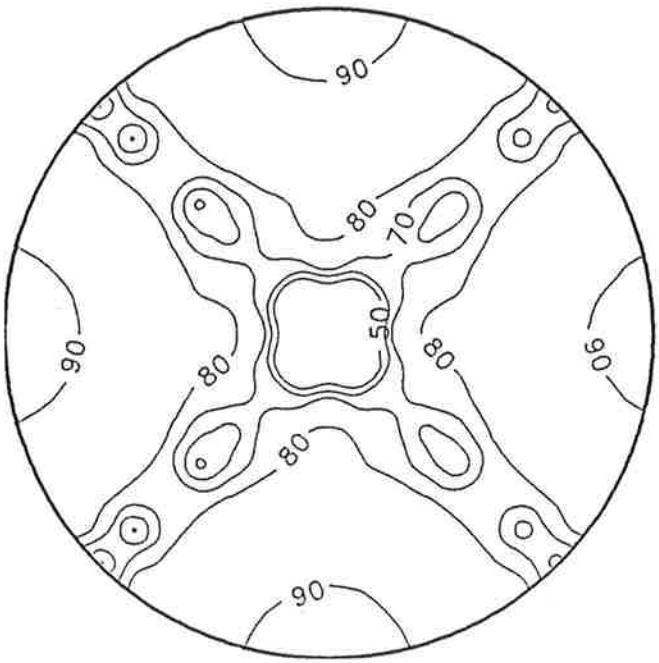

Figure 5.3. Theoretical primary source sound pressure levels, 270 Hz.

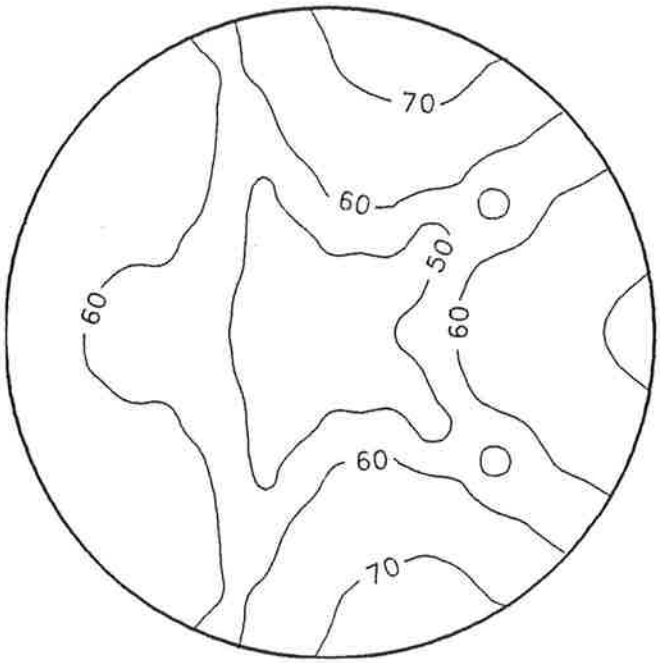

Figure 5.4. Theoretical residual sound field, 1 control at 180°, 1 error sensor at 180°, 270 Hz.

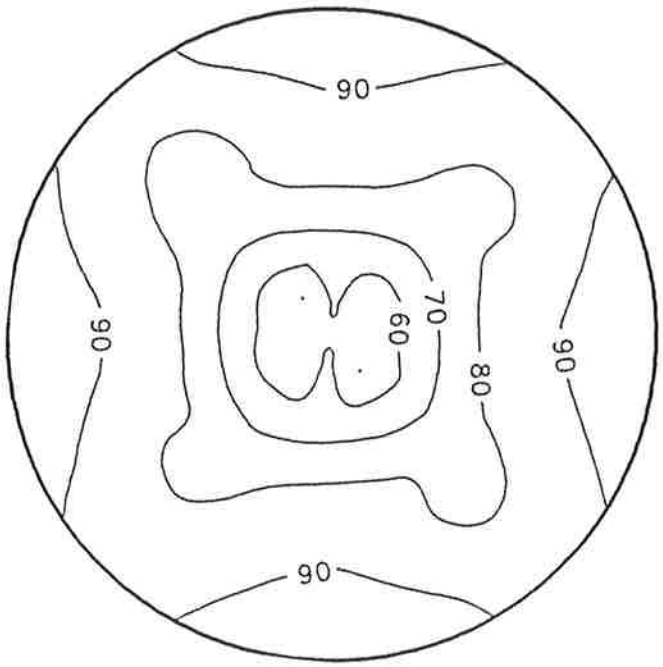

Figure 5.5. Experimental primary source sound pressure levels, 258 Hz.

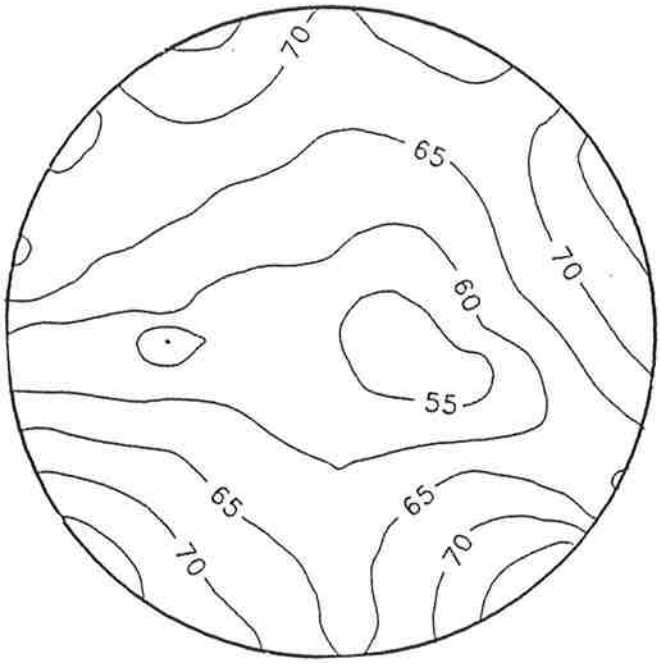

Figure 5.6. Experimental residual sound field, 1 control at 180°, 1 error sensor at 180°, 258 Hz.

Consider first the structure controlled case, near the (1,2) structural resonance. The effect of applying a single vibration control force at the 180° angular location, and minimizing the sound pressure at the 180° angular location, is shown theoretically in figures 5.3 and 5.4, and experimentally in figures 5.5 and 5.6. These plots depict the interior sound pressure levels in one cylinder cross section, midway along the length of the cylinder.

Consider first the interior response under primary excitation, illustrated in figures 5.3 and 5.5 for the theoretical and experimental cases, respectively. The influence of the nearly-resonant (1,2) structural mode is the salient feature of both of these figures, producing the distinctive 4 lobed pattern of a circumferential cosine(2θ) modal indice. In viewing these, it is clear that the general agreement between the predicted and measured sound pressure levels is good.

Consider now the effect of applying active vibration control, shown theoretically in figure 5.4 and experimentally in figure 5.6. In comparing these results, the first point to note is that the analytical model predicts a global sound attenuation in the order of 20 dB, an attenuation matched experimentally. Next, consider the general pattern of the theoretical and experimental residual sound fields. Theoretically, several lobes of a sound pressure level of approximately 70 dB are predicted close to the cylinder edges, symmetric about the 0° angular location. These lobes do appear experimentally; however, the top (90°) lobe is somewhat distorted. This is possibly due to the presence of the cylinder fabrication butt joint at this location. The second point to note is that the analytical model predicts an area of enhanced sound attenuation "reaching" from the center of the cylinder towards the error microphone location (located at an angular location of 180°). This effect is also evident in the experimental result. In general the agreement between the theoretical and experimental residual sound fields is good.

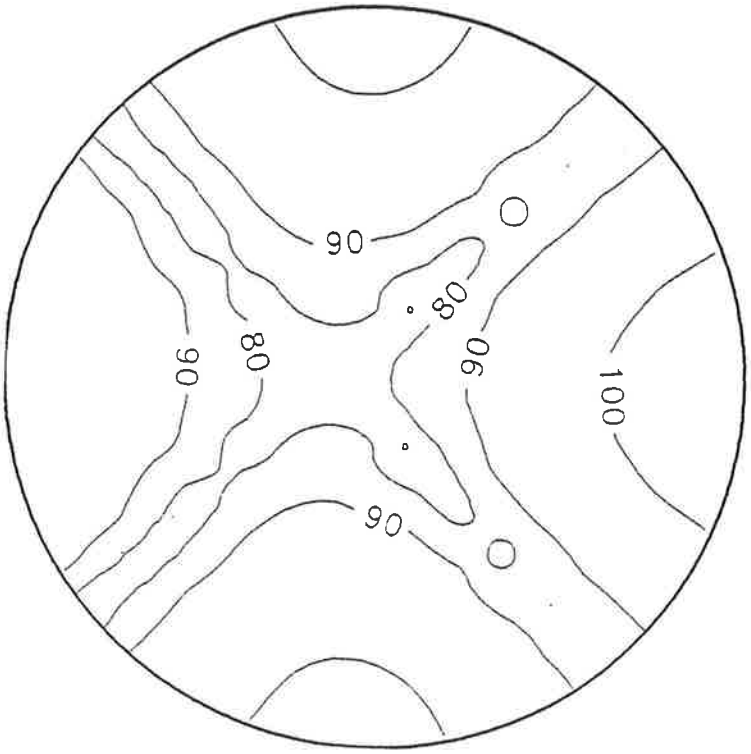

Figure 5.7. Theoretical primary source sound pressure levels, 656 Hz.

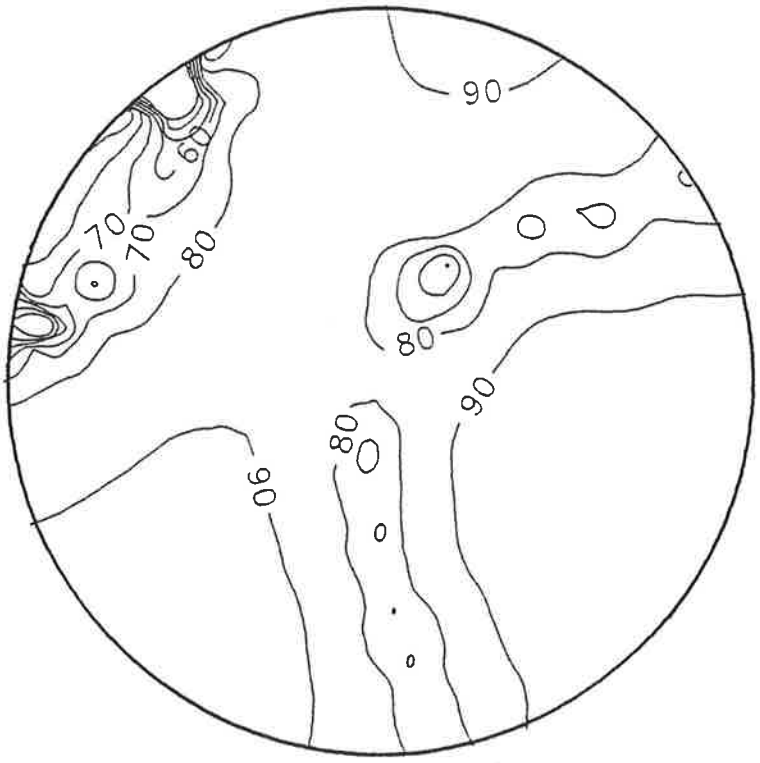

Figure 5.8. Theoretical residual sound field, 2 controls at 45° and 180°, two error sensors at 135° and 180°, 656 Hz.

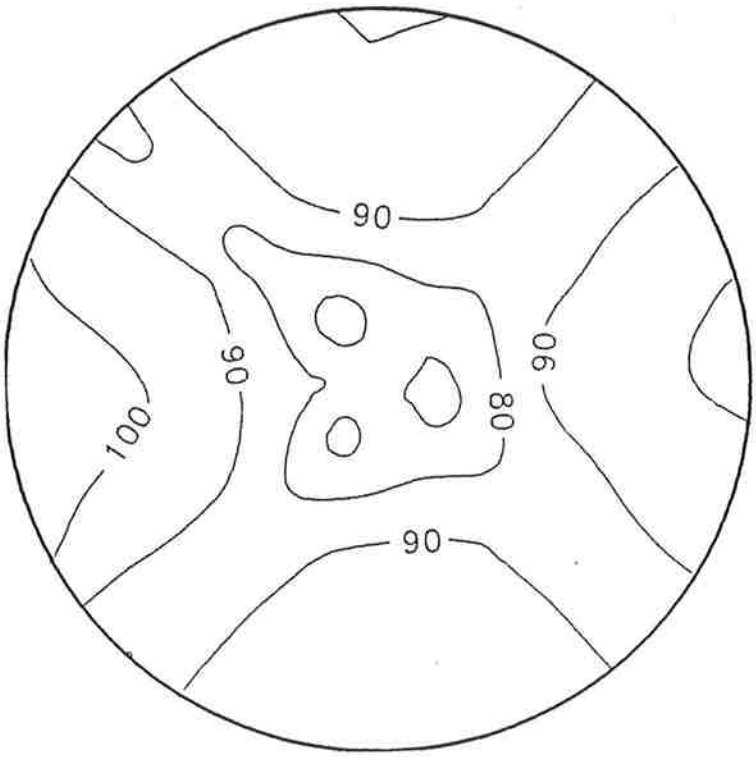

Figure 5.9. Experimental primary source sound pressure levels, 669 Hz.

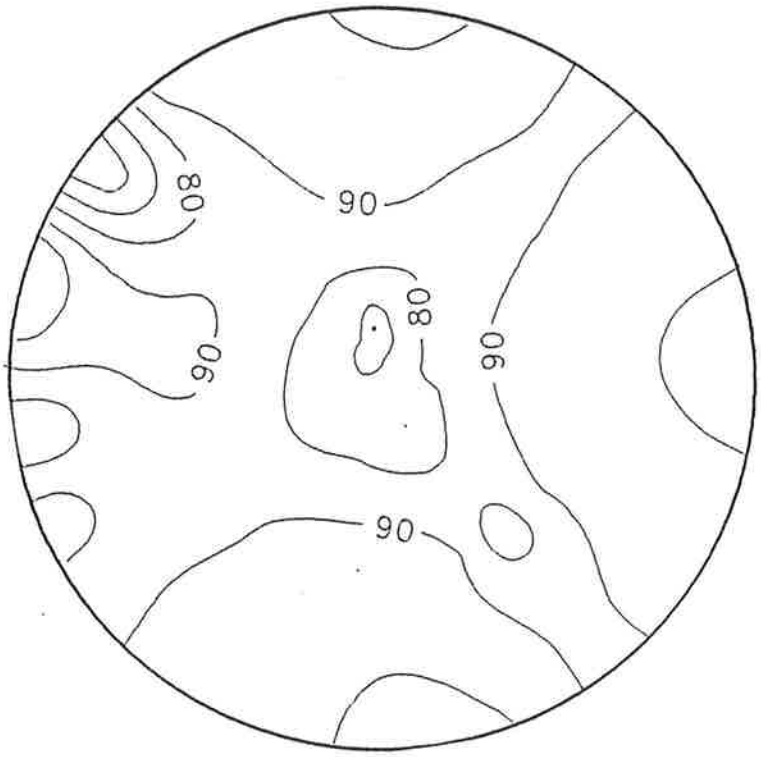

Figure 5.10. Experimental residual sound field, 2 controls at 45° and 180°, two error sensors at 135° and 180°, 669 Hz.

Consider now the acoustic cavity controlled case, near the acoustic (0,2,1) acoustic modal resonance. The effect of applying vibration control at both the 45° and 180° angular locations, and minimizing the sound pressure at both the 135° and 180° angular locations, is shown theoretically in figures 5.7 and 5.8, and experimentally in figures 5.9 and 5.10. Again, these plots depict the interior sound pressure levels in one cylinder cross section midway along the length.

Compare first the predicted and measured primary excitation sound fields, illustrated in figures 5.7 and 5.9, respectively. In viewing these figures, it is again clear that there is good agreement between theory and experiment. The influence of the nearly resonant (0,2,1) acoustic mode is clearly evident in both cases, creating the distinctive 4 lobed pattern.

Consider now the effect of applying vibration control, shown analytically in figure 5.8 and experimentally in figure 5.10. In viewing these, it is again clear that there is good agreement between the theory and experiment. The most interesting point to note is the lack of significant overall sound level attenuation, both predicted and measured. It would appear that the relationship between the acoustic modes has somehow altered to achieve destructive interference only at the error sensing locations, which differs from the structure controlled case considered previously. A detailed examination of this phenomena, however, is beyond the scope of this thesis; the work presented here is concerned only with demonstrating the ability of the analytical model to predict the residual sound field under the action of active control.

5.4 SUMMARY

The analytical and experimental results presented here demonstrate the ability of the modal coupling based analytical model to predict the residual sound fields under the application of vibration sources used to control sound transmission into a cylindrical enclosure. Two distinct frequency cases were examined, the first being a frequency close to that of a structure controlled modal resonance and the second being a frequency close to that of an acoustic controlled modal resonance. It was found that when the coupled system response is dominated by the structural response, a single control source could provide significant levels of global sound attenuation. However, for the case considered here, when the system was dominated by the acoustic cavity controlled response, a single control source did not provide significant levels of global sound attenuation.

CHAPTER 6.

INTRODUCTION TO ELECTRONIC CONTROL SYSTEM ANALYSIS

6.1 OVERVIEW

Research in the field of active noise control has increased dramatically in recent years. This has been spurred on in part by advances in microprocessors which allow adaptive (or self-tuning) systems to be implemented. Adaptive systems provide the flexibility required for the practical use of active noise control, as changing conditions would render a non-adaptive active noise control system ineffective after a period of time.

The majority of adaptive active noise control systems currently under investigation use a modified signal processing approach to do this. This is based usually on a transversal filter architecture, implemented either as a finite impulse response (FIR) or infinite impulse response (IIR) filter.

One important characteristic of transversal filters is that their weight coefficients are non-orthogonal. As a result, all of the weight coefficients must be tuned together for guaranteed optimization. This is commonly done using a gradient descent based optimization procedure.

Adaptive control systems implementing a finite impulse response filter appear more commonly in published literature than infinite impulse response filter implementations, owing to their reduced complexity (this is in spite of the fact that IIR filters may be better suited to active

noise control implementations, owing to their ability to compensate for feedback to the error sensor). The most common gradient descent algorithm utilized in active noise control for these is the least mean square (LMS) algorithm. This algorithm is used frequently in adaptive signal processing for telecommunications, in biomedical research, for antennae beamforming, and for adaptive control applications (Widrow et al, 1975; Widrow and Stearns, 1985; Cowan and Grant, 1985; Honig and Messerschmitt, 1984; Alexander, 1986; Ljung, 1977). It must be modified, however, for active noise control implementations to accomodate the inherent acoustic, structural/acoustic, and electro-acoustic system transfer functions. These modifications lead to a version of the algorithm commonly referred to as the filtered-x LMS algorithm (Widrow and Stearns, 1985).

There is a large body of work concerned with various aspects of the LMS algorithm as applied in adaptive signal processing systems. Much of the work addressing practical implementation issues, such as limited precision effects (Gitlin et al, 1982; Caraiscos and Liu, 1984; Cioffi, 1987; Zimmerman and Cudney, 1989), is directly applicable to active noise control systems. Studies of the convergence properties of the algorithm (Widrow et al, 1976; Horowitz and Senne, 1981; Gardner, 1984; Boland and Foley, 1987; Foley and Boland, 1987), however, are not. This is because the previously mentioned transfer functions, which do not occur in general adaptive signal processing systems, and errors in their measurement, will have an effect upon the convergence properties of the filtered-x LMS algorithm used in active noise and vibration control applications. Further, if multiple input/output channels are used, the effect of channel "cross coupling", arising from the non-orthogonal nature of the placement of the control sources and error sensors in terms of the structural / acoustic system modes which can be excited and sensed, must be taken into account. Also, the effect of using a delayed error signal in the the

6.2 HISTORICAL BACKGROUND

One of the primary reasons that active noise control has become a topic of increased research activity is that parallel advances in microprocessor technology have made it possible to practically implement adaptive systems. This allows active noise control systems to remain "tuned" despite environmental and system changes. It also increases the bandwidth over which active noise control systems are effective.

An early approach to developing an adaptive control strategy for active noise control systems was a method based on trial and error waveform generation (Chaplin, 1980; Crocker, 1983; Nadim and Smith, 1983; Chaplin and Smith, 1983; Smith and Chaplin, 1983; Chaplin, 1983). The advantage of this method is that the control system requires only an RMS error signal (providing a measure of the residual sound or vibration field after the application of active control). As no phase information about the error signal is required, the electro-acoustic transfer functions of the system's transducers, as well as the acoustic or structural/acoustic transfer functions, do not need to be considered in the adaptive controller design. The disadvantage of such a system is that it is limited to periodic disturbances, and the adaption times can be long.

Another adaptive approach involves modelling of the system transfer functions, and directly using the estimated solution to the active noise control governing physical equations, which provides the maximum levels of sound attenuation (Ross, 1982, 1982a; White and Cooper, 1984; Roure and Nayroles, 1984; Roure, 1985). The error signal is used to adjust this solution.

This technique has been shown to produce high levels of broadband attenuation, although the adaption times may again be long.

The most popular modern adaptive control stategy, however, is the use of a modified adaptive signal processing architecture. This is usually a transversal filter-based implementation, either a finite impulse response (FIR) or infinite impulse response (IIR) filter.

One of the first such implementations was a computer simulation of active, adaptive control of plane wave sound propagation in an air handling duct using an FIR filter arrangement (Burgess, 1981). Optimization of the system was done using a modified version of a popular gradient-descent type algorithm, the least mean square (LMS) algorithm (referred to as the "filtered-x" LMS algorithm (Widrow and Stearns, 1985) with the modifications). The modifications were incorporations of estimates of the acoustic and electro-acoustic system transfer functions. These are required to determine an accurate estimate of the gradient of the active noise control error criterion (or "cost function"), where the necessary measurements must be made in the "physical" domain, then converted to usable electric signals. Without knowledge of the above-mentioned transfer functions, the algorithm could become unstable (due to errors in the gradient estimate). Since this initial computer simulation, this form of single input, single output algorithm has received widespread use (for example, Zalas and Tichy, 1984; Poole et al, 1984; Elliott and Darlington, 1985; Kang and Fransen, 1987; Mikhael and Hill, 1988; Schuck, 1988).

The filtered-x LMS algorithm has also been extended for use in multiple input, multiple output active noise control systems (Elliott and Nelson, 1985, 1985a; Elliott and Nelson, 1986; Elliott

et al, 1987a). This extension is necessary, as many practical active noise control systems will require multiple control sources to achieve significant levels of global sound attenuation.

Recently, it has been suggested that IIR filter architectures may be better suited to active noise control implementations than FIR filter architectures (Warner and Bernhard, 1987; Eriksson et al, 1987, 1988; Eriksson and Allie, 1988; Billoud et al, 1989). This is because the IIR filter has pole-zero characteristics, whereas the FIR filter is an all-zero device. Poles can occur in practical active noise control systems due to acoustic feedback from the control source(s) to the reference sensor (providing a measure of the primary disturbance without the addition of active noise control). The IIR filter can theoretically account for these poles.

Both FIR and IIR filter implementations in active noise systems require estimates of the electro-acoustic, acoustic, and structural/acoustic system transfer functions to insure the stability of the gradient descent algorithms which are commonly used to optimize them. These transfer functions, and errors in their measurement, will have an influence upon the algorithm stability characteristics. For the single channel filtered-x LMS algorithm, it has been shown that the (total) estimation of the transfer functions must be within 90° of the actual value for the algorithm to remain stable (Burgess, 1981; Elliott et al, 1987). Also, the acoustic time delays inherent in an active noise control system will have an influence upon the system performance (Elliott and Nelson, 1985). Some computer simulation of the multi-channel LMS algorithm convergence characteristics has also been conducted (Elliott and Nelson, 1985; Elliott et al, 1987), although no rigorous examination of the influence of active noise control system variables (such as the number of error sensors, and the amplitude and phase of the structural / acoustic system transfer function) was undertaken.

Gradient descent algorithms, such as the LMS algorithm, optimize the filter coefficients by adding to them a portion of the current estimate of the negative gradient of the error criterion. The maximum size of the variable that defines this portion, referred to as the convergence coefficient, that can be used in stable operation will be influenced by the active noise control system parameters. Some investigation of this effect has already been conducted (McNichol, 1985) (although there are some errors in some of the mathematical techniques employed, specifically the use of an orthonormal transform on a non-symmetric matrix). A more thorough examination is required, and will be undertaken in this thesis. Also, no such examination of the multi-channel LMS algorithm has been published, and will also be undertaken in this thesis. Here the effects of additional system parameters, such as the number of error sensors and cross-coupling between channels, must be taken into account.

CHAPTER 7.

THE SINGLE INPUT, SINGLE OUTPUT LMS ALGORITHM

7.1 INTRODUCTION

As outlined in Chapter 6, the use of a modified version of the LMS algorithm (the filtered-x LMS) in a transversal filter-based architecture has been widely implemented in active noise control systems. However, a details of the effects which these required modifications have upon the convergence characteristics of the algorithm still require investigation.

The following is an analysis of the effect which the acoustic time delay and electro/acoustic transfer functions have on the convergence and stability properties of the LMS algorithm as utilized in a single input, single output active noise control system. For simplicity, the "ideal" LMS algorithm is considered in the analysis. In this case, the error signal and reference signal are assumed to be stationary, stochastic quantities, and the samples of these are taken to be equal to the mean value of the process at that time (that is, the expected value, E[]). Although this assumption may not be correct in all implementations (Horowitz and Senne, 1981; Gardner, 1984; Feuer and Weinstein, 1985), the results obtained provide a basis against which to assess the effects of the acoustic time delay and transducer transfer functions on the algorithm characteristics. The basic LMS algorithm, without a time delay and without transfer functions, will first be reviewed to provide this basis. Following this, the effects of the time delay and transducer electro/acoustic transfer functions will be examined separately. A single actuator,

single error sensor system will be studied in this chapter. This will be extended to multiple sensors and actuators in the following chapter.

7.2 REVIEW OF THE LMS ALGORITHM

7.2.1 Formulation of error criterion

One of the most common methods of generating a secondary (or control) source signal in an active noise control system is by means of a transversal filter, or tapped delay line (see Figure 7.1). With this arrangement, a reference signal is sampled, providing a discrete filter input value, x. This value propagates through the filter, progressing one stage with every new sample taken. Thus, at any particular time k, the values present in the delay chain can be represented as a vector:

$$X_k = \left[\begin{array}{cccc} x_k & x_{k-1} & x_{k-2} & \cdots & x_{k-(N-1)} \end{array} \right]^T \qquad (7.1)$$

where N is the number of stages in the filter, and ^{T} denotes the transpose of the matrix. Throughout this chapter, vectors and matrices will be denoted by capital letters, scalars by lower case letters.

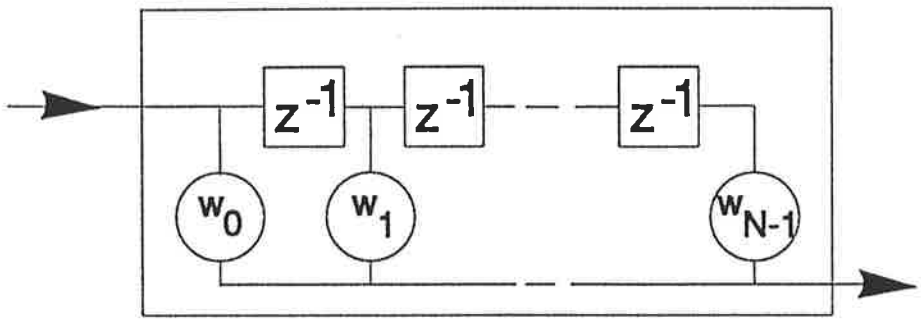

Figure 7.1. The transversal filter. Note that z^{-1} denotes a single time delay.

Each time a new input sample enters the transversal filter, the previous N samples are shifted one position, and the values at each stage are multiplied by a weight coefficient assigned to that stage. The results are summed to produce a filter output. Representing the weight coefficients at time k as a vector:

$$W_k = \left[\begin{array}{cccc} w_{0,k} & w_{1,k} & w_{2,k} & \cdots & w_{(N-1),k} \end{array} \right]^T \qquad (7.2)$$

the filter output at time k is equal to:

$$y_k = \sum_{i=0}^{N-1} w_{i,k}\, x_{k-i} = W_k^T X_k = X_k^T W_k \qquad (7.3)$$

The ideal output from the transversal filter at time k would closely match some "desired signal", d_k. The resulting estimation error, e_k, is the difference between the actual filter output and this desired signal:

$$e_k = d_k - y_k = d_k - W_k^T X_k = d_k - X_k^T W_k \qquad (7.4)$$

The mean square estimation error (simply called the mean square error), ξ, is often used as a system error criterion. That is, the weight coefficient vector is adapted so as to minimize the value of the mean square error, ξ, defined as:

$$\xi_k \equiv E\left[e_k^2 \right] \tag{7.5}$$

where E [] denotes the expected value in the brackets.

Substituting equation(7.4) into equation(7.5):

$$\xi_k = E\left[(d_k - X_k^T W_k)^2 \right] \tag{7.6}$$

$$= E\left[d_k^2 \right] - 2\, E\left[d_k X_k^T \right] W_k + W_k^T E\left[X_k X_k^T \right] W_k \tag{7.7}$$

$$= E\left[d_k^2 \right] - 2\, P_k^T W_k + W_k^T R_k W_k \tag{7.8}$$

where P_k is the cross correlation vector between the desired response and the input signal:

$$P_k = E\left[d_k X_k \right] \tag{7.9}$$

and R_k is the input autocorrelation matrix:

$$R_k = E\left[X_k X_k^T \right] \tag{7.10}$$

7.2.2 Derivation of the LMS algorithm

Assuming that the reference signal and desired signal are stationary, stochastic variables, it can be seen from equation (7.8) that the mean square error is a quadratic function of the weight coefficient vector, W. Thus, the "performance surface", the shape of the mean square error, is a hyper-paraboloid of dimension (N+1), where N is the number of filter weights. Considering the

three dimensional case of two filter weights, the performance surface is bowl-shaped, with only one (global) minimum. This trait applies to the entire family of performance surfaces of (N+1) dimensions. It is therefore possible to find the optimum weight vector, that produces the minimum mean square error, by setting the gradient of the mean square error equal to zero.

From equation (7.8):

$$\nabla_k = \text{gradient of error surface} = \frac{\partial \xi_k}{\partial W_k} = 2R_k W_k - 2P_k \qquad (7.11)$$

Thus, the optimum weight vector, W^*, that results in a gradient of zero, is:

$$W^* = R_k^{-1} P_k \qquad (7.12)$$

Note that as the process is assumed to be stationary, the optimum weight vector is independent of time; so the subscript $_k$ has been dropped.

Substituting equation (7.12) into equation (7.8), the minimum mean square error, ξ^*, is:

$$\begin{aligned}
\xi_k^* &= E[d_k^2] - 2 P_k^T W^* + W^{*T} R_k W^* \\
&= E[d_k^2] - P_k^T W^* - P_k^T R_k^{-1} P_k + P_k^T R_k^{-1} R_k R_k^{-1} P_k \\
&= E[d_k^2] - P_k^T W^* - P_k^T R_k^{-1} P_k + P_k^T R_k^{-1} P_k \\
&= E[d_k^2] - P_k^T W^* \qquad (7.13)
\end{aligned}$$

Thus, the mean square error can be restated as:

$$\xi_k = E[d_k^2] - P_k^T W^* + P_k^T W^* - 2 P_k^T W_k + W_k^T R_k W_k$$

$$= \xi_k^* + P_k^T R_k^{-1} P_k - 2 P_k^T W_k + W_k^T R_k W_k$$

$$= \xi_k^* + P_k^T R_k^{-1} R_k R_k^{-1} P_k - 2 P_k^T W_k + W_k^T R_k W_k$$

$$= \xi_k^* + W^{*T} R_k W^* + W_k^T R_k W_k - W^{*T} R_k W_k - W_k^T R_k W^*$$

$$= \xi_k^* + [W_k - W^*]^T R_k [W_k - W^*] \qquad (7.14)$$

$$= \xi_k^* + V_k^T R_k V_k \qquad (7.15)$$

where V_k is the weight variance vector:

$$V_k = W_k - W^* \qquad (7.16)$$

Geometrically, restating the algorithm in terms of the weight variance vector simply has the effect of an axis translation, moving the "bottom of the bowl" to the origin of the coordinate system.

It is usually not computationally efficient (or sometimes possible) to determine the input autocorrelation matrix or the cross correlation matrix. For this reason, a gradient descent algorithm is often implemented to adapt the filter weights towards their optimum value. The gradient descent algorithm operates by adding to the weight vector at time k a portion of the negative gradient of the error surface, causing the weight vector to descend downwards towards the "bottom of the bowl". Thus:

$$W_{k+1} = W_k - \mu \nabla_k \qquad (7.17)$$

where μ is called the convergence coefficient, which is equal to the portion of the negative gradient vector added to the weight vector.

It was shown in equation (7.11) that the gradient of the error surface at time k is dependent upon the values of the input autocorrelation matrix and cross correlation matrix, those quantities whose calculation it is desirable to avoid. However, as mentioned previously, the signals considered here are stationary and stochastic, thus the gradient can be estimated by basing it upon a single sample of the error at time k. Using equation (7.4) the estimated gradient, ∇_k, is:

$$\nabla_k = \frac{\partial e_k^2}{\partial W_k} = \frac{\partial (d-W_k^T X_x)^2}{\partial W_k} = -2e_k X_k \qquad (7.18)$$

Using this estimated gradient in equation (7.17), the weight update equation becomes:

$$W_{k+1} = W_k + 2\mu e_k X_k \qquad (7.19)$$

This is the well known least mean square (LMS) algorithm (Widrow and Stearns, 1985).

7.2.3 Characteristics of the "ideal" algorithm

To produce a set of qualitative characteristics of the LMS algorithm against which to compare the results obtained for the active noise control implementation, the "ideal" case, where the samples used to calculate the gradient estimate are equal to the mean value of the variable at that time, will be considered. With this assumption, equation (7.17) can be written in terms of equation (7.11):

$$W_{k+1} = W_k + 2\mu [P_k - R_k W_k] \qquad (7.20)$$

As the input autocorrelation matrix, R, is symmetric, it can be diagonalized using an orthonormal transformation:

$$R = Q \Lambda Q^{-1} = Q \Lambda Q^{T} \qquad (7.21)$$

where Q is the orthonormal modal matrix of R (the column vector of eigenvectors) and Λ is the diagonal matrix of eigenvalues of R (the sample subscript $_k$ has been omitted for generality). The geometric significance of the eigenvector matrix, Q, is that it defines the principal axis of the error surface. Therefore, expressing the algorithm in terms of Q has the effect of rotating the coordinate system to line up with the principal axis of the performance surface. If the algorithm in equation (7.19) is expressed in terms of the principal axis coordinate system, it can be viewed as a set of N scalar equations. Defining:

$$V_k' = Q^{-1} V_k = Q^{T} V_k \qquad (7.22)$$

(note that $Q^{-1} = Q^{T}$ by definition)

The mean square error (equation 7.15) becomes:

$$\xi_k = \xi^* + V_k'^{T} \Lambda V_k' \qquad (7.23)$$

$$\xi_k = \xi^* + tr[\Lambda_k V_k' V_k'^{T}] \qquad (7.24)$$

$$= \xi^* + tr[\Lambda_k C_k] \qquad (7.25)$$

where tr[] denotes the trace of the matrix (that is, the sum of the diagonal elements), and C_k is the weight covariance vector:

$$C_k = [V_k' V_k'^{T}] \qquad (7.26)$$

Thus it can be deduced that the mean square error will converge to some finite value if the weight covariance vector converges to some finite value.

Defining

$$W' = Q^{-1} W \tag{7.27}$$

and

$$W^{*\prime} = Q^{-1} W^{*} = Q^{-1} R^{-1} P = \Lambda^{-1} P' \tag{7.28}$$

equation (7.20) can be rewritten as

$$W'_{k+1} = W'_k = 2\mu [P'_k - \Lambda_k W'_k] \tag{7.29}$$

In terms of the weight variance vector:

$$\begin{aligned} V'_{k+1} &= (W'_k - W^{*\prime}) + 2\mu([P'_k - \Lambda_k W^{*\prime}] + [\Lambda_k W^{*\prime} - \Lambda_k W'_k]) \\ &= V'_k + 2\mu [P'_k - P'_k - \Lambda_k V'_k] \\ &= (I - 2\mu\Lambda_k) V'_k \end{aligned} \tag{7.30}$$

From equation (7.26):

$$C_{k+1} = (I-2\mu\Lambda_k)^2 C_k \tag{7.31}$$

Hence, the behaviour of the weight covariance matrix (in the principal axis coordinate system) can be viewed in terms of N scalar equations. The i^{th} equation is:

$$c_{i,k+1} = (1-2\mu\lambda_{i,k})^2 c_{i,k} \tag{7.32}$$

All of these equations are convergent if:

$$|1-2\mu\lambda_{max}| < 1 \qquad (7.33)$$

or

$$0 < \mu\,\lambda_{max} < 1 \qquad (7.34)$$

therefore:

$$\mu_{max} = \frac{1}{\lambda_{max}} \qquad (7.35)$$

From equation (7.32), it may be concluded (Horowitz and Senne, 1981) that the convergence rates of all of the natural "modes" of the system will increase as μ increases up to $\mu\lambda_{max} < 1/2$. At this point, however, the mode with eigenvalue λ_{max} will begin to slow down again, beginning to oscillate in direction. This result can be expressed as (Widrow and Stearns, 1985):

$0 < \mu < 1/(2\lambda_{max})$: overdamped

$\mu = 1/(2\lambda_{max})$: critically damped

$1/(2\lambda_{max}) < \mu < 1/\lambda$: underdamped.

Hence, a choice of μ approximately equal to $1/(2\lambda_{max})$ will generally yield the best overall convergence rate.

From the preceeding analysis, it can been deduced that for the "ideal" algorithm, the bounds on μ for the convergence of the mean square error to some finite value are the same as the bounds for convergence of the weight vector to its optimum value (hence convergence of the weight covariance vector). Therefore, it will be sufficient for the remainder of this article to consider only the conditions required for convergence of the weight vector. As mentioned previously, this may not be true in practice (Horowitz and Senne, 1981; Gardner, 1984; Feuer and Weinstein, 1985); however, it does provide a basis against which to assess the effects that the

acoustic time delay and the electro/acoustic transfer functions, inherent in an active noise control system, have on the algorithm characteristics.

Finally, one other conclusion that can be drawn from equation (7.32) is that the convergence of the mean square error towards its minimum value has a geometric ratio of $(1 - 2\mu\lambda_p)^2$. Hence the convergence rate, r_p, is exponential with a time constant, τ_p, defined as (Widrow et al, 1976):

$$r_p = e^{-1/\tau_p} \qquad (7.36)$$

where

$$\tau_p = \frac{1}{4\mu\lambda_p} \qquad (7.37)$$

and p denotes the p^{th} "mode", or scalar equation corresponding to the p^{th} eigenvector of the input autocorrelation matrix..

7.3 FORMULATION OF THE FILTERED-X LMS ALGORITHM

Certain active noise control systems exist where only one actuator and one error sensor are required to achieve global attenuation of noise levels. Depending on the characteristics of the offending primary noise source, the control actuator can either generate an acoustic control disturbance, such as in ducts where only the plane wave mode is to be controlled (as was considered in Chapter 2), or a structural control disturbance in a coupled structural/acoustic system, such as in the control of sound transmission through a thin wall into a "live" rectangular enclosure (Pan et al, 1990), where all acoustic modes have an antinode in the corners. A block diagram of the active noise control system is shown in Figure 7.2. The control system is simply

trying to adaptively model the inverse of the acoustic or structural/acoustic system (labelled the "plant"). It follows that for a single actuator, single error sensor system to be effective on a global basis, it must be able to observe and control all of the offending acoustic or coupled structural/acoustic modes at a single location (not necessarily the same location for observing and controlling).

It will be assumed in the following analysis that an uncorrupted reference signal is available to the control system. This may not be true, for example, in a duct where acoustic feedback contributes to the sound at a reference microphone. In these instances the location of the reference microphone will have a significant influence upon the performance of the active noise control system, as any decrease in the coherence between the reference signal and the targetted primart source disturbance will have a detrimental effect upon the levels of sound attenuation obtained. An in-depth analysis of this, however, is beyond the scope of this thesis.

With reference to Figure 7.2, the signal sensed at the error microphone can be modelled as the sum of two parts; that due to the primary signal (from the primary source), ρ_k, and that due to the control source, s_k (note that if these signals are equal in magnitude but opposite in phase, the sound pressure at the error microphone will be nulled; if the system is observable and controllable at a single location, as mentioned earlier, this may produce global sound attenuation). Thus, the error signal is:

$$e_k = \rho_k + s_k \tag{7.38}$$

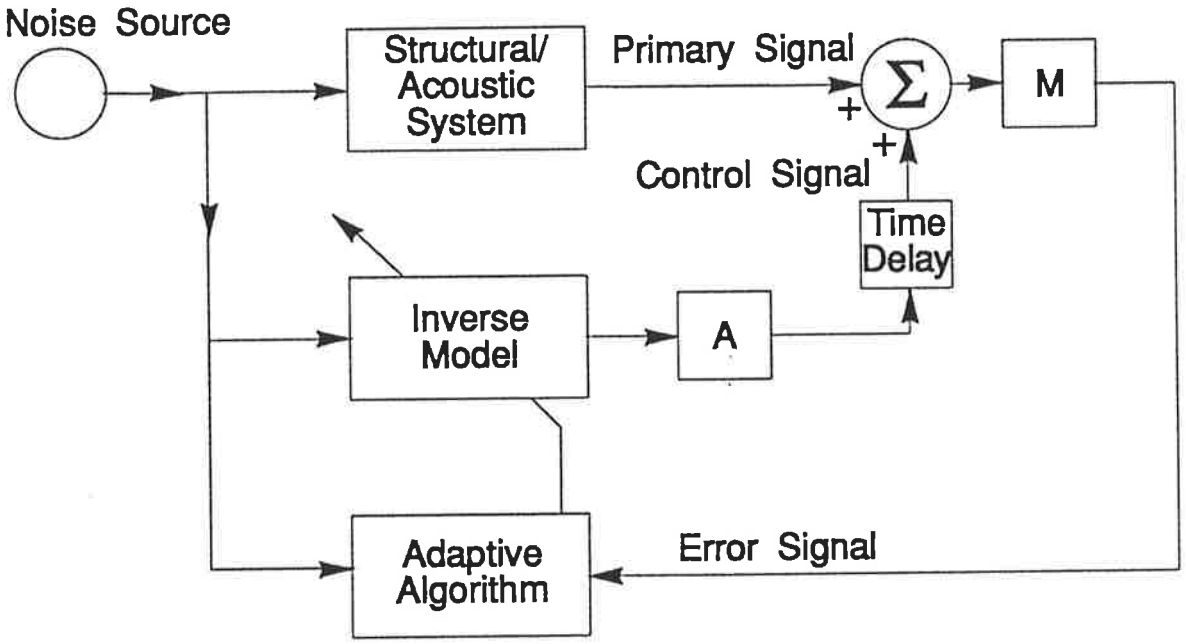

Figure 7.2. Block diagram of a single actuator, single error sensor active noise control system.

The secondary signal sensed at the error microphone at time k is not the signal sent out by the controller at time k. Rather, the control signal has been modified by the characteristic transfer function of the actuator, A, and delayed by n samples due to the finite separation distance between the actuator and the error sensor. Also, the total error signal has been modified due to the error microphone transfer function, M. Representing the transfer functions as finite impulse response functions, the actual error signal received by the system is:

$$e_k = (\rho_k + \mathbf{w}_{k-n}^T \mathbf{x}_{k-n} * A) * M \qquad (7.39)$$

where * is the convolution operator.

To simplify equation (7.39), the filtered primary source signal, G, and filtered reference signal, F, at time k are defined as:

$$g_k = \rho_k * M \tag{7.40}$$

$$F_k = X_{k-n} * A * M \tag{7.41}$$

The gradient estimate based on the instantaneous error signal squared is:

$$\hat{\nabla}_k = \frac{\partial e_k^2}{\partial W} = 2 e_k F_k \tag{7.42}$$

Therefore, the modified LMS algorithm is:

$$W_{k+1} = W_k - 2\mu e_k F_k \tag{7.43}$$

This is widely referred to as the filtered-X algorithm (Widrow and Stearns, 1985), and has been associated with active noise control in ducts for some time (Burgess, 1981). There are two characteristics of equations (7.42) and (7.43) that should be noted in particular. The first is the effect of the (acoustic) delay on the error estimate, equation (7.42). If the weights are updated at every sample, the gradient estimate at time k is based on the system response of n samples ago. This can significantly affect the system bounds of stability. Also, the right hand side of equation (7.43) involves subtraction, rather than addition (as in equation (7.19)). This is a result of the fact that acoustic signals must be "added", as opposed to electrical signals that can be "subtracted" (inverted and added).

In the practical implementation of the algorithm, the reference signal, X, is delayed by an estimate of n samples, then convolved with an estimate of the actuator and error microphone

transfer functions before being used in the adaptive algorithm. Thus, the calculations are based upon an estimate of the filtered reference signal:

$$\hat{F}_k = X_{k-\hat{n}} \hat{A} \hat{M} \tag{7.44}$$

where $\hat{}$ denotes an estimated quantity.

Therefore, the practical implementation of the algorithm is:

$$W_{k+1} = W_k - 2\mu e_k \hat{F}_k \tag{7.45}$$

$$= W_k - 2\mu \hat{F}_k (G_k + W_{k-n}^T F_k) \tag{7.46}$$

$$= W_k - 2\mu (\hat{F}_k G_k + \hat{F}_k F_k^T W_{k-n}) \tag{7.47}$$

7.4 CONVERGENCE COEFFICIENT STABILITY BOUNDS

There are two possible schemes for implementing the weight updating algorithm given in equation (7.43). The first is not to modify the weights at every sample; rather, send a signal to the actuator and wait for the resulting residual error signal to propagate back to the controller before adjustment. In this case, $W_{k-n} = W_k$ and, provided the system disturbances and response characteristics are time invariant (or only slowly varying), the delay will have no effect upon the system bounds of stability. The other scheme, mentioned previously, is to update the weights at every sample, thereby basing the adjustment on an "old" version of the system response. The delay has a significant effect upon the bounds of stability in this instance. To examine the effect, the limits placed on the convergence coefficient for stable operation will first be derived for the non-continuously updating system. The "ideal" case, as defined in the introduction, will again be considered. Following this, the effect of the time delay will be included. The stability bounds obtained will be compared with those derived in Section 7.2.3 for the standard LMS algorithm, to determine the effects of the algorithm modifications required for the active noise control implementation.

7.4.1 Base case stability criterion

For the "ideal" case, equation (7.47) can be modified to include expected values:

$$W_{k+1} = W_k - 2\mu \left(E[\hat{F}_k G_k] + E[\hat{F}_k F_k^T W_{k-n}]\right) \qquad (7.48)$$

As only the effects due to the time delay are being examined, it will be assumed that the estimates of the time delay and microphone and actuator transfer functions are accurate.

Therefore:

$$\hat{F}_k = F_k \tag{7.49}$$

Thus,

$$W_{k+1} = W_k - 2\mu\,(C_k + B_k\,W_{k-n}) \tag{7.50}$$

where:

$$B_k = E[F_k F_k^T] \tag{7.51}$$

$$C_k = E[F_k G_k] \tag{7.52}$$

Similar to the result obtained in section 7.2.2, the optimum weight vector, W^*, is that which sets the error criterion gradient estimate (the bracketted part of equation (7.50)) equal to zero:

$$W^* = -B_k^{-1}\,C_k \tag{7.53}$$

Thus B_k will be a symmetric matrix, allowing it to be diagonalized by an orthonormal matrix, Q, as outlined in the previous section. Using the notation described in section 7.2.3, equation (7.49) becomes:

$$W'_{k+1} = W'_k - 2\mu[C'_k + \Lambda_k W'_{k-n}] \tag{7.54}$$

As before, this can be expressed in terms of the weight variance vector:

$$V'_{k+1} = (W'_k - W^{*\prime}) - 2\mu([\Lambda_k W'_{k-n} - \Lambda_k W^{*\prime}] + [C'_k + \Lambda W^{*\prime}_k]) \tag{7.55}$$

Noting that:

$$W^{*\prime} = Q^{-1}W^{*} = -Q^{-1}B_k^{-1}C_k = -\Lambda_k^{-1}C_k' \tag{7.56}$$

equation (7.55) becomes:

$$V_{k+1}' = V_k' - 2\mu \Lambda_k V_{k-n}' \tag{7.57}$$

As the matrices in this equation are decoupled (contain no off-diagonal elements), they can be considered as N scalar "modal" equations of the form:

$$v_{i,k+1}' = v_{i,k}' - 2\mu \lambda_{i,k-n} v_{i,k-n}' \tag{7.58}$$

For the LMS algorithm to be stable over time, the weight coefficient vector variances must converge to some finite value for each scalar "modal" equation, or:

$$\left| \frac{v_{i,k+1}'}{v_{i,k}'} \right| < 1 \text{ for all } i \tag{7.59}$$

By re-expressing equation (7.58) as:

$$v_{i,k+1}' = v_{i,k}' \left(1 - 2\mu \lambda_{i,k-n} \frac{v_{i,k-n}'}{v_{i,k}'} \right) \tag{7.60}$$

it can be deduced that:

$$0 < \mu \lambda_{i,k-n} \frac{v_{i,k-n}'}{v_{i,k}'} < 1$$

or

$$0 < \mu < \frac{1}{\lambda_{i,k-n}} \frac{v_{i,k}'}{v_{i,k-n}'} \tag{7.61}$$

For the non-continuously updating case being considered here, the variance ratio term on the right hand side of equation (7.61) will be equal to 1. Therefore, the bounds placed on the convergence coefficient, μ, for stable operation reduce to:

$$0 < \mu < \frac{1}{\lambda_{max}} \qquad (7.62)$$

These bounds are identical in form to the bounds placed on the convergence coefficient for stability in the implementation of the standard LMS algorithm, given in equation (7.35). The difference here, however, is the the eigenvalues of interest are those of the *filtered* input autocorrelation matrix, defined in equation (7.51), rather than the standard input autocorrelation matrix of equation (7.10). Thus, the transfer functions inherent in an active noise control system modify the stability bounds of the algorithm by modifying the characteristic eigenvalues of the electronic system.

7.4.2 Effect of continuously updating the weight coefficients

The bounds placed on the convergence coefficient, μ, for algorithm stability given in equation (7.62) were derived with the assumption that the weight coefficient vectors were adjusted only after the result of the previous modification was known. In this case, the explicit effect of the acoustic time delay can be ignored (assuming that the system is stationary or only slowly time varying). However, if the system is continuously adapting, the time delay will have a significant effect upon the stability of the algorithm. This is because the present weight coefficient vector modification is based upon the results of a previous modification conducted n samples ago.

The starting point for including this effect is the weight vector variance adaption equation (7.58). Taking the z-transform of the i^{th} variance produces (Kabal, 1983):

$$V_i'(z) = \frac{z^{n+1} v_i(o)}{z^{n+1} - z^n + 2\mu\lambda_i} \qquad (7.63)$$

For the algorithm to be stable, the poles of equation (7.63) (determined by the roots of the characteristic equation) must be within the unit circle.

The values of $2\mu\lambda_i$ for which the characteristic equation has roots on the unit circle can be found by substituting $e^{i\phi}$ for z, and setting the equation equal to zero, or:

$$2\mu\lambda_i = e^{in\phi} - e^{i(n+1)\phi} \qquad (7.64)$$

As the matrix B is symmetric, the eigenvalues will all be real. Therefore, equating real and imaginary parts of equation (7.64):

$$2\mu\lambda_i = \cos(n\phi) - \cos((n+1)\phi) \qquad (7.65)$$

$$0 = \sin(n\phi) - \sin((n+1)\phi) \qquad (7.66)$$

From equation (7.66):

$$\phi = \frac{\pi}{2n+1} \qquad (7.67)$$

where n = the acoustic time delay expressed in sample periods, as defined earlier.

Substituting this value of ϕ into equation (7.65) produces:

$$2\mu\lambda_i = 2 \sin \frac{\pi}{2(2n+1)} \qquad (7.68)$$

This result can be introduced as a multiplying factor into equation (7.61), derived for the non-continuously updating case, producing the following bounds placed on the convergence coefficient for stable operation of the continuously updating implementation:

$$0 < \mu < \sin\frac{\pi}{2(2n+1)} \frac{1}{\lambda_{i,k-n}} \frac{v'_{i,k}}{v'_{i,k-n}} \qquad (7.69)$$

7.4.3 Discussion of the effect of active noise control system parameters upon the stability of the filtered-x LMS algorithm

There are two active noise control system parameters which explicitly alter the stability criteria for the LMS algorithm in this implementation. The first is the necessary convolution of the input signal with the system transfer functions, illustrated in equations (7.41) and (7.44). As mentioned previously, these convolutions will alter the eigenvalues which characterize the electronic system "modes" which, from equation (7.64), explicitly limit the maximum allowable value of convergence coefficient, μ, for stable operation.

To illustrate this effect, a single control source, single error sensor system was computer simulated. In this simulation, the transfer function between the control source and error sensor was increased in magnitude, and kept constant in phase. For a given magnitude, the convergence coefficient was increased in size until the system was only marginally stable. The results of this simulation are shown in Figure 7.3, plotted as the maximum allowable value of convergence coefficient for system stability, against relative transfer function magnitude. By comparing the definitions of the filtered input autocorrelation matrix, given in equation (7.51), with the standard input autocorrelation matrix, given in equation (7.10), it can be deduced that

the decrease in maximum stable convergence coefficient should be inversely proportional to the change in transfer function magnitude squared. This relationship is evident in Figure 7.3.

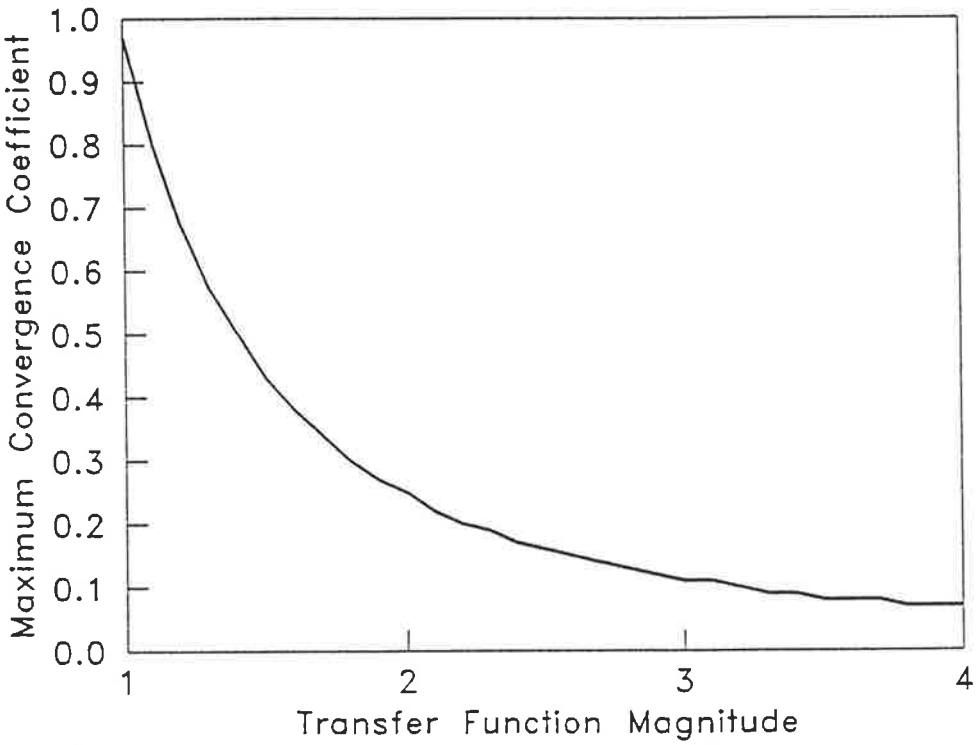

Figure 7.3. Effect of transfer function magnitude on the maximum stable value of convergence coefficient.

The second effect of interest is that which the time delay has on stability for the continuously adapting implementation. This effect appears explicitly in the sin() term in equation (7.69). However, it also appears implicitly in the variance ratio terms, as the ratio is the present variance of the (transformed) weight coefficient of interest divided by the sum of the past variances of all corresponding (transformed) weight coefficients. These combined effects are illustrated in Figure 7.4, which depicts the maximum allowable value of convergence

coefficient for system stability for the previously outlined computer simulated single control source, single error sensor system, plotted as a function of acoustic time delay (in samples). With this simulation, the primary disturbance is taken to be single frequency sinusoidal excitation. Two sets of data are shown, one where the sampling rate is equal to 10 times the excitation frequency, the other where it is equal to 50 times the excitation frequency. The effect of the sin() term is evident in the general shape of the data curves. What is interesting, however, is the enhancement of algorithm stability occurring at numbers of delay samples equivalent to quarter, and especially half, wavelength intervals. This enhancement is a combined effect of a sinusiodal input and the form of the variance ratio term. Note that the concept of sampling at quarter wavelength intervals has been referred to elsewhere as synchronous sampling (Elliott and Darlington, 1985).

An interesting point to note, however, is that while the acoustic time delay reduces the maximum stable value of convergence coefficient when the weights are continuously updated, the choice of continuously updating the weight coefficient vectors, or updating only after the effect of the previous change is known (waiting for the delay) appears to have no significant effect upon the convergence speed of the algorithm. Figure 7.5 depicts the convergence of the mean square error for a single control source, single error sensor system where the acoustic time delay between the source and sensor is equal to 10 samples. Two curves are plotted, one for the continuously updating system and one where the weight coefficients are updated every 10 samples. The convergence coeffiicents for these are equivalent, scaled by a factor of $\sin(\pi/(2(2n+1)))$. Clearly, the difference in convergence speed is minimal.

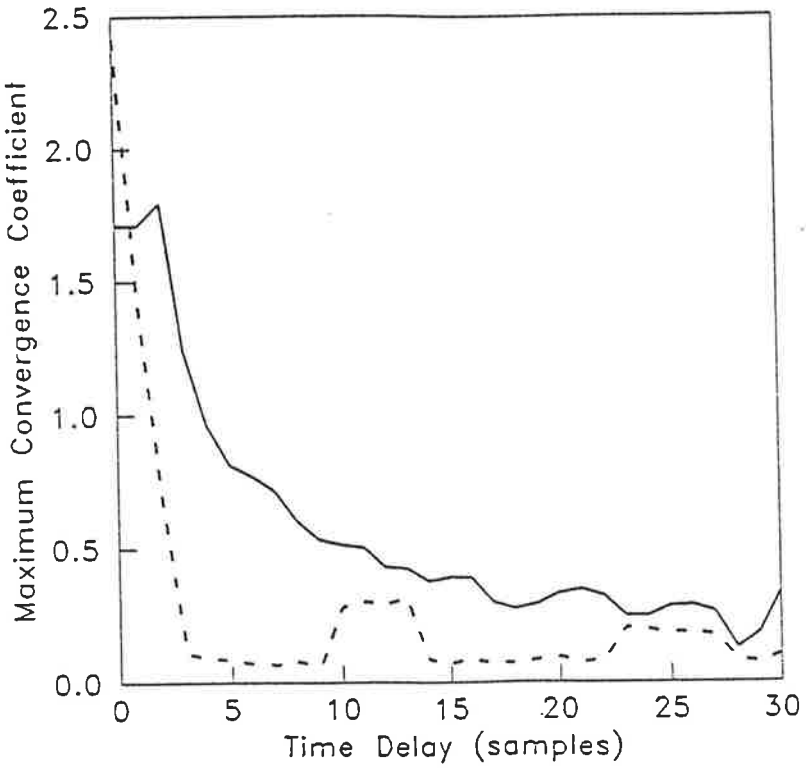

Figure 7.4. Maximum stable value of convergence coefficient as a function of time delay between the control source and error sensor, —— = sampling rate equal to 10 time the excitation frequency, - - - = sampling rate equal to 50 times the excitation frequency.

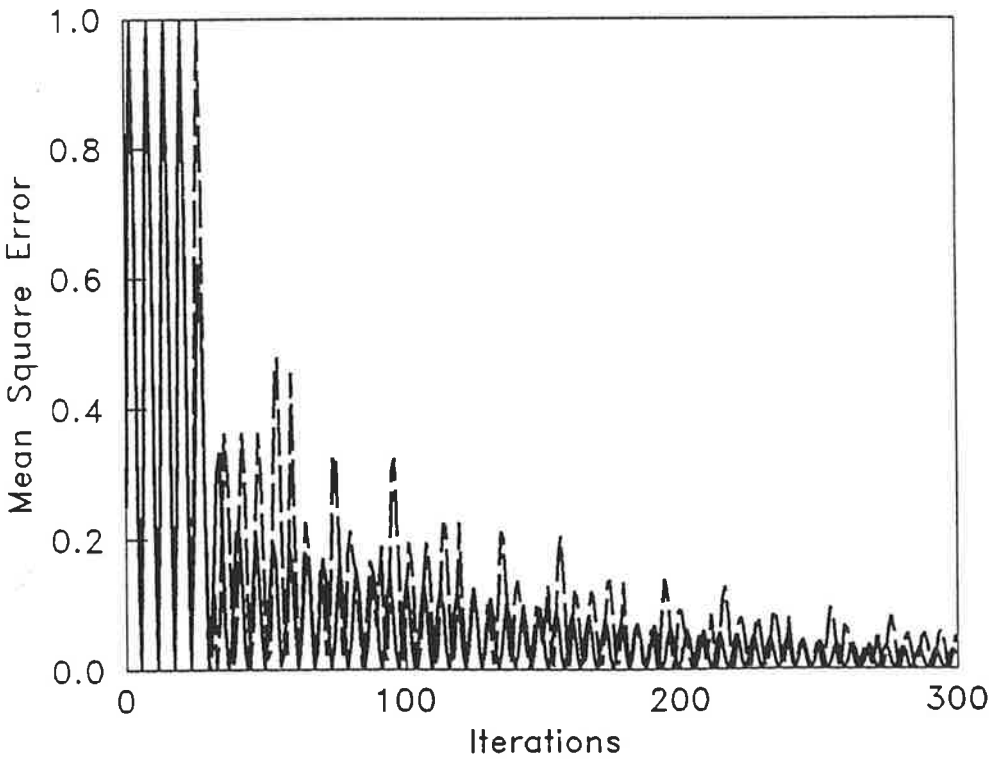

Figure 7.5 Convergence of mean square error, —— = continuous adaption, — — = delayed adaption

7.5. EFFECT OF TRANSFER FUNCTION ESTIMATION ERRORS - SINE WAVE INPUT

As outlined in Section 7.3, the practical implementation of the filtered-x LMS algorithm includes estimation of the error loop time delay, as well as the error microphone and actuator transfer functions. These estimates will, in general, be imperfect. As alluded to before, such imperfections will have an influence upon the system stability bounds. To examine the effect due to the estimation errors only, the actual time delay and error sensor and control source electro/acoustic transfer functions will be omitted from the system, and a single "estimation error transfer function", H, will be inserted as shown in Figure 7.6. If the system input signal is a sine wave, the transfer function can be thought of as a simple gain and phase change, h and ϕ_h, respectively.

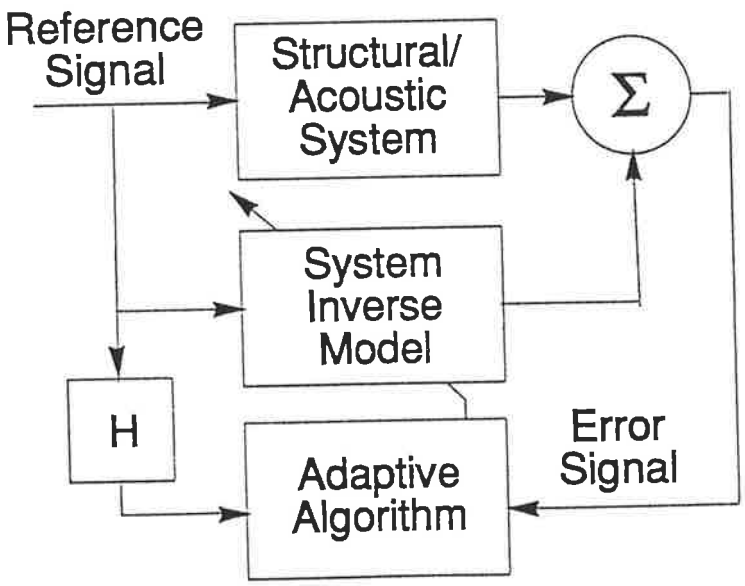

Figure 7.6. Block diagram of the single actuator, single error sensor active noise control system with transfer function estimation errors represented as a filter, H.

Consider first the simplified case of the filtered-LMS algorithm operating with complex numbers. This is the form of the algorithm which would be implemented in the frequency domain. For the system shown in figure 7.6, the LMS algorithm is:

$$W_{k+1} = W_k - 2\mu e_k (hX_k^*) \tag{7.70}$$

where * denotes complex conjugate, and h is the (complex) gain of the error transfer function:

$$h = h_R + i\, h_I \tag{7.71}$$

For the ideal (deterministics) case, equation (7.70) can be rewritten in the form of equation (7.50) (where C is now equal to P, and B is now equal to R) as

$$W_{k+1} = W_k - 2\mu h (P_k + R_k W_k) \tag{7.72}$$

As R_k is a symmetric matrix, it can be diagonalized by use of an orthonormal matrix as described in equation (7.21). Using the previously outlined notation, equation (7.72) becomes:

$$W'_{k+1} = W'_k - 2\mu h[P'_k + \Lambda_k W'_k] \tag{7.73}$$

In terms of the weight variance vector, V, this can be restated as

$$V'_{k+1} = V'_k - 2\mu h\Lambda_k V'_k = (I - 2\mu h\Lambda_k)V'_k \tag{7.74}$$

As equation (7.74) is decoupled, it can be viewed as a set of N scalar equations. Each of these must converge as $k \rightarrow \infty$ for the algorithm to be stable. The i^{th} scalar equation is:

$$v'_{i,k+1} = (1 - 2\mu h\lambda_{i,k})v'_{i,k} \tag{7.75}$$

Note that i^{th} eigenvalue, λ_i, is a real quantity here as the input autocorrelation matrix is symmetric..

For equation (7.75) to converge as $k \rightarrow \infty$:

$$| 1 - 2\mu h\lambda_i | < 1 \tag{7.76}$$

As h is complex, rewriting equation (7.76) in terms of the real and imaginary parts gives

$$[(1 - 2\mu h_R\lambda_i)^2 + (2\mu h_I\lambda_i)^2]^{1/2} < 1 \tag{7.77}$$

or

$$(1 - 2\mu h_R\lambda_i)^2 + (2\mu h_I\lambda_i)^2 < 1 \tag{7.78}$$

Expanding this:

$$1 - 4\mu h_R\lambda_i + 4\mu^2 h_R^2\lambda_i^2 + 4\mu^2 h_I^2\lambda_i^2 < 1 \tag{7.79}$$

or

$$\mu^2\lambda_i^2 (h_R^2 + h_I^2) - \mu\lambda_i h_R < 0 \tag{7.80}$$

or

$$\mu\lambda_i |h|^2 - h_R < 0 \tag{7.81}$$

Equation (7.81) can be rewritten:

$$\mu < \frac{h_R}{\lambda_i |h|^2} \tag{7.82}$$

or $$\mu < \frac{\cos \phi_h}{\lambda_i |h|} \tag{7.83}$$

where ϕ_h = the phase change caused by the transfer function. Thus, the bounds placed on μ for convergence are:

$$0 < \mu < \frac{\cos \phi_h}{\lambda_{max} |h|} \tag{7.84}$$

Thus, for a sinusoidal input signal operating with a complex number algorithm, the effect of imperfections in the estimates of the error loop time delay and error microphone and actuator transfer functions can be considered in two parts. Firstly, an error in the estimation of the phase delay will reduce the maximum convergence coefficient by an amount proportional to cos ϕ_h. It follows that if the estimate is in error by more than ±90°, the algorithm will become unstable regardless of the size of the convergence coefficient. This agrees with previous results (Morgan, 1980; Burgess, 1981; Elliott and Nelson, 1985; McNichol, 1985). Secondly, errors in

the estimation of the magnitude of the transfer function will reduce the size of the maximum allowable convergence coefficient by an amount proportional to the inverse of that error.

The majority of implementations of the filtered-x LMS algorithm in active noise control systems will not, however, be done with complex numbers. Rather, the algorithm will be implemented in the time domain with strictly real numbers. For this case errors in the estimation of the transfer functions will alter the eigenvalues of the filtered input autocorrelation matrix, which in a practical system will be equal to

$$B_k = E[F_k \hat{F}_k^T] \tag{7.85}$$

This can be compared to equation (7.51), for perfect tranfer function estimates. Therefore, these eigenvalues must be examined to determine the effect which transfer function estimation errors have upon the algorithm stability. To do this, a simple 2-tap system will be investigated.

For the system shown in Figure 7.6, with a single frequency sinusoidal input signal, the input autocorrelation matrix will be:

$$R_h = E[X_{k,h} X_k^T] \tag{7.86}$$

where:

$$X_k = [\sin(\theta+\gamma), \quad \sin(\theta)]^T \tag{7.87}$$

$$X_{k,h} = h[\sin(\theta+\gamma+\phi_h), \quad \sin(\theta+\phi_h)]^T \tag{7.88}$$

where θ is an arbitrary reference angle, and γ is the angular increment of each new sample:

$$\gamma = 2\pi \frac{\text{input frequency}}{\text{sampling rate}} \tag{7.89}$$

By definition (Bendat and Piersol, 1980) the i,jth element of the autocorrelation matrix is found by evaluating:

$$r_{i,j} = \frac{1}{2\pi} \int_0^{2\pi} x_i \, x_{h,j} \, d\theta \qquad (7.90)$$

Performing this integration (Bendat and Piersol, 1980) produces and input autocorrelation matrix equal to:

$$R_h = \frac{h}{2} \begin{bmatrix} \cos(\phi_h) & \cos(\phi_h + \gamma) \\ \cos(\phi_h - \gamma) & \cos(\phi_h) \end{bmatrix} \qquad (7.91)$$

The eigenvalues of R_h can be found by solving for the characteristic determinant of the expression:

$$|\lambda I - R_h| = 0 \qquad (7.92)$$

Solving for the determinant produces the following expression for the eigenvalues of R_h:

$$\lambda = \frac{h}{2} \left(\cos(\phi_h) \pm (\cos(\phi+\gamma) \cos(\phi-\gamma))^{0.5} \right) \qquad (7.93)$$

From equation (7.93), it can be seen that errors in the estimation of the magnitude of the transfer functions have a simple multiplying effect upon the magnitude of the eigenvalues. Therefore, as the maximum allowable convergence coefficient for system stability is inversely proportional to the system eigenvalues:

$$\mu_{max} \propto \frac{1}{h} \qquad (7.94)$$

This fact is illustrated in Figure 7.7, which depicts the maximum stable value of convergence coefficient for the previously described computer simulated system, plotted against the

magnitude of the transfer function estimation error expressed as a multiplying factor. In viewing this, it is clear that an inverse proportional relationship exists.

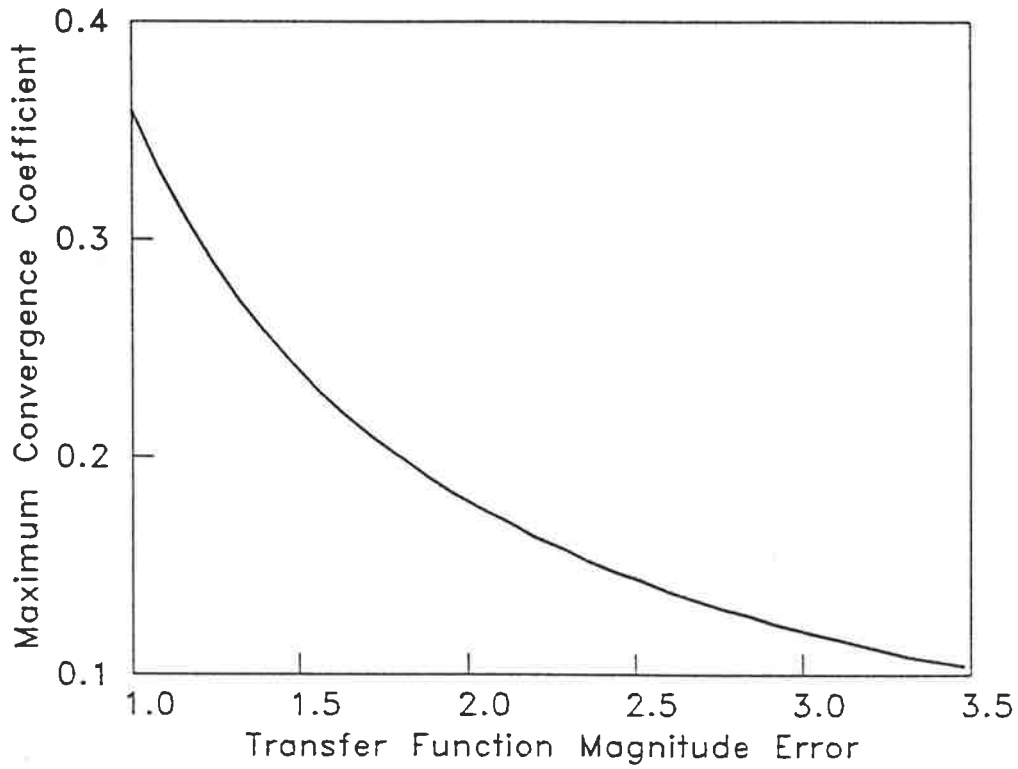

Figure 7.7. Effect of transfer function magnitude estimation error on the maximum stable value of convergence coefficient.

The effect of phase estimation error is more complicated. The first point to note is that, regardless of sampling rate, an error of more ±90° will guarantee algorithm instability, as one of the eigenvalues will be a negative number (it should also be noted that at some symmetric positive / negative value of phase error, governed by the sampling rate, the eigenvalues will become complex). This point was mentioned previously in regard to the complex number implementation of the algorithm. However, analysis of the effect which other values of phase estimation error has upon the stability of the algorithm is complicated by the fact that the "phase errored" filtered input autocorrelation matrix, stated in equation (7.91), is no longer symmetric. As a result, it can no longer be said that it will in general have orthogonal eigenvalues, so that

the algorithm can no longer be decoupled by the use of an orthonormal transformation. Therefore, while it is possible to generalise that a phase error in excess of 90° will cause algorithm stability, that is all that can be said. Different cases with differing sample rates (the effects of which appear explicitly in equation (7.91)) must be considered individually.

7.6 SUMMARY

The acoustic time delay and the electro/acoustic transfer functions of the actuators and error sensors inherent in an active noise control system must be taken into account when implementing the LMS algorithm in a single actuator, single error sensor system. Estimates of these must be included in any practical active noise control system.

For the single actuator, single error sensor case the effect of the system transfer functions is to reduce the maximum stable value of the convergence coefficient by an amount proportional to the square of the transfer function magnitude. The effect of the time delay is implementation dependent. For the non-continuously updating case (where the weights are updated only after the result from the previous update has been received from the error sensor) there is no effect (provided the system is time invariant or only slowly varying). For the continuously updating case (where the weights are updated at every sample), the maximum allowable convergence coefficient is reduced by a baseline multiplying factor of $\sin[\pi/(2(2n+1))]$, where n is the number of samples corresponding to the acoustic time delay between the control actuator and error sensor. Additive to this, areas of enhanced algorithm stability can occur at discrete quarter and half wavelength intervals, if the disturbance is sinusoidal. Despite this, there is not a

significant difference in convergence speed between the continuous and non-continuous weight updating strategies where the convergence coefficient is scaled as stated.

Errors in the estimation of the time delay and the transducer electro/acoustic transfer functions also have an influence on the system bounds of stability. The reduction in the maximum allowable value of the convergence coefficient is inversely proportional to the error in the estimated magnitude of the electro/acoustic transfer function. The effect of phase estimation errors is more complicated, and varies with varying sampling rate. However, for the single input, single output system considered here, if the error in phase estimation is greater than $\pm 90^{\circ}$, the algorithm will become unstable regardless of the value of the convergence coeffiicent, μ, and regardless of whether continuous or non-continuous updating is used.

CHAPTER 8.

THE MULTIPLE INPUT, MULTIPLE OUTPUT LMS ALGORITHM

8.1. INTRODUCTION

A major hindrance to the development of practical active noise control systems for a variety of low frequency problems is related to the complexity of the multi-modal response of most structural/acoustic systems. For an active system to provide global noise attenuation, all of the primary offending acoustic or coupled structural/acoustic modes must be observable to, and controllable by, the system. It follows that, for a single mode system, such as plane wave sound propagation in a duct, a relatively simple combination of a single control source and error sensor can achieve the desired result. For more complex systems, the required number of control sources and error sensors can increase dramatically.

Recently, the single input, single output "filtered-x" LMS algorithm, examined in chapter 7, has been extended to allow its use in active noise control systems requiring multiple control sources and error sensors (Elliott et al, 1987). As with the single channel version of the filtered-x LMS algorithm, the multi-channel filtered-x LMS algorithm requires estimates of transducer transfer functions and acoustic time delays, as well as estimates of the transfer functions of the acoustic or coupled structural/acoustic system's response, for stable operation. The transfer functions will have an effect upon the bounds of stability placed on the algorithm, as too will the acoustic time delays if the weight coefficient vectors are updated at a rate which is faster than the propagation time of the error signal(s) (however, if the weight coefficient vectors are updated at

time intervals which are sufficiently long to include all of the delays associated with the acoustic propagation, then the time delays will have no effect upon the system stability for a (relatively) stationary disturbance). Further, in a system using more than one error sensor and control source, the indirect effect that the control sources have on one another due to feedback through the error sensors will also change the convergence behaviour of the algorithm.

The following analysis examines the stability of the multiple input, multiple output LMS algorithm as applied to active noise control systems, with the results obtained here providing some insights into efficient algorithm implementation. The first two sections develop the bounds of stability for the algorithm. The following section examines the effect which various system parameters have upon this bounds.

Finally, it should again be noted that part of the reason for the choice of the LMS algorithm for analysis here, as well as for implementation in many practical systems, is its relative simplicity as compared to other signal processing algorithms. It may not be, in fact is likely not to be, the optimal algorithm in many situations. However, the results presented here may be applied qualitatively to other algorithm implementations.

8.2. MULTIPLE CONTROL SOURCE, MULTIPLE ERROR SENSOR LMS ALGORITHM

The following sections of this chapter aim to assess the effects which the electro/acoustic transfer functions and acoustic time delays inherent in an active noise control system have upon the algorithm performance. In this way, the design requirements for this type of system can be

determined qualitatively. The derivations are directed at obtaining an expression for the bounds on the algorithm which will ensure stability. It assumes the "ideal" case, where the value of the signal sampled at time k is taken to be the mean of the variable at that time (the expected value, E[]). While the absolute results obtained may not be correct for all implementations (Horowitz and Senne, 1981; Gardner, 1984), they do provide a basis against which to assess the effects of the important system parameters.

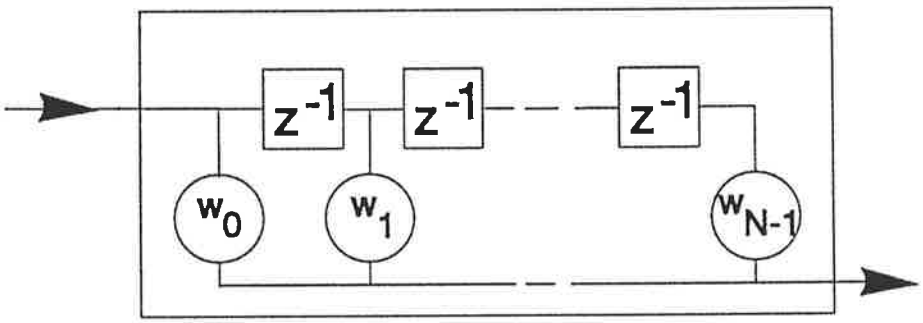

Figure 8.1. The transversal filter. Note that z^{-1} denotes a single time delay.

As with the single channel filtered-x LMS algorithm studied in chapter 7, the analysis is based on the premise that the control source signals are generated by using transversal filters, or tapped delay lines, as shown in Figure 8.1. With this system, a reference signal (a signal which is correlated with the sound or vibration field) is sampled, providing a discrete filter input value,

x. This value propagates through the filter, progressing one stage with every new sample taken. Thus, at any particular time k, the values present in the delay line can be represented as a vector:

$$X_k = \left[\begin{array}{cccc} x_k & x_{k-1} & x_{k-2} & \cdots & x_{k-(N-1)} \end{array} \right]^T \qquad (8.1)$$

where N is the number of stages in the filter, and ^{T} denotes the transpose of the matrix. Throughout this chapter, vectors and matrices will be denoted by upper case letters, scalars by lower case letters.

Each time a new input sample enters the transversal filter, the previous N samples are shifted one position, and the values at each stage are multiplied by a weight coefficient assigned to that stage. The results are summed to produce a filter output. Representing the weight coefficients at time k as a vector:

$$W_k = \left[\begin{array}{cccc} w_{0,k} & w_{1,k} & w_{2,k} & \cdots & w_{(N-1),k} \end{array} \right]^T \qquad (8.2)$$

the filter output at time k is equal to:

$$y_k = \sum_{i=0}^{N-1} w_{i,k} \, x_{k-i} = W_k^T X_k = X_k^T W_k \qquad (8.3)$$

For the multiple control source, multiple error sensor control system considered here, there are m error sensors and r control sources. The control source signals are generated by transversal filters, each using the same reference signal but different weight coefficients.

Whilst the physical and electronic control systems can be considered separately in the design process, it will be useful here to "attach" the design to some specific problem. In this way some

of the concepts to be presented can be better visualized. The system considered here will be designed for controlling the radiation of sound from a vibrating rectangular baffled panel, shown in Figure 8.2. As discussed in chapters 3 and 4, global sound attenuation can be achieved by using either an acoustic control source, such as a horn driver, or a vibration control source, such as an electrodynamic shaker or piezoelectric crystal, or a combination of the two. For the case considered here, several vibration (point) sources will be attached to the panel, and the residual sound field will be sensed by several error microphones. Owing to the directivity of the panel sound radiation, the placement of the microphones, and the different attachment points of the control sources, the transfer functions between each control source and each error sensor, represented in the time domain as finite impulse responses, will be different.

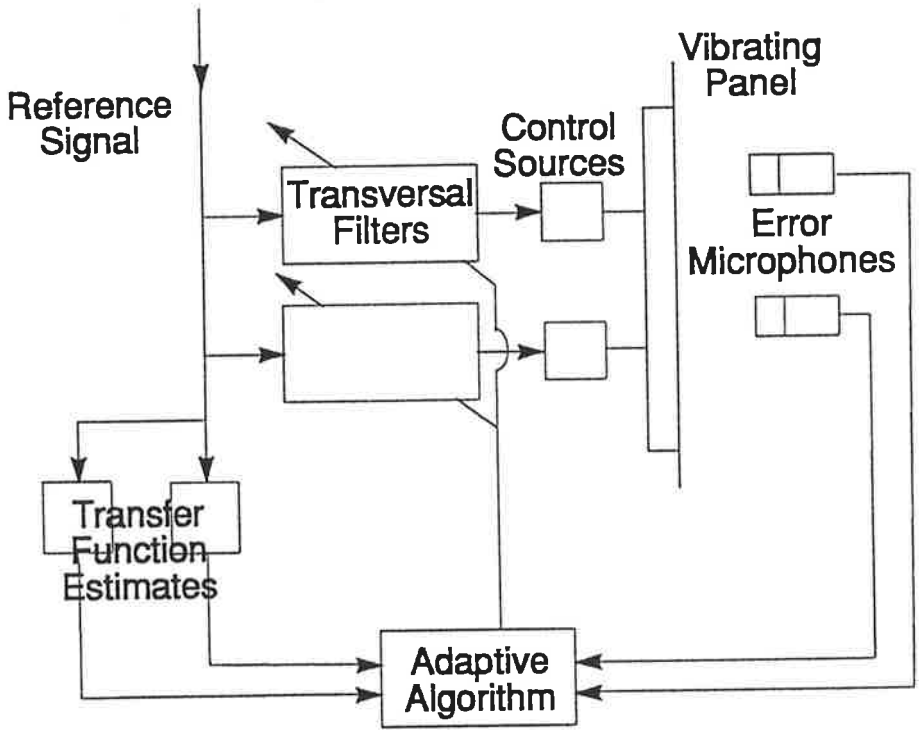

Figure 8.2. Block diagram of the practical implementation of a multiple actuator, multiple error sensor system for the active control of sound radiation from a vibrating panel.

It will be assumed in the following analysis that an uncorrupted reference signal is available to the control system. This may not always be true, especially in systems using acoustic control sources and "reference microphones". In these instances, the location of the reference microphone is critical to the performance of the active noise control system (owing to observability constraints). Any decrease in the coherence between the reference signal and the targeted primary source disturbance will have a detrimental effect upon the levels of attenuation achieved. However, an in-depth discussion of this area is beyond the scope of this thesis).

It should be noted that although the algorithm will be formulated with respect to the above described system, it can be applied directly to any system fulfilling observable/controllable conditions, where all parts of the sound field are observable by one or more error sensors and all parts can be controlled by one or more control sources.

8.2.1 Derivation of the practical multiple input, multiple output LMS algorithm

The required extension of the LMS algorithm to enable its use in multiple input, multiple output active noise control systems was derived Elliott et al (1987). An outline of the derivation of this algorithm will be briefly described here to provide the basis for the results presented later in this chapter.

With reference to Figure 8.2, the sound field presented to the i^{th} error sensor at time k can be thought of as being comprised of two parts; that due to the primary source(s), $\rho_{i,k}$, and that due to each of the $\imath$ control sources, $s_{i,j,k}$. Thus, the sound field at the i^{th} error sensor at time k is:

$$p_{i,k} = \rho_{i,k} + \sum_{j=1}^{\imath} s_{i,j,k} \qquad (8.4)$$

That part of the sound field arriving at the i^{th} error sensor at time k which can be thought of as originating from the j^{th} control source is not simply that signal sent out by the adaptive control system at time k, given in equation (8.3). Rather, the control signal has been modified by both the characteristic (frequency dependent) transfer function of the j^{th} control source and some factor arising from the directivity of the panel radiation. These two transfer functions are combined and expressed as a single finite impulse response function, $\Gamma_{i,j}$. Also, the signal has been delayed by $n_{i/j}$ samples due to the finite separation distance between the j^{th} control source and i^{th} error sensor (this value will be taken as constant for all control source / error sensor combinations, equal to n samples, to simplify the equation notation). Finally, the sound field arriving at the error sensor at time k is not that presented to the adaptive controller at time k. Rather, in producing an output, the i^{th} error sensor modifies the signal by some electro/acoustic transfer function, represented in the time domain as a finite impulse response function, M_i. Hence, the actual error signal received by the adaptive control system at time k from the i^{th} error sensor is:

$$e_{i,k} = p_{i,k} * M_i = \left(\rho_{i,k} + \sum_{j=1}^{I} s_{i,j,k} \right) * M_i$$

$$= \left(\rho_{i,k} + \sum_{j=1}^{I} W_{j,k-n}^{T} X_{k-n} * \Gamma_{i,j} \right) * M_i \qquad (8.5)$$

where * is the convolution operator.

To simplify equation (8.5), two quantities will be defined. Firstly, the filtered primary source signal, g, received at the output of the i^{th} error sensor at time k is defined as:

$$g_{i,k} = \rho_{i,k} * M_i = \sum_{u=0}^{N-1} \rho_{i,k-u}\, m_{i,u} \qquad (8.6)$$

where $m_{i,u}$ is the u^{th} element of the i^{th} error sensor finite impulse response vector of length N. Secondly, the filtered reference input sample at time k, $f_{i,j,k}$ is defined as

$$f_{i,j,k} = X_{k-n}\, T_{i,j} \qquad (8.7)$$

and $T_{i,j}$ is the (N x 1) vector (time domain) representation of the transfer function between the i^{th} error sensor and j^{th} control source. Therefore, the filtered reference input vector can be expressed as

$$F_{i,j,k} = \chi_k\, T_{i,j} \qquad (8.8)$$

where χ_k is a vector of (k-N) input vectors,

$$\chi_k = [\, X_k\ X_{k-1}\ \ldots\ X_{k-N}\,]^T \qquad (8.9)$$

In terms of the quantities defined in equations (8.6) and (8.8), equation (8.5) can be rewritten as:

$$e_{i,k} = g_{i,k} + \sum_{j=1}^{I} W_{j,k-n}^T\, F_{i,j,k} \qquad (8.10)$$

The error criterion is that the sum of the mean square values, $E[p_i^2]$, of the signals presented at each error sensor should be a minimum. This is equivalent to the sum of the mean square values $E[e_i^2]$ of the signal received by the control system from each error sensor being a minimum. The gradient descent algorithm operates by adding a portion of the negative gradient of the error at the present control source weight coefficient values to the weight coefficient vector (the portion being determined by the convergence coefficient, μ). The gradient of the error for the i^{th} microphone with respect to the j^{th} weight coefficient vector is *estimated* based

upon the instantaneous signal at time k. This estimate is commonly obtained (Widrow and Stearns, 1985) by squaring the instantaneous error (equation (8.10)) and differentiating with respect to the j^{th} weight vector, W_j, producing:

$$\frac{\partial e_{i,k}^2}{\partial W_j} = 2\, e_{i,k}\, F_{i,j,k} \qquad (8.11)$$

Note that the error signal at time k is matched to the signal originating from the controller producing the error, which has been delayed by n samples.

Summing this result for all the error sensors will provide an estimate of that part of the total error gradient attributable to the j^{th} control actuator:

$$\hat{\nabla}_{j,k} = \sum_{i=1}^{m} \frac{\partial e_{i,k}^2}{\partial W_j} = 2 \sum_{i=1}^{m} F_{i,j,k}\, e_{i,k} \qquad (8.12)$$

where $\hat{}$ denotes an estimated quantity.

Therefore, the multiple actuator, multiple error sensor LMS algorithm is:

$$W_{j,k+1} = W_{j,k} - 2\mu \sum_{i=1}^{m} F_{i,j,k}\, e_{i,k} \qquad (8.13)$$

Equation (8.13) agrees with the previously presented derivation by Elliott et al (1987). For the simple case of a single actuator and single error sensor, equation (8.13) reduces to the "filtered-x" algorithm examined in chapter 7.

In a practical system, estimates of the previously mentioned transfer functions and time delays, rather than actual values, will be used. Therefore, for the j^{th} weight vector, the practical implementation of the algorithm is:

$$W_{j,k+1} = W_{j,k} - 2\mu \sum_{i=1}^{m} \hat{F}_{i,j,k}\, e_{i,k} \qquad (8.14)$$

Two aspects of the algorithm given in equation (8.14) that should be noted are as follows: Firstly, the updating of the weight coefficients in the practical algorithm is based upon a reference signal that is convolved with estimates of the transfer functions of the control sources and error sensors as well as the structural / acoustic transfer functions. Secondly, due to the inherent acoustic time delays, the updating of the weight vector at time k is based on an "old" version of the system response. These will both affect the bounds placed on the convergence coefficient, μ, for system stability, as will be discussed later in this article.

8.2.2 Solution for the optimum set of weight vectors

The system error criterion, taken to be the minimization of the mean square values of the error transducer output, $E[e_i^2]$, can be expressed, using equation (8.10), as:

$$\Xi_k = \sum_{i=1}^{m} E[\, e_{i,k}^2 \,]$$

$$= \sum_{i=1}^{m} E\Big[\Big(g_{i,k} + \sum_{j=1}^{I} W_{j,k-n}^T F_{i,j,k} \Big)^2 \Big] \qquad (8.15)$$

This can be expanded:

$$\Xi_k = \sum_{i=1}^{m} \Big(E[g_{i,k}^2] + 2 \sum_{j=1}^{l} C_{i,j,k}^T W_{j,k-n} + \sum_{j=1}^{l} W_{j,k-n}^T E\Big[F_{i,j,k} \sum_{j=1}^{l} F_{i,j,k}^T \Big] W_{j,k-n} \Big) \qquad (8.16)$$

where $C_{i,j,k}^T$ = the cross correlation matrix between the filtered primary source signal, $g_{i,k}$, from the ith error sensor and the transpose of the filtered reference signal, $F_{i,j,k}^T$, between the i^{th} error sensor and the jth control source at time k:

$$C_{i,j,k}^T = E[\, g_{i,k} \, F_{i,j,k}^T] \qquad (8.17)$$

Equation (8.16) can be re-expressed in augmented matrix form as

$$\Xi_k = \epsilon_k^T \epsilon_k = W_k^T B_k W_k + C_k^T W_k + W_k^T C_k + D_k \qquad (8.18)$$

where

$$\epsilon_k^T = E[e_{1,k} \; e_{2,k} \; \cdots \; e_{m,k}] \qquad (8.19)$$

$$W_k^T = [w_{1,1,k} \cdots w_{1,N,k} \mid w_{2,1,k} \cdots w_{2,N,k} \mid \cdots \mid w_{l,1,k} \cdots w_{l,N,k}] \qquad (8.20)$$

$$B_k = E[F_k^T F_k] \qquad (8.21)$$

$$F_k = \begin{bmatrix} F_{1,1,k} & \cdots & F_{m,1,k} \\ F_{1,2,k} & \cdots & F_{m,2,k} \\ & \cdots\cdots\cdots & \\ F_{1,l,k} & \cdots & F_{m,l,k} \end{bmatrix} \qquad (8.22)$$

$$C_k^T = E[g_k^T F_k^T] \tag{8.23}$$

$$g_k^T = [g_{1,k}\ g_{2,k}\ \cdots\ g_{m,k}] \tag{8.24}$$

$$D_k = E[g_k^T g_k] \tag{8.25}$$

Expressed in this form, the optimum set of weight coefficients, W^*, is

$$W^* = -B_k^{-1} C_k \tag{8.26}$$

Substituting this back into equation (8.18), the minimum mean square error, Ξ^*, is

$$\Xi^* = D_k + C_k^T W^* \tag{8.27}$$

8.2.3 Solution for a single optimum weight coefficient vector

The solution for the optimum set of weight vectors in the previous section assumes that all of these vectors are optimized together. It may be more hardware efficient in some cases, however, to optimize single weight coefficient vectors in a round robin arrangement. It will therefore be useful to re-express the optimum weight vector solution in terms of a single weight vector, interacting with the others, rather than a solution for the entire set.

The optimum j^{th} weight coefficient vector, W_j^*, is found by differentiating equation (8.16) with respect to the weight coefficient vector, $W_{j,k-n}$, and setting this gradient expression equal to zero, will enable the determination of this quantity. Before doing this, it will be advantageous to re-express equation (8.16) in terms of equation (8.8),

$$\Xi_k = \sum_{i=1}^{m} \Big(E[g_{i,k}^2] + 2 \sum_{j=1}^{l} C_{i,j,k}^T W_{j,k-n} + \sum_{j=1}^{l} W_{j,k-n}^T E\Big[\chi_k T_{i,j} \sum_{j=1}^{l} T_{i,j}^T \chi_k^T \Big] W_{j,k-n} \Big) \qquad (8.28)$$

Noting that χ_k is a symmetric matrix, equation (8.28) can be written as

$$\Xi_k = \sum_{i=1}^{m} \Big(E[g_{i,k}^2] + 2 \sum_{j=1}^{l} C_{i,j,k}^T W_{j,k-n} + \sum_{j=1}^{l} W_{j,k-n}^T R_k \sum_{q=1}^{l} \tilde{W}_{j/q,k-n} \Big) \qquad (8.29)$$

where the subscript q refers to control source q and

$$R_k = E[\chi_k \chi_k^T] \qquad (8.30)$$

$$\tilde{W}_{j/q,k-n} = T_{i,j} T_{i,q}^T W_{q,k-n} = T_{i,j/q} W_{q,k-n} \qquad (8.31)$$

Differentiating equation (8.29), the gradient expression for the jth weight coefficient vector (corresponding to the j^{th} control source) is:

$$\frac{\partial \Xi_k}{\partial W_j} = \sum_{i=1}^{m} \Big(\sum_{q=1}^{l} (2 R_{k-n} \tilde{W}_{j/q,k-n} + 2 C_{i,j,k}) \Big) \qquad (8.32)$$

Setting equation (8.32) equal to zero produces the j^{th} optimum weight coefficient vector:

$$W_j^* = \sum_{i=1}^{m} \Big(- T_{i,j/j}^{-1} R_{k-n}^{-1} C_{i,j,k} - \sum_{q=1,\neq j}^{l} \tilde{W}_{j/q,k-n} \Big) \qquad (8.33)$$

It is interesting to consider the solution for the j^{th} optimum weight coefficient vector, given in equation (8.33), in terms of the physical placement of the control sources and error sensors in the structural acoustic system. The transformation of equation (8.31) projects the q^{th} weight coefficient vector into the vector space whose basis is the j^{th} weight coefficient vector (the vector of interest), the projection defined by the transfer function matrices, $T_{i,j}$ and $T_{i,q}$. If the transfer functions are identical, then the vector spaces lay on top of each other. If, however, the transfer function matrices are orthogonal, the transformation maps the q^{th} weight coefficient vector into the nullspace of the j^{th} weight coefficient vector.

Physically, this means that if the placement of the control sources and error sensors is orthogonal in terms of the structural / acoustic system modes which can be excited and sensed, in a round robin adaption process the presence of the other control sources has no effect upon the convergence behaviour of the control source being adapted. However, if the placement of the control sources and error sensors is non-orthogonal (as will usually be the case), the solution for the optimum j^{th} weight coefficient vector is dependent upon the present values of the other weight coefficient vectors, mapped into the j^{th} weight coefficient vector space. Thus, if the system is effectively underdetermined, there may *not* be a unique set of optimum weight coefficient vectors. This point will be elaborated on later in this article.

8.3 CONVERGENCE COEFFICIENT STABILITY BOUNDS

There are two common schemes for updating the j^{th} weight coefficient vector via the algorithm given in equation (8.14). The first is not to modify the weights at every sample; rather, to send a signal to the actuator and wait for the resulting residual error signal to propagate back to the

controller before adjustment (non-continuous adaption). In this case, $W_{j,k-n} = W_{j,k}$ and, provided the system disturbance and response is time invariant (or only slowly varying), the acoustic time delays will have no effect upon the system bounds of stability. The other scheme, mentioned previously, is to update the weights at every input sample (continuous adaption), thereby basing the adjustment on an "old" estimate of the gradient of the error. The delays have a significant effect upon the bounds of stability in this instance.

The following analysis examines the stability of the active noise control version of the multiple input, multiple output LMS algorithm for the "base" case, where "perfect" transfer function estimates are available and non-continuous weight vector updating is implemented. The analysis follows on from the "single weight vector" formulation of section 8.2.3. This will then be extended to include the effect of continuous adaption in the section that follows.

8.3.1. Base case stability criterion

With the assumption that the estimates of the transfer functions and time delays in equation (8.14) are exact, expanding the sampled error term of that equation produces, for the j^{th} control source,:

$$W_{j,k+1} = W_{j,k} - 2\mu \sum_{i=1}^{m} F_{i,j,k} \left(g_{i,k} + \sum_{q=1}^{l} F^{T}_{i,q,k} W_{q,k-n} \right) \qquad (8.34)$$

It is useful here to partition the primary source disturbance measurement provided by the i^{th} error sensor, $g_{i,k}$, into two components; the "excess" which will be "cancelled" under optimal

conditions (where $W_j = W_j^*$ for all weight coefficient vectors), and the "minimum" component which will not be cancelled, $g^*_{i,k}$. The part of the primary source disturbance which will be cancelled can be further partitioned into components "assigned" to each control source, $g_{i,j,k}$. For some multi-channel systems, this analytical partitioning procedure will not produce a unique set of primary source components assigned to each control source because the placement of the control sources and error sensors in the structural / acoustic system will be non-orthogonal in terms of the system modes which can be excited and sensed. The final combination actually arrived at by the adaptive control system is dependent upon the optimization procedure used (this point will be discussed later in this chapter). However, for the purposes of the analysis, it is sufficient to say that, for the given optimization procedure, the component assigned to each control source is equivalent in amplitude, and opposite in phase, to the control signal sensed at each microphone if, under final optimized conditions, the primary source and all other control sources were switched off. Thus, the measured primary source disturbance provided by the i^{th} error sensor can be represented as:

$$g_{i,k} = \sum_{j=1}^{I} g_{i,j,k} + g^*_{i,k} \qquad (8.35)$$

where:

$$g_{i,j,k} = - F^T_{i,j,k} W^*_j \qquad (8.36)$$

It should be noted that g^* will only be equal to zero for all error sensors if the number of non-redundant control sources is equal to the number of non-redundant error sensors.

Substituting equations (8.35) and (8.36) into equation (8.34) produces:

$$W_{j,k+1} = W_{j,k} - 2\mu \sum_{i=1}^{m} F_{i,j,k} \left[g^{*}_{i,k} + \sum_{q=1}^{l} (g_{i,q,k} + F^{T}_{i,q,k} W_{q,k-n}) \right]$$

$$= W_{j,k} - 2\mu \sum_{i=1}^{m} \left(F_{i,j,k} \sum_{q=1}^{l} F^{T}_{i,q,k} (W_{q,k-n} - W^{*}_{q}) + F_{i,j,k} g^{*}_{i,k} \right) \qquad (8.37)$$

The weight "variance" vector is defined as the vector of signed weight coefficient deviations from their optimum values (Horowitz and Senne, 1981; Gardner, 1984; Widrow and Stearns, 1985):

$$V_{j,k} = W_{j,k} - W^{*}_{j} \qquad (8.38)$$

Equation (8.37) can be re-expressed in terms of this quantity as:

$$V_{j,k+1} = V_{j,k} - 2\mu \sum_{i=1}^{m} \left(F_{i,j,k} \sum_{q=1}^{l} F^{T}_{i,q,k} V_{q,k-n} + F_{i,j,k} g^{*}_{i,k} \right) \qquad (8.39)$$

Using the same transformation operation as in equation (8.37) to define the projected weight variance vector:

$$\tilde{V}_{j/q,k-n} = T_{i,j/q} V_{q,k-n} \qquad (8.40)$$

enables equation (8.39) to be expressed as:

$$V_{j,k+1} = V_{j,k} - 2\mu \sum_{i=1}^{m} \left(R_{k-n} \sum_{q=1}^{l} \tilde{V}_{j/q,k-n} + C^{*}_{i,j,k} \right) \qquad (8.41)$$

where $C^{*}_{i,j,k}$ is the cross correlation matrix between the filtered input signal between the ith error sensor and the jth weight coefficient vector and that part of the primary source signal detected by the ith error sensor which will not be cancelled under optimal conditions:

$$C^{*}_{i,j,k} = F_{i,j,k}\, g^{*}_{i,k} \tag{8.42}$$

To examine the convergence behaviour of equation (8.41), which will govern the convergence behaviour (hence stability) of the algorithm, the equation must first be decoupled. As R is a symmetric matrix, this can be accomplished by using an orthonormal transform:

$$R = Q\,\Lambda\,Q^{-1} = Q\,\Lambda\,Q^{T} \tag{8.43}$$

where Λ is the diagonal matrix of eigenvalues of R, and Q is the eigenvector matrix (column vector of eigenvectors). Premultiplying equation (8.41) by Q^{-1} produces:

$$V'_{i,j,k+1} = V'_{i,j,k} - 2\mu \sum_{i=1}^{m} \left(\Lambda_{k-n} \sum_{q=1}^{l} \tilde{V}'_{j/q,k-n} + C^{*\prime}_{i,j,k} \right)$$

$$= V'_{i,j,k} - 2\mu \sum_{i=1}^{m} \left(\Lambda_{k-n} \sum_{q=1}^{l} \tilde{V}'_{j/q,k-n} \right) \tag{8.44}$$

where

$$V' = Q^{-1}\, V \tag{8.45}$$

Note that in equation (8.44) the orthonormal projection has mapped $C^{*}_{i,j,k}$ into the nullspace. This is because that "minimum" part of the primary source signal which is uncontrolled when all of the weight coefficient vectors are optimized is orthogonal to the input reference signal. Physically, this implies that the optimum (final) value of sound attenuation achieved does not have any influence upon the stability of the algorithm. This has been found to be the case in both simulation and in practice.

As equation (8.44) is decoupled, it can be viewed as a set of scalar equations. For algorithm stability to be maintained, the sum of the m scalar equations for any given transformed weight coefficient variance, v'_j, of V'_j, must converge to some finite value over time. Therefore, for the r^{th} scalar equation,

$$\left| \sum_{i=1}^{m} \frac{v'_{r,i,j,k+1}}{v'_{r,i,j,k}} \right| < 1 \qquad (8.46)$$

From equation (8.44), this sets a bounds on the convergence coefficient, μ, of:

$$0 < \mu_{r,j} < \sum_{i=1}^{m} \left(\lambda_{r,k-n} \sum_{q=1}^{I} \frac{\tilde{v}'_{r,j/q,k-n}}{v'_{r,i,j,k}} \right)^{-1} \qquad (8.47)$$

where $\lambda_{r,k-n}$ is the eigenvalue of the scalar equation of interest.

8.3.1. Effect of continuous updating of weight coefficient vector

The bounds placed on the convergence coefficient, μ, given in equation (8.47) were derived with the assumption that the weight coefficient vectors were adjusted only after the results of the previous adjustment were known; hence, the algorithm was not continuously adapting. In this case, the explicit effect of the acoustic time delay can be ignored (for a stationary, or nearly so, system). However, the time delay between the j^{th} control actuator (the one of interest) and the error sensors will have an influence upon these bounds of stability for the continuously updating case. This is because the j^{th} weight variance vector of n samples ago, upon which the adjustment is based, differs from the present variance vector. The effect which this has will manifest itself in the self-variance part of equation (8.44), which is:

$$v'_{r,i,j,k+1} = v'_{r,i,j,k} - 2\mu\,\lambda_{r,k-n}\,v'_{r,j/j,k-n}$$

$$= v'_{r,i,j,k} - 2\mu\,\lambda_{r,k-n}\,v'_{r,i,j,k-n} \qquad (8.48)$$

Taking the z-transform of equation (8.48) produces (Kabal, 1983):

$$v'_{r,i,j}(z) = \frac{z^{(n+1)}\,v'_{r,i,j}(0)}{z^{(n+1)} - z^{n} + 2\mu\,\lambda_{r,k-n}} \qquad (8.49)$$

For the algorithm to be stable, the poles of equation (8.49) (determined by the roots of the characteristic equation) must lie within the unit circle.

The values of the convergence coefficient for which the characteristic equation has roots on the unit circle can be found by substituting $e^{i\phi}$ for z, and setting the denominator on the right side of the equation equal to zero:

$$2\mu\,\lambda_{r,k-n} = e^{i(n\phi)} - e^{i(n+1)\phi} \qquad (8.50)$$

As R is symmetric, it will have real eigenvalues. Therefore, equating the real and imaginary parts of equation (8.50) gives:

$$2\mu\,\lambda_{r,k-n} = \cos(n\phi) - \cos((n+1)\phi) \qquad (8.51)$$

$$0 = \sin(n\phi) - \sin((n+1)\phi) \qquad (8.52)$$

From equation (8.52):

$$\phi = \frac{\pi}{(2n+1)} \qquad (8.53)$$

Substituting this value of ϕ into equation (8.51) produces:

$$2\mu\,\lambda_{r,k-n} = 2\,\sin\left[\frac{\pi}{2(2n+1)}\right] \qquad (8.54)$$

Therefore, for convergence (Kabal, 1983):

$$\mu_{max} < \lambda_{max}^{-1} \sin\left[\frac{\pi}{2(2n+1)} \right] \qquad (8.55)$$

The overall bounds placed on the convergence coefficient for system stability for the case of continuously updating the weight coefficient vector can be found by combining equations (8.47) and (8.55):

$$0 < \mu_{r,j} < \left(\sum_{i=1}^{m} \lambda_{r,k-n} \sum_{q=1}^{\imath} \frac{\tilde{v}'_{r,j/q,k-n}}{v'_{r,i,j,k}} \right)^{-1} \sin\left[\frac{\pi}{2(2n+1)} \right] \qquad (8.56)$$

This can be compared to the commonly stated bounds placed on the convergence coefficient for the "standard" LMS algorithm analysed under similar "ideal" mean-value assumptions (using expected values, E[], of the variables) (Widrow and Stearns, 1985):

$$0 < \mu_{max} < \frac{1}{\lambda_{max}} \qquad (8.57)$$

8.4. EFFECT OF SYSTEM PARAMETERS UPON ALGORITHM STABILITY

There are several characteristics of the multiple input, multiple output LMS algorithm that become clear on examination of the bounds (given in equation (8.56)) placed on the convergence coefficient, μ, for system stability. The first is the extent to which the convergence behaviour of the $\imath$ weight coefficient vectors is coupled. There is a term in equation (8.56) which appears as the sum of the ratios of the variances of the j^{th} weight coefficient of interest to the other corresponding orthonormal transformed weight coefficients in the system. Each of these weight coefficient variances forms the basis for a different vector

space. As described previously, the transformation of equation (8.40) provides a measure of the independence of these vector spaces. If, at one extreme, all of the transfer functions between each control source and the i^{th} error microphone were orthogonal, then all of the transformed ratios (using equation (8.40)) would be equal to zero, except for the j^{th} variance of interest, and the system stability would be enhanced. At the other extreme, if all of the vector spaces laid on top of each other, then from equation (8.40) the transformed variance ratio would be equal to the "raw" variance ratio, and the maximum stable value of the convergence coefficient would be reduced. This conclusion, that orthogonality of control source placement in terms of the structural / acoustic modal response has an effect on the maximum allowable convergence coefficient for system stability, would seem intuitively obvious; that it is predicted explicitly by the algorithm stability bounds is therefore not surprising.

Continuing with this same line of thought, there is another aspect of the transformed weight vector variance ratio terms which must be taken into account in system design. In a system with many control sources and error sensors, where convergence time is not of major concern, it may be tempting to update the weight coefficient vectors on a "round robin" basis, one weight coefficient vector at a time, to save hardware costs. As was discussed previously in this article, if the control source placement is non-orthogonal in terms of the structural / acoustic system modes which can be excited, there may not be a unique set of optimum weight coefficient vectors. If all of the weight coefficient vectors are adjusted simultaneously, the algorithm will inherently try to find a solution which requires the least amount of overall weight coefficient adjustment from the initial values. In doing this, it tends to divide up the overlapping parts of the primary source disturbance which can be "cancelled" by a number of control sources. However, if one control source is adjusted at a time, the algorithm tries to adjust the first weight

coefficient vector to control all of the primary source disturbance which it possibly can before beginning to adjust the next weight coefficient vector; that is, there is no division of the overlapping parts of the primary source components, but rather an "all or nothing" solution.

This has two implications for active control system design. The first is concerned with control effort. Clearly, updating a multi-channel control system on a round robin basis could easily result in one control source being overdriven while others are hardly driven at all. Thus, in this case control effort would need to be included in the criteria used to decide when a control source is adjusted sufficiently, and the algorithm begins to adjust the next control source in the round robin, so that no control sources are overdriven.

The second implication is concerned with algorithm stability. Considering the bounds placed on the convergence coefficient for algorithm stability given in equation (8.56), the variance ratio can be written as:

$$\left(\sum_{j=1}^{I} \frac{\tilde{v}'_{j/q,k-n}}{v'_{j,k}} \right)^{-1} = \left(\frac{\tilde{v}'_{j/j,k-n}}{v'_{j,k}} + \sum_{j=1,\neq q}^{I} \frac{\tilde{v}_{j/q,k-n}}{v'_{j,k}} \right)^{-1} \qquad (8.58)$$

The first term on the right hand side of equation (8.58) will be approximately the same, regardless of whether one or all weight coefficient vectors are adapted at the same time. The second term, however, will differ. This is because if the overlapping parts of the primary source components are not divided up, the final (optimized) output of the control sources which are updated later in the round robin procedure will have a reduced output (from the all or nothing primary source component division) compared to the output they would have if all weight coefficient vectors are updated simultaneously (dividing up the overlapping primary source

components). Thus, if the initial weight coefficients are all set to a value of zero (as is commonly done), the weight coefficient vector variances adapted later in the round robin will be reduced. From equation (8.56) this will enhance system stability.

To test these ideas, a two control source, two error sensor system was computer simulated. The transfer functions between a given control source and each error sensor were set equal, with the transfer function variable between the two control sources. The primary disturbance was a single frequency sinusoid, and the transfer functions were pure phase shifts, with no amplitude gain. For a given system arrangement, the convergence coefficient was increased in amplitude until the system was marginally stable.

Figure 8.3 illustrates the maximum stable value of convergence coefficient for both the simultaneous adaption and round robin adaption strategies, plotted against the phase difference between the control sources transfer function sets. In viewing these results, it is clear that the transfer function phase difference does have a significant influence upon the system stability. Further, the round robin adaption strategy is more stable than the simultaneous adaption strategy. Also, it was found that for any given system arrangement, the final (converged) value of mean square error was the same for the simultaneous and round robin adaption strategies, but the final weight coefficient values would differ by up to four orders of magnitude between the optimization strategies, illustrating the need in a practical system for inclusion of some measure of control effort in the optimization procedure.

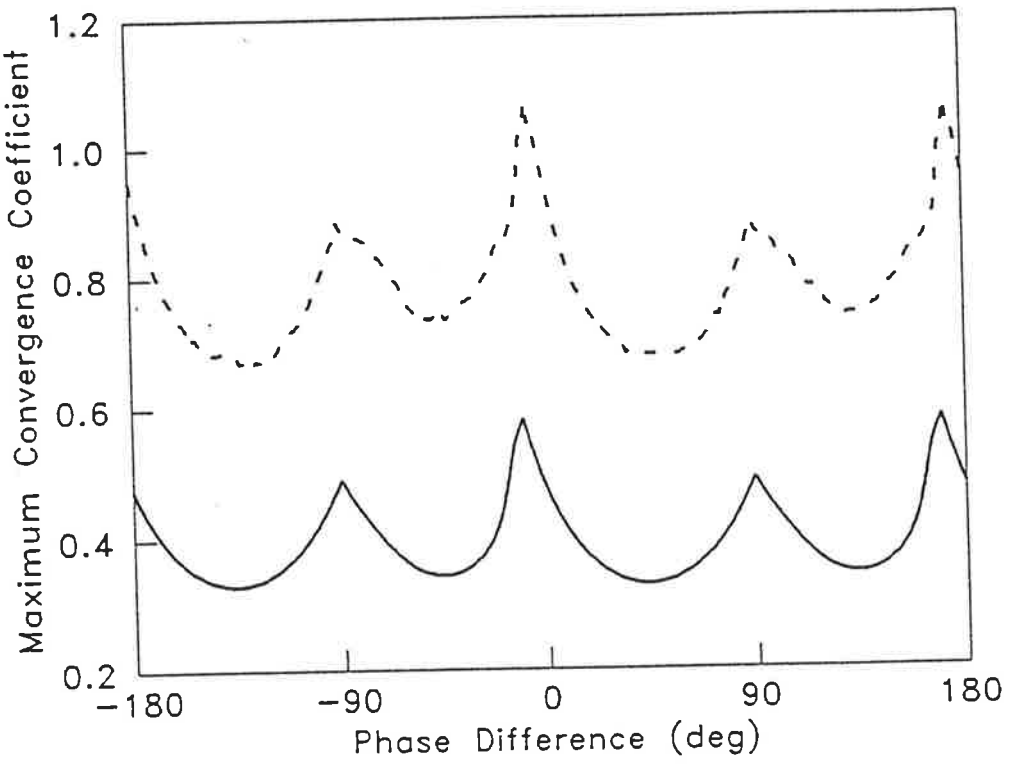

Figure 8.3. Maximum stable value of convergence coefficient for a two control source, two error sensor system where the transfer functions between a given control source and each error microphone are equal, plotted against the phase difference between the control source transfer function sets, —— = simultaneous weight coefficient vector updating, - - - = round robin weight coefficient vector updating.

The next item to note is that increasing the number of error sensors will tend to decrease the maximum stable value of convergence coefficient. This effect, which will be weighted by a multiplying factor proportional to the magnitude of the transfer function between the control source(s) and additional error sensor, can be seen explicitly in figure 8.4, which depicts the maximum stable value of convergence coefficient, μ, for a single control source system plotted against the number of error sensors. To obtain these data, a computer simulation of a single

control source system was conducted. For a given number of error sensors, the algorithm convergence coefficient was increased until the system was marginally stable. The transfer functions between the control source and each error sensor were made the same, to avoid any additional effects. Under these circumstances, equation (8.56) predicts that the maximum stable value of convergence coefficient would decrease proportionally with increasing numbers of error sensors, a fact which is borne out in figure 8.4.

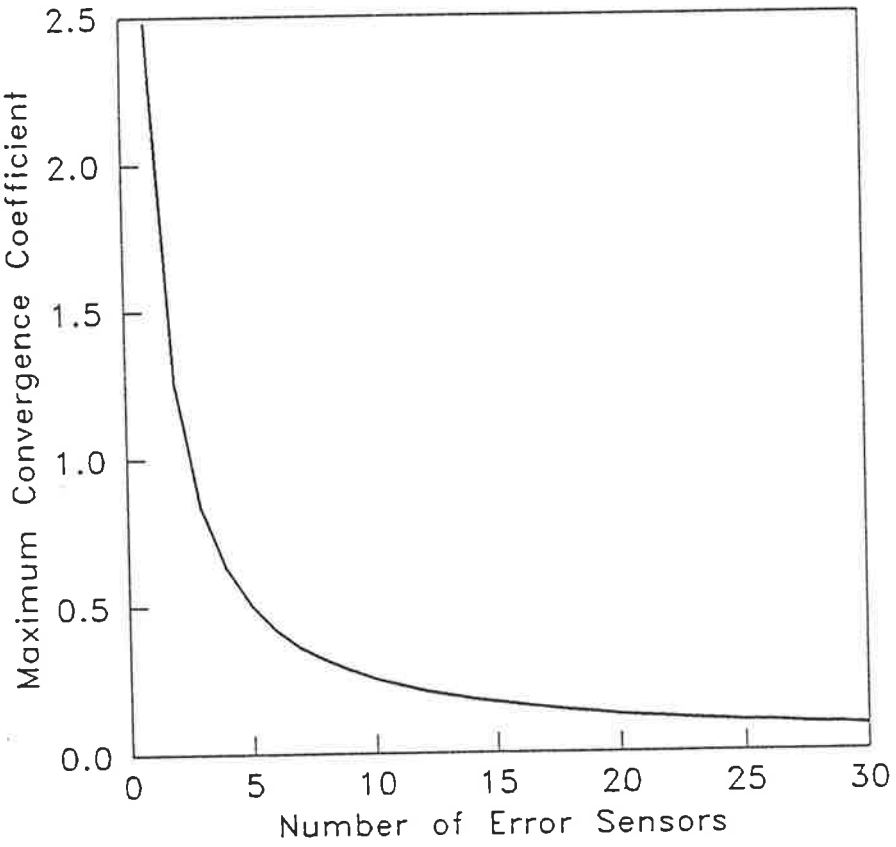

Figure 8.4. Maximum stable value of convergence coefficient for a single control source system as a function of the number of error sensors.

Consider next the effect of increasing the magnitude of the transfer function(s) between the control source(s) and error sensor(s). From equation (8.40), it can be deduced that as the magnitudes are increased, the values of $\tilde{\mathbf{v}}$ are increased proportionally squared. From equation (8.56) it can be seen that the convergence coefficient should therefore be decreased proportionally squared. This point was previously considered in chapter 7, and illustrated in computer simulation in figure 7.3.

The final effect of interest is that which the acoustic time delay has upon the bounds of stability for the continuously adapting system. This effect appears explicitly in the sin() term in equation (8.56). However, it also appears implicitly in the variance ratio terms, as the ratio is is between the present variance of the (transformed) weight coefficient of interest with the past variance of all corresponding (transformed) weight coefficients. This is identical to the single input, single output filtered-x LMS algorithm, for which the implications were dicussed in chapter 7, and illustrated in figure 7.4.

8.5. SUMMARY

The inherent acoustic time delays and the electro/acoustic transfer functions of the control sources and error sensors, as well as the response of the acoustic or coupled structural/acoustic system, must be taken into account when implementing the multiple actuator, multiple error sensor LMS algorithm in an active noise control system. Estimates of these quantities must be included in any practical control system.

The control source weight coefficient vectors are coupled through the non-orthogonal nature of the structural / acoustic system. For orthogonal control source placement (in terms of the structural / acoustic system modal response), the marginally stable value of convergence coefficient is maximized. In this case the stability is the same whether round robin weight coefficient vector adaption or continuous adaption is used. Deviations from this ideal arrangement will reduce this maximum stable value.

For the (common) non-orthogonal control source placement, round robin weight coefficient vector adaption is more stable than simultaneous weight coefficient vector adaption. It is, however, generally slower to reach a final solution and may lead to control effort problems, such as overdriving of one control source while others are barely driven.

Increasing the number of error sensors used in the system decreases the maximum stable value of convergence coefficient. So too does increasing the magnitude of the transfer functions between the control source(s) and error sensor(s). The effect of the time delay on the maximum allowable convergence coefficient used in the filtered-x LMS algorithm is implementation dependent. For the non-continuously updating case (where the weights are updated only after the result from the previous update has been received from the error sensor) there is no effect (provided the system is time invariant or only slowly varying). For the continuously updating case (where the weights are updated at every sample), the maximum allowable convergence coefficient is limited to a reduction by a factor of $\sin[\pi/(2(2n+1))]$, where n is the number of samples corresponding to the acoustic time delay between the control source of interest and the error sensors (assuming that the acoustic time delays between the control source and each error

sensor is the same). However, for sinusoidal excitation, areas of enhanced stability can occur at delays equal to half or quarter wavelength intervals of the propagating disturbance.

CHAPTER 9.
GENERAL SUMMARY

The goals of this thesis were to identify the control mechanisms employed in a feedforward active noise control system, to provide general analytical models to aid in the design of active noise control systems, and in the process, to quantify the influence of common system parameters upon system performance. This chapter provides a brief summary of the results relating to these goals.

The mechanisms employed by feedforward active noise control systems were all found to be impedance altering effects, as would have been expected by the nature of feedforward control. (It is well known (see, for example, Franklin, Powell, and Workman, 1990) that feedforward systems alter the dynamic response of a system by introducing zeroes into the transfer function, thereby effectively altering the impedance of the system. This is in contrast to the nature of feedback control systems, in which the poles of the dynamic system are altered, changing the characteristic system eigenvalues and eigenvectors, and hence the transient response characteristics.) In chapter 2 it was shown, both analytically and experimentally, that acoustic sources actively controlling plane wave sound propagation in an air handling ducts do so by altering the radiation impedance "seen" by the sound sources, causing them to radiate less power, or in some cases absorb power. In chapter 4 it was shown, both analytically and experimentally, that vibration sources used to actively control sound radiation into free space achieve the desired result in two possible ways. Firstly, they can reduce the amplitude(s) of the primary radiating structural mode(s) (effectively increasing the structural input impedance seen

by the primary disturbance). Secondly, they alter the relative amplitudes and phases of the dominant structural modes in such a way that the total radiated sound pressure (which is the sum of contributions from all the radiating modes) is reduced (effectively reducing the overall radiation impedance seen by the structure). In chapter 5 it was seen that this second mechanism, modal rearrangement, is more complicated for the problem of controlling sound transmission into a coupled enclosure. This complication arises from the modal coupling characteristics of the structural / acoustic system, where it is not possible for all modes to globally interact. Still, the two vibration source control mechanisms apply.

The design of active noise control systems was considered in two separate sections; the design of the physical control system, comprising the arrangement of the actuators and error sensors, and the design of the electronic control system. The design of both of these must be optimized if the total active noise control system is to perform to its fullest potential. The design of the physical control system sets the absolute bounds on the levels of sound attenuation which can be achieved with an ideal electronic controller, while the design of the electronic control system determines how close to the absolute bounds the actual sound attenuation is.

In considering the design of the physical control system it was not found possible to the placement of the control sources and error sensors directly and analytically. This is because sound power attenuation is not a linear function of control source location, and because the optimum error sensor location is a function of the control source placement. It was, however, possible to determine the optimum control source volume velocities or forces for a given actuator arrangement using quadratic optimization theory. For a simple single mode problem

such as controlling plane wave sound propagation in an air handling duct it was then feasible to implement this in a numerical search routine to optimally place the control source. (It should be noted that for the single mode case it was found to be theoretically possible to completely suppress acoustic power output at any control source location; however, the control source volume velocity required to do so varied greatly. This control effort should therefore be a quantity of interest in the numerical search routine, with the optimization error criterion assuming the from of an optimal control problem.)

For multi-modal cases, however, it was impractical to directly implement the quadratic optimization routines in a numerical search procedure owing to the computational requirements. Therefore, a "shortcut" method of determining the optimum control source volume velocities or forces was formulated using standard multiple regression routines. This had the added benefit of determining the optimum error sensor locations as part of the procedure, which were shown to be at the locations of maximum sound pressure reduction in the residual sound field obtained by theoretically optimizing the control sources to minimize the radiated acoustic power.

In addition to control source and error sensor location, other physical and geometric system variables were shown to have a significant influence upon the levels of active attenuation which could be achieved, and upon the mechanisms employed in achieving it. These variables include radiating structure size relative to the frequency of interest, structural modal density and damping, and the characteristics of the primary excitation. For acoustic control, sources the distance from the primary radiating source, and the size of the control source, were also found to be important (with an increase in either of these quantities proving detrimental). Also, it was

shown that large levels of acoustic pressure attenuation at the error sensing locations do not necessarily lead to large levels of acoustic power attenuation, and conversely extreme levels of acoustic pressure attenuation at the error sensing location are not necessarily required to achieve the maximum possible levels of acoustic power attenuation.

For the electronic control system, it was shown that the inherent acoustic time delays and the electro/acoustic transfer functions of the control sources and error sensors, as well as the response of the acoustic or coupled structural/acoustic system, must be taken into account when implementing the LMS algorithm in either single channel or multi-channel systems. In general it was found that increasing the number of error sensors used in the system decreased the maximum stable value of the convergence coefficient. So too did increasing the magnitude of the transfer functions between the control source(s) and error sensor(s). The effect of the time delay on the maximum allowable convergence coefficient used in the filtered-x LMS algorithm was implementation dependent. For the non-continuously updating case (where the weights are updated only after the result from the previous update has been received from the error sensor) there was no effect (provided the system is time invariant or only slowly varying). For the continuously updating case (where the weights are updated at every sample), the maximum allowable convergence coefficient was reduced by a factor of $\sin[\pi/(2(2n+1))]$, where n is the number of samples corresponding to the acoustic time delay between the control source of interest and the error sensors (assuming that the acoustic time delays between the control source and each error sensor is the same). However, for sinusoidal excitation, areas of enhanced stability can occur at delays equal to half or quarter wavelength intervals of the propagating disturbance. Despite this required smaller convergence coefficient, the difference in

convergence speed between the continuously and non-continuously updating cases was found to be minimal.

For the multi-channel implementation of the LMS algorithm, the control source weight coefficient vectors were found to be coupled through the non-orthogonal nature of the structural / acoustic system. For orthogonal control source placement (in terms of the structural / acoustic system modal response), the marginally stable value of convergence coefficient was maximized. In this case the stability was the same whether round robin weight coefficient vector adaption or continuous adaption is used. Deviations from this ideal arrangement reduced this maximum stable value.

For the (common) non-orthogonal control source placement, round robin weight coefficient vector adaption was found to be more stable than simultaneous weight coefficient vector adaption. It was, however, generally slower to reach a final solution and may lead to control effort problems, such as overdriving of one control source while others are barely driven.

APPENDIX 1.

DERIVATION OF EQUATION 3.25

As stated in Chapter 3, equation (3.24), the pressure $p_i(\vec{x}')$ at the inner surface of a weakly coupled enclosure can be expressed in terms of the *in vacuo* structural mode shape functions according to:

$$p_i(\vec{x}') = \sum_{j=1}^{\infty} m(\vec{x}')\, \dot{v}_j\, \psi_j(\vec{x}') \qquad (A.1.1)$$

Substituting this into equation (3.19), and expanding the velocity at $\vec{x}$ in terms of the complex structural modal velocity amplitudes, v_j, produces the following equation:

$$\sum_{j=1}^{\infty} m(\vec{x}')\, \dot{v}_j\, \psi_j(\vec{x}') + i(\rho_o c_o)^2 \omega \sum_{j=1}^{\infty} \left[\int_A G_a(\vec{x}|\vec{x}')\, \psi_j(\vec{x})\, d\vec{x} \right] v_j = 0 \qquad (A.1.2)$$

Multiplying equation (A.1.2) by the rth structural mode shape, $\psi_r(x')$, integrating over the surface of the structure and using the modal orthogonality property, results in:

$$\dot{v}_r M_r + i(\rho_o c_o)^2 \omega \sum_{j=1}^{\infty} \left\{ \int_A \psi_r(\vec{x}') \cdot \left[\int_A G_a(\vec{x}|\vec{x}')\, \psi_j(\vec{x})\, d\vec{x} \right] d\vec{x}' \right\} v_j = 0 \qquad (A.1.3)$$

Similarly, equation (3.18) can be expanded in terms of the structural mode shapes (using equation (3.6) and equation (3.19)):

$$\sum_{j=1}^{\infty} v_j \psi_j(\vec{x}) = i\omega \left\{ \int_A G_s(\vec{x}|\vec{x}') \, p_e(\vec{x}') \, d\vec{x}' - \int_A G_s(\vec{x}|\vec{x}') \left[\sum_{j=1}^{\infty} m(\vec{x}') \, \dot{v}_j \, \psi_j(\vec{x}') \right] d\vec{x}' \right\} \qquad (A.1.4)$$

Expanding the Green's function into its components (using equation (3.6)) and using the orthogonality property of the modes, the second integral on the right hand side of equation (A.1.4) can be rewritten as:

$$\int_A G_s(\vec{x}|\vec{x}') \left\{ \sum_{j=1}^{\infty} m(\vec{x}') \, \dot{v}_j \, \psi_j(\vec{x}') \right\} d\vec{x}' = \sum_{j=1}^{\infty} \frac{\dot{v}_j \psi_j(\vec{x})}{Z_j} \qquad (A.1.5)$$

Therefore, equation (A.1.4) can be restated as:

$$\sum_{j=1}^{\infty} v_j \psi_j(\vec{x}) + i\omega \sum_{j=1}^{\infty} \frac{\dot{v}_j \psi_j(\vec{x})}{Z_j} = i\omega \int_A G_s(\vec{x}|\vec{x}') \, p_e(\vec{x}') \, d\vec{x}' \qquad (A.1.6)$$

Multiplying equation (A.1.6) through by the surface density and the rth mode shape, $m(\vec{x})\psi_r(\vec{x})$, and integrating over the surface of the structure results in:

$$v_r M_r + i\omega \frac{\dot{v}_r M_r}{Z_r} = i\omega \int_A m(\vec{x}) \, \psi_r(\vec{x}) \left\{ \int_A G_s(\vec{x}|\vec{x}') \, p_e(\vec{x}') \, d\vec{x}' \right\} d\vec{x} \qquad (A.1.7)$$

By expanding the Green's function, the right hand side of equation (A.1.7) can be rewritten as:

$$i\omega \int_A m(\vec{x})\ \psi_r(\vec{x}) \left\{ \int_A G_s(\vec{x}|\vec{x}')\ p_e(\vec{x}')\ d\vec{x}' \right\}$$

$$= i\omega \int_A m(\vec{x})\ \psi_r(\vec{x}) \sum_{j=1}^{\infty} \frac{\psi_j(\vec{x})}{M_j Z_j} \left\{ \int_A p_e(\vec{x}')\ \psi_j(\vec{x}')\ d\vec{x}' \right\} d\vec{x} \qquad (A.1.8)$$

$$= i\omega \sum_{j=1}^{\infty} \left\{ \int_A p_e(\vec{x}')\ \psi_j(\vec{x}')\ d\vec{x}' \right\} \left\{ \frac{1}{M_j Z_j} \int_A m(\vec{x})\ \psi_r(\vec{x})\ \psi_j(\vec{x})\ d\vec{x} \right\} \qquad (A.1.9)$$

Thus, using modal orthogonality, for the rth structural mode gives:

$$v_r M_r + i\omega \frac{\dot{v}_r M_r}{Z_r} = i\omega \frac{\gamma_r}{Z_r} \qquad (A.1.10)$$

where γ_r is the rth modal generalized force, as defined by equation (3.12). The pressure on the surface of the structure has been expanded in terms of the structural mode shapes resulting in the following expression for the rth structural mode shape:

$$\dot{v}_r = \frac{\gamma_r}{M_r} + i\frac{v_r Z_r}{\omega} \qquad (A.1.11)$$

Equation (A.1.11) can be substituted into equation (A.1.3) to express the latter in terms of the external pressure distribution. Thus, for the rth structural mode:

$$\left\{ i(\rho_o c_o)^2 \omega \int_S \psi_r(\vec{x}') \left\{ \int_S G_a(\vec{x}|\vec{x}')\ \psi_r(\vec{x})\ d\vec{x} \right\} d\vec{x}' + \frac{iM_r Z_r}{\omega} \right\} v_r$$

$$+ \sum_{j=1,\neq r}^{\infty} \left\{ i(\rho_o c_o)^2 \omega \int_S \psi_r(\vec{x}') \left\{ \int_S G_a(\vec{x}|\vec{x}')\ \psi_j(\vec{x})\ d\vec{x} \right\} d\vec{x}' \right\} v_j = -\gamma_r \qquad (A.1.12)$$

The Green's function for the interior space can be expanded using equation (3.20) to produce for the rth structural mode:

$$\left\{ i(\rho_o c_o)^2 \omega \left\{ \sum_{l=1}^{\infty} \frac{1}{M_l Z_l} \int_S \psi_r(\vec{x}') \, \phi_l(\vec{x}') \left\{ \int_S \psi_r(\vec{x}) \, \phi_l(\vec{x}) \, d\vec{x} \right\} d\vec{x}' \right\} \right.$$

$$\left. + \frac{iM_r Z_r}{\omega} \right\} v_r \; +$$

$$\sum_{j=1, \neq r}^{\infty} i(\rho_o c_o)^2 \omega \left\{ \sum_{l=1}^{\infty} \frac{1}{M_l Y_l} \int_S \psi_r(\vec{x}') \, \phi_l(\vec{x}') \left\{ \int_S \psi_j(\vec{x}) \, \phi_l(\vec{x}) \, d\vec{x} \right\} d\vec{x}' \right\} v_j$$

$$= -\gamma_r \qquad \text{(A.1.13)}$$

where

$$Z_l = (\kappa_l^2 - k^2) c_o^2 \qquad \text{(A.1.14)}$$

Equation (A.1.13) can be restated as:

$$\left\{ i (\rho_o c_o)^2 S^2 \omega \left\{ \sum_{l=1}^{\infty} \frac{B_{l,r} B_{l,r}}{M_l Z_l} \right\} + i \frac{M_r Z_r}{\omega} \right\} v_r \; +$$

$$\sum_{j=1, \neq r}^{\infty} i (\rho_o c_o)^2 S^2 \omega \left\{ \sum_{l=1}^{\infty} \frac{B_{l,r} B_{l,j}}{M_l Z_l} \right\} v_j = -\gamma_{r,p}$$

(A.1.15)

which is equation (3.25).

APPENDIX 2.

IMPLEMENTATION OF THE LMS ALGORITHM IN A TRANSPUTER BASED MULTIPLE INPUT, MULTIPLE OUTPUT ACTIVE NOISE CONTROL SYSTEM

Part of the reason that active noise control has become an increasingly popular field of research is that parallel advances in microprocessor technology have allowed adaptive systems to be implemented efficiently and effectively. Adaptive systems provide the flexibility required for the practical application of active noise control, as slight changes in ambient conditions would render a non-adaptive system ineffective after a period of time. One microprocessor that would appear well suited to the implementation of multiple error microphone, multiple secondary source active noise control systems is the Transputer. The architecture of the Transputer is designed for parallel processing, complementing the multi-tasking nature of practical active noise control systems. Also, communications between microprocessors is straightforward, making it ideal for large (distributed) systems. The following appendix provides a brief overview of the implementation of the LMS algorithm in a Transputer based adaptive active noise control system.

As outlined in chapters 7 and 8, the updating of the jth weight coefficient vector requires a version of the input signal, X, which has been convolved with the appropriate control source, error sensor, and structural / acoustic system transfer functions, as well as delayed by the

associated acoustic propagation time. A block diagram of one possible arrangement for updating the jth weight coefficient vector is shown in Figure A.2.1.

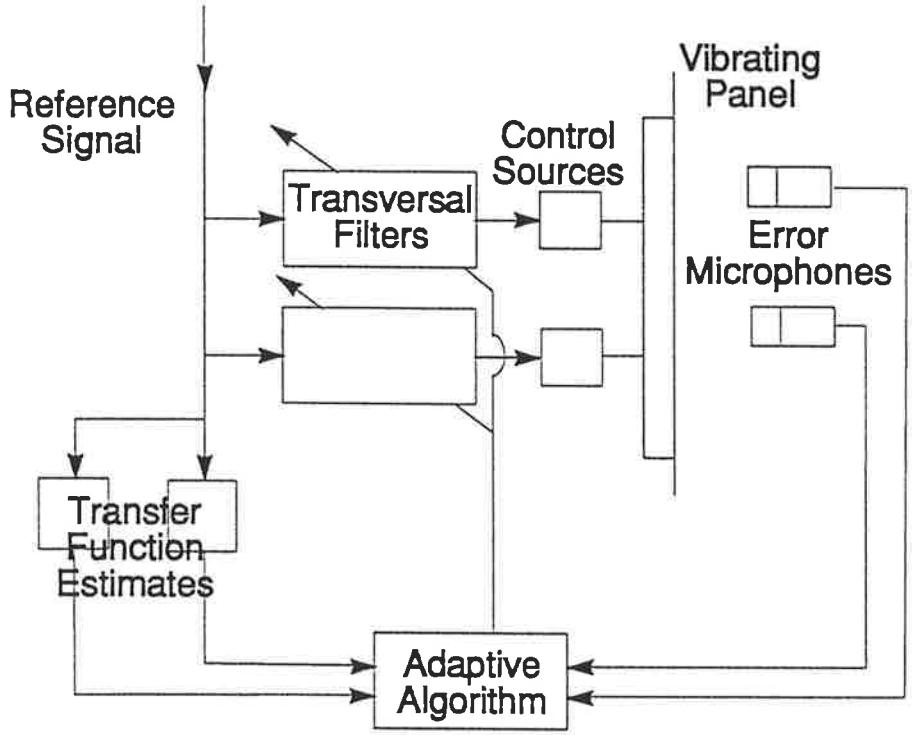

Figure A.2.1. Block diagram of the active noise control implementation of the multiple actuator, multiple error microphone LMS algorithm.

The active noise control version of the multiple input, multiple output LMS algorithm can be practically implemented in a transputer based system as shown in Figure A.2.2. In this case, one secondary source at a time has its weight coefficient vector updated in a "round robin" manner. As discussed in chapter 8, this arrangement will produce the optimum set of weight coefficient vectors, with a savings in hardware costs.

The primary components of the system shown in Figure A.2.2 are the T800 Transputer and the A100 signal processing chip, both made by Inmos. The T800 Transputer is a high speed microprocessor whose architecture is designed to allow parallel processing. This type of processor is needed to practically implement an active noise control system with many channels owing to the multi-tasking nature of the problem. The A100 signal processing chip is designed to be used with the transputer. It is a 32 point transversal filter, with an architecture that allows cascading of the chips if more tap points are required. This may be necessary for systems with only light acoustic damping (hence long reverberation, or impulse response, times).

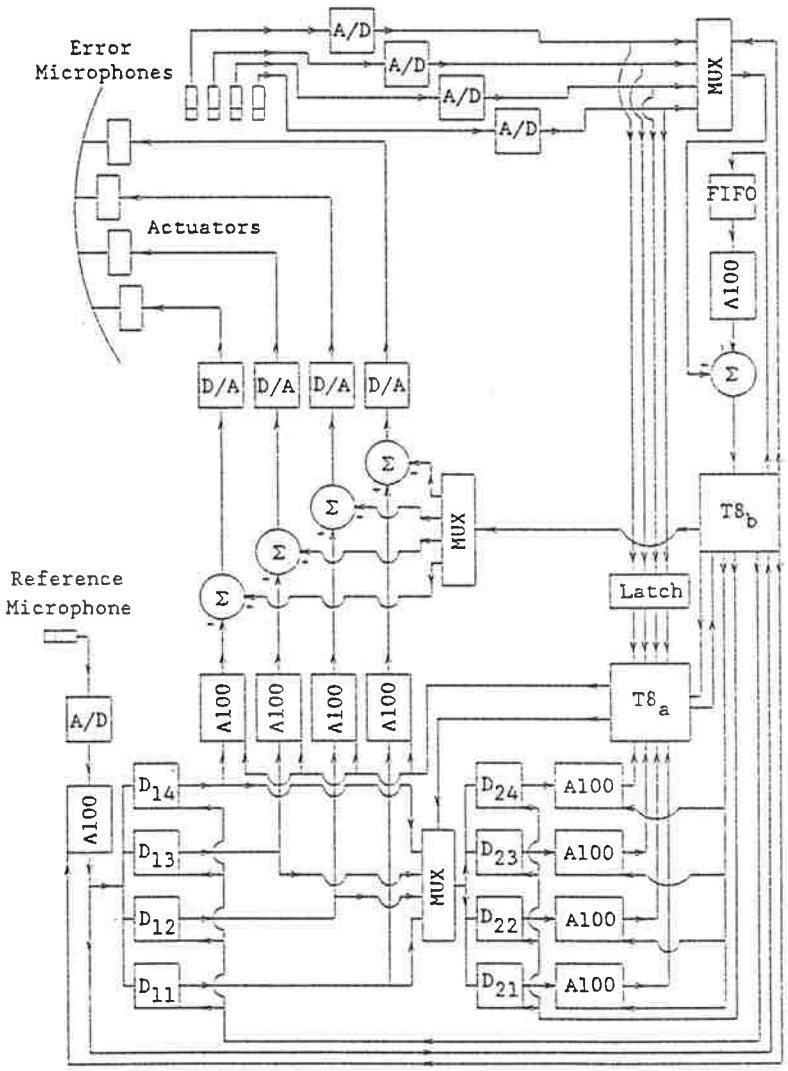

Figure A.2.2. Practical implementation of the multiple actuator, multiple error microphone algorithm in a Transputer based system.

The active control system can be roughly divided into three sections, corresponding to three tasks; the generation of the secondary source driving signals, estimation of the reference signal transducer transfer function(s), and the estimation of the error loop actuator and error microphone transfer functions and associated time delays. These sections will be described separately. (It should be noted that if the noise targetted for active control is completely periodic in nature, the part of the circuit concerned with estimating the reference signal transducer transfer function(s) may be omitted).

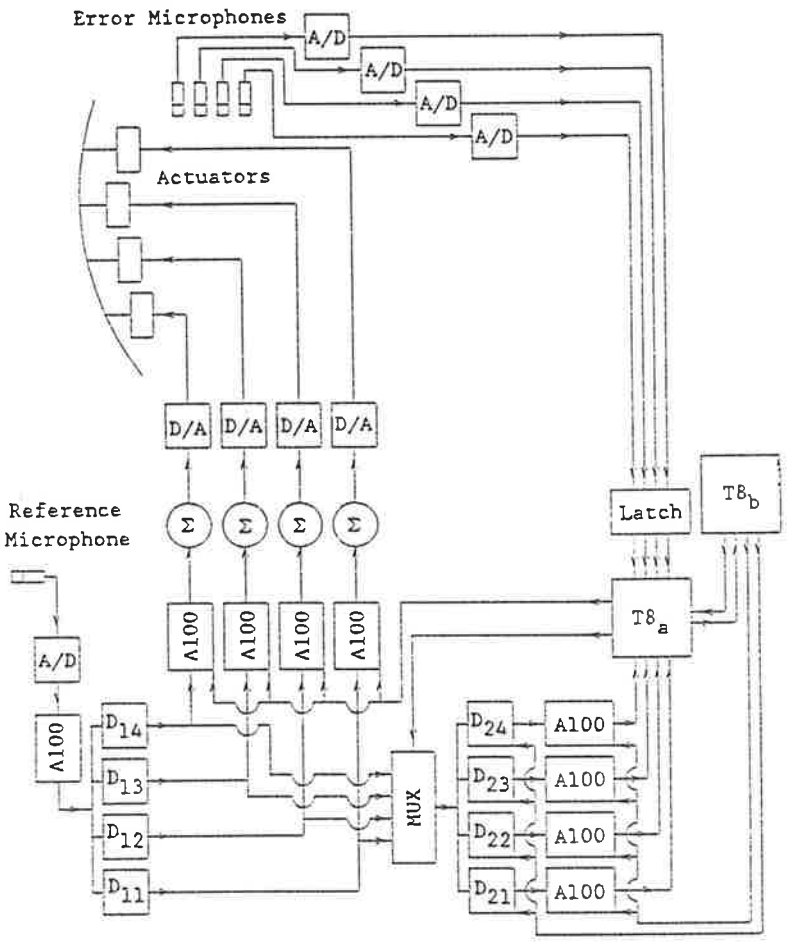

Figure A.2.3. Driving signal generation and modification section of the Transputer based system.

The section of the system concerned with generating and modifying the control actuator driving signals is shown in Figure A.2.3. The driving signals are provided by passing the reference signal through the A100 signal processing chips. Before reaching these, however, the reference signal is first conditioned via an A100 signal processing chip which models the inverse of the frequency response of the reference signal transducer, thereby providing a phase linear reference signal. Also, the reference signals are delayed in programmable FIFO buffers, which serve to "align" in the time domain the incoming acoustic disturbance (which is at least partially correlated with the reference signal) with the control source signals. This stage may not be necessary in systems where only periodic noise problems are targetted, but in systems where random noise is to be "absorbed" by the control sources (such as in a duct, where a correlated reference signal may be obtained), it is required.

As stated previously, the updating of the weight coefficient vectors is handled in a round robin manner. When it is time for the jth weight coefficient vector to be updated, T800A (the master) signals T800B (the slave) to load the estimates of the combined transfer functions and acoustic time delay between the jth actuator and each error microphone into a bank of A100 signal processing chips and programmable FIFO buffers. It also sets a multiplexer to allow the appropriately delayed reference signal to be fed into the A100's/FIFO's. The T800A then has access to the required "filtered" reference signals for weight coefficient vector adaption.

At the same time the T800A begins receiving the conditioned reference signals, it also begins sampling the error signals. This is accomplished using a latch to allow multiple error signals to be sampled simultaneously.

Once it is has the filtered reference and error signals, T800A can update and reload the jth weight coefficient vector. It will continue to do this until a specified minimum positive error change occurs (outlined in the next section), at which time it begins adjusting the next weight coefficient vector.

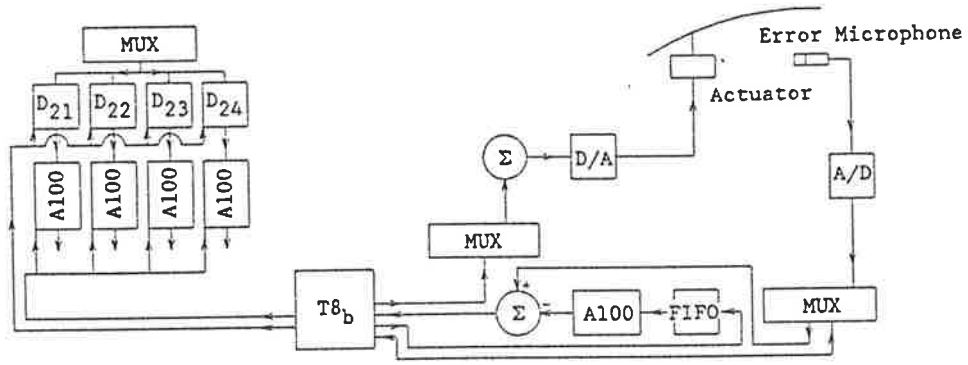

Figure A.2.4. Error loop transducer transfer function and acoustic time delay estimation section of the Transputer based system.

The functioning of the part of the system concerned with estimating the reference transducer transfer function(s) and associated time delay, and the error loop combined transfer functions and and associated time delays are similar, so only the error loop estimation section will be described here. An outline of this section of the system is shown in Figure A.2.4. The transputer T800B models each error loop using an A100 chip and programmable FIFO, then transfers these estimates to the bank of A100's/FIFO's to allow conditioning of the reference signal when requested by transputer T800A. To do this, T800B first sends a pulse or "chirp" out to an actuator, and measures the time taken (in samples) for it to be sensed. This value is used to set up the FIFO. The A100 can then be adapted using a standard LMS algorithm to model the combined error loop transfer functions. In theory, this must be done between each actuator and each error microphone. However, in a large system with sufficient acoustic damping, some control signals may not be observable by all error microphones. Hence, they may be omitted from consideration.

BIBLIOGRAPHY

Abler, S.B. and Silcox, R.J. (1987) "Experimental evaluation of active noise control in a thin cylindrical shell", *Proc. Noise-con 87*, 341-347.

Alexander, S.T. (1986) *Adaptive Signal Processing: Theory and Applications*, Springer-Verlag, New York.

Angevine, O.L. (1978) "Active acoustic attenuation of electric transformer noise", *Proc. Internoise 81*, 303-306.

Bendat, J.S. and Piersol, A.G. (1980) *Engineering Applications of Correlation and Spectral Analysis*, John Wiley, New York.

Beranek, L.L. (1986) *Acoustics*, Acoustical Society of America, New York.

Berengier, M. and Roure, A. (1980) "Broad-band active sound absorption in a duct carrying uniformly flowing fluid", *J. Sound Vib.*, **68**, 437-449.

Berengier, M. and Roure, A. (1980a) "Radiation impedance of one or several real sources mounted in a hard-walled rectangular waveguide", *J. Sound Vib.*, **71**, 389-398.

Berge, T. (1983) "Active noise cancellation of low frequency sound inside vehicle cabs", *Proc. Internoise 83*, 457-460.

Berge, T, Petterson, O.Kr.O., and Sorsdal, S. (1987) "Active noise cancellation of transformer noise", *Proc. Internoise 87*, 537-540.

Bies, D.A. and Hansen, C.H. (1988) *Engineering Noise Control - Theory and Practice*, Unwin Hyman, London.

Billoud, G., Galland, M., and Sunyach, M. (1989) "The use of time algorithms for the realization of an active sound attenuator", *Proc. ICASSP 89.*

Boland, F.M. and Foley, J.B. (1987) "Stochastic convergence of the LMS algorithm in adaptive systems", *Signal Process.*, **13**, 339-352.

Bullmore, A.J., and Nelson, P.A., and Elliott, S.J. (1986) "Active minimization of acoustic potential energy in harmonically excited cylindrical enclosed sound fields", AIAA paper **AIAA-86-1958**.

Bullmore, A.J., Nelson, P.A., Curtis, A.R.D., and Elliott, S.J. (1987) "The active minimization of harmonic enclosed sound fields, part II: A computer simulation", *J. Sound Vib.*, **117**, 15-33.

Bullmore, A.J., Nelson, P.A., and Elliott, S.J. (1990) "Theoretical studies of the active control of propeller-induced cabin noise", *J. Sound Vib.*, **140**, 191-217.

Burgess, J.C. (1981) "Active adaptive sound control in a duct: A computer simulation", *J. Acoust. Soc. Am.*, **70**, 715-726.

Canevet, G. (1978) "Active sound absorption in an air handling duct", *J. Sound Vib.*, **58**, 333-345.

Caraiscos, C. and Liu, B. (1984) "A roundoff error analysis of the LMS adaptive algorithm", *IEEE Trans. Acoust. Speech Signal Process.*, **ASSP-32**, 34-41.

Chaplin, B. (1980) "The cancellation of repetitive noise and vibration", *Proc. Internoise 80*, 699-702.

Chaplin, B. (1983) "Anti-noise - The Essex breakthrough", *Chart. Mech. Engr.*, **30**, 41-47.

Chaplin, G.B.B. and Smith, R.A. (1983) "Waveform synthesis: The Essex solution to repetitive noise and vibration", *Proc. Internoise 83*, 399-402.

Cioffi, J.M. (1987) "Limited-precision effects in adaptive filtering", *IEEE Trans. Circuits Syst.*, **CAS-34**, 821-833.

Conover, W. (1956) "Fighting noise with noise", *Noise Control*, **92**, 78-82.

Cowan, C.F.N. and Grant, P.M. (1985) *Adaptive Filters*, Prentice-Hall, New Jersey.

Croker, M.D. (1983) "The active control of internal combustion engine exhaust noise", *Proc. Internoise 83*, 457-460.

Curtis, A.R.D., Nelson, P.A., Elliott, S.J. and Bullmore, A.J. (1987) "Active suppression of acoustic resonance", *J. Acoust. Soc. Am.*, **81**, 624-631.

Deffayet, C. and Nelson, P.A. (1988) "Active control of low-frequency harmonic sound radiated by a finite panel", *J. Acoust. Soc. Am.*, **84**, 2192-2199.

Dimitriadis, E.K. and Fuller, C.R. (1989) "Investigation on active control of sound transmission through elastic plates using piezoelectric actuators", AIAA Paper **AIAA 89-1062**.

Doelman, N.J. (1989) "Active control of sound fields in an enclosure of low modal density", *Proc. Internoise 89*, 451-454.

Dorling, C.M., Eatwell, G.P., Hutchins, S.M., Ross, C.F., and Sutcliffe, S.G. (1989) "A demonstration of active noise reduction in an aircraft cabin", *J. Sound Vib.*, **128**, 358-360.

Eghtesadi, Kh. and Leventhall, H.G. (1981) "Active attenuation of noise: The Chelsea dipole", *J. Sound Vib.*, **75**, 127-134.

Eghtesadi, Kh. and Leventhall, H.G. (1982) "Active attenuation of noise- The monopole system", *J. Acoust. Soc. Am.*, **71**, 608-611.

Eghtesadi, Kh., Hong, W.K.W., and Leventhall, H.G. (1985) "Applications of active attenuators in controlling low-frequency noise", *Proc. Noise-Con 85*, 193-198.

Eghtesadi, Kh., Hong, W.K.W., and Leventhall, H.G. (1986) "Evaluations of active noise attenuator systems", *Proc. Internoise 86*, 577-582.

Eghtesadi, Kh., Hong, W.K.W., and Leventhall, H.G. (1987) "The tight-coupled monopole (TCM) and tight-coupled tandem (TCT) attenuators: Theoretical aspects and experimental attenuation in an air duct", *J. Acoust. Soc. Am.* **81**, 376-388.

Elliott, S.J. and Nelson, P.A. (1984) "Models for describing active noise control in ducts", *ISVR Technical Report 127.*

Elliott, S.J. and Nelson, P.A. (1985) "The application of adaptive filtering to the active control of sound and vibration", ISVR Technical Report **136**.

Elliott, S.J. and Nelson, P.A. (1985a) "Algorithm for multichannel LMS adaptive filtering", *Electron. Lett.*, **21**, 979-981.

Elliott, S.J. and Darlington, P. (1985) "Adaptive cancellation of periodic, synchronously sampled interference", *IEEE Trans. Acoust. Speech Signal Process.*, **ASSP-33**, 715-717.

Elliott, S.J. and Nelson, P.A. (1986) "The implications of causality in active control", *Proc. Internoise 86*, 583-588.

Elliott, S.J. and Nelson, P.A. (1986a) "An adaptive algorithm for multichannel active control", *Proc. Inst. Acoust.*, **8**, 135-147.

Elliott, S.J., Curtis, A.R.D., Bullmore, A.J., and Nelson, P.A. (1987) "The active minimization of harmonic enclosed sound fields, part III: Experimental verification", *J. Sound Vib.*, **117**, 35-58.

Elliott, S.J., Stothers, I.M., and Nelson, P.A. (1987) "A multiple error LMS algorithm and its application to the active control of sound and vibration", *IEEE Trans. Acoust. Speech Signal Process.*, **ASSP-35**, 1423-1434.

Elliott, S.J., Nelson, P.A., Stothers, I.M., and Boucher, C.C. (1989) "Preliminary results of in-flight experiments on the active control of propeller-induced cabin noise", *J. Sound Vib.*, **128**, 355-357.

Elliott, S.J., Nelson, P.A., Stothers, I.M., and Boucher, C.C. (1990) "In-flight experiments on the active control of propeller-induced cabin noise", *J. Sound Vib.*, **140**, 219-238.

Eriksson, L.J., Allie, M.C., and Greiner, R.A. (1987) "The selection and application of an IIR adaptive filter for use in active sound attenuation", *IEEE Trans. Acoust. Speech Signal Process.*, **ASSP-35**, 433-437.

Eriksson, L.J. and Allie, M.C. (1988) "A practical system for active attenuation in ducts", *Sound Vib.*, **22**, 30-34.

Eriksson, L.J., Allie, M.C., Bremigan, C.D., and Greiner, R.A. (1988a) "Active noise control using digital signal processing", *Proc. ICASSP 88.*

Fahy, F. (1985) *Sound and Structural Vibration: Radiation, Transmission, and Response*, Academic Press, London.

Ffowcs-Williams, J.E. (1984) "Anti-sound", *Proc. R. Soc. Lond.*, **A395**, 63-88.

Ffowcs-Williams, J.E., Roebuck, I., and Ross, C.F. (1985) "Anti-phase noise reduction", *Phys. Tech.*, **16**, 19-22.

Foley, J.B. and Boland, F.M. (1987) "Comparison between steepest descent and LMS algorithms in adaptive filters", *IEE Proc. Pt. F*, **134**, 283-289.

Franklin, G.F, Powell, J.D., and Workman, M.L. (1990) *Digital Control of Dynamic Systems, 2nd Ed.*, Addison-Wesley, Reading, Mass.

Fuller, C.R. and Jones, J.D. (1987) "Experiments on reduction of propeller induced interior noise by active control of cylinder vibration", *J. Sound Vib.*, **112**, 389-395.

Fuller, C.R. and Jones, J.D. (1987a) "Influence of sensor and actuator location on the performance of active control systems", paper presented at ASME winter annual meeting, Boston.

Fuller, C.R. (1987) "Free-field correction factor for spherical acoustic waves impinging on cylinders", AIAA paper **AIAA-87-2735**.

Fuller, C.R. (1988) "Analysis of active control of sound radiation from elastic plates by force inputs", *Proc. Internoise 88*, 1061-1064.

Fuller, C.R. (1990) "Active control of sound transmission / radiation from elastic plates by vibration inputs. I. Analysis", *J. Sound Vib.*, **136**, 1-15.

Gardner, W.A. (1984) "Learning characterisitics of stochastic-gradient-descent algorithms: A general study, analysis, and critique", *Signal Process.*, **6**, 113-133.

Gitlin, R.D., Meadors, H.C.Jr., Weinstein, S.B. (1982) "The tap-leakage algorithm: An algorithm for the stable operation of a digitally implemented, fractionally spaced adaptive equalizer", *Bell Sys. Tech. J.*, **61**, 1817-1839.

Guicking, D. (1990) "On the invention of active noise control by Paul Lueg", *J. Acoust. Soc. Am.*, **87**, 2251-2255.

Hesselman, N. (1978) "Investigation of noise reduction on a 100 KVA transformer tank by means of active methods", *Appl. Acoust.*, **11**, 27-34.

Honig, M.L. and Messerschmitt, D.G. (1984) *Adaptive Filters: Structures, Algorithms, and Applications*, Kluwer, Netherlands.

Horowitz, L.L. and Senne, K.D. (1981) "Performance advantage of complex LMS for controlling narrow-band adaptive arrays", *IEEE Trans. Circuits Syst.*, **CAS-28**, 562-576.

Jessel, M and Mangiante, G.A. (1972) "Active sound absorbers in an air duct", *J. Sound Vib.*, **23**, 383-390.

Jones, J.D. and Fuller, C.R. (1987) "Active control of sound fields in elastic cylinders by multi-control forces", AIAA paper **AIAA-87-2707**.

Joplin, P.M. and Nelson, P.A. (1990) "Active control of low-frequency random sound in enclosures", *J. Acoust. Soc. Am.*, **87**, 2396-2404.

Joseph, P., Nelson, P.A., and Elliott, S.J. (1989) "Near field zones of quiet in the pure tone diffuse sound field", *Proc. Internoise 89*, 489-494.

Junger, M.C. and Feit, D. (1986) *Sound, Structures, and Their Interaction*, MIT, Cambridge.

Kang, G.S. and Fransen, L.J. (1987) "Experimentation with an adaptive noise-cancellation filter", *IEEE Trans. Circuits Syst.*, **CAS-34**, 753-758.

Kempton, A.J. (1976) "The ambiguity of acoustic sources - A possibility of active control", *J. Sound Vib.*, **48**, 475-483.

Kido, A. (1975) "Reduction of noise by use of additional sound sources", *Proc. Internoise 75*, 647-650.

Leich, R.R. and Tokhi, M.O. (1987) "Active noise control systems", *IEE Proc.*, pt. A, **134**, 525-546.

La Fontaine, R.F. and Shepherd, I.C. (1983) "An experimental study of broadband active attenuation for cancellation of random noise in ducts", *J. Sound Vib.*, **91**, 351-362.

Leissa, A.W. (1973) "Vibration of shells", *NASA SP-288.*

Lester, H.C. and Fuller, C.R. (1986) "Active control of propeller induced noise fields inside a flexible cylinder", AIAA paper **AIAA-86-1957**.

Lester, H.C. and Fuller, C.R. (1987) "Mechanisms of active control for noise inside a vibrating cylinder", *Proc. Noise-con 87*, 371-376.

Leventhall, H.G. (1976) "Developments in active attenuators", *Proc. Noise-Con 76*, 33-42.

Leventhall, H.G. and Eghtesadi, Kh. (1979) "Active attenuation of noise: Dipole and monopole systems", *Proc. Internoise 79*, 175-180.

Ljung, L. (1977) "Analysis of recursive stochastic algorithms", *IEEE Trans. Automat. Contr.*, **AC-22**, 551-575.

Long, G., Ling, F., and Proakis, J.G. (1989) "The LMS algortihm with delayed coefficient adaption", *IEEE Trans. Acoust. Speech Signal Process.*, **ASSP-37**, 1397-1405.

McNichol, I.D. (1985) *Active Adaptive Cancellation of Sound in Ducts*, M.Engr.Sc. Thesis, Dept. of Electrical Engineering, University of Adelaide.

Mace, B.R. (1987) "Active control of flexural vibrations", *J. Sound Vib.*, **114**, 253-270.

Magliozzi, B. (1984) "Advanced turboprop noise: A historical review", AIAA paper **AIAA 84-226**.

Mandic, D.S. and Jones, J.D. (1989) "Active noise control in damped elastic cylinders using vibrational force inputs", *Proc. Internoise 89*, 441-446.

Meirovich, L. and Thangjitham, S. (1990) "Control of sound transmission from submerged plates", *J. Acoust. Soc. Am.*, **88**, 402-407.

Meirovitch, L., Baruh, H. and Oz, H. (1983) "A comparison of control techniques for large flexible systems", *J. Guidance*, **6**, 302-301.

Meirovich, L. and Bennighof, J.K. (1986) "Modal control of travelling waves in flexible structures", *J. Sound Vib.*, **111**, 131-144.

Mikhael, W.B. and Hill, P.D. (1988) "Performance evaluation of a real-time TMS 32010-based adaptive noise canceller (ANC)", *IEEE Trans. Acoust. Speech Signal Process.*, **ASSP-36**, 411-412.

Mollo, C.G. and Bernhard, R.J. (1987) "A generalized method for optimization of active noise controllers in three-dimensional spaces", AIAA paper **AIAA-87-2705**.

Moore, C.J. (1979) "Measurement of radial and circumferential modes in annular and circular fan ducts", *J. Sound Vib.*, **62**, 235-256.

Morgan, D.R. (1980) "An analysis of multiple correlation cancellation loops with a filter in the auxillary path", *IEEE Trans. Acoust. Speech Signal Process.*, **ASSP-28**, 454-467.

Morse, P.M. and Ingard, K.U. (1968) *Theoretical Acoustics*, McGraw-Hill, New York.

Nadim, M. and Smith, R.A. (1983) "Synchronous adaptive cancellation in vehicle cabs", *Proc. Internoise 83*, 461-464.

Nelson, P.A., Curtis, A.R.D., and Elliott, S.J. (1985) "Quadratic optimization problems in the active control of free and enclosed sound fields", *Proc. Inst. Acoust.*, **7**, 45-53.

Nelson, P.A. and Elliott, S.J. (1986) "The minimum power output of a pair of freefield monopole sources", *J. Sound Vib.*, **105**, 173-178.

Nelson, P.A. and Elliott, S.J. (1987) "Active minimisation of acoustic fields", *J. Theor. App. Mech.*, **6** (supp), 39-98.

Nelson, P.A., Curtis, A.R.D., Elliott, S.J., and Bullmore, A.J. (1987) "The minium power output of free field point sources and the active control of sound", *J. Sound Vib.*, **116**, 397-414.

Nelson, P.A., Curtis, A.R.D, Elliott, S.J., and Bullmore, A.J. (1987a) "The active minimization of harmonic enclosed sound fields, part I: Theory", *J. Sound Vib.*, **117**, 1-13.

Nelson, P.A., Hammond, J.K, Joseph, P., and Elliott, S.J. (1990) "Active control of stationary random sound fields", *J. Acoust. Soc. Am.*, **87**, 963-975.

Ochs, J. and Snowden, J. (1975) "Transmissibility across simply supported thin plates, 1. Rectangular and square plates with and without damping layers", *J. Acoust. Soc. Am.*, **58**, 832-840.

Olson, H.F. and May, E.G. (1953) "Electronic Sound Absorber", *J. Acoust. Soc. Am.*, **25**, 1130-1136.

Olson, H.F. (1956) "Electronic control of noise, vibration, and reverberation", *J. Acoust. Soc. Am.*, **28**, 966-972.

Pan, J., Hansen, C.H., and Bies, D.A. (1990) "Active control of noise transmission through a panel into a cavity: I. Analytical study", *J. Acoust. Soc. Am.*, **87**, 2098-2108.

Pan, J. and Hansen, C.H. (1990a) "Active control of sound transmission through a panel into a cavity: II. Experimental study", *J. Acoust. Soc. Am.*, submitted for publication.

Poole, J.H.B. and Leventhall, H.G. (1976) "An experimental study of Swinbank's method of active attenuation of sound in ducts", *J. Sound Vib.*, **49**, 257-266.

Poole, L.A., Warnaka, G.E., and Cutter, R.C. (1984) "The implementation of digital filters using a modified Widrow-Hoff algorithm for the adaptive concellation of acoustic noise", *Proc ICASSP 84.*

Pope, L.D. (1971) "On the transmission of sound through finite closed shells: Statistical energy analysis, modal coupling, and nonresonant transmission", *J. Acoust. Soc. Am.*, **50**, 1004-1018.

Pope, L.D., Rennison, D.C., and Wilby, E.G. (1980) "Analytical prediction of the interior noise for cylindrical models of aircraft fuselages for prescribed exterior noise fields", *NASA CR-159363.*

Pope, L.D., Rennison, D.C., Willis, C.M. and Mayes, W.H. (1982) "Development and validation of preliminary analytical models for aircraft noise prediction", *J. Sound Vib.*, **82**, 541-575.

Press, W.H., Flannery, B.P., Teukolsky, S.A., and Vetterling, W.T. (1986) *Numerical Recipes: The Art of Scientific Computing*, Cambridge University Press, Cambridge.

Roebuck, I (1990) "Energy considerations in active noise control", *Proc. International Congress on Recent Developments in Air- and Structure-Borne Sound and Vibration*, 509-516.

Ross, C.F. (1982) "Experiments on the active control of transformer noise", *J. Sound Vib.*, **61**, 473-480.

Ross, C.F. (1982a) "Application of digital filtering to active control of sound", *Acustica*, **51**, 135-140.

Ross, C.F. (1982b) "An adaptive digital filter for broadband active sound control", *J. Sound Vib.*, **80**, 381-388.

Roure, A. and Nayroles, B. (1984) "Autoadaptive broadband active absorbtion in ducts by means of transversal filtering", *Proc. Internoise 84*, 493-496.

Roure, A. (1985) "Self-adaptive broadband active sound control system", *J. Sound Vib.*, **101**, 429-441.

Schuck, P.L. (1988) "Investigation into the use of the filtered-x LMS algorithm for noise reduction in a duct", *J. Acoust. Soc. Am.*, supp QQ3.

Sha Jiazheng and Tian Jing (1987) "Acoustical mechanism of active noise attenuator in duct", *Proc. Internoise 87*, 541-544.

Silcox, R.J. and Lester, H.C. (1982) "Sound propagation through a variable area duct: Experiment and theory", *AIAA Jour.*, **20**, 1377-1384.

Silcox, R.J., Fuller, C.R., and Lester, H.C. (1987) "Mechanisms of active control in cylindrical fuselage structures", AIAA paper **AIAA-87-2703**.

Silcox, R.J., Lester, H.C., and Abler, S.B. (1987a) "An evaluation of active noise control in a cylindrical shell", NASA TM-89090.

Silcox, R.J. and Lester, H.C. (1988) "Energy flows for active noise control systems in a cylindrical shell", *Proc. Internoise 88*, 1003-1008.

Silcox, R.J., Lester, H.C., and Abler, S.B. (1989) "An evaluation of active noise control in a cylindrical shell", *J. Acoust. Stress Rel. Design*, **111**, 337-342..

Smith, R.A. and Chaplin, G.B.B. (1983) "A comparison of some Essex algorithms for major industrial applications", *Proc. Internoise 83*, 407-410.

Snyder, S.D. and Hansen, C.H. (1990) "The influence of transducer transfer functions and acoustic time delays on the implementation of the LMS algorithm in active noise control systems", *J. Sound Vib.*, **141**, 409-424.

Swinbanks, M.A. (1973) "The active control of sound propagation in long ducts", *J. Sound Vib.*, **27**, 411-436.

Tabachnick, B.G. and Fidell, L.S. (1989) *Using Multivariate Statistics*, 2nd ed., Harper and Row, New York.

Thomas, D.R, Nelson, P.A., and Elliott, S.J. (1990) "Experiments on the active control of the transmission of sound through a clamped rectangular plate", *J. Sound Vib.*, **139**, 351-355.

Tohyama, M. and Suzuki, A. (1987) "Active power minimization of a sound source in a closed space", *J. Sound Vib.*, **119**, 562-564.

Trinder, M.C.J. and Nelson, P.A. (1983) "Active noise control in finite length ducts", *J. Sound Vib.*, **89**, 95-105.

Wallace, C.E. (1972) "Radiation resistance of a rectangular panel", *J. Acoust. Soc. Am.*, **51**, 946-952.

Warnaka, G.E. (1982) "Active attenuation of noise: The state of the art", *Noise Control Eng.* **18**, 100-110.

Warner, J.V. and Bernhard, R.J. (1987) "Digital control of sound fields in three-dimensional enclosures", AIAA paper **AIAA-87-2706**.

White, A.D. and Cooper, D.G. (1984) "An adaptive controller for multivariable active noise control", *App. Acoust.*, **17**, 99-109.

Widrow, B., Glover, J.R.Jr., McCool, J.M., Kaunitz, J., Williams, C.S., Hearn, R.H., Zeidler, J.R., Dong, E.Jr., and Goodlin, R.C. (1975) "Adaptive noise cancelling: Principles and applications", *Proc. IEEE*, **63**, 1692-1716.

Widrow, B., McCool, J.M., Larimore, M.G., and Johnson, C.R.Jr. (1976) "Stationary and non-stationary learning characteristics of the LMS adaptive filter", *Proc. IEEE*, **64**, 1151-1162.

Widrow, B. and Stearns, S.D. (1985) *Adaptive Signal Processing*, Prentice-Hall, New Jersey.

Zalas, J.M. and Tichy, J. (1984) "Active attenuation of propeller blade passage noise", NASA CR-172386.

Zimmerman, D.C. and Cudney, H.H. (1989) "Practical implementation issues for active control of large flexible structures", *J. Vib. Acoust. Stress Rel. Des.*, **111**, 283-289.

PUBLICATIONS ORIGINATING FROM THIS THESIS WORK

PAPERS PUBLISHED IN REFEREED JOURNALS

Snyder, S.D. and C.H. Hansen 1990. The influence of transducer transfer functions and acoustic time delays on the LMS algorithm in active noise control systems. Journal of Sound and Vibration, **141**, 409-424.

Snyder, S.D. and C.H. Hansen 1989. Active noise control in ducts: some physical insights. Journal of the Acoustical Society of America, 86, 184-194.

PAPERS ACCEPTED FOR PUBLICATION IN REFEREED JOURNALS

Snyder, S.D. and C.H.Hansen 1990. Mechanisms of active noise control using vibration sources. Accepted for publication in the Journal of Sound and Vibration.

Snyder, S.D. and C.H. Hansen 1990. Using multiple regression to optimise active noise control system design. Accepted for publication in the Journal of Sound and Vibration

Fuller, C.R. C.H. Hansen and S.D. Snyder 1990. Experiments on active control of sound radiation from a panel using a piezo ceramic actuator. Accepted for publication in the Journal of Sound and Vibration.

Fuller, C.R., C.H. Hansen and S.D. Snyder 1990. Active control of sound radiation from a vibrating rectangular panel by sound sources and vibration inputs: an experimental comparison. Accepted for publication in the Journal of Sound and Vibration.

PAPERS CURRENTLY UNDER REVIEW FOR PUBLICATION IN REFEREED JOURNALS

Snyder, S.D., R.L. Clark and C. H. Hansen 1990. Convergence characteristics of the multiple input, multiple output LMS algorithm. Submitted for publication in the Journal of Intelligent Material Systems and Structures.

Pan, J., C.H. Hansen and S.D. Snyder 1990. Dynamic modelling of an elastic beam excited by a piezoceramic actuator. Submitted for publication in the Journal of the Acoustical Society of America.

Snyder, S.D. and C.H. Hansen 1990. Design requirements for active noise control systems implementing the multiple input, multiple output LMS algorithm. Submitted to the Journal of Sound and Vibration.

Pan, J., S.D. Snyder, C.H. Hansen and C.R. Fuller 1990. Active control of far field sound radiated by a rectangular panel - a general analysis. Submitted to the Journal of the Acoustical Society of America.

Snyder, S.D. and C.H. Hansen 1990. A general approach to the design of active systems to control sound radiation from vibrating structures. Part 1. Analytical models. Submitted for publication in the Journal of the Acoustical Society of America.

Snyder, S.D. and C.H. Hansen 1990. A general approach to the design of active systems to control sound radiation from vibration structures. Part 2. Radiation into free space. Submitted for publication in the Journal of the Acoustical Society of America.

PAPERS PUBLISHED IN REFEREED CONFERENCE PROCEEDINGS

Snyder, S.D. and Hansen, C.H. 1991. The effect of modal coupling characteristics on one mechanism of active noise control. To be presented at the Conference on Recent Advances in the Active Control of Sound and Vibration, Virginia Polytechnic Institute and State University, USA, in April.

Hansen, C.H. and Snyder, S.D. 1991. Effect of geometric and structural / acoustic variables on the active control of sound radiation from a vibrating structure. To be presented at the Conference on Recent Advances in the Active Control of Sound and Vibration, Virginia Polytechnic Institute and State University, USA, in April.

Fuller, C.R., S.D. Snyder, C.H. Hansen and R.J. Silcox 1990. Active control of interior noise in model aircraft fuselages using piezoceramic actuators. Proceedings of the 13th AIAA Aeroacoustics Conference, Talahessee, Florida, USA, October 1990. AIAA paper 909-3922.

Snyder, S.D., Hansen, C.H. and J. Pan 1990. A general design methodology to control sound radiation into enclosed spaces. Proceedings of the Australian Vibration and Noise Conference, Melbourne, September 1990.

Hansen, C.H. and S.D. Snyder 1990. The influence of source size location and number upon power flow attenuation achieved with duct active noise control systems. Proceedings of the Australian Vibration and Noise Conference, Melbourne, September 1990.

Hansen, C.H., S.D. Snyder and J. Pan 1990. A methodology for the design of systems to actively control sound from vibrating structures. Proceedings of The International Congress on Recent Developments in Air- and Structure-borne Sound and Vibration, Auburn University, Alabama, March 6-8, 1990.

Fuller, C.R., C.H. Hansen and S.D. Snyder 1989. Active control of structurally radiated noise using piezo-ceramic actuators. Proceedings Internoise '89, Newport Beach, December 4-6.

Snyder, S.D., C.H. Hansen and C.R. Fuller 1989. An experimental investigation of the active control of sound transmission into a cylindrical enclosure. Proceedings of INTERNOISE '89, International Conference on Noise Control Engineering, December 4-6, Newport Beach, CA.

Hansen, C.H., S.D. Snyder and C.R. Fuller 1989. Reduction of noise radiated by a vibrating square panel by use of active sound sources and active vibration sources: a comparison. Proceedings of Noise and Vibration '89 Singapore, August 16-18.

OTHER CONFERENCE PAPERS AND INVITED LECTURES

Fuller, C.R., S.D. Snyder and C.H. Hansen 1990. Near field intensity and pressure distributions of actively controlled panel radiated sound. Journal of the Acoustical Society of America, 87 Suppl. 1.

Snyder, S.D., C.H. Hansen and J. Pan 1989. A general analysis of the active control of sound radiation from a baffled panel. J.Acoust. Soc. Am. 86, Suppl.1.

Hansen, C.H., S.D. Snyder and D.A. Bies 1988. Mechanisms of active sound control. Journal of the Acoustical Society of America Suppl. 1. 84, S183.